STATE OF CALIFORNIA • DEPARTMENT OF TRANSPORTATION
TECHNICAL REPORT DOCUMENTATION PAGE
TR0003 (REV 10/98)

1. REPORT NUMBER	2. GOVERNMENT ASSOCIATION NUMBER	3. RECIPIENT'S CATALOG NUMBER
CA14-2280		

4. TITLE AND SUBTITLE
Probabilistic Damage Control Approach for Seismic Design of Bridges

5. REPORT DATE
June 2014

6. PERFORMING ORGANIZATION CODE
UNR/

7. AUTHOR
Amarjeet Saini and M. Saiid Saiidi

8. PERFORMING ORGANIZATION REPORT NO.
UNR/CA14-2280

9. PERFORMING ORGANIZATION NAME AND ADDRESS
Department of Civil and Environmental Engineering
University of Nevada, Reno
Reno, Nevada 89557-0152

10. WORK UNIT NUMBER

11. CONTRACT OR GRANT NUMBER
65A0419

12. SPONSORING AGENCY AND ADDRESS
California Department of Transportation, Engineering Service Center
1801 30th Street, MS 9-2/5i, Sacramento, California 95816
California Department of Transportation, Division of Research, Innovation & System Info
1227 O Street, Sacramento, CA 95814

13. TYPE OF REPORT AND PERIOD COVERED
Final Report
7/11/2011 – 5/31/2014

14. SPONSORING AGENCY CODE

15. SUPPLEMENTARY NOTES
Prepared in cooperation with the State of California Department of Transportation.

16. ABSTRACT
Probabilistic seismic design is a relatively new concept for seismic design of bridges subjected to earthquakes. Through this method, uncertainties in seismic response and seismic demand are taken into account. The concept can be extended to control damage by designing for certain target apparent damage with an associated probability of exceedance. Through a study funded by the California Department of Transportation (Caltrans), a probabilistic damage control approach (PDCA) and reliability analysis was used to develop performance based seismic design of bridge columns. The PDCA uses the extent of lateral displacement nonlinearity defined by "Damage Index" (DI) to measure the performance of bridge columns. The performance objective was defined based on predefined apparent damage states and the damage states were correlated to DIs based on a previous study at the University of Nevada, Reno. The correlation between DI and DS was determined from a statistical analysis (resistance model) of over 140 response data measured from testing of 22 bridge column models subjected to seismic loads. Extensive analytical modeling of seismic response of single column and multicolumn bents was conducted. A wide range of variables was included in the study to address the effect of aspect ratio, longitudinal steel ratio, site class, distance to active faults, earthquake return period, and number of columns per bent. Each column was analyzed under 25 near-field and far-field ground motions. A statistical analysis of the demand damage index (DIL) was performed to develop fragility curves (load model) and to determine the reliability index for each DS. The results of reliability analysis were

17. KEY WORDS	18. DISTRIBUTION STATEMENT
bridge, damage, earthquake, PDCA, probabilistic design, reliability index, return period,	No restrictions. This document is available to the public through the National Technical Information Service, Springfield, VA 22161

19. SECURITY CLASSIFICATION *(of this report)*	20. NUMBER OF PAGES	21. COST OF REPORT CHARGED
Unclassified	216	

Abstract

Probabilistic seismic design is a relatively new concept for seismic design of bridges subjected to earthquakes. Through this method, uncertainties in seismic response and seismic demand are taken into account. The concept can be extended to control damage by designing for certain target apparent damage with an associated probability of exceedance. Through a study funded by the California Department of Transportation (Caltrans), a probabilistic damage control approach (PDCA) and reliability analysis was used to develop performance based seismic design of bridge columns. The PDCA uses the extent of lateral displacement nonlinearity defined by "Damage Index" (DI) to measure the performance of bridge columns. The performance objective was defined based on predefined apparent damage states and the damage states were correlated to DIs based on a previous study at the University of Nevada, Reno. The correlation between DI and DS was determined from a statistical analysis (resistance model) of over 140 response data measured from testing of 22 bridge column models subjected to seismic loads. Extensive analytical modeling of seismic response of single column and multicolumn bents was conducted. A wide range of variables was included in the study to address the effect of aspect ratio, longitudinal steel ratio, site class, distance to active faults, earthquake return period, and number of columns per bent. Each column was analyzed under 25 near-field and far-field ground motions. A statistical analysis of the demand damage index (DI_L) was performed to develop fragility curves (load model) and to determine the reliability index for each DS. The results of reliability analysis were analyzed and a direct PDCA was developed to calibrate design DI to obtain a desired reliability index against failure. The calculated reliability indices and fragility curves showed that the proposed method could be effectively used in seismic design of new bridges as well as seismic assessment of existing bridges. Included in the current project was an exploratory study to extend the PDCA to earthquake-damaged columns that have been repaired. Like conventional original (not repaired) columns, different damage states (DSs) were defined for repaired columns associated with varying degree of damage

DISCLAIMER STATEMENT

Final Report No. CA14-2280, CCEER 14-02

PROBABILISTIC DAMAGE CONTROL APPROACH FOR SEISMIC DESIGN OF BRIDGE COLUMNS

Amarjeet Saini
M. Saiid Saiidi

Final Report Submitted to the California Department of Transportation (Caltrans) under contract No. 65A0419

Center for Civil Engineering Earthquake Research

University of Nevada, Reno
Department of Civil and Environmental Engineering, MS 258
1664 N. Virginia St.
Reno, NV 89557

June 2014

Acknowledgements

The research presented herein was sponsored by California Department of Transportation (Caltrans) under Grant No. 65A0419. However, conclusions and recommendations are those of the authors and do not necessarily present the views of the sponsor.

The contribution of Dr. Ashkan Vosooghi, a former post-doctoral fellow at UNR, on providing valuable and constructive suggestions during the planning and development of this study is much appreciated. The authors would like to express their appreciation to Mr. Abbas Tourzani, Dr. Amir Malek, Dr. Mark Mahan, Mr. Sam Ataya, Dr. Charles Sikorsky, Dr. Tom Shantz, Mr. Kyoung Lee, and Mr. Mark Yashinsky of Caltrans for their feedback and interest in different aspects of the project. Special thanks are due to Mr. Peter Lee, the Caltrans Research Program manager, for his support and advice.

Table of Contents

List of Tables

Chapter 5

Chapter 6

Appendix A

List of Figures

Chapter 2

Chapter 3

Chapter 4

Chapter 5

Chapter 6

Appendix A

Chapter 1. Introduction

1.1 Introduction

Performance-based seismic design (PBSD) become of interest to researchers and structural engineers after the Loma Prieta earthquake in 1989. PBSD is based largely on displacement consideration rather than strength used in conventional seismic design methods (Priestley et al. 2007; Suarez and Kowalsky 2010). Most of the existing PBSD for bridge columns are based on deterministic approaches. Due to uncertainties in seismic demand and response, deterministic seismic design and evaluation of a structure may be unsafe and unrealistic, especially for important structures. It is more realistic to analyze the structure using probabilistic approach by incorporating the uncertainties in seismic demand and structure response to better control the seismic performance. In the present study, a probabilistic damage control approach (PDCA) was used to develop PBSD for bridge columns. PDCA is a new procedure for seismic design of bridges that takes into account the uncertainties in seismic response and seismic demand. The PDCA design procedure explicitly evaluates how a given structure is likely to perform under a given seismic hazard. To evaluate the performance of the bridge column, PDCA incorporates the extent of column lateral plastic deformation at different earthquake levels. The extent of lateral plastic deformation was quantified by Malek et al. (2007) based on limited experimental results and engineering judgments for different bridge categories subjected to earthquakes with various return periods (T). The extent of lateral plastic deformation was quantified using damage index (DI). The DI was defined as the ratio of plastic deformation demand to plastic deformation capacity (Eq. 1-1).

$$DI = \frac{\Delta_D - \Delta_Y}{\Delta_C - \Delta_Y} \tag{1-1}$$

Where Δ_D, Δ_Y, and Δ_C are the column displacement demand induced by earthquake, the effective yield displacement, and the ultimate displacement capacity, respectively.

Probabilistic damage control approach (PDCA) for seismic design of single column and multi-column bridge bents was developed and discussed in this present study. Each bent was designed for a predefined performance level under the design earthquake. Because PBSD is largely based on displacement considerations, DI was selected as a representative parameter of the column response. The DI is the ratio of column plastic deformation demand and plastic deformation capacity and varies from zero to one. To quantify the performance of a column, each performance level was correlated to a possible apparent damage state (DS). Subsequently, each damage state was correlated to an associated DI (Vosooghi and Saiidi 2012).

To determine reliability of the columns designed as per PDCA, a reliability analysis was conducted. To develop a resistance model for reliability analysis, the fragility curves that correlate DSs to an associated DI (Vosooghi and Saiidi 2012) were utilized. To develop a load model for reliability analysis, extensive analytical modeling of seismic response of single column and multi columns bents was conducted. A wide range of variables was included in the study to address the effect of aspect ratio, support conditions, longitudinal steel ratio, site class, distance to active faults, and number of columns per bent. After having distribution of resistance and load model, reliability analysis was conducted. The reliability analysis results were analyzed, and a direct probabilistic design method was developed to calibrate the design DI and to obtain a target reliability index (β_6') against failure.

Included in the current project was an exploratory study to extend the PDCA and reliability analysis approach to earthquake-damaged columns that have been repaired. This part of the study was focused on columns that are repaired using carbon fiber reinforced polymer (CFRP) jackets. Like conventional original (not repaired) columns, different damage states (DSs) were defined for repaired columns associated with varying degree of damage. The goal of this study was to demonstrate the process of using PDCA for repaired columns, realizing that the study is of limited scope due to the scarcity of data for repaired columns.

1.2 Previous Relevant Research

Probabilistic performance-based design (PPBD) methodology has become of central interest in risk mitigation decision making for structures and infrastructure systems (Cornell and Krawinkler, 2000; Mackie and Stojadinovic, 2001). Such methodologies aim to better understand the seismic risk to structural systems, and design structures to achieve goals of life safety, reduce economic loss, and minimize recovery downtime in the aftermath of a seismic event. In the evolving world of performance-based earthquake engineering, engineers are transitioning away from development of deterministic design criteria for site-specific seismic hazard (Mackie and Stojadinovic, 2001). Describing the resulting structural performance as safe or unsafe can be misleading when considering the uncertainty in structural demand and response parameters. Therefore, current seismic performance assessment methodologies are tending toward fragility curves (probabilistic techniques). Fragility curves describe probabilities of exceeding design or performance criteria at different levels of seismic input intensity. There are several reports and codes available to provide guidelines on probabilistic/reliability based design of bridges (National Cooperative Highway Research Program (NCHRP Report 489, 2003), American Association of State Highway and Transportation Officials (AASHTO, 2010), HAZUS-MH (2011). In the following sections, a brief overview of the past research on probabilistic design and structural reliability based assessment of bridges is presented.

1.2.1. Probabilistic Based Design

Mackie and Stojadinovic (2005) conducted a study on developing fragility curves for California overpass bridge seismic decision making. In that study, a rational method to evaluate damage potential and to assess probable highway bridge losses for critical decision making regarding the post-earthquake safety and repair of highway network was presented. Loss fragilities were defined for each individual bridge using PEER's performance-based earthquake engineering framework. Decision variables were related to earthquake intensity through a series of disaggregated models (demand, damage, and loss). The fragility curves provided in that study were intended for application in two ways. First, bridge designers may use them to investigate how variation of bridge design parameters is reflected in the amount of expected losses after an earthquake. Second, highway network planners may use bridge fragilities to more reliably evaluate the losses in a highway transportation network. In the process of developing bridge fragilities, intensity measures were first coupled with engineering demand parameters to formulate probabilistic demand models. Two damage models were then formulated. Component damage models utilized experimental data to predict response levels at which observable damage states were reached. System damage models utilized finite element reliability analysis to predict the loss of lateral and vertical load-carrying capacity. Improved methods for computing system damage were introduced. Two loss models were formulated. Component damage states were described in terms of repair costs of returning bridges to full functionality. System load-loss states were described in terms of bridge traffic capacity and collapse prevention. System loss fragilities were enhanced using the same improved methods developed for damage models.

Tourzani et al. (2008) presented a performance-based design procedure for bridge columns. In their study, PDCA was used to assess the performance of column subjected to various probabilistic seismic events. The reserved deformation capacity of the column was quantified using DI and compared to various levels of deformation demand imposed by probabilistic seismic events. The damage level of the bridge was established for a specific seismic event known as "Design Earthquake". Then, additional probabilistic seismic excitations were imposed to study various damage levels. To design columns, acceleration response spectrum (ARS) curves instead of a certain averaged deterministic curve were used. However, in the study by Tourzani et al. (2008), uncertainties in earthquake demands and bridge responses were not included.

Vosooghi and Saiidi (2012) developed a method for PPBD and probabilistic performance based assessment (PPBA) of reinforced concrete bridge columns using the fragility curves. These fragility curves include the uncertainties in seismic response parameters. Data from 32 bridge column models, mostly tested on shake tables, were used to develop fragility curves for six seismic response parameters at six distinct apparent DSs. The DSs were: flexural cracks (DS1), minor concrete cover spalling (DS2), extensive spalling of cover concrete (DS3), visible bars (DS4), start of concrete core damage (DS5), and bar fracture (DS6). The six response parameters defined by Vosooghi and Saiidi (2012) were: the maximum drift ratio (MDR), residual drift ratio (RDR), frequency ratio (FR), inelasticity index (II), maximum longitudinal steel strain (MLS), and maximum transverse steel strain (MTS). In the present study, inelasticity index is referred as damage index (DI) to be consistent with the rest of the study. A PPBD method was used to design columns for one or more probabilistic performance objectives. The probabilistic performance objective was defined as a DS under specified earthquake intensity with a given probability of occurrence. However, in the study by Vosooghi and Saiidi (2012), uncertainties in earthquake demands were not included.

Liang and Lee (2013) conducted a study on establishing practical multi-hazard design limit states for bridges. This study was mainly focused on formulating a criterion to combine the time variant load effects (extreme load effects such as earthquake, and vessel collisions) in the load and resistance factor design (LRFD) (AASHTO). The

LRFD is a reliability-based design that considers failure probabilities of bridge components due to the actions of typical dead load and frequent vehicular loads (time invariant loads). The study conducted by Liang and Lee (2013) describes the establishment of a criterion to include only the necessary load combinations to establish the design limit states. This criterion was established by examining the total failure probabilities for all possible time-invariant and time-varying load combinations and breaking them down into partial terms. Then, important load combinations were readily determined quantitatively. However, in the study by Liang and Lee (2013) the uncertainties in bridge response were not discussed.

Alipour et al. (2013) developed a multi-hazard reliability-based framework to evaluate the bridge response subjected to combined effect of pier scour and earthquake events. This framework was used to calibrate the scour load-modification factors for the design of bridges located in high seismic areas. A series of case studies were investigated. For each bridge case, the joint probability of failure associated with scour and earthquake hazards determined for a range of expected combinations of these two extreme events. The occurrence probability of each scour-earthquake scenario was identified by taking into account all of the major sources of load uncertainty through scour risk and seismic hazard curves. Furthermore, the uncertainties inherent in the structural response of bridges were included in the framework to improve the accuracy of estimated failure probabilities. The calculated probabilities were then compared with an equivalent target reliability index given by current design codes to obtain scour load-modification factors.

1.2.2. Reliability Based Assessment of Bridges

Researchers have adopted different techniques to probabilistically model the structural response and demand by utilizing fragility curves. The derivation of component based fragility curves is straightforward and is a closed-form solution (Eq. 1-2), considering that the demand and capacity are log-normally distributed (Mackie and Stojadinovic (2001), Cornell et al. (2002), Bazzurro and Cornell (2002), Ellingwood and Wen (2005), Nielson and DesRoches (2007), Padgett et al. (2008), Celik and Ellingwood (2010)). In Eq. 1-2, D and C denote demand and capacity, S_D and S_C denote the median values of demand and capacity, IM denotes the intensity measure, and $\beta_{D|IM}$ and β_C denote the dispersions (logarithmic standard deviation) of the demand and capacity, respectively. It must be noted that S_C and β_C are defined based on the limit state under consideration.

Mackie and Stojadinovic (2005) used a mean value, first order, second-moment analysis for each of the limit state functions describing the components that contribute to the system vulnerability. Having determined the mean and standard deviation for each of the response quantities (drift ratio, residual displacement, etc.), parametric first order reliability method (FORM) analysis was used to determine the probability of failure for each of the response measures. The series system assumption was then used to determine the system level fragility curves. Choi et al. (2004) developed first order bounds for system reliability assuming series systems, as one of the earliest attempts to account for some level of correlation among bridge components.

Zhang and Huo (2009) adopted a weighting scheme to establish correlation between component failure and bridge system level failure based on the components that contribute the most to the load carrying capacity or post event functionality criterion. Although the approach realizes that not all components contribute equally to system level damage states, the establishment of weights is particularly subjective and difficult as the number of components characterizing the system vulnerability increases. Kim et al. (2006), Lupoi et al. (2006), Zhang and Huo (2009) used other approaches to define system reliability such as parallel system, combination of series and parallel components, or adaptive systems that add components as damage accumulates.

Although there are numerous studies on probabilistic based seismic design and/or assessment of bridges, studies on displacement-based probabilistic seismic design of bridge columns by considering uncertainties in both the response and demand parameters are very limited. Additionally, there is no research available which explicitly correlates the probability of exceedance of a certain damage state in bridge columns with an associated reliability against failure and other damage states.

1.3 Objectives and Scope of PDCA

The primary objectives of the present study were: (1) to develop a method for seismic design of bridge columns for different probability of exceedance of different apparent damage states that are correlated to a quantifiable damage index (DI) and to determine the associated reliability index against failure and other damage states, and (2) to develop a method for seismic design of bridge columns for a target reliability against failure (β_6'), and to determine probability of exceedance of other damage states. In addition, an exploratory study to extend the PDCA and reliability analysis approach to earthquake-damaged columns that have been repaired is presented in this report.

To accomplish these objectives, the study was divided into four parts. The first part was to establish a resistance model for the reliability analysis. To develop resistance model, over 140 seismic performance data points from testing of 22 bridge column models mostly tested on shake tables were used to develop fragility curves for DIs at six apparent DSs (Vosooghi and Saiidi 2012). In the second part of the study, a load model was developed by conducting a large number of non-linear dynamic analyses on bridge bents. The uncertainties in ground motions, site class, bent configuration, earthquake return period were included in the analyses. Each bent was analyzed under 25 earthquake records consisting of 10 far-field and 15 near field ground motions. For each ground motion, the maximum displacement was determined and consequently DI was calculated. Reliability analysis was conducted upon having distribution of resistance and load model. In the third part, the results of the reliability analyses were investigated, and a direct probabilistic design procedure was developed to calibrate design DI based on a target reliability against failure. Finally, the same PDCA methodology that was used for conventional columns was used to extend the PDCA and reliability analysis approach to earthquake-damaged columns that have been repaired. Because seismic performance data for different damage states in repaired column models was very limited, the results of the last part of the study should be viewed only as an example of the potential application of PDCA to repaired columns and the results should be used with caution.

Chapter 2. Probabilistic Damage Control Approach for Seismic Design of Bridge Columns

2.1 Introduction

To develop PDCA, six apparent DSs defined in a previous study by Vosooghi and Saiidi (2010) were utilized (Figure *2-1*). To establish correlation between DS and DI, a database of 22 bridge columns were studied (Vosooghi and Saiidi 2012). In that study, in addition to DI, five other response parameters were defined. The response parameters were divided into two categories, internal and external. The external response parameters consist of the maximum drift ratio (MDR), residual drift ratio (RDR), frequency ratio (FR), and damage index (DI); whereas, the internal response parameters consist of the maximum longitudinal steel stain (MLS) and the maximum transverse steel strain (MTS). Out of 32 columns, only 21 were used to develop fragility curves for damage indices. This is because 11 of the columns had not failed in the tests. The models used to develop fragility curves are shown with bold letters in Table 2-1. The column database of 32 columns was further expanded to 38 columns by adding data from six columns of a four-span bridge model tested at UNR (Saiidi et al. 2013). The six column models are listed at the bottom of Table 2-1. Out of these six, only one column was subjected to failure and was added to the previous database of 21 columns. Utilizing the columns database, fragility curves were developed to establish correlation between DS and DI (Figure 2-2). These fragility curves serve as resistance model in the reliability analysis. Implicit in these curves is variability in concrete and steel properties. The expansion of column database is further discussed in detail in Chapter 11. In Figure 2-2, no curves are shown for DS-6, because DS-6 corresponds to failure with 100% probability of DI of one.

To develop a load model for reliability analysis, extensive analytical modeling of seismic response of single column and multi columns bents was conducted. A wide range of variables was included in the study to address the effect of aspect ratio, support conditions, longitudinal steel ratio, site class, distance to active faults, and number of columns per bent. Each bent was analyzed under 15 near-field and 10 far-field ground motions. For each ground motion, the maximum displacement was determined and consequently DI was calculated. After having distribution of resistance and load model, reliability analysis was conducted. The reliability analysis results were analyzed, and a direct probabilistic design method was developed to calibrate the design DI and to obtain a target reliability index (β_6') against failure. The β_6' is based on combined probability of failure including the probability of earthquake exceedance during the life span of bridge (P_{EQ})

2.2 Fragility Curves to Correlate Damage States with Damage Indices

The fragility analysis approach was used to establish the correlation between DS and DI, taking into account the effect of uncertainties in seismic response parameters. To develop fragility curves a cumulative lognormal distribution function was used. Development of fragility curves is discussed in the following sections.

2.2.1. Fragility Function Definition

According to ATC-58, fragility functions are probability distributions that are used to indicate the probability that a component, element or system will be damaged to a given or more severe DS as a function of a single predictive demand parameter. In the present study, fragility curves take the form of cumulative lognormal distribution functions, with median value θ and logarithmic standard deviation of x. The mathematical form for such a fragility function is:

$$F\left(RP\right)=\Phi\left(\frac{\ln\left(RP/\theta\right)}{x}\right) \tag{2-1}$$

Where $F(RP)$ is the conditional probability that the component will be damaged to a given DS as a function of RP, RP is the response parameter at a given DS, Φ denotes the standard normal cumulative distribution function, θ denotes the median value of the probability distribution, and x denotes the logarithmic standard deviation. Both θ and x are established for each DS. In simple terms, median value θ represents the 50% probability of exceeding a given DS and can be calculated as:

$$\theta = \exp\left(\frac{1}{N}\sum_{i=1}^{N}\ln\left(RP\right)_i\right) \tag{2-2}$$

Where, N is the total number of specimens at a given DS. The logarithmic standard deviation of the response parameter at the given DS is calculated as follows:

$$x=\sqrt{\frac{1}{N-1}\sum_{i=1}^{N}\left(\ln\left(RP/\theta\right)\right)_i^2} \tag{2-3}$$

All the parameters were defined previously.

2.2.2. Development of Fragility Curves

Fragility functions were calculated for the DI associated with each DS. The procedure to develop fragility curves was as follows: the response parameters (DI) were sorted in an ascending order. The cumulative frequencies were calculated for the i^{th} DI as i/N, where i is the sequential position of the DI, and N is the total number of columns. Natural logarithm magnitudes of DI were calculated. The θ and x were calculated using Eq. 2-2 and 2-3. Substituting θ and x in Eq. 2-1, fragility curve was developed. Figure 2-3 shows the typical form of a fragility function when plotted using the lognormal cumulative distribution function.

The Smironov-Kolmogorov goodness-of-fit test (Massey et al. 1951) and graphical methods were used as acceptance criteria for lognormal distribution. To use the Kolmogorov goodness of fit test, it was assumed that the DI data is the representative of the population. This assumption was satisfied by conducting extensive analyses with a reasonable scatter in data to develop an approximately continuous distribution function for DI. In the Smironov-Kolmogorov test, the hypothesis that the data has lognormal distribution is accepted if all test data points in resistance and load model lie between the lower and upper confidence limits (LCL and UCL). These confidence limits can be calculated as follow:

$$LCL = F(RP) - d_{\alpha}(N) \tag{2-4}$$

$$UCL = F(RP) + d_{\alpha}(N) \tag{2-5}$$

Where $d_{\alpha}(N)$ is a parameter determined based on the level of significance (α) and the total number of the samples (N). Massey et al. (1951) tabulated the magnitudes of $d_{\alpha}(N)$ as a function of significance level and the total number of samples (Table 2-2). The critical values of $d_{\alpha}(N)$ (Table 2-2) represent the maximum absolute difference between the sample and population cumulative distribution. Table 2-2 can be used to determine the confidence intervals for cumulative distribution function $F(RP)$. Thus 100(1-α) represents the confidence limits for $F(RP)$. The level of confidence is the probability that the data points lie outside the limits. For example, significance level of 0.05 represents the confidence level of 95%, which means there is 5% probability that the data points lie outside the limits. In the present study, a significance level of 10% was selected based on Naeim et al. (2005) recommendation.

2.2.3. Application of Fragility Curves in Performance Based Design

Seismic fragility curves for highway bridges are conditional probability statements about the vulnerability of a bridge subjected to seismic loading. This vulnerability is typically expressed in terms of predefined DSs that have some physical meaning in terms of bridge functionality levels. The fragility curves are useful for performance-based design of bridge columns. In simple terminology, fragility curves are graphs that describe the probability of structure being damaged beyond a specific DS for various levels of ground shaking. These curves offer valuable insight to decision makers and bridge owners seeking to reduce the risk of damage to bridges. To develop any fragility curve, a response parameter needs to be selected.

In the present study, a PDCA method was developed for bridge columns that utilized fragility curves to define performance levels for a certain bridge category under a specified earthquake level. The performance levels were quantified in terms of DSs. To design columns, DSs were correlated with column response parameter (DI). The columns were designed for one or more target performance levels with stated probabilities. Given the performance level (DS) and its stated probability, a response parameter was selected from the fragility curves. For example, in the present study, the columns were designed for 50% probability of exceeding DS3, and the corresponding DI was 0.35 (Figure 2-2). To satisfy the given performance level, the response parameter was selected to be higher than the earthquake demand on the column. In order to provide flexibility to designers, different performance levels were assigned to distinct bridge categories and earthquake levels as discussed in the following section.

2.3 Design Performance Levels

Performance based design begins with the selection of design criteria stated in the form of one or more performance objectives. Each performance objective is a statement of the acceptable risk of being at specific level of damage at a specified level of seismic hazard. Current design codes (American Association of State Highway and Transportation Officials (AASHTO) (2010) and Caltrans SDC (2010) have adopted different approaches to achieve required performance objectives. AASHTO (2010) states that "bridges shall be designed to have a low probability of collapse but may suffer significant damage and disruption to service when subject to earthquake ground motions that have a seven percent probability of exceedance in 75 years. Partial or complete replacement may be required. Higher levels of performance may be used with the authorization of the Bridge Owner". AASHTO (2010) defines damage levels depending on the importance of the bridge, and earthquake return period. However, the performance objectives in the design codes are defined qualitatively in terms of design principles. Damage levels are not quantified in terms of response parameters of a bridge. In general, current design codes have the following shortcomings: (1) damage levels are defined qualitatively and not correlated to bridge response parameters; (2) they do not provide enough flexibility to designer/owner to select different performance levels under different earthquake return periods.

To address these shortcomings, a comprehensive design matrix was developed in the present study to correlate the performance objective with bridge category, earthquake return period, and bridge response parameter (DI) (Table 2-3). Both qualitative and quantitative performance levels are described in Table 2-3. An average DI from fragility curves was selected as a representative of the given DS. Based on discussion with the Caltrans engineers, different service levels to distinct DSs were assigned (column 2 and 3 of Table 2-3). Based on Table 2-3, at DS1 (DI=0), the bridge will remain fully operational after the earthquake with no repair needed, and the bridge will be open to both public and emergency vehicles. At DS2, the bridge will remain fully operational after the earthquake, repair is needed only at plastic hinges and DI is equal to 0.15. At DS3, the bridge is closed to public vehicles, limited service will be allowed to emergency vehicles, repair is needed perhaps for all columns, and DI is equal to 0.35. At DS4, the bridge is closed to public vehicle, limited service is allowed to emergency vehicles, repair is needed for the entire column, and DI is equal to 0.55. At DS5, the bridge is not usable after the earthquake, major repair is needed for entire column, and DI is equal to 0.8. At DS6, the bridge is not usable after the earthquake, major repair or reconstruction is needed, and DI is equal to one.

Four bridge categories defined by Caltrans (standard bridges, ordinary non-standard bridges, recovery bridges, and important bridges) were used to correlate with performance objectives. Even though only one of these were utilized in the present study (standard bridges), other categories were included for the sake of completeness. Different earthquake return periods ranging from 100 to 2500 years are tied with various performance objectives and bridge categories. It is to be noted that the design matrix presented in this study is somewhat subjective and can be modified based on the desired performance objectives.

2.4 Limit State Function and Probability of Failure

The term "failure" means different things to different people. Failure does not necessarily mean catastrophic failure but is used to indicate that the structure does not perform as intended. Before conducting reliability analysis, failure needs to be clearly defined. The concept of limit state is used to define failure in the context of structural reliability analysis. Limit state is a boundary between desired and undesired performance of a structure. The structural performance is usually expressed in terms of the mathematical equations and limit state functions involving various load and resistance parameters. Let L and R be the load and resistance parameters, respectively. Then, the structural failure corresponds to R being less than L. The corresponding limit state function, Z, is (Nowak and Collins 2000)

$$Z = R - L \tag{2-6}$$

$$P_f = P(Z < 0) \tag{2-7}$$

A negative value of Z indicates failure. The probability of failure, P_f, can be expressed by Eq. 2-7. In this study, parameters L and R were represented in terms of DI. Probability distribution functions of load, resistance, and safety margin are shown in Figure 2-4 (Nowak & Collins 2000).

2.5 Resistance Model

The proposed design approach in this study is based on apparent DS and its associated DI. DI is a measure of the lost plastic deformation capacity in the column at certain DS. Therefore, in this study, the DI is focused on for investigation. The resistance or capacity of the bridge column is determined based on material properties and dimensions. To model a resistance, fragility curves developed by Vosooghi and Saiidi (2012) correlating DSs with DIs were utilized (Figure 2-2). Column model database in their study consisted of 25 columns studied at the UNR and seven columns from the Pacific Earthquake Engineering Research Center (PEER) (PEER 2003). Out of these 24 models were tested on shake tables and the rest were tested under lateral quasi-static loading. The concrete strength ranged between 4 and 6 ksi (28 and 41 MPa), and the reinforcement yield stress was between 60 and 70 ksi (414 and 483 MPa). Single columns and columns of two-span and four-span bridge model were included in the database. Columns used in their study were designed based on recent or current seismic design provisions. All columns were placed in a single category to obtain the database. To account for the effect of data scatter, a probabilistic approach was used to correlate the DSs and DIs. To characterize the probabilistic nature of the problem, fragility curves were developed for five damage states, DS1 to DS5 (Figure 2-2). DS6 corresponds to failure with DI equal to one. Consequently, no scatter in the data was accounted for DS6. In reliability analysis, mean and standard deviation of DS6 for resistance model were assumed to be one and zero, respectively.

2.6 Load Model

The load component used in this study was the demand DI for the column imposed by different earthquake ground motions. The load component was determined by modeling a large number of single column and multicolumn bents, and analyzing them under 25 near field and far field ground motions. One of the most challenging aspects of the modeling was to incorporate uncertainties in the load model. To incorporate uncertainties in the load model the following parameters were used:

2.6.1. Site Class

Bridge site class was divided into two categories; site class B/C and site class D. In various codes (AASHTO (2010), Caltrans SDC (2010), and American Society of Civil Engineers (ASCE 7-10)) these site classes are defined based on soil type and shear wave velocity (V_{S30}). According to the definition given in these codes, site classes B, C, and D corresponds to rock, soft rock, and stiff soil, respectively. Because site B and C both represents rock, they were lumped together into one site class as B/C. USGS de-aggregation beta website (USGS 2008 Interactive Deaggregations Beta) was utilized to determine design spectrum for these site classes. To determine the design spectrum, a shear wave velocity (V_{S30}) of 760 m/s [2500 ft/s] and 270 m/s [886 ft/s] was used for site B/C and site D, respectively. The shear wave velocities used were based on the code recommendations (Caltrans ARS Online V2.3.06 and Caltrans SDC 2010). The V_{S30} of 760 m/s [2500 ft/s] represents the median of V_{S30} of site class B and C, whereas, 270 m/s [886 ft/s] represents the average V_{S30} of site class D (Table 2-4).

2.6.2. Ground Motion Selection

Ground motion records were initially selected from PEER strong ground motion database (http://peer.berkeley.edu/peer_ground_motion_database/), but were subsequently scaled to match the design spectral acceleration of the bent at one second. The scale factor was limited to 3 because it was felt that higher factors would lead to records that do not represent strong earthquakes despite their high scaled acceleration. To account for the uncertainties in ground motions, various site parameters were assumed. Parameters used in the selection of far-field and near-field ground motions were: VS30, earthquake magnitude, distance to the fault (Rjb), and scaling factors (SF). The range of VS30 between 500 to 1500 m/s [1640 to 4821 ft/s] and 200 to 360 m/s [656 to 1181 ft/s] was used to select ground motions for site class B/C and D, respectively. All the ground motions were selected for earthquake magnitude greater than six. Rjb between 0 to 15 km [0 to 1500 m] and 15 to 30 km [1500 to 3000 m] was selected for near-field and far-field ground motions, respectively. Based on these parameters, 15 near-field and 10 far-field ground motions were selected for each site class. The number of near field motions was higher because this type of motion is generally more demanding.

2.6.3. Bents Properties

The expected material properties as specified in SDC Caltrans (2010) were used to design bents. Grade 60 steel was used for longitudinal and spiral reinforcement. The expected concrete compressive strength and steel yield strength were used as 5 ksi [34.47 MPa] and 68 ksi [468.84 MPa], respectively. No uncertainty was considered in the concrete compressive and steel yield strength. To capture the effect of column diameter, three different diameters of four, five, and six feet [1219, 1524, and 1829 mm] were used in the analyses. The longitudinal steel ratio in the columns was 1%, 2%, and 3%. To account for the effect of column aspect ratio, two different column heights of 30 feet [9144 mm] and 60 feet [18288 mm] were used in the study. To account for the variability in bent support conditions, cantilever, fixed-pinned and fixed-fixed connections were used. To study the effect of redundancy on reliability, single column bent (SCB), two columns bents (TCB), and four columns bents (FCB) were used in the analyses and axial load index of 10% was used in all columns. The axial load index is defined as the compressive axial force divided by the product of the cross section area of the column and the specified concrete compressive strength.

2.6.4. Earthquake Return Period

The return period is generally defined as the average number of trials (usually years) to the first occurrence of an event of magnitude greater than a predefined critical event (Benjamin and Cornell 1970). If the events are independent and the exceedance probability (P) of the critical event at any trial remains constant, the return period T can be computed as $T = 1/P$. The return period is usually used for risk analysis. Risk analysis assumes that the probability of the event occurring does not vary over time and is independent of past events. Since earthquakes are random events, an uncertainty concerning earthquake occurrence always exists, and a structure located in a seismically active region will be exposed to some earthquake loads during its lifetime. Therefore, an appropriate description of the seismic hazard needs to be incorporated for valid estimation of structural reliability. In this context, reliability refers to the probability that the structure will resist any seismic loads result from a given earthquake level. In the present study, the reliability of bents was investigated under the earthquakes with return period of 1000, 1500, and 2500-year.

2.7 Reliability Analysis

Society expects bridges to be designed with a reasonable safety level. In practice, this expectation is achieved by implementing current design code requirements specifying design values for strength, displacement, and so on. Over the past few years, design code requirements have advanced to include design criteria that take into account some of the sources of uncertainty in seismic design of bridge component (AASHTO 2010). Such criteria are often referred to as reliability-based design criteria. The reliability of a component is defined as the probability that the component would perform according to a specified performance criterion for at least a specified period under specified conditions (Ayyub and McCuen 2003). Reliability is often expressed as the probability that a structure will not fail to perform its intended function.

In order to determine the probability of failure, first order second moment method (FOSM) (Ayyub and McCuen 2003) was used in the reliability analysis. First order implies that this method considers only linear limit state function, while second moment refers to the fact that, the first two moments of a random variable, the mean value and the standard deviation, are considered. This method measures the structural performance in terms of the reliability or probability of failure. The mean and standard deviation of Z in Eq. 2-6 are estimated using the information on means and standard deviation of the basic random variables. In the present study, the random variable was DI.

The reliability of bents was quantified by "reliability index" (β). The β is often used as a measure of structural safety. Graphically, reliability index (also known as safety index) is the distance of the mean of limit state function from failure surface measured in terms of standard deviations. The graphical representation of β (Cornell 1969) is shown in Figure 2-5. In the present study, reliability analysis was conducted to calibrate design DI for bridge columns to obtain a target β against failure. The objective of the analysis was the assurance of some level of safety. Load and resistance were treated as random variables. As discussed before, there was significant scatter in the seismic response and demand of bents, therefore, the reliability of bents needs to be determined. The β was calculated as follows for lognormal distributions (Ayyub and McCuen 2003):

$$\beta = \frac{\ln\left(\frac{\mu_R}{\mu_L}\sqrt{\frac{\delta_L^2+1}{\delta_R^2+1}}\right)}{\sqrt{\ln\left[\left(\delta_R^2+1\right)\left(\delta_L^2+1\right)\right]}} \tag{2-8}$$

Where L=load, R=resistance, μ=mean, σ=standard deviation, and δ=coefficient of variation (σ/μ). The statistical parameters associated with fragility curves for seismic response (Figure 2-2) were used for resistance parameters and those obtained from non-linear dynamic analyses were used for loading parameters. The reliability index calculated by Eq. 2-8 was modified to include the probability of occurrence of design earthquake during the lifetime of a bridge.

The probability of column failure is related to the return period and exceedance probability of the design earthquake. Therefore, it is important to determine the probability of column failure by incorporating the probability of earthquake exceedance during the lifetime of a structure. Considering that annual earthquake events are independent, the probability of earthquake exceedance during lifetime of a structure can be calculated using Eq.2-9 (Yen 1970):

$$P_{EQ} = 1 - \left(1 - \frac{1}{T}\right)^t \tag{2-9}$$

Where, P_{EQ}, t and T are the probability of earthquake exceedance during the life-time of a structure, life time of a structure and return period, respectively. The probability of column failure (P_{CF}) and at the same time to have an earthquake occurrence can be calculated using conditional probability as:

$$P_{CF} \cap P_{EQ} = (P_{CF}|P_{EQ}) \times (P_{EQ}) \tag{2-10}$$

$$P_{CF}|P_{EQ} = 1\ )\ \beta(\Phi \quad \text{or} \quad P_{CF} \cap P_{EQ} = 1'\ \beta)'\ \beta(\Phi - \tag{2-11}$$

$$\left(\Phi = 1 - P_{CF} \cap P_{EQ}\right) \tag{2-12}$$

$P_{CF}|P_{EQ}$ is the probability of column failure given the design earthquake has occurred, Φ is the normal standard distribution function, and $'\beta$ is the reliability index corresponds to combined probability of failure. Having β calculated from Eq. 2-8, $P_{CF}|P_{EQ}$ was calculated using Eq. 2-11 (Ayyub and McCuen 2003). By substituting P_{EQ} and $P_{CF}|P_{EQ}$ in Eq. 2-10, $P_{CF} \cap P_{EQ}$ was determined. Having $P_{CF} \cap P_{EQ}$, β' was calculated from Eq.2-12. The level of reliability at DS3, DS4, and DS5 was also investigated.

2.8 Calibration of Design Damage Index

A reliability analysis was conducted to calibrate design DI to obtain a specified β against failure. In general, calibration process in reliability analysis is iterative, until the desired reliability level is achieved. To overcome this iterative process, a new direct PDCA was developed to calibrate design. Calibration of design DI using direct PDCA consists of the following steps:

Step 1. Development of load and resistance model: The load and resistance models were treated as continuous random variables. Their scatter was described by cumulative distribution functions (CDF) (Section 2.6 and 2.7). The CDF's for load and resistance models were derived using the available statistical database.

Step 2. Reliability analysis: Structural performance was measured in terms of the probability of failure. After having cumulative distributions of load and resistance models, combined reliability index was calculated using Eqs. 2-8 to 2-12.

Step 3. Selection of target reliability index: After achieving a methodology and database to calculate β, the next step was the selection of target β_6' for the design DI calibration. Selection of a target β_6' was based on the margin of safety implied in current design codes. Typically, reliability values in the range of 2.0 to 4.0 are used in formulating AASHTO LRFD design criteria. AASHTO LRFD recommends a reliability of 3.5 for bridges under gravity loading while not accounting for the effect of earthquake loading. Earthquake loading is uncertain and not always present on the structure; therefore, in this study a target β_6' of 3 against failure was selected for columns under seismic loading. In general, selection of a β_6' is somewhat subjective. Ideally, the selection of the target β_6' is based on economic issue that reflects both the cost of increasing the safety margins and the implied costs associated with component failure.

Step 4. Direct PDCA and calibration of DI: In step 1, design DI was tentatively specified as 0.35. Using steps 1 and 2, β was calculated against failure. To achieve the target β_6' as described in step 3, one approach is to perform iterations by selecting different design DI and repeating the entire process from step 1 and 2 until the desired reliability level is achieved. This approach is time consuming and not practical. A second approach is to fix the reliability index and calculate the design DI associated with it. Using the second approach, direct PDCA was developed in this study for DI calibration. Design DI could be precisely determined based on a target β_6'. The development and evaluation of direct PDCA is discussed in detail in Chapter 5.

Chapter 3. Expansion of Column Database

3.1 Introduction

The database used to develop fragility curves in the study conducted by Vosooghi and Saiidi (2012), was expanded with addition of six columns. The three two-column bents of a large-scale 4-span bridge that had been tested on the three shake tables at the University of Nevada Reno (UNR) (Saiidi et al. 2013) were used in this part of the study. The objectives of their study was to investigate the response, performance, and interaction of components of a quarter-scale four-span bridge system to increasing levels of seismic excitation until failure. The columns were subjected to varying degree of damage. Their project scope included the biaxial (no vertical excitation) testing of a highway bridge that utilizes a continuous superstructure supported on drop cap piers. After each run of shake table tests, the columns were investigated for damage. In this Chapter, the six response parameters defined in a previous study at UNR (Vosooghi and Saiidi 2012) were calculated for each column. Bridge properties, configuration, and calculation of response parameters (RPs) are discussed in the following sections.

3.2 Four Span Bridge Model

Saiidi et al. (2013) tested a quarter-scale four-span conventional bridge model on three shake tables at the UNR. Figure 3-1 shows the plan and elevation view of the bridge. The prototype was scaled into an equivalent quarter-scale model for shake table testing. The superstructure was composed of a solid slab that was post-tensioned in both the longitudinal and transverse direction. The model also included abutment seats at both ends of the bridge that were driven in the longitudinal direction by hydraulic actuators to incorporate the abutment interaction with the bridge system. The interior two spans were 348 inch [8839 mm] and the exterior two spans were 294.25 inch [7474 mm] for a total length of approximately 1320 inch [33528 mm]. The clear height of the bents were 60, 72 and 84 inch [1524, 1829, and 2134 mm], with the tallest bent in the middle. The bridge consisted of three, two-column bents. The columns were of same diameter and height. However, the height of each bent varies making the bridge asymmetric relative to the transverse axis passing through the center to include the effect of in plane torsion. Figure 3-2 shows the bent configuration.

The columns met the current seismic design and detailing requirement. The compressive concrete strength used was 5.7 ksi [39.3 MPa] and the reinforcement yield stress was 59 ksi [406.8 MPa]. The longitudinal bar of size #3 and spiral of size W 2.9 wire was used in the columns. Bent 1 was the shortest and stiffest as compared to the Bent 2 and 3.

3.3 Loading Protocol

The motion selected for bridge excitation was a modified version of the Century City station recording of the 1994 Northridge, California earthquake. The earthquake motion used in the experimental testing consisted primarily of biaxial motions. This motion was applied in multiple runs, with gradually increasing amplitudes that caused increasing damage in columns. Table 3-1 lists the complete test schedule for the 4-span bridge testing.

3.4 Observed Performance

The columns were flexure dominated. At the end of each earthquake run, the visual evidence of damages was investigated to determine the DS. The definition of apparent DS was discussed previously in Chapter 1 (Vosooghi and Saiidi 2012). The DSs in columns varied from DS1 to DS6.

3.4.1. Bent 1 Observations

Bent 1, being the shortest of the bents, attracted a relatively large portion of lateral forces. The plastic hinges in bent 1 exhibited flexural cracks at the end of Test 1D. By the end of Test 3, minor concrete spalling was observed on all faces of the bottom hinge of the East column. Whereas in the West column concrete cover spalling was observed after Test 4C. Extensive concrete spalling occurred in the bottom hinge of East column by the end of Test 4D. By the end of Test 5, spirals were visible in the lower hinge of the East column. By the end of Test 6, start of core damage occurred in the bottom hinge of East column; whereas, in the West column start of core damage began by the end of Test 7. Finally, by the end of Test 7 all longitudinal bars were visible, 5 of which fractured in the East column while numerous others buckled in both columns. Figures 3-3 to 3-6 show the damage in the East and West column of Bent 1. The description of damage after each run is presented in Tables 3-2 to 3-5.

3.4.2. Bent 2 Observations

Bent 2 was the tallest and most flexible of the bents, and therefore, the amount of damage was relatively small due to the small share of shear it carried. Virtually no cracking was observed until Test 1D. Small amount of flexural cracking occurred by the end of Test 3 in the bottom and top hinges of East and West columns; whereas, in the West column, flexural cracking occurred by the end of Test 2. The extensive spalling of cover concrete occurred by the end of Test 5 in the bottom hinge of East column while minor spalling occurred in the West column. By the end of Test 6, few spirals were visible in the East column while the West column underwent extensive spalling in the bottom hinge. Few spirals were visible in the West column by the end of Test 7. Figures 3-7 to 3-10 show the damage in the East and West column of Bent 2. The description of damage after each run is presented in Tables 3-6 to 3-9.

3.4.3. Bent 3 Observations

Bent 3 was the intermediate height bent. Flexural cracks were visible after Test 3 in the bottom hinge of East and West columns. By the end of Test 4D, East column exhibited minor spalling in the top and bottom hinge; whereas, West column bottom hinge exhibited extensive spalling in the concrete with visible spirals. In the East column, extensive spalling and visible spirals were observed by the end of Test 5 and 7, respectively. The West column exhibited imminent concrete core failure with visible longitudinal reinforcement by the end of Test 6. Figures 3-11 to 3-14 show the damage in the hinges of East and West column of Bent 3. The description of damage after each run is presented in Tables 3-10 to 3-13.

3.5 Measured Force-Displacement Relationship

The bridge was subjected to uniaxial and biaxial motions. The target peak ground acceleration (PGA) applied in the transverse direction was different from the PGA in the longitudinal direction in each run. Because biaxial motions were applied, force-displacement envelopes were determined using peak resultant lateral force and the corresponding resultant displacements. Figures 3-15 to 3-20 show the measured force-displacement envelopes and idealizations for all the bents. The envelopes were idealized by setting the elastic branch to pass through the first yield point and adjusting the plastic portion so that the areas above and below the idealized curve is balanced with the envelope in each bent. The first yield point was assumed to be at one-half of the peak force because the actual first yield point varied even within the plastic hinges of each bent and for different loading directions. Utilizing the idealized force-displacement curves, DS in each column was correlated with the corresponding peak displacements. Figures 3-21 to 3-26 show the maximum displacement corresponding to a given DS of Bent 1, 2 and 3 columns.

3.6 Response Parameters

The six response parameters defined in a previous study (Vosooghi and Saiidi 2012) were used as indicators of seismic performance. Even though only one of these were utilized in the present study (DI), the data are included for the sake of completeness. The RPs were: the maximum drift ratio (MDR), residual drift ratio (RDR), frequency ratio (FR), damage index (DI), the maximum longitudinal steel strain (MLS), and the maximum transverse steel strain (MTS). Tables 3-14 to 3-19 show the calculated RPs for all the columns.

3.7 Updated Fragility Curves

The RPs calculated in this study were combined with those calculated in a previous study of Vosooghi and Saiidi (2012) to expand the database. The fragility curves calculated in their study were updated to reflect this expansion (Figure 3-27). Cumulative lognormal distribution function was used to calculate these fragility curves. Because the fragility function is a logarithmic function, it cannot be calculated for negative RPs. As a result, instead of lognormal distribution function, a normal distribution function was used to calculate the fragility curve for DIs at DS1 in Figure 3-27. The corresponding fragility functions were calculated as:

$$F(DI)_1 = \Phi\left(\frac{DI_1 - \mu}{\sigma}\right) \tag{3-1}$$

where DI_1 is for DS1; and μ and σ are the mean and standard deviation of DI_1, respectively. The μ and σ of DI_1 were calculated as 0.016 and 0.072, respectively. For each of the other DIs and RPs, Table 3-20 lists the median and logarithmic standard deviation. Depending on data scatter, the median of each RP should be consistent with the value read from the respective fragility curve with a 50% probability of occurrence. For example, the median of the DI at DS3 is 0.36 (Table 3-20) and the corresponding value read from the fragility curves is 0.36.

Chapter 4. Seismic Demand Analysis and Development of Load Model

4.1 Introduction

The structural analysis program SAP 2000 version 15.0.1 (Computer and Structures, Inc. 2011) and Xtract (Chadwell 2007) were used in the analytical studies. The bent models that were used to develop load model for the reliability analysis are described in this chapter. Single column, two-column, and four-column bents (SCB, TCB, and FCB) were studied. To design SCBs, curvature capacity and strains required for bond slip calculations were determined using Xtract for moment-curvature analysis. Due to the variation in the axial load of columns in TCB and FCB under cyclic loading, it was not practical to use the same design procedure as was used for SCB. Therefore, SAP 2000 was used to obtain the pushover curves for multi-column bents. The pushover curve was idealized with an elasto-plastic relationship to estimate the plastic shear force and the effective yield displacement (Caltrans SDC 2010).

Followed by bent design, non-linear dynamic analyses were conducted using SAP 2000. To account for uncertainties in the load model, the effect of longitudinal steel ratio, site class, return period, aspect ratio, and number of columns per bent was included in the study. The bents were analyzed under a large number of near-field and far-field ground motions of different intensities. For each ground motion, the maximum displacement was determined and subsequently, DI_L was calculated. Where DI_L is the damage index corresponds to load model. To analyze the scatter in DI_{LS}, statistical analyses were conducted. Finally, the log-normal fragility curves were developed for DIs for each bent. These fragility curves served as a load model in the reliability analysis.

4.2 Ground Motions Selection

Un-scaled ground motions (GMs) were selected from the PEER strong ground motion database (http://peer.berkeley.edu/peer_ground_motion_database/). Out of three ground motion components in each record set, two horizontal and one vertical, the horizontal motion with high spectral acceleration at period of one second was selected. Parameters that were used in the selection of far-field and near-field GMs were: shear wave velocity (V_{S30}), earthquake magnitude, distance to fault (R_{jb}), and scale factor (SF). The range of V_{S30} between 500 m/s [1640 ft/s] to 1500 m/s [4921 ft/s] and 200 m/s [656 ft/s]to 360 m/s [1181 ft/s] was used to select GMs for site class B/C and D, respectively. The GMs with magnitude greater than six were used. The R_{jb} distance between 0 to 15 km and 15 to 30 km was used to distinguish near-field and far-field ground motions. The GMs were selected so that the SF calculated based on spectral acceleration associated with period of one second ($(S_a)_{1\ sec}$) is not greater than 3. This is because it was felt that records amplified by larger scale factors would not necessarily have the characteristics of strong earthquakes. The limitation of SF of 3 was based on the design spectrum of 1000-year return period earthquake. Then, the same GMs were used to analyze the bents under 2500-year earthquake.

Based on the above parameters, 15 near field and 10 far-field GMs were selected for each site class (Site B/C and Site D). Tables 4-1 and 4-2 list the GMs selected for site class B/C and D respectively. In these tables, NGA is the new generation attenuation number and PGA is the peak ground acceleration. The other parameters are defined previously. Every GM presented in PEER database has its unique new generation attenuation number (NGA). The GMs response spectrums are presented in Figures 4-1 to 4-4.

4.3 Design Spectra

The United States Geological Survey (USGS 2008) Interactive Deaggregations Beta tool (https://geohazards.usgs.gov/deaggint/2008/) was utilized to calculate the design spectrum for site class B/C and D. This tool provides spectral acceleration (S_a) for the following spectral periods anywhere in the conterminous U.S: 0.0 s (PGA), 0.1 s, 0.2 s, 0.3 s, 0.5 s, 1.0 s, 2.0 s, 3 s, 4 s, and 5 s. The calculation of design spectrum requires 10 separate deaggregation calculations, one for each period. For example, Figure 4-5 shows the design spectrum calculation for the spectral period of 1 sec for site B/C. This Figure shows that, for period of one second, the spectral acceleration is 0.6733 g. The USGS Interactive Deaggregations tool has an option to develop a design spectrum for various site classes and earthquake return periods.

To determine design spectrum, V_{S30} of 760 m/s [2500 ft/s] and 270 m/s [886 ft/s] were used for site B/C and site D, respectively. The design spectra were calculated for a site in Los Angeles with latitude 34.05 and longitude -118.25 degree (Figure 4-6). All the design spectra were calculated for 5% damping. Given the site parameters (latitude and longitude), spectral period, and V_{S30}, design spectra were calculated for 1000, 1500, and 2500-year return period earthquake (Figures 4-7 and 4-8). Table 4-3 lists the structural period, S_a, and return period for site class B/C and D.

4.4 Bent Design

The Caltrans SDC version 1.6 (Caltrans 2010) was used to design the bents. The Xtract software, SAP 2000, and design spectrum were used to design the columns. Within each multicolumn bent, all the columns were designed identically. Circular cross section was selected because of its widespread use. Each bent was designed for a tentative design DI of 0.35 under an earthquake with a 1000-year return period. The DI of 0.35 corresponds to a 50% probability of exceedance of DS3. The DI was calculated using elasto-plastic pushover curve based on SDC 3.1 (Caltrans 2010). Seismic displacement demands were determined based on the rule of "equal displacement" and the effective stiffness of the column bents. Each bent was designed for two site classes: site class B/C and site class D. To investigate the effect of different design performance levels on the reliability, SCBs were also designed for DI of 0.35 under 1500-year earthquake.

The shear design was conducted based on SDC 3.6 (Caltrans 2010). The bents with double-curvature and high longitudinal steel ratio, reached a DI smaller than 0.35, even with zero confinement, because they nearly remained elastic under the design earthquake. Therefore, these columns were not included in the present study. A similar trend was observed in some of the tall columns because of their relatively low stiffness. In cases where the bents reached DI of 0.35, but shear rather than confinement controlled the design, the columns were redesigned for shear. Because of the extra transverse steel, the actual DIs were less than 0.35 in the columns that were controlled by shear.

4.4.1. Material and Section Properties

To account for uncertainties in the bent properties, a large number of bents were designed with different longitudinal steel ratios, heights, column diameter, and support conditions. A practical range was used for each parameter to represent actual bridge construction. A specified and expected concrete compressive strength of 3.6 and 5 ksi were used. Grade 60 steel with expected yield strength of 68 ksi was assumed for column longitudinal reinforcement. For each bent, the transverse steel was designed to provide sufficient confinement pressure to meet the target DI of 0.35. The axial load index of 10% was specified for all the columns. The minimum and maximum area of the longitudinal reinforcement for compression members are specified in Caltrans SDC 3.7 (2010) at $0.01A_g$ and $0.04A_g$, respectively. Therefore, the ratio of the column longitudinal bars was assumed at 0.01, 0.02, and 0.03. Table 4-4 lists the longitudinal steel ratio and reinforcement provided for different column diameters.

The Mander et al. (1988) constitutive stress-strain model was used for confined core concrete and unconfined cover concrete. The typical curves for unconfined and confined concrete are shown in Figure 4-9. In this Figure, $f_c^{'}$ is the compression strength of unconfined concrete, $f_{cc}^{'}$ is the compression strength of confined concrete, $f_{cu}^{'}$ is the maximum stress at failure of core concrete, ε_{cc} is the maximum strain at $f_{cc}^{'}$, ε_{cu} ultimate compression strain at $f_{cu}^{'}$, ε_{sp} is the spalling strain, and ε_{co} is the strain at $f_c^{'}$. The reduced ultimate strain capacity for reinforcing steel was used per SDC 3.2.3 (Caltrans 2010) (Figure 4-10). It is Caltrans practice to reduce the ultimate strain by up to thirty-three percent to decrease the probability of fracture of the reinforcement. In Figure 4-10, ε_{ye} is the yield strain, ε_{sh} is the strain at strain hardening, ε_{su}^{R} is the reduced ultimate tensile steel strain, and ε_{su} is the ultimate tensile stain in steel.

4.4.2. Moment Curvature Analysis

Moment-curvature analysis was conducted to design the SCBs and calculate the strains required for bond slip calculations using Xtract (Chadwell 2007) based on SDC 3.3.1 (Caltrans 2010). The expected material properties for steel and concrete were used in the analyses. The moment-curvature curve was idealized by an elasto-plastic relationship to estimate the plastic moment capacity and the effective yield curvature. The elastic portion of the idealized curve passes through the point marking the first longitudinal reinforcing bar yield. The idealized plastic moment capacity was obtained by balancing the areas between the calculated and the idealized curves beyond the first reinforcing bar yield point. The effective yield and ultimate curvatures were used to estimate the effective yield and ultimate displacement of the bents using SDC 3.1.3 (Caltrans 2010).

4.4.3. Bond Slip Effect

Because the plastic hinge length (L_P) calculated for columns was based on the Paulay and Priestley (1992) (Eq. 4-1), the effect of bond slip is implicit in the plastic deformations. Therefore, in the present study, the bond slip calculations were only performed for the linear part of the elasto-plastic pushover curve.

$$L_P = 0.08L + 0.15 d_b f_{ye} \geq 0.3 d_b f_{ye} \tag{4-1}$$

Bond slip rotation is a result of yield penetration of the longitudinal bars into the footing. The bond slip effect was modeled using a lumped linear moment-rotation spring at the bottom of the column. Wehbe et al. (1999) developed a method to calculate the bond slip rotations associated with cracking, yielding, and ultimate capacity of reinforced concrete columns. The bond-slip rotation is assumed to occur about the neutral axis of the column cross section at the connection interface. The neutral axis location, and the strain and stress in the extreme tensile steel at a given lateral load are determined from moment-curvature analysis of the section. The basic bond strength of tension bars can be found using the following equations:

$$u = \frac{9.5\sqrt{f_c'}}{d_b} \leq 800 \qquad \textit{(psi)} \tag{4-2}$$

Where, u is the constant bond stress and d_b is the bar diameter. Assuming a constant bond stress distribution along the embedded bar length, the development length can be calculated from equilibrium of forces as follows:

$$l_d = \frac{f_s d_b}{4u} \tag{4-3}$$

Where, l_d is the development length, f_s is the bar stress at the interface, and d_b is the bar diameter. The bar extension can be calculated by integrating the strain profile along the development length as follows:

$$\delta l = \int_0^{l_d} \varepsilon_s dz \tag{4-4}$$

Where, δl is the bar extension at the interface, ε_s is the bar strain at the depth of z from the interface, and l_d is the development length. The bond-slip rotation can be calculated as follows:

$$\theta_b = \frac{\delta l}{d - c} \tag{4-5}$$

Where, θ_b is the bond-slip rotation, d is the effective depth of the column section, and c is the compression depth of the column section at the interface.

In the present study, it was found that, the effect of inclusion of bond slip on DI was negligible in many cases. Because the calculation of DI is relative, the increase in yield displacement due to bond slip was compensated by the increase in displacement demand and ultimate displacement. Although the effect of bond slip was negligible on the DI, it was still included in the bents design for practical reasons.

4.4.4. Transverse Steel Design

The spirals were designed for the target DI of 0.35 while ensuring that the column shear strength is sufficient. The requirements for the maximum spacing for spiral in SDC 8.2.5 (Caltrans 2010) were satisfied. The maximum pitch in the plastic hinge zone shall not exceed the smallest of the following:

One fifth of the column diameter
Six times the nominal diameter of the longitudinal bars
8 inches [200 mm]

4.4.5. Seismic Shear Design

The shear design was conducted based on SDC 3.6 (Caltrans 2010). The seismic shear demand was calculated based on the overstrength shear, V_o, associated with the overstrength moment, M_o, defined in SDC 4.3 (Caltrans 2010). The overstrength moment is 1.2 times the idealized plastic moment capacity, M_P, to account for (1) material strength variations and strain rate effects, and (2) actual column moment capacity being greater than M_P.

According to SDC 3.2.1 (Caltrans 2010), the seismic shear capacity was conservatively calculated using the specified material properties instead of expected values. The columns were designed so that the shear demand to capacity ratio (D/C) was less than one. This ratio is calculated as follow:

$$D/C = \frac{V_o}{\phi(V_c + V_s)} \tag{4-6}$$

where V_S is nominal shear strength provided by spirals, V_C is nominal shear strength provided by concrete, and ϕ is the strength reduction factor for shear with a value of 0.9. Other parameters were defined previously.

4.4.6. Pushover Analysis

SAP 2000 was used to design the two-column and four-column bents (TCBs and FCBs). In case of single column bents (SCBs), elasto-plastic pushover curve was derived from the moment curvature analysis by utilizing Xtract. Unlike SCBs, under lateral loading, the axial load varies among the columns of multicolumn bents. To account for the variation in the axial load, multicolumn bents were modeled in SAP 2000, and pushover analyses were conducted. To account for bond slip in the columns, frame partial fixity springs were modeled at the supports. The spring rotational stiffness was determined based on the initial yield moment and bond slip rotation. It is to be noted that, the bond slip calculations were performed only for the pre-yielding portion of the pushover curve. In the post yielding, bond slip effect was already included in the calculated plastic hinge length. In SAP 2000, Fiber P-M2-M3 hinge element was used to model plastic hinges. To calculate the DI, the effective yield displacement (Δ_Y), the ultimate displacement (Δ_C), and the displacement demand (Δ_D) were calculated for each bent.

Given the structural period, the seismic demand force was calculated utilizing design spectrum. Based on the linear dynamic analysis method, having seismic force and bent stiffness, the Δ_D was calculated.

To find the effective yield displacement, pushover envelopes were idealized by elasto-plastic curves. Each envelope was idealized by setting the initial slope to pass through the point marking the first longitudinal tensile reinforcing bar yield in any of the column. The idealized force-displacement was obtained by balancing the area between the actual and the idealized force-displacement curves beyond the first reinforcing bar yield point (Caltrans 2010). Figure 4-11 shows the typical idealized force displacement curve.

4.5 Bent Models Description

All the bents designed in the present study were assumed to be in the standard bridge category as defined by SDC 1.1 (Caltrans 2010). To account for the effect of redundancy on the reliability analysis, three bent configurations (SCBs, TCBs, and FCBs) were used. The bents were designed for different support conditions (cantilever in SCBs, fixed-fixed, fixed-pinned). The columns within each multicolumn bent were designed identically. In the multicolumn bents, a massless bent cap with rectangular cross section was assumed. The minimum bent cap width provided was equal to the column diameter plus two feet (600 mm) (Caltrans 2010). The bent cap was modeled as a rigid element with a rigid zone factor of 0.5.

4.5.1. Single Column Bents

Two sizes of column diameter, 4 ft [1219 mm] and 6 ft [1905 mm] were assumed in SCBs. For each diameter, two different column heights of 30 ft [9.14 m] and 60 ft [18.28 m] were assumed corresponding to aspect ratios of five to 15. Figure 4-12 shows the SCBs configurations. By utilizing SDC 3.1.3 (Caltrans 2010), the columns were designed based on their rotation capacity determined from curvature capacity obtained from moment curvature analyses. Some of the bents reached a DI smaller than 0.35 even with no confinement because they nearly remained elastic under the design earthquake. These bents were not included in the reliability analysis presented in this study. The general procedure used to design the bents for the target DI consisted of two steps: (1) calculations for Δ_Y, and Δ_C, and (2) calculations for Δ_D. The procedure was as follow:

Step 1. Calculations of Δ_Y and Δ_C: Based on Caltrans SDC 3.1.3 (2010), Δ_Y and the Δ_C were calculated for the columns using Eqs. 4-7a to 4-7e.

$$\Delta_C = \Delta_Y + \Delta_p \tag{4-7a}$$

$$\Delta_Y = \frac{L^2}{3} \times \phi_Y \tag{4-7b}$$

$$\Delta_P = \theta_p \times \left(L - \frac{L_p}{2} \right) \tag{4-7c}$$

$$\theta_p = L_p \times \phi_p \tag{4-7d}$$

$$\phi_p = \phi_u - \phi_Y \tag{4-7e}$$

where:
L = Distance from the point of maximum moment to the point of contra-flexure (in)
L_P = Equivalent analytical plastic hinge length (in)
Δp = Plastic deformation capacity due to rotation of the plastic hinge (in)
Δ_Y = Effective yield displacement of the column (in)
ϕ_Y = Idealized yield curvature defined by an elastio-plastic representation of the moment-curvature curve (rad/in)
ϕ_p = Idealized plastic curvature capacity (assumed constant over Lp) (rad/in)
ϕ_u = Curvature capacity at the failure, defined as the concrete strain reaching ε_{cu} or the longitudinal reinforcing steel reaching the reduced ultimate strain ε_{su}^R (rad/in)
θ_p = Plastic rotation capacity (radian)

Step 2. Calculations for Δ_D: The Δ_D was calculated based on the linear dynamic analysis utilizing the design spectrum using Eqs. 4-8a to 4-8e.

$$k_i = \frac{V_o}{\Delta_Y} \tag{4-8a}$$

$$F = \frac{1.2M_p}{L} \tag{4-8b}$$

$$T = 2\pi\sqrt{\frac{W}{gk_i}} \tag{4-8c}$$

$$F_D = ma = \frac{W}{g} \times a \tag{4-8d}$$

$$\Delta_D = \frac{F_D}{k_i} \tag{4-8e}$$

where:
k_i = initial slope of the column (kip/in)
V_o = shear force (kips)
M_p = plastic moment capacity (kip-in)

T = fundamental period of the structure
W = weight corresponds to ALI of 10% (kips)
F_D = seismic force demand (kips)
m = W/g = mass acting on the column
a = spectral acceleration corresponds to *T* (g)

By having Δ_Y, Δ_C, and Δ_D, the DI was calculated from Eq. 1-1. Table 4-5 lists the SCB models with different longitudinal steel ratios, height to depth ratios (H/D), site classes, and boundary conditions designed for an earthquake with a 1000-year return period. In site class B/C, the columns with higher aspect ratio (H/D = 10) remained elastic under the design earthquake due to their low stiffness. Consequently, the DI in these columns was smaller than 0.35, even with zero confinement. Therefore, these columns were not included in the present study. Table 4-6 lists the SCBs designed for 1500-year return period. The transverse steel in the columns shown in italic in these tables was controlled by shear, and therefore could not reach the target DI=0.35.

4.5.2. Two Column Bents

Two different column diameters of 5 ft [1524 mm] and 6 ft [1829 mm] were assumed in TCBs. For each diameter, two different column heights of 30 ft [9144 mm] and 60 ft [1828 mm] were used. Because in SCBs it was found that, only one bent was able to reach DI of 0.35 with site class of B/C, the TCBs were only designed for site class D. Figure 4-13 shows a typical TCB configuration used in the analyses. All TCBs were designed for a target DI of 0.35. To determine the DI, pushover curves were idealized by elasto-plastic curves. In cases where shear controlled the transverse steel, the bents were redesigned for shear. Like SCBs, Δ_D was calculated using Eqs. 4-8a to 4-8e. Table 4-7 lists the TCB models used in the analyses. The bents shown with italic font style were redesigned for shear and therefore, could not reach the target DI=0.35. In some cases, the bents with higher aspect ratio (H/D = 12) remained elastic under the design earthquake due to their low stiffness. Consequently, the DI in these columns was smaller than 0.35, even with zero confinement. Therefore, these columns were not included in the present study (fixed-pinned 2 and 3% and fixed-fixed 3% for H/D = 12) (Table 4-7).

4.5.3. Four Column Bents

All FCBs were designed with columns of diameter 4ft [1219 mm]. The bents were designed for a height of 30 ft [9144 m]. Figure 4-14 shows a typical FCBs configuration used in the analyses. All FCBs were designed for a target DI of 0.35. To determine the DI, pushover envelopes were idealized by elasto-plastic curves. In cases where shear controlled, the transverse steel was redesigned for shear. The Δ_D was calculated using Eqs. 4-8a to 4-8e. Table 4-8 lists the FCB models used in the analyses. The bents shown with italic font style were redesigned for shear and therefore, could not reach the target DI=0.35.

4.6 Non-Linear Dynamic Analysis

SAP 2000 was utilized to perform the non-linear response history analyses to determine the demand DI. To develop a load model, non-linear dynamic analyses (NLDA) were conducted on SCBs, TCBs, and FCBs. The expected material properties of reinforcing steel and concrete were used. The Takeda hysteresis model (Takeda et al. 1970) available in SAP 2000 was used. The P-M2-M3 was used to model the plastic hinge. Except in the plastic hinge, the cracked (effective) section properties were used throughout the length of the column. The effective section properties were calculated from the yield moment, yield curvature, and concrete elastic modulus (Eq. 4-9).

$$I_{eff} = \frac{M_y}{\phi_y E_c} \tag{4-9}$$

To account for bond slip in the columns, frame partial fixity spring was modeled at the supports. The spring rotational stiffness was determined based on the initial yield moment and bond slip rotation. Bents designed for target DI of 0.35 under 1000-year earthquake were analyzed under both 1000 and 2500-year earthquakes. The purpose of the latter analysis was to determine the reliability under longer return period in columns that are typically designed for earthquakes with1000-year return period. Each bent was analyzed under 10 far field and 15 near field GMs. The number of near field motions was higher because this type of motion is generally more demanding.

4.6.1. NLDA for Single Column Bents

Non-linear dynamic analyses were conducted into two parts: (1) columns that were designed for 1000-year earthquakes were analyzed under GMs corresponding to 1000-year earthquakes, and (2) columns designed for 1000-year earthquakes were analyzed under GMs corresponding to 2500-year earthquakes. Each bent was analyzed under 25 GMs selected for site B/C and D. The GMs were scaled to match the design spectra corresponding to the 1000 and 2500-year earthquake. The GMs were scaled at the fundamental period of the bents. For each GM, the maximum displacement demand was determined, and subsequently DI_L was calculated. Figures 4-15 and 4-16 show a few examples of the force-displacement hysteretic curves for the far-field and near-field GMs, respectively. The Figures show the results for SCB with column diameter and height of 6 ft [1829 mm] and 30 ft [9144 mm], respectively, that were analyzed under 1000-year earthquake for site D. Tables 4-9 to 4-28 list the displacement demands and DI_Ls for SCBs designed for 1000-year earthquake, and analyzed under 1000 and 2500-year earthquake. Some of the SCBs underwent very large displacements under some of the ground motions and became unstable. The Δ_D in these bents was assumed to be equal to Δ_C (presented in italic font in Tables 4-9, 4-10, 4-13, 4-14, 4-15, 4-16, 4-22, and 4-26). The SCBs were also designed and analyzed under 1500-year earthquake to generate additional information and determine the sensitivity of reliabilities to the return period of the design earthquake. The design DI was kept at 0.35 under 1500-year earthquake. Tables 4-29 to 4-32 list the displacement demands (Δ_D) and DI_Ls of SCBs analyzed under 1500-year earthquake level.

4.6.2. NLDA for Two Column Bents

Like SCBs, the TCBs that were designed for a target DI of 0.35 for 1000-year earthquake, but were analyzed under 1000 and 2500-year earthquake. The Each bent was analyzed under 25 GMs selected for site B/C and D. The GMs were scaled to match the design spectra corresponding to the 1000 and 2500-year earthquake. The GMs were scaled at the fundamental period of the bents. For each GM, the maximum displacement demand was determined, and subsequently the DI_L was calculated. Tables 4-33 to 4-42 list DI_Ls of TCBs designed for 1000-year, and analyzed under 1000 and 2500-year earthquakes. Some of the TCBs underwent very large displacements under some of the ground motions and became unstable. The Δ_D in these bents was assumed to be equal to Δ_C (presented in italic font in Tables 4-33 and 4-34). Some of the bents with higher aspect ratio (H/D = 12) remained elastic under the design earthquake due to their low stiffness. Consequently, the DI in these columns was smaller than 0.35, even with zero confinement. Therefore, these columns were not included in the analyses (fixed-pinned 2 and 3% and fixed-fixed 3% for H/D = 12) (Tables 4-37 and 4-38).

4.6.3. NLDA of Four Column Bents

Four column bents designed for 1000-year earthquake were analyzed under 1000 and 2500-year earthquake levels. Like SCBs and TCBs, FCBs were designed for a target DI of 0.35. The Each bent was analyzed under 25 GMs selected for site D. The GMs were scaled to match the design spectra corresponding to the 1000 and 2500-year earthquake. The GMs were scaled at the fundamental period of the bents. For each GM, the maximum displacement demand was determined, and subsequently DI_L was calculated. Tables 4-43 to 4-46 list the Δ_Ds and DI_Ls of FCBs. Two of the FCBs underwent very large displacements under some of the ground motions and became unstable. The Δ_D in these bents was assumed to be equal to Δ_C (presented in italic font in Tables 4-43 and 4-44).

4.7 Fragility and Reliability Analysis

To model the scatter in DI_Ls, fragility curves were developed for all the bents. To develop fragility curves, cumulative lognormal distribution function was used. The Smironov-Kolmogorov goodness-of-fit test (Massey et al. 1951) and graphical methods (histograms) were used as acceptance criteria for lognormal distribution. To use the Kolmogorov goodness of fit test, it was assumed that the DI_L data is the representative of the population. This assumption was satisfied by conducting extensive analyses with a reasonable scatter in data to develop an approximately continuous distribution function for DI_L. In the Smironov-Kolmogorov test, the hypothesis that the data has lognormal distribution is accepted if all test data points in resistance and load model lie between the lower and upper confidence limits (LCL and UCL). These fragility curves serve as load model in the reliability analysis. By utilizing the resistance and load fragility curves, the reliability index was calculated against failure (DS6). In the present study, the reliability index against failure is denoted by "β_6". The reliability analysis presented in this document is based on large experimental test data and comprehensive analysis of column resistances and load models. Because the DI_L data was log-normally distributed, β

corresponds to lognormal distribution was calculated using equations Eqs. 2-8 to 2-12. The level of reliability at DS3 (β_3), DS4 (β_4), and DS5 (β_5) was also determined.

4.7.1. Fragility and Reliability Analyses of Single Column Bents

To develop fragility curves for SCBs, the DI_L data tabulated in Tables 4-9 to 4-32 was utilized. The fragility curves were developed for each bent for 1%, 2%, and 3% longitudinal steel ratios. For each steel ratio, the fragility curves and reliability indices were calculated for 1000 and 2500-year return period earthquake.

4.7.1.1. Analyses of Four Foot Diameter Single Column Bents for Site D

To develop fragility curves for SCBs with 4ft [1219 mm] diameter columns for Site D, the DI_L data tabulated in Tables 4-9 to 4-16 was utilized. Figures 4-17 and 4-18 show the fragility curves and reliability indices, respectively, for SCBs with 4 ft [1219 mm] diameter column. The fragility curves and reliability indices were calculated for 1000 and 2500-year return period earthquake. With high aspect ratios of 7.5 and 15, the columns designed for Site B/C were not able to reach a DI of 0.35, even at nearly zero confinement. Therefore, these bents were not included in the study, and the fragility curves were only developed for Site D.

Figure 4-17 shows that for the same probability of exceedance, the earthquakes with 2500-year earthquake are more demanding as expected. For example, under 1000-year earthquake, in a cantilever bent with 30 ft [9144 mm] height and 2% steel, the DI_L corresponding to 40% probability of exceedance was about 0.20 compared to 0.40 under 2500-year earthquake. Even though, the earthquakes with higher return periods are more demanding; the probability of occurrence of these earthquakes (P_{EQ}) during the life span of a bridge (75-year (AASHTO 2010)) is relatively low. For example, P_{EQ} for 1000-year return period is 0.072256514; whereas for 2500-year return period it is equal to 0.029554466. This effect is reflected in reliability indices (Figure 4-18). Figure 4-18 shows the reliability indices for damage states of three or higher. Note that the reliability indices are based on combined probability of failure including the P_{EQ}. The method used to calculate the combined probability of failure is described in Section 2.7.

Because the bents were designed to be at 50% probability of exceeding DS3 (DI = 0.35), theoretically the reliability index corresponds to DS3 should be zero. However, Figure 4-18 shows that, the reliability indices in all cases are greater than 1.5. This is because these reliability indices have included P_{EQ}, and the reliability index (β) corresponds to P_{EQ} itself is 1.5. The β of 1.5 is based on the probability of exceedance of 1000-year earthquake in 75-year (life span of bridge). Therefore, no matter for which DI the column is designed for, the reliability index would always be greater than or equal to 1.5.

The effect of various parameters on the reliability index is discussed below:

- Longitudinal steel ratio: In general, the reliability was almost unchanged, when the steel ratio was increased from 1% to 3%. For example, in cantilever bents with 30ft [9144 mm] height analyzed under 1000-year earthquake, the reliability for DS6 increased from 3.1 to 3.2, when the steel ratio was increased from 1% to 3%. However, in tall fixed-fixed bents with 60 ft [18288 mm] height and analyzed under 2500-year earthquake, the reliability was decreased from 3.1 to 2.7, when the steel ratio was increased from 1% to 3%.

- H/D ratio: In general, the effect of different aspect ratios on the reliability of bents was insignificant. For example, for 1000-year earthquake, in a cantilever bent with 30ft [9144 mm] height and 1% steel, the reliability for DS6 was 3.1, compared to 2.8 in tall cantilever bent (H = 60 ft [18288 mm]) for the same earthquake level and steel ratio.
- Boundary conditions: The reliability was almost unaltered when the support condition was changed from cantilever to fixed-fixed. For example, for 1000-year earthquake, in a cantilever bent with 30ft height and 3% steel ratio, the reliability for DS6 was 3.2, compared to 3.5 in fixed-fixed bent for the same steel ratio and earthquake return level.

The small effect of various parameters on reliability as discussed for DS6 can be noticed for other damages states (DS3, DS4, and DS5) as well. Because the bents were designed for 50% probability of exceeding DS3, the reliability is increased from DS3 to DS6. For example, in cantilever bents with 3% steel, 30ft [9144 mm] height, and analyzed under 1000-year earthquake, the reliability for DS3 is 2.0 compared to 3.5 for DS6. The reliability indices for DS3 to DS5 provide a vision of damage that might occur when the bent is designed for a target reliability index against failure.

4.7.1.2. Analyses of Six Foot Diameter Single Column Bents for Site B/C

To develop fragility curves for SCBs with 6ft [1905 mm] diameter columns for Site B/C, the DI_L data presented in Tables 4-17 to 4-20 was utilized. The fragility curves were developed for 1% and 2% longitudinal steel ratios (Figure 4-19). When the columns designed for Site B/C were not able to reach the DI of 0.35, even at nearly zero confinement, they were not included in the results. This was especially the case for fixed-fixed columns, and the columns with higher longitudinal steel ratios because these columns remained nearly elastic.

Figure 4-19 shows that, for the same probability of exceedance, the earthquakes with 2500-year earthquake are more demanding. For example, for 1000-year earthquake, in cantilever bent with 2% steel, the DI_L corresponding to 60% probability of exceedance was about 0.20, compared to 0.45 under 2500-year earthquake.

The reliability indices were calculated for 1000 and 2500-year earthquake (Figure 4-20). Figure 4-20 shows the reliability indices for damage states of three or higher. The effect of various parameters on the reliability of bents is discussed below:

- Longitudinal steel ratio: The reliability was almost unchanged when the steel ratio was increased from 1% to 2%. For example, in cantilever bents analyzed under 1000-year earthquake, the reliability for DS6 decreased from 3.9 to 3.7 when the steel ratio was changed from 1% to 2%.
- Boundary conditions: The reliability remained nearly the same, when the support condition was changed from cantilever to fixed-fixed for 2500-year earthquake. However, under 1000-year earthquake, the reliability increased significantly when the support condition was changed from cantilever to fixed-fixed. For example, in a cantilever bent with 1% steel and analyzed under 1000-year earthquake, the reliability for DS6 was 3.9, compared to 4.7 in fixed-fixed bent.

4.7.1.3. Analyses of Six Foot Diameter Single Column Bents for Site D

To develop fragility curves for SCBs with 6ft [1905 mm] diameter columns for Site D, the DI_L data tabulated in Tables 4-21 to 4-28 was utilized. Figure 4-21 shows the fragility curves for SCBs for 6-ft [1905-mm] diameter column. The fragility curves and reliability indices were calculated for 1000 and 2500-year return period earthquake.

Figure 4-21 shows that for the same probability of exceedance of DI_L, the earthquakes with 2500-year earthquake are more demanding. For example, for 1000-year earthquake, in fixed-fixed bent with 30 ft [9144 mm] height and 1% steel, the DI_L corresponding to 60% probability of exceedance was about 0.40 compared to 0.65 under 2500-year earthquake. However, the reliability did not change significantly (except in fixed-fixed bent with 30ft [9144 mm] height), when the return period was changed from 1000-year to 2500-year (Figure 4-22). For example, for 1000-year earthquake, in a cantilever bent with 30 ft height and 1% steel, the reliability for DS6 is 3.6, compared to 3.2 for 2500-year earthquake for the same bent height and steel ratio. This is because these reliability indices are based on combined probability of failure including the P_{EQ}. The earthquakes with longer return periods will also have lower probability of exceedance as discussed in section 4.7.1.1. Therefore, the overall effect on the reliability index is not significant. Figure 4-22 shows the reliability indices for damage states of three or higher. The various parameters that affect the reliability are described below:

- Longitudinal steel ratio: Figure 4-22 shows that, the reliability decreased when the steel ratio was increased from 1% to 3% in cantilever bents with 30 ft [9144 mm] height. In tall cantilever and fixed-fixed bents with 60 ft [18288 mm] height, the reliability remained nearly the same when the steel ratio was changed from 1% to 3%. For example, in a cantilever bent with 60ft [18288 mm] height, the reliability was decreased from 3.1 to 2.9 for DS6, when steel ratio was changed from 1% to 3%.
All fixed-fixed bents with 30 ft [9144 mm] height were controlled by shear, and the actual DI was less than 0.35. The DI for these columns decreased when the longitudinal steel ratio was increased from 1% to 3%. Consequently, β was increased when the steel ratio was changed from 1% to 3%. For example, in a fixed-fixed bent with 30 ft [9144 mm] height, the reliability was increased from 3.0 to 5.3 for DS6, when steel ratio was changed from 1% to 3%.
- H/D ratio: In general, the effect of different aspect ratios on the reliability of bents was insignificant. For example, for 1000-year earthquake, in a cantilever bent with 30 ft [9144 mm] height and 2% steel, the reliability for DS6 was 3.3, compared to 3.0 in tall cantilever bent with 60 ft [18288 mm] for the same height and steel ratio.
- Boundary conditions: The reliability did not change significantly when the support condition was changed from cantilever to fixed-fixed. For example, for 1000-year earthquake, in a cantilever bent with 60 ft [18288 mm] height and 2% steel, the reliability for DS6 was 3.0, compared to 3.2 in fixed-fixed bent for the same height and steel ratio.

4.7.2. Sensitivity of Reliability Index to Design Earthquake Return Period for Single-Column Bents

To investigate the effect of design earthquake return period on the reliability of the structure, the single-column bents were redesigned by increasing the return period to 1500-year while maintaining the target DI of 0.35. Because the majority of bents were from Site D, the bents were only designed for this site class. The bents were designed using 6 ft [1829 mm] diameter column for heights of 30 ft [9144 mm] and 60 ft [18288 mm] for 1%, 2%, and 3% longitudinal steel ratios. The DI_L data tabulated in Tables 4-29 to 4-32 was utilized to calculate fragility curves and reliability index. To compare the reliability of bents designed for 1000-year and 1500-year earthquake, the columns were designed for flexure to reach a target DI of 0.35 while ignoring the shear demand.

Figure 4-23 shows the fragility curves for DI_L for the bents analyzed under 1500-year earthquake. This Figure shows that the demand (DI_L) increased when the steel ratios was changed from 1% to 3%, except in tall cantilever bent with 60 ft [18288 mm] height. The fragility curves calculated for 1500-year earthquake were compared with those calculated for 1000-year earthquake. It was found that, the demand (DI_L) is nearly the same, when the bents were redesigned by increasing the return period to 1500-year, while maintaining the target DI of 0.35. For example, for 1500-year earthquake, in a cantilever bent with 30 ft [9144 mm] height and 2% steel, the DI_L corresponding to 40% probability of exceedance was about 0.25, which is nearly the same as that for the cantilever bent designed and analyzed under1000-year earthquake (Figure 4-21).

Figure 4-24 shows the average DI_L for 1000-year and 1500-year earthquakes. The comparison shown in Figure 4-24 is based on the combined data for 1%, 2%, and 3% steel for cantilever and fixed-fixed bents. In general, the mean DI_L is almost the same for 1000-year and 1500-year earthquake, except in fixed-fixed bents with 30 ft [9144 mm] height and 3% steel. For example, for 1000-year earthquake, the mean DI_L for cantilever bent with 30 ft [9144 mm] height and 1% steel is 0.29, compared to 0.31 in1500-year earthquake. This is because designing and analyzing the bents for higher earthquake levels affects both the capacity and seismic demand parameters. In the present study, it was found that, the effect on the capacity and the demand balanced each other. This was due to the following reasons: (1) bents designed for higher earthquake levels results in higher transverse steel ratio to obtain a target DI of 0.35. The higher transverse steel ratio results in higher confinement and consequently leads to higher ultimate displacement capacity, while not effecting the yield displacement considerably, and (2) on the demand side, the GMs are relatively strong for longer return periods and consequently they lead to higher displacement demand. Therefore, the increase in displacement capacity was balanced by the increase in displacement demand, and resulted in negligible effect on the fragility analysis.

Figure 4-25 shows the reliability indices for damage states of three or higher for the bents analyzed under 1500-year earthquake. This Figure shows that, the reliability decreased when the steel ratios was increased from 1% to 3%, except in tall cantilever bents with 60 ft [18288 mm] height. The reliability indices calculated for 1500-year earthquake were compared with those calculated for 1000-year earthquake. It was found that, the reliability indices were nearly the same when the return period was changed from 1000-year to 1500-year. For example, for 1500-year earthquake, the reliability index for cantilever column with 30 ft [9144 mm] height is 3.11 at DS6, compared to 3.10 in 1000-year earthquake. This is because the probability of exceedance of earthquake with higher return period is relatively low. For example, the P_{EQ} for 1000-year earthquake is 0.072256514, compared to 0.048770575 for 1500-year earthquake. The comparison shown in Figure 4-26 is based on the combined data for 1%, 2%, and 3% steel for cantilever and fixed-fixed bents.

4.7.3. Fragility and Reliability Analyses of Two Column Bents

To develop fragility curves for TCBs, the DI_L data tabulated in Tables 4-33 to 4-42 was utilized. The fragility curves were developed for 1%, 2%, and 3% longitudinal steel ratios. The TCBs were designed for a target DI of 0.35 under 1000-year earthquake for Site D. These bents were then analyzed under 1000-year and 2500-year earthquake.

4.7.3.1. Analyses of Five Foot Diameter Two Column Bents for Site D

To develop fragility curves for TCBs with 5ft [1524 mm] diameter columns, the DI_L data presented in Tables 4-33 to 4-38 was utilized. The fragility curves were developed for 1%, 2%, and 3% longitudinal steel ratios (Figure 4-27). For each steel ratio, the fragility curves and reliability indices were calculated for 1000 and 2500-year earthquake.

Figure 4-27 shows that, for the same probability of exceedance, the earthquakes with 2500-year earthquake are more demanding. For example, for 1000-year earthquake, in fixed-pinned bent with 30 ft [9144 mm] height and 1% steel, the DI_L corresponding to 40% probability of exceedance was about 0.20, compared to 0.35 under 2500-year earthquake.

The demand in fixed-pinned bents with 30 ft [9144 mm] height was nearly the same when the steel ratio was changed from 1% to 3% for 1000-year earthquake. For example, the DI_L corresponding to 40% probability of exceedance was about 0.20, 0.20, and 0.18 for 1%, 2% and 3% steel, respectively. However, in fixed-fixed bent with the same height and earthquake level, the demand decreased when the steel ratio was changed from 1% to 3%. This is because in fixed-fixed bents with 2% and 3% steel ratios, the transverse steel was controlled by shear leading to a relatively large amount of transverse steel that increased the ultimate displacement. Consequently, the actual DI in these bents was less than 0.35. The effect of higher transverse steel in 2% and 3% steel ratio also reflected in reliability indices (Figure 4-28). Figure 4-28 shows the reliability indices for damage states of three or higher. The various parameters that affect the reliability are described below:

- Longitudinal steel ratio: Figure 4-28 shows that the reliability was almost unchanged in fixed-pinned bents with 30 ft [9144 mm] height when the steel ratio was increased from 1% to 3%. For example, under 1000-year earthquake, the reliability decreased from 3.0 to 2.9 for DS5, when steel ratio was changed from 1% to 3%. In fixed-fixed bents with 30 ft height, the reliability increased when the steel ratio was changed from 1% to 3%. For example, the reliability increased from 3.2 to 4.8 for DS6, when steel ratio was changed from 1% to 3%. This is because all the fixed-fixed bents with 30 ft [9144 mm] height were controlled by shear and the actual DI was less than

0.35. The DI for these column decreased when the longitudinal steel ratio was changed from 1% to 3%. Consequently, the reliability increased when the steel ratio was changed from 1% to 3%.

- H/D ratio: In fixed-pinned bents, the effect of different aspect ratios on the reliability of bents was insignificant. For example, for 1000-year earthquake, in a fixed-pinned bent with 30 ft [9144 mm] height and 1% steel, the reliability for DS6 was 3.1, compared to 2.9 in tall fixed-pinned bent with 60 ft [18288 mm] height. However, in tall fixed-fixed bent with 60 ft [18288 mm] height, the pattern of reliability indices was the opposite of the one observed in fixed-fixed bent with 30 ft [9144 mm] height. This is because in tall bents the design was governed by the design DI of 0.35 instead of shear. Therefore, the transverse steel for the column with 2% steel ratio was relatively low for the same design DI of 0.35.
- Boundary conditions: The reliability in short bents (H = 30 ft [9144 mm]) with different support conditions cannot be compared. This is because the actual DI in the fixed-fixed bents was less than the one in fixed-pinned bents (DI of 0.35). However in tall bents (H = 60 ft [18288 mm]), the reliability increased when the support condition was changed from fixed-pinned to fixed-fixed. For example, in fixed-pinned bent with 1% steel, the reliability for DS6 was 2.9, compared to 4.4 in fixed-fixed bent for the same steel ratio.

Because in TCBs with 30 ft [9144 mm] height the difference in reliability indices for 1000-year and 2500-year earthquake was insignificant, the tall bents were not analyzed under 2500 years earthquake.

The fixed-pinned TCBs with 60 ft [18288 mm] height were not able to reach DI of 0.35 for 2% and 3% steel ratio even with zero confinement. Therefore, these bents were not included in the analyses. The same was true for the fixed-fixed TCBs with 3% steel ratio.

4.7.3.2. Analyses of Six Foot Diameter Two Column Bents for Site D

To develop fragility curves for TCBs with 6-ft [1829-mm] diameter columns, the DI_L data presented in Tables 4-39 to 4-42 was utilized. Because the difference in reliability for 1000 and 2500-year earthquake was found to be insignificant, the fragility curves and reliability indices were calculated for 1000-year earthquake only.

Figure 4-29 shows the fragility curves for TCBs with 6 ft diameter columns analyzed under 1000-year earthquakes. The demand in fixed-pinned bent with 30 ft height was nearly unaffected by the steel ratio. For example, for 1% steel, the DI_L corresponding to 40% probability of exceedance was about 0.20 compared to 0.18 for 3% steel. However, in fixed-fixed bents with 30 ft height the demand decreased when the steel ratio was changed from 1% to 3%. This is because fixed-fixed bents with 2% and 3% steel ratio were controlled by shear leading to a relatively large amount of transverse steel that increased the ultimate displacement. Consequently, the actual DI in these bents was less than the target design DI of 0.35.

In tall fixed-pinned bents with 60 ft height, the difference in demand was not significant when the steel ratio was changed for 1% to 3%. For example, the DI_L corresponding to 40% probability of exceedance was about 0.18, 0.20, and 0.17 for 1%, 2%, and 3% steel, respectively. In tall fixed-fixed bents with 60 ft height, the demand decreased when the steel ratio was changed for 1% to 3%.

Figure 4-30 shows the reliability indices for TCBs with 6 ft diameter columns analyzed under 1000-year earthquake. Various parameters that affect the reliability are described below:

- Longitudinal steel ratio: Figure 4-30 shows that the reliability in fixed-pinned bents with 30 ft [9144 mm] height increased when the steel ratio was changed from 1% to 3%. For example, the reliability increased from 2.9 to 3.2 for DS5, when steel ratio was changed from 1% to 3%. In fixed-fixed bents with 30 ft height, the increase in reliability was significant when the steel ratio was changed from 1% to 3%. For example, the reliability increased from 2.9 to 7.2 for DS6, when steel ratio was changed from 1% to 3%. This is because fixed-fixed bents with 2% and 3% steel ratios were controlled by shear causing the design DI to be less than 0.35. The DI for these columns decreased when the longitudinal steel ratio was changed from 1% to 3%. Consequently, the reliability increased when the steel ratio was changed from 1% to 3%.
- H/D ratio: In fixed-pinned bents, the reliability decreased when the height was changed from 30 ft to 60 ft. For example, for 1000-year earthquakes in a fixed-pinned bent with 30 ft [9144 mm] height and 1% steel, the reliability for DS6 was 3.5 compared to 3.1 in tall fixed-pinned bent with 60 ft height. The reliability in fixed-fixed bents with different H/D ratio cannot be compared. This is because the actual DI in the fixed-fixed bents (for 2% and 3% steel) with 30 ft height was less than the one in bents with 60 ft height (DI of 0.35).
- Boundary condition: The reliability in short bents (H = 30 ft) with different support conditions cannot be compared. This is because the actual DI in the fixed-fixed bents with 2% and 3% steel was less than the one in fixed-pinned bents (DI of 0.35). However in tall bents (H = 60 ft), the reliability increased when the support condition was changed from fixed-pinned to fixed-fixed. For example, in fixed-pinned bent with 1% steel, the reliability for DS6 is 3.0, compared to 3.8 in fixed-fixed bent for the same steel ratio

4.7.4. Fragility and Reliability Analyses of Four Column Bents

To develop fragility curves for FCBs with 4 ft [1219 mm] diameter columns, the DI_L data presented in Tables 4-43 to 4-46 was utilized. These bents were only designed for the height of 30 ft [9144 mm]. The fragility curves were developed for 1%, 2% and 3% longitudinal steel ratios (Figure 4-31). For each steel ratio, fragility curves and reliability indices were calculated for 1000 and 2500 years return period.

Figure 4-31 shows that for the same probability of exceedance of DI_L, the earthquakes with 2500-year earthquake are more demanding. For example, for 1000-year earthquakes in fixed-pinned with 1% steel, the DI_L corresponding to 40% probability of exceedance was about 0.25 compared to 0.50 under 2500-year earthquakes. The same pattern was noticed in fixed-fixed bents. Figure 4-31 shows that the demand decreased in fixed-pinned and fixed-fixed bents when the steel ratio was changed from 1% to 3%. The decrease in demand in fixed-fixed bents is relatively high. This is because fixed-fixed bents with 2% and 3% steel ratio were revised for shear. In these bents, the transverse steel was controlled by shear leading to a relatively large amount of transverse steel that increased the ultimate displacement. Consequently, the actual DI in these bents was less than the target design DI of 0.35.

As discussed previously, even though the earthquakes with higher return period are more demanding, the probability of occurrence of these earthquakes is relatively low (P_{EQ}). Because the reliability is based on the combined probability of failure including P_{EQ}, this effect is reflected in reliability indices (Figure 4-32). The effect of various parameters on the reliability index is discussed below:

- Longitudinal steel ratio: The reliability in fixed-pinned bents did not vary significantly when the steel ratio was changed from 1% to 3%. For example, in fixed-pinned bents analyzed under 1000-year earthquake, the reliability varied from 3.0 to 3.4 for DS6 when the steel ratio was changed from 1% to 3%. However, in fixed-fixed bents, the reliability increased significantly when the steel ratio was changed from 1% to 3%. For example, in fixed-fixed bents analyzed under 1000-year earthquakes the reliability changed from 3.6 to 4.9 for DS6, when the steel ratio was changed from 1% to 3%
- Boundary condition: The reliability increased when the support condition was changed from cantilever to fixed-fixed. For example, under1000-year earthquake, in a fixed-fixed bent with 3% steel ratio, the reliability for DS6 was 3.0, compared to 3.6 in fixed-fixed bent for the same steel ratio and earthquake return period.

4.8 Discussion of Results

Reliability analysis results show that β_6 in SCBs varies from 2.7 to 3.9, except in cases where column shear controlled the design of transverse reinforcement. The reliability analyses were conducted based on combined probability of failure, including the probability of earthquake exceedance (P_{EQ}). The reliability of bents was greater than 1.5. The β of 1.5 is based on the probability of exceedance of 1000-year earthquake in 75-year (life span of bridge) itself. Because the bents were designed for 50% probability of exceeding DS3, the reliability increased from DS3 to DS6. Because the reliability against failure was the controlling parameter in calibrating the design DI, most of the discussion is focused on reliability against DS6. However, the reliability indices for DS3 to DS5 are also useful in providing a vision of damage and repair that one can expect when the bent is to be designed for a target reliability index against failure.

Because the variation in β was not significant, all the data for SCBs were combined to obtain a uniform reliability against failure. The fragility and reliability analysis was conducted on the combined data. The cumulative lognormal distribution was used to conduct the fragility analysis. Because PDCA approach is displacement based, the bents in which shear controlled the transverse steel design were excluded. The validity of fragility curve was determined using Smironov-Kolmogorov test with 10% level of significance. Figure 4-33 shows that the data follows the lognormal distribution. The reason some of the data lies outside or on the limit curve is that the bandwidth of the limit curves are inversely proportional to the number of data points. The empirical data falling outside the lower limit curve shows that the theoretical distribution used is conservative. To validate the current distribution, the histogram with lognormal fit was plotted utilizing Minitab 15 software (Figure 4-33). Figure 4-34 shows that the data closely follow the lognormal distribution.

The same approach as that used for SCBs was applied to develop a combined fragility curves for TCBs and FCBs. Figures 4-35 and 4-36 show the fragility curve and histogram for TCBs, respectively. Figure 4-37 shows that all the data for FCBs are falling inside the curve limits.

The combined data for each bent type (single column, two-column, and four-column bents) was used to determine and compare the reliability indices for different bents. Figure 4-38 shows the reliability indices for SCBs, TCBs, and FCBs. This Figure shows that, for each steel ratio, β increased slightly from SCBs to FCBs. The reliability indices against failure were calculated as 3.1, 3.2, and 3.3 for SCBs, TCBs, and FCBs, respectively. The present study shows that β_6 is higher than 3.0 when bents are designed for 50% probability of exceeding DS3 (DI = 0.35) under 1000-year earthquake. β of 3.0 is approximately a probability of failure of 1 in 1000 (Table 4-47). However, the bents can be designed for higher probability of exceeding DS3 without causing a concern for failure. In general, the selection of β is somewhat subjective. Ideally, the selection of the target β is based on economic considerations that reflect both the cost of increasing the safety margins and the implied costs associated with component repair, bridge closure, or failure.

The current study shows that, the new approach of PDCA by incorporating reliability index provides much flexibility to the structural engineer to design a bridge column to reach a given damage state with a specified reliability under an earthquake with a given return period. To correlate the target β6 with design DI, a direct probabilistic design method was developed. This method is described in Chapter 5.

Chapter 5. Development of Direct Probabilistic Design Method

5.1 Introduction

In Chapter 4, the reliability indices were calculated for bents that were designed to be at 50% probability of exceeding DS3 (*DI* = 0.35). The designer does not have a control over the reliably index for higher damage states including failure. To achieve the desired reliability level, one needs to select different design *DI*s, and conduct the reliability analyses until the desired β_6' is obtained. Therefore, to calibrate the design *DI*, an iterative process has to be used to achieve a certain level of reliability index for different damage states. Although this process of calibrating the design *DI* is exact, it can be time consuming and impractical. To overcome this iterative approach used in the exact method, a new direct PDCA method was developed.

The direct PDCA was developed by calibrating the design *DI* for a given β_6', while calculating the probability of exceeding other DSs (DS3, DS4 and DS5). The direct PDCA is approximate but it can be used quickly with no iteration involved. The methodology used in direct PDCA, is inverse of the methodology used for the exact method. In this method, instead of selecting different *DI*s, and then calculate the β_6', the *DI* is directly determined for a given target β_6', which is based on combined probability of failure ($P_{CF} \cap P_{EQ}$), including the probability of earthquake exceedance and the life span of bridge (P_{EQ}). The development of direct PDCA is described in this chapter.

5.2 Objective

To develop a probabilistic method for seismic design of bridge columns, that have been repaired with CFRP, for a target reliability against failure (β_6'), and to determine probability of exceedance of other damage states.

5.3 Assumptions and Simplifications

In developing direct PDCA, it was assumed that the Δ_Y and Δ_D are independent of transverse steel ratio. In general, the Δ_Y and Δ_D are mostly controlled by the yielding of column longitudinal bar and the column period, respectively. For example, Figure 5-1 shows Δ_D for the SCBs with columns designed for different spiral ratios (0.44% and 1.05%). The Δ_D was 10.08 in [256.0 mm] and 10.07 in [255.8 mm] for the columns with 0.44% and 1.05 spiral ratio, respectively. Whereas Δ_Y was 3.32 in [84 mm] and 3.51 in [89 mm] for the columns with 0.44% and 1.05 spiral ratio, respectively. This shows that the assumptions made was reasonable. These assumptions are further verified in the design example presented for SCBs in Appendix A.

5.4 Calibration of Damage Index

The design *DI* was calibrated for a given β'_6. The calibration was performed using Eqs. 5-1 to 5-6.

$$DI_L = \frac{\Delta_D - \Delta_Y}{\Delta_C - \Delta_Y} \tag{5-1}$$

$$DI'_L = \frac{\Delta_D - \Delta_Y}{\Delta'_C - \Delta_Y} \tag{5-2}$$

$$\frac{DI'_L}{DI_L} = \frac{\Delta_C - \Delta_Y}{\Delta'_C - \Delta_Y} = \text{constant} = \alpha \tag{5-3}$$

$$\frac{\mu'_L}{\mu_L} = \frac{\sigma'_L}{\sigma_L} = \alpha, \quad \frac{\delta'_L}{\delta_L} = 1 \tag{5-4}$$

$$\beta''_6 = \frac{\ln\left(\frac{\mu_R}{\alpha\mu_L}\sqrt{\frac{\delta'^2_L + 1}{\delta^2_R + 1}}\right)}{\sqrt{\ln\left[\left(\delta^2_R + 1\right)\left(\delta'^2_L + 1\right)\right]}} \tag{5-5}$$

$$DI' = \alpha DI \tag{5-6}$$

Where, DI = tentative design damage index, DI′ = calibrated design damage index for a given reliability, DI_L = damage index calculated from earthquake ground motions for bents designed for *DI*, DI'_L = damage index calculated from earthquake ground motions for bents designed for *DI′*, Δ_C = ultimate displacement based on *DI*, Δ'_C = ultimate displacement based on *DI′*, Δ_D = displacement demand, Δ_Y = effective yield displacement, *L* = load, *R* = resistance, δ = coefficient of variation (σ/μ), μ'_L = mean of DI'_L, σ'_L = standard deviation of DI'_L, μ_L = mean of DI_L, σ_L = standard deviation of DI_L, and β''_6 = target reliability index corresponding to probability of column failure ($P_{CF} \mid P_{EQ}$). The μ_R and σ_R are the mean and standard deviation of fragility curves of damage indices (DI_R) developed by Vosooghi and Saiidi (2012). The μ_R and σ_R for all DSs are listed in Table 5-1.

Because for a given earthquake level, P_{EQ} is constant, the calibration of *DI* is based on $P_{CF} \mid P_{EQ}$ and its corresponding reliability index (β''_6). For example, for a 1000-year earthquake, to obtain a desired β'_6 of 3.5, the required combined probability of exceedance is equal to 0.000232629 ($P_{CF} \cap P_{EQ} = 1 - \Phi(\beta'_6)$) (Eq. 2-11), in which the P_{EQ} is equal to 0.072256514 (Eq. 2-9). Having $P_{CF} \cap P_{EQ}$ and P_{EQ}, $P_{CF} \mid P_{EQ}$ can be calculated as 0.003219489 ($P_{CF} \cap P_{EQ} \div P_{EQ}$) (Eq. 2-10). The β''_6 for $P_{CF}|P_{EQ}$ of 003219489 is 2.72 ($-\Phi^{-1}(P_{CF}|P_{EQ})$) (Eq. 2-12). By plugging β''_6 in Eq. 5-5, the constant α can be calculated.

Having μ'_L and σ'_L calculated using Eqs. 5-1 to 5-6, the new reliability indices corresponding to DI' was back calculated from Eq. 2-8. Once the new reliability indices were calculated, the P_{EQ} was included to calculate the desired β'_6 utilizing Eqs. 2-9 to 2-12. Table 5-3 lists values of β''_6 to be used to obtain desired β'_6. The parameters in Table 5-3 were defined previously in Section 2.7.

To demonstrate direct PDCA, an example is presented in Appendix A. The results of direct method were compared with the exact method. The results in Appendix-A show that, the direct PDCA was very effective in calibrating the design *DI* and providing flexibility to determine reliability indices for a column designed for different damage indices.

5.5 Reliability Based Design Matrix

The reliability based design matrix was developed assuming a 1000-year earthquake return period. The design example presented in Appendix A shows that, the direct PDCA could be effectively applied to calibrate the design *DI*. This design example was presented only for SCB. In order to apply direct PDCA to all types of bents regardless of the number of columns, the design *DI* was calibrated by combining all the data of DI_L for different bent categories. Because the variation in βs was not significant in the bents with different configurations and steel ratios, the decision of combining the data was considered to be reasonable. Table 5-2 lists the μ_L and σ_L of the combined DI_L data for each bent category (SCBs, TCBs and FCBs).

Utilizing direct PDCA, the DI' was calibrated for SCBs, TCBs, and FCBs for various β'_6s. Table 5-4 shows different DI's for various β'_6s for SCBs. In this Table, for a given β'_6, the probability of exceedance of other DSs was also investigated. Because the P_{EQ} is implicit in β'_6, the probabilities of exceeding DSs are very low. For example, for β'_6 of 3.0, the probability of exceeding DS1 is only 7%. However, the probability of exceeding these DSs is much higher when P_{EQ} is not included in the β'_6 (Table 5-5). Table 5-5 shows that, for β'_6 of 3.0, the probability of exceeding DS1 is 100%. This is because the reliability index (β) corresponds to P_{EQ} itself is 1.46. The β of 1.46 corresponds to the 7% probability of exceedance. Therefore, no matter for which DI' the column is designed, the probability of exceedance of any given DS will always be less than or equal to 7%.

Similarly, the DI's were calculated for TCBs and FCBs for various β'_6s. Tables 5-6 and 5-7 show different DI's for distinct β'_6s for TCBs and FCBs, respectively. For a given β'_6, the probability of exceedance of other DSs was also investigated. Like SCBs, the probabilities of exceeding DSs are very low due to the inclusion of P_{EQ} in β'_6.

As discussed previously in Chapter 4, the TCBs and FCBs were more reliable than SCBs. Consequently, the DI's calculated for TCBs and FCBs were higher compared to the SCBs designed for the same β_6'. For example, in SCBs, DI' of 0.38 is required to obtain β_6' of 3.0 (Table 5-4), while requiring 0.41 and 0.43 for TCBs, and FCBs, respectively (Tables 5-6 and 5-7), to achieve the same β_6'.

5.6 Difference between Theoretical and Actual Failure of Columns

Thus far, in the present study, the βs were calculated based on the compressive failure of concrete core edge (code-defined failure, which is the theoretical failure). Accordingly, the ultimate displacement capacity (Δ_C) of the bents was calculated based on the compressive failure of concrete core edge in determining *DI*. Numerous column tests have shown that the Δ_C at the actual failure, which is generally associated with reinforcing bar fracture and extensive core damage, exceeds the theoretical displacement capacity, as shown in Figure 5-2. Consequently, the reliability indices corresponding to the actual failure is higher those based on the theoretical failure. In order to determine *DI* based on the actual failure, the fragility curves developed by Vosooghi and Saiidi (2012) were utilized. From these fragility curves, it was found that the actual failure displacement is approximately 20% higher than the theoretical displacement. The factor of 1.2 was calculated by dividing the average of DI_6 by DI_5 using the resistance fragility curves (Vosooghi and Saiidi 2012). Where, DI_6 and DI_5 are the damage indices correspond to DS6 and DS5, respectively. For DS6, the average of DI_6 was taken equal to one. In the direct PDCA, the βs were calculated based on both the core edge failure (DS5) and the actual failure (DS6). To determine βs based on the actual failure, the following steps were used:

Step 1. Determine the *DI* corresponding to the actual failure using resistance fragility curves.

$$DI^R = 1.2 \times DI \tag{5-7}$$

Step 2. Determine the mean and standard deviation corresponding to actual failure using Eq. 5-9.

$$\mu_L^R = \mu_L / 1.2 \qquad \sigma_L^R = \sigma_L / 1.2 \tag{5-9}$$

In the above equations, the superscript "R" represents the actual failure. In Eq. 5-9, the load parameters were divided by 1.2 in order to reduce DI_L, which consequently leads to an increase in β. Having μ_L^R and σ_L^R, βs were back calculated from Eq. 2-8.

5.7 Comparison of Reliability Indices Based on Theoretical and Actual Failure

As discussed in section 5.6, the reliability index based on the actual failure is higher for a given design DI'. The β_6' based on the actual failure was calculated, and compared with the one based on theoretical failure. Figures 5-3, 5-4 and 5-5 show the comparison of β_6' calculated based on theoretical and actual failure for SCBs, TCBs, and

FCBs, respectively. It is evident from these Figures that, for a given DI', the β_6' for actual failure is relatively high. For example, in SCBs, for design DI' of 0.38, β_6' is 3.0 and 3.2 for theoretical and actual failure, respectively (Figure 5-3). The same pattern was observed in TCBs and FCBs (Figures 5-4 and 5-5Figure 5-5).

These results show that, the reliability based design matrix developed for SCBs, TCBs, and FCBs is conservative, indicating a higher safeguard against actual failure. To be consistent with the code requirements, it is recommended that, the reliability based design matrix based on the theoretical failure rather than actual failure to be used.

5.8 Discussion of Results

The results show that the direct method can precisely calibrate the design damage index for a desired β_6'. The DI' Tables presented for SCBs, TCBs, and FCBs provides flexibility to the structural designers to design a bridge column to reach a given DS with a specified reliability level. For the same β_6', DI' in multicolumn bents was higher compared to SCBs. This confirms the general perception that multicolumn bents are more reliable than single column bents. Therefore, to achieve an optimum reliability index against failure, multicolumn bents can be designed for higher probability of exceeding DS3 without causing a concern for failure. The reliability based design matrices developed in this study are based on the theoretical failure. Therefore, these design matrices are conservative and have a higher safeguard against actual failure.

Chapter 6. Preliminary Development of PDCA for Repaired Bridge Columns

6.1 Introduction

Thus far, the PDCA and reliability analysis was used to develop performance based seismic design for conventional bridge columns. In this Chapter, the PDCA and reliability analysis were further extended for earthquake-damaged columns that have been repaired. This study focused on columns repaired using carbon fiber reinforced polymer (CFRP) jackets. Retrofitted columns were not included in this study. PDCA was developed based on limited experimental test results and engineering judgments for repaired columns subjected to various earthquake levels. Like conventional columns, different damage states (DSs) were defined for repaired columns associated with varying degree of damage. In order to define the apparent DSs, the experimental data from the study conducted by Vosooghi and Saiidi 2010 was utilized. The goal of this Chapter is to demonstrate the process to use PDCA for repaired columns, realizing that the study is of limited scope due to the scarcity of data for repaired columns.

6.2 Assumptions and Simplifications

In repaired columns subjected to different earthquake intensities, because the column is wrapped with CFRP, the apparent damage states (DSs) are substantially different from original columns DSs except for possibly DS6, which is associated with column failure. Even DS6 in repaired columns may be due to the CFRP jacket fracture, which is not applicable to original columns. Generally, the CFRP jacket does not exhibit any visit damage until failure. Therefore, the only visible damage may be noted at the jacket gaps provided at column ends to prevent bearing of jacket on the footing or the cap beam. As a result, pre-failure DSs were investigated based on the type of damage in the gap region. Out of six possible damage states, only two DSs, DS3 and DS6 were defined. The other damage states are not applicable for repaired columns. The DS3 and DS6 correspond to extensive spalling in the gap region and CFRP fracture, respectively (Figure 6-1). In developing PDCA for repaired columns, it was assumed that, the repair was applied to standard columns that have undergone damage states of 1 to 5 (with DS5 being theoretical failure) to restore their lateral load strength and shear capacity. Columns that are repaired after undergoing DS6 (with fractured bars) were excluded. Also, repaired substandard columns were not included.

6.3 Resistance Model for Repaired Columns

To develop resistance model for reliability analysis, a literature search was made to collect the experimental data for repaired columns. The goal was to gather this data and calculate the DIs at different DSs to develop fragility curves (resistance model) for repaired columns. However, comprehensive data could be found only for two repaired columns (NHS1-R and NHS2-R) tested in a previous study of Vosooghi and Saiidi. These two columns were used to define apparent DSs (DS3 and DS6) and calculate the corresponding DI_R. Because DI for DS6 is one, the DI_R was only calculated for DS3. The DI_Rs calculated for DS3 were 0.10 and 0.23 for NHS1-R and NHS2-R, respectively (Table 6-1).

The DI_{RS} for repaired columns are lower than the DI_{RS} for conventional columns subject to the same DS. For example, DI_R for DS3 in NHS1-R is 0.10 compared to 0.18 in NHS1 (Table 6-1 andTable 6-2). NHS1 and NHS2 were the designation of the original columns (Vosooghi and Saiidi 2010). It was found that, the DI_{RS} (0.10 and 0.23) calculated for repaired columns (NHS1-R and NHS2-R) for DS3, fall in the range of DS2 in original standard columns (Figure 6-2). This is attributed to the lower initial stiffness of repaired columns. Therefore, the DI_R fragility curve for DS2 in conventional columns was utilized as a resistance model for DS3 in repaired columns for reliability analysis.

6.4 Analytical Model

To demonstrate the applicability of PDCA to repaired columns, a cantilever single column bent was designed (original column), and then repaired with CFRP (repaired column). The properties of the original column (undamaged) used in this study are listed in Table 6-3. Because DS3 in repaired columns is equivalent to the DS2 in conventional columns with respect to DI, the column was repaired to be at 50% probability of exceeding DS3 with DI = 0.15 (Table 3-20). The DI of 0.15 corresponds to the 50% probability of exceeding DS2 in conventional columns. The expected material properties were used in the analyses (f_c' = 5 ksi [34.5 MPa] and f_{ye} = 68ksi [468.8 MPa]). Figure 4-10 (Chapter 4) was used for stress-strain relationship of steel in the original column.

6.4.1. Modification of Steel Properties

In damaged columns under cyclic loading, the stress-strain properties of steel become different from those associated with purely tensile or compressive stress. This is known as the Bauschinger effect (Kent & Park 1973) and results in lowering of the reversed yield stress and the reversed stiffness (Figure 6-3). The column was assumed to have been damaged to DS5 prior to repair. A tri-linear stress-strain relationship proposed by Vosooghi and Saiidi (2010) was used for the repaired column longitudinal bars (Figure 6-4). The slope of the first branch was calculated as a fraction of the steel modulus of elasticity. In their study, the modification factor (α) was determined based on the damage state. For instance, the factor of 0.2, 0.5, and 0.67 were proposed for DS5, DS3, and DS2, respectively. In the present study, α equal to 0.2 was used. In Figure 6-4, Point A represents the yield stress and the strain associated with the modified stiffness. The second branch connects Point A to Point B. Point B is related to the maximum strain in longitudinal steel (MLS) at the given damage state. The third branch connects Point B to the ultimate point (Point C). Table 6-4 lists the parameters of the modified stress-strain relationship for the repaired columns. Figure 6-5 shows the modified stress-strain relationship for steel used for the repaired column.

6.4.2. CFRP Confined Concrete Properties

It was assumed that the spiral contribution to confinement in the repaired columns is negligible at DS5 (Vosooghi and Saiidi 2010). Therefore, the concrete properties of the repaired columns were determined based on CFRP confined concrete properties.

Saiidi's (Saiidi et al. 2005) bilinear stress-strain relationship for CFRP-confined concrete was used in this study. To define the bilinear relationship, the coordinate of the break point and the ultimate point were determined. At the break point, the strain was assumed to be at 0.002 and the stress was found as follows:

$$f'_{co} = f'_c + 0.003\rho_{cf}E_j \tag{6-1}$$

Where ρ_{cf} is volumetric ratio of CFRP jacket, E_j is elastic modulus of CFRP, and f'_c is the unconfined concrete strength. The ultimate strain and stress were determined using the following equations:

$$\varepsilon_{cu} = \frac{\varepsilon_j}{0.1 - 0.25\ln\left(f_r / f'_c \right)} \tag{6-2}$$

$$f'_{cu} = f'_c + 3.5 f_r^{0.7} \quad \text{[ksi]} \tag{6-3a}$$

$$f'_{cu} = f'_c + 6.2 f_r^{0.7} \quad \text{[MPa]} \tag{6-3b}$$

Where ε_{cu} is the ultimate strain, f'_{cu} is the ultimate stress, f_r is the confinement pressure, and ε_j is the jacket strain. Saiidi et al. (2005) recommend 50% of the failure strain of CFRP for the jacket strain to account for the fact that jacket failure strain is typically lower than the ultimate strain obtained in coupon testing of FRP. Unidirectional CFRP fabrics with fibers in the horizontal direction were used in the analysis. Unidirectional CFRP fabrics produced by the FYFE Co. SCH41/Tyfo S, with fibers in the horizontal direction were assumed. The material properties of CFRP fabrics used are shown in Table 6-5. Because in practice, the cover concrete and the edge of core concrete are replaced with the repair mortar, the CFRP confined properties were calculated for core and cover concrete separately using the original concrete and repair mortar properties, respectively. The nominal strength of 4 ksi [27.6 MPa] was used for repair mortar. The properties of CFRP confined concrete are listed in Table 6-6.

6.4.3. Moment Curvature Analysis

Moment-curvature analyses were conducted to calculate strains required for bond-slip calculations. The modified Wehbe's method (Section 4.4.3) was applied for bond-slip calculations. Xtract was used in the analyses (Chadwell 2007) utilizing the modified steel properties and the CFRP confined concrete properties. The moment-curvature relationships for the original and repaired column are plotted in Figure 6-6. Since the column was repaired after reaching DS5 (compressive failure of core concrete edge), the moment curvature analyses were also continued until the ultimate strain in core concrete was reached.

6.4.4. Column Design

Initially the column was designed for site class D under 1000-year earthquake level. The column diameter and height of 6 ft [1829 mm] and 30 ft [9144 mm] were used. The column was designed for 2% longitudinal steel ratio. This column was served as the original column (undamaged). Later, it was assumed that the original column underwent DS5. The longitudinal steel properties of the original column were modified to reflect the softening due to damage to the original column (Section 6.4.1). Finally, the repair was designed for a target DI of 0.15. The properties of the repaired column are listed in Table 6-7.

The DI was calculated using elasto-plastic pushover curve based on SDC 3.1 (Caltrans 2010). By utilizing SDC 3.1.3 (Caltrans 2010), the columns were designed based on their rotation capacity determined from moment curvature analyses. The general procedure used to design the bent for the target DI was explained in Section 4.5.1. Seismic displacement demands were determined based on the rule of "equal displacement" and the effective stiffness of the column. The idealized force-displacement relationship for the original and repaired column is plotted in Figure 6-7.

6.5 Load Model for Repaired Columns

To develop a load model, non-linear dynamic analyses (NLDA) were conducted. SAP 2000 was utilized to perform the analyses. The column was analyzed under 10 far field and 15 near field ground motions (GMs). The GMs were scaled at the fundamental period of the column. For each GM, the maximum displacement demand was determined, and subsequently DI_L was calculated. Table 6-8 lists the displacement demands (Δ_D) and DI_Ls of the repaired column designed for DI of 0.15, and analyzed under 1000 years earthquake level for site class D. Because in some cases the displacement demand imposed by the ground motions was less than the column effective yield displacement, the DI_L in these cases was a negative value (Table 6-8).

To model the scatter in DI_Ls, a fragility analysis was conducted (Figure 6-8). To develop the fragility curve, cumulative lognormal distribution function was used. Because lognormal distribution is not defined at negative values, such values were excluded from the fragility analysis. The Smironov-Kolmogorov goodness-of-fit test (Massey et al. 1951) was used as acceptance criteria for lognormal distribution. In the Smironov-Kolmogorov test, the hypothesis that the data has lognormal distribution is accepted if all test data points in the load model lie between the lower and upper confidence limits (LCL and UCL). This fragility curve served as the load model in the reliability analysis.

6.6 Reliability Analysis

By utilizing the resistance and load fragility curves, the reliability analysis was conducted. The reliability index was calculated for DS3 and DS6. To calculate the reliability index, Eqs. 2-8 to 2-12 were utilized. The level of reliability index calculated for DS3 (β_3') and DS6 (β_6') was 1.67 and 2.96, respectively (Figure 6-9).

The results show that, the reliability index against failure is 3.0, when the column was repaired for 50% probability of exceeding DS3 (DI = 0.15) under 1000-year earthquake, whereas in the original column with the same height, diameter, and earthquake return period, the reliability against failure was 3.3 (Figure 4-22). Note that the original column was designed to be at 50% probability of exceeding DS3 (DI = 0.35). The results show that, for the same probability of exceeding DS3, the failure reliability index in the repaired column is lower than that of the original column. Inversely, the results suggest that, to accomplish the same reliability against failure, the repair should be designed for a smaller DI. The PDCA procedure provided herein is based on very limited information about the damage progression in repaired columns. The findings from this limited study should be considered to be tentative. Nonetheless, the procedure can serve as a framework, which could be further refined in the future as more data for repaired columns becomes available.

Chapter 7. Summary and Conclusions

7.1 Summary

A performance based seismic design for bridge columns was developed in this study by incorporating probabilistic damage control approach (PDCA) and reliability analysis. The PDCA design procedure was used to evaluate the structural performance of bridge columns under a given seismic hazard. To quantify the performance of a column, each performance level was correlated to a possible apparent damage state (DS). Subsequently, each damage state was correlated to an associated damage index (DI). The fragility curves that correlate DSs with DIs were utilized (Vosooghi and Saiidi 2012). An average DI from fragility curves was selected as a representative of the given DS. A comprehensive design matrix was developed to correlate the performance objective with bridge category, earthquake return period, and bridge response parameter (DI). Both qualitative and quantitative performance levels were defined in the matrix. A PDCA method was developed for single column bents (SCBs), two-column bents (TCBs), and four-column bents (FCBs) and discussed. Each bent was designed for a predefined performance level (or DI) under the design earthquake.

The global goal of this study was to provide flexibility to designers to design a bridge column for different probability of exceedance of certain DS and determine the reliability index against failure (β_6') or design the column for a target reliability index against failure (β_6') and determine the probability of exceedance of different DS. Because the knowledge of probability of exceedance of lower damage states (DS3 to DS5) is also important from repair and down time prospective, the reliability against these DSs was also investigated while designing a column for desired β_6'.

To accomplish these objectives, the study was divided into three parts. The first part was to determine the scatter on DI due to earthquake ground motions of different intensities. The reliability of the bents designed as per PDCA was determined in the second part. In the third part, a direct probabilistic design procedure was developed to calibrate design DI based on the desired β_6'.

To conduct reliability analysis, a statistical distribution of the resistance parameter (DI_R) and load parameter (DI_L) was determined. To determine statistical distribution of DI_R, the updated fragility curves to reflect the expansion of column database were utilized (Section 3.7). The statistical distribution of DI_R was developed by utilizing the experimental data of 22 bridge columns. To develop a load model, extensive analytical modeling of seismic response of many SCBs, TCBs, and FCBs bents was conducted. To account for uncertainties in the reliability analysis, a wide range of column variables such as the aspect ratio, support conditions, longitudinal steel ratio, site class, distance to active faults, and the number of columns per bent were included in the study. Each bent was analyzed under 25 earthquake records consisting of 15 near-field and 10 far-field ground motions. For each ground motion, the maximum displacement was determined and consequently DI_L was calculated. A large database of DI_L for SCBs, TCBs, and FCBs was generated. Utilizing this database, a fragility analysis was conducted for SCBs, TCBs, and FCBs to develop load model. After having the resistance and load models, reliability analysis was conducted. The reliability analysis results were analyzed, and a direct probabilistic design method was developed to calibrate the design DI for a desired β_6'.

Finally, an exploratory study was conducted to extend the PDCA and reliability analysis approach to earthquake-damaged columns that have been repaired. This part of the study was focused on columns that are repaired using carbon fiber reinforced polymer (CFRP) jackets. Retrofitted columns were not included in this study. Neither were columns that have been repaired after fracture of reinforcing steel. PDCA was developed based on limited experimental test results and engineering judgments for repaired columns subjected to various earthquake levels. Like conventional original (not repaired) columns, different damage states (DSs) were defined for repaired columns associated with varying degree of damage. In order to define the apparent DSs, the experimental data from the study conducted by Vosooghi and Saiidi 2010 was utilized. The goal of this study was to demonstrate the process to use PDCA for repaired columns, realizing that the study is of limited scope due to the scarcity of data for repaired columns.

7.2 Conclusions

The following conclusions were drawn based on the analytical studies presented in this document:

1. The proposed probabilistic damage control approach (PDCA) for bridge columns provides flexibility to engineers to design a column for different probability of exceedance of certain apparent damage state (DS) that is correlated to a quantifiable damage index (DI) and to determine the associated reliability index against failure and other damage states or design the column for a given target reliability against failure, damage state 6 (DS6) (β_6'), and determine probability of exceedance of other damage states.
2. Even though the design DI was calibrated for the bents based on desired target β_6', the reliability indices for lower damage states (DS3 to DS5) are useful in providing a vision of damage and repair that one can expect when the bent is to be designed for a desired β_6'.
3. The reliability indices against failure were calculated as 3.1, 3.2, and 3.3 for SCBs, TCBs, and FCBs, respectively. The present study shows that β_6 is higher than 3.0 when bents are designed for 50% probability of exceeding DS3 (DI = 0.35) under 1000-year earthquake.
4. The reliability against failure in multicolumn bents is slightly higher than that of single-column bents. This confirms the general perception that multicolumn bents are more reliable than single column bents. The results show that, multicolumn bents can be designed for higher probability of exceeding DS3 without causing a concern for failure.
5. In general, the effect of different steel ratios, support conditions, and aspect ratio on the reliability index was insignificant, except in cases where the bents were controlled by shear.
6. The results show that, the effect of design earthquake return period on the reliability of the structure is insignificant. This is because the lower probability of

exceedance for longer return periods balances the higher demand for these earthquakes.

7. The direct method presented herein can calibrate the design damage index for a desired β_6'. The DI' Tables presented for SCBs, TCBs, and FCBs provides flexibility to the structural designers to design a bridge column for various reliability levels.
8. The reliability based design matrices developed in this study are based on the theoretical failure (start of concrete core damage). Therefore, these design matrices are conservative and have a higher safeguard against the actual failure (bar fracture and/or major concrete core damage).
9. It was found that, the DI_R calculated for repaired columns for DS3, falls in the range of DI_R for DS2 in original standard columns. This is attributed to the lower initial stiffness of repaired columns. Therefore, the DI_R fragility curve for DS2 in conventional columns were utilized as a resistance model for DS3 in repaired columns for reliability analysis.
10. The results show that, the reliability index against failure is 3.0, when the column was repaired for 50% probability of exceeding DS3 (DI = 0.15) under 1000-year earthquake. Whereas in the original column with the same height, diameter, and earthquake return period, the reliability against failure was 3.3. This shows that, to accomplish the same reliability index against failure (β_6'), the repair should be designed for a relatively low design DI.
11. The PDCA procedure developed for repaired columns is based on very limited information about the damage progression in repaired columns. Nonetheless, the procedure can serve as a framework which could be further refined in the future as more data becomes available.

References

AASHTO 2010. "AASHTO LRFD Bridge Design Specification," American Association of State Highway and Transportation Officials, 5th Edition, Washington, D. C.

Alipour, A., Shafei B., and Shinozuka M. (2013). “Reliability-Based Calibration of Load and Resistance Factors for Design of RC Bridges under Multiple Extreme Events: Scour and Earthquake,” Journal of Bridge Engineering, ASCE, Vol. 18. No. 5. May 1, 2013, pp: 362-371.

ASCE/SEI 7-10 (2010), “Minimum Design Loads for Buildings and Other Structures,” American Society of Civil Engineers,” Reston, Virginia 20191.

ATC (2009). “Guidelines for Seismic Performance Assessment of Buildings,” Applied Technology Council, ATC-58 50% Draft, Washington, D.C.

Ayyub, B. and McCuen, R. H. (2003). “Probability, Statistics, and Reliability for Engineers and Scientists,” CRC Press LLC, Boca Raton, Florida.

Bazzurro, P., Cornell, A. C. (2002). “Vector-Values Probabilistic Seismic Hazard Analysis (VP-SHA),” Proceedings of the 7th U.S. National Conference on Earthquake Engineering, Boston, MA.

Benjamin, J. R., and Cornell, C. A. (1970). “Probability, Statistics, and Decision for Civil Engineers,” McGraw-Hill, New York.

Caltrans 2010. “Seismic Design Criteria (SDC),” version 1.6, California Department of Transportation, Sacramento, CA.

Celik, O. C., Ellingwood, B. R. (2010). “Seismic Fragilities for Non-ductile Reinforced Concrete Frames - Role of Aleatoric and Epistemic Uncertainties,” Structural Safety, 32, pp: 1-12.

Choi, E., DesRoches, R., Nielson, B. G. (2004). “Seismic Fragility of Typical Bridges in Moderate Seismic Zones,” Engineering Structures, 26(2), pp: 187-199.

Choi, H., M. Saiidi, P. Somerville, and S. El-Azazy, “An Experimental Study of RC Bridge Columns Subjected to Near-Fault Ground Motions,” American Concrete Institute, ACI Structural Journal, Vol. 107, No. 1, January-February 2010, pp. 3-12.

Cornell, A. C., Krawinkler, H. (2000). “Progress and Challenges in Seismic Performance Assessment,” PEER Center News <http://peer.berkeley.edu/news/2000spring/index.html>.

Cornell, A. C., Jayaler, F., Hamburger, R. O., and Foutch, A. D. (2002). “Probabilistic Basis for 2000 SAC Federal Emergency Management Agency Steel Moment Frame Guidelines,” Journal of Structural Engineering, 128(4), pp: 526-533.

Correal, J., Saiidi, M., Sanders, D. & El-Azazy, S. (2006). “Shake Table Studies of Bridge Columns with Double Interlocking Spirals”, ACI structural journal, June, pp. 393-401.

Ellingwood, B. R., Wen, Y.-K. (2005). “Risk-Benefit-Based Design Decisions for Low-Probability/High Consequence Earthquake Events in Mid-America,” Progress on

Structural Engineering and Materials, 7(2), pp: 56-70.

HAZUS-MH (2011). "Multi-Hazard Loss Estimation Methodology," Earthquake Model HAZUS-MH MR5 Technical Manual, Federal Emergency Management Agency, Washington DC.

Johnson, N., Ranf T., Saiidi, M., Sanders, D. and Eberhard, M. (2008). "Seismic Testing of a Two-Span Reinforced Concrete Bridge", Journal of Bridge Engineering, ASCE, V. 13, No. 2, pp. 173-182.

Kim, S. H., Mha, H. S., Lee, S. W. (2006). "Effects of Bearing Damage upon Seismic Behavior of a Multi-Span Girder Bridge," Engineering Structures, 28(7), pp: 1071-1080.

Liang, Z., and Lee, G. (2013). "Towards Establishing Practical Multi-Hazard Bridge Design Limit States," Earthquake Engineering and Engineering Vibration, Vol. 13. No. 3, September, pp: 333-340.

Lupoi, G., Franchin, P., Lupoi, A., Pinto, P. (2006). "Seismic Fragility Analysis of Structural Systems," Journal of Engineering Mechanics, 132(4), pp: 385-395.

Mackie, K., Stojadinovic, B. (2001). "Probabilistic Seismic Demand Model for California Bridges," Journal of Bridge Engineering, 6, pp: 468-480.

Mackie, K., and Stojadinovic, B. (2005). "Fragility Basis for California Highway Overpass Bridge Seismic Decision Making," PEER Report 2005/02, Pacific Earthquake Engineering Research Center, University of California, Berkeley, CA.

Malek, A., Tourzani, A., Ataya, S. and Mahan, M. (2007), "Probabilistic Damage Control Approach for Seismic Design of Bridges," The 24th Annual International Bridge Conference-IBC 07-76, June 4-6, Hilton Pittsburgh.

Mander, J. B., Priestley, M. J. N., and Park, R. (1988). "Theoretical Stress-Strain Model for Confined Concrete," Journal of Structural Engineering, ASCE, V. 114, No. 8, August, pp. 1804-1826.

Massey, F.J. (1951). "The Kolmogorov-Smirnov Test for Goodness of Fit," Journal of the American Statistical Association, V. 46, No. 253, March, pp. 68-78.

Naeim, F., Hagie, S., Alimoradi, A., and Miranda, E. (2005). "Automated Post-Earthquake Damage Assessment and Safety Evaluation of Instrumented Buildings," Report No. 2005-10639, John A. Martin Associates, Inc., Los Angeles, CA.

NCHRP Report 489 (2003). "Design of Highway Bridges for Extreme Events", National Cooperative Highway Research Program, Transportation Research Board, Washington, D.C.

Nielson, B. G., DesRoches, R. (2007). "Analytical Seismic Fragility Curves for Typical Bridges in the Central and Southeastern United States," Earthquake Spectra, 23, pp: 615-633

Nowak, A.S. and Collins, K.R. (2000). "Reliability of Structures," McGraw-Hills Companies

Nowak, A.S. and Zhou, J. H., (1985), "Reliability Models for Bridge Analysis," Report No. UMCE85-9, University of Michigan, March 1985.

Padgett, J. E., Nielson, B. G., DesRoches, R. (2008). "Selection of Optimal Intensity Measures in Probabilistic Seismic Demand Models of Highway Bridge Portfolios," Earthquake Engineering and Structural Dynamics, 37(5), pp: 711-725.

PEER (2011), "Users Manual for the PEER Ground Motion Database Web Application," Beta Version, November, http://peer.berkeley.edu/peer_ground_motion_database/.

Priestley, M. J. N., Calvi G. M., and Kowalsky M. J. (2007). "Displacement-Based Seismic Design of Structures," IUSS Press, Pavia, Italy.

Saiidi, M., Vosooghi, A., and Nelson, R.B. (2013). "Shake Table Studies of a Four-Span Reinforced Concrete Bridge," Journal of Structural Engineering, ASCE, Special Issue on NEES: Advances in Earthquake Engineering, In press, http://ascelibrary.org/doi/abs/10.1061/%28ASCE%29ST.1943-541X.0000790.

USGS (2008). "NSHMP PSHA Interactive Deaggregation," https://geohazards.usgs.gov/deaggint/2008/index.php, Geologic Hazard Science Center.

Vosooghi, A. and Saiidi, M. (2010). "Seismic Damage States and Response Parameters for Bridge Columns," ACI Special Publications, SP271-02, Structural Concrete in Performance-Based Seismic Design of Bridges, V. 271, May 24, pp. 29-46.

Vosooghi, A. and Saiidi, M. (2012). "Experimental Fragility Curves for Seismic Response of Reinforced Concrete Bridge Columns," ACI Structural Journal, V. 109, No. 6, November-December, pp. 825-834.

Yen, B. C. (1970). ''Risks in Hydrologic Design of Engineering Projects,'' Journal Hydrologic Division, ASCE, 96(4), 959–966.

Zhang, J., Huo, Y. (2009). Evaluating Effectiveness and Optimum Design of Isolation Devices for Highway Bridges using the Fragility Function Method, Engineering Structures, 31, pp: 1648-1660.

Tables

Chapter 2. Tables

Table 2-1. Database of single column and bridge models

Column model		Scale	Design code	Ground motion	Aspect ratio	Section dimensions, in	Long. steel ratio, %	Trans. steel ratio, %
328 [a]		0.5	BDS 1993	Quasi-static	3.0	24	2.8	0.9
828 [a]		0.5	ATC-32	Quasi-static	8.0	24	2.8	0.9
Bridge II [b]	B2E-II	0.25	NCHRP 12-49	Synthetic fault rupture	4.0	12	1.56	0.84
	B2W-II	0.25	NCHRP 12-49	Synthetic fault rupture	4.0	12	1.56	0.84
MN [b]		0.29	Caltrans 2004	Rinaldi	4.5	14	2.86	1.37
ETN [b]		0.29	Caltrans 2004	Rinaldi	7.75	14	2.86	1.54
SETN [b]		0.29	New spectrum	Rinaldi/RRS (Synthetic)	7.75	14	3.62	2.05
SVTN [b]		0.2	New spectrum	Rinaldi/RRS (Synthetic	8.21	12	3.0	1.82
ISH 1.0 [c]		0.2	Caltrans 2001	Sylmar Hospital	2.0	10 x 14.5	2.9	0.6
ISH 1.25 [c]		0.2	Caltrans 2001	Sylmar Hospital	2.0	10 x 15.62	2.8	0.9
ISH 1.50 [c]		0.2	Caltrans 2001	Sylmar Hospital	2.1	10 x 16.75	2.9	0.9
ISH 1.50T [c]		0.2	Caltrans 2001	Sylmar Hospital	2.1	10 x 16.75	2.9	0.9
ISL 1.0 [c]		0.25	Caltrans 2001	Sylmar Hospital	3.3	12 x 17.5	2.0	1.1
ISL 1.5 [c]		0.25	Caltrans 2001	Sylmar Hospital	3.6	12 x 20.25	2.0	1.1
Bridge-I [d]	N1E-I	0.25	NCHRP 12-49	CCN	3.0	12	1.56	0.84
	B1W-I	0.25	NCHRP 12-49	CCN	3.0	12	1.56	0.84
	B2E-I	0.25	NCHRP 12-49	CCN	4.0	12	1.56	0.84
	B2W-I	0.25	NCHRP 12-49	CCN	4.0	12	1.56	0.84
	B3E-I	0.25	NCHRP 12-49	CCN	2.5	12	1.56	0.84
	B3W-I	0.25	NCHRP 12-49	CCN	2.5	12	1.56	0.84
407 [e]		0.33	Caltrans 1991	Quasi-static	4.0	24	0.75	0.7
415 [e]		0.33	Caltrans 1991	Quasi-static	4.0	24	1.50	0.7
430 [e]		0.33	Caltrans 1991	Quasi-static	4.0	24	3.0	0.7
825 [e]		0.33	Caltrans 1991	Quasi-static	8.0	24	1.50	0.7
1015 [e]		0.33	Caltrans 1991	Quasi-static	10.0	24	1.50	0.7
NF-1 [f]		0.33	Caltrans 2004	Rinaldi	4.5	16	2.0	0.92
NF-2 [f]		0.33	AASHTO 2002	Rinaldi	4.5	16	2.2	1.10
RSC [g]		0.2	NCHRP 12-49	Quasi-static	4.5	10	2.04	0.74
SC-CAL [h]		0.25	Caltrans 1994	Artificial	4.5	12	2.83	0.66
SC-PBD [h]		0.25	PBD	Artificial	4.5	12	2.83	1.05
NHS1 [i]		0.33	Caltrans 2006	Sylmar Hospital	2.5	16	3.08	1.38
NHS2 [i]		0.33	Caltrans 2006	Sylmar Hospital	2.5	16	3.08	1.38
BENT 1 [j]	**B1E**	0.25	NCHRP 12-49	Northridge	5.0	12	1.56	0.86
	B1W	0.25	NCHRP 12-49	Northridge	5.0	12	1.56	0.86
BENT 2 [j]	B2E	0.25	NCHRP 12-49	Northridge	7.0	12	1.56	0.86
	B2W	0.25	NCHRP 12-49	Northridge	7.0	12	1.56	0.86
BENT 3 [j]	B3E	0.25	NCHRP 12-49	Northridge	6.0	12	1.56	0.86
	B3W	0.25	NCHRP 12-49	Northridge	6.0	12	1.56	0.86

[a] Calderone et al. (2001), [b] Choi et al. (2007, 2010), [c] Correal et al. (2006), [d] Johnson et al. (2008)
[e] Lehman and Moehle (2000), [f] Phan et al. (2007), [g] Saiidi et al. (2009), [h] Saiidi and Mortensen (2002)
[i] Vosooghi and Saiidi (2010), [j] Nelson et al. (2010)

Table 2-2. Magnitudes of $d_{\alpha}(N)$ (Massey et al. 1951)

Sample size (N)	Level of significance (α)				
	0.20	0.15	0.10	0.05	0.01
1	0.900	0.925	0.950	0.975	0.995
2	0.684	0.726	0.776	0.842	0.929
3	0.565	0.597	0.642	0.708	0.828
4	0.494	0.525	0.564	0.624	0.733
5	0.446	0.474	0.510	0.565	0.669
6	0.410	0.436	0.470	0.521	0.618
7	0.381	0.405	0.438	0.486	0.577
8	0.358	0.381	0.411	0.457	0.543
9	0.339	0.360	0.388	0.432	0.514
10	0.322	0.342	0.368	0.410	0.490
11	0.307	0.326	0.352	0.391	0.468
12	0.295	0.313	0.338	0.375	0.450
13	0.284	0.302	0.325	0.361	0.433
14	0.274	0.292	0.314	0.349	0.418
15	0.266	0.283	0.304	0.338	0.404
16	0.258	0.274	0.295	0.328	0.392
17	0.250	0.266	0.286	0.318	0.381
18	0.244	0.259	0.278	0.309	0.371
19	0.237	0.252	0.272	0.301	0.363
20	0.231	0.246	0.264	0.294	0.356
25	0.21	0.22	0.24	0.27	0.32
30	0.19	0.20	0.22	0.24	0.29
35	0.18	0.19	0.21	0.23	0.27
over 35	$\frac{1.07}{\sqrt{N}}$	$\frac{1.14}{\sqrt{N}}$	$\frac{1.22}{\sqrt{N}}$	$\frac{1.36}{\sqrt{N}}$	$\frac{1.63}{\sqrt{N}}$

Table 2-3. Design performance levels

Damage State DS	Service to Public	Service to Emergency	Emergency Repair	Design Damage Index DI	Earthquake Levels (Years)			
					O-ST	O-NST	Rec.	Imp.
DS-1	Yes	Yes	No	0	100	500	1000	1500
DS-2	Yes	Yes	Yes, only plastic hinge	0.15	500	1000	1500	2500
DS-3	No	Yes, 1 lane	Yes, entire column	0.35	1000	1500	2500	NA
DS-4	No	Yes, 1 lane	Yes, entire column	0.55	1500	2500	NA	NA
DS-5	No	No	Yes, entire column	0.8	2500	NA	NA	NA
DS-6	No	No	NA	1	NA	NA	NA	NA

O-ST = Ordinary Standard Bridge
O-NST = Ordinary Non Standard Bridge
Rec. = Recovery Bridge
Imp. = Important Bridge
NA = Not Applicable

Table 2-4. Soil profile types

Soil Profile Type	Soil Profile Description[a]
A	**Hard rock with measured shear wave velocity $v_{S30} > 5000$ ft/s (1,500 m/s)**
B	**Rock with shear wave velocity $2{,}500 < v_{S30} < 5000$ ft/s (760m/s $< v_{S30} <$ 1,500 m/s)**
C	**Very dense soil and soft rock with shear wave velocity $1{,}200 < v_{S30} < 2{,}500$ ft/s (360m/s $< v_{S30} <$ 760 m/s) or with either standard penetration resistance $N > 50$ or undrained shear strength $s_u \geq 2{,}000$ psf (100 kPa)**
D	**Stiff soil with shear wave velocity $600 < v_{S30} < 1{,}200$ ft/s (180 m/s $< v_{S30} <$ 360 m/s) or with either standard penetration resistance $15 \leq N \leq 50$ or undrained shear strength $1{,}000 < s_u < 2{,}000$ psf ($50 < s_u < 100$ kPa)**
E	**A soil profile with shear wave velocity $v_{S30} < 600$ ft/s (180 m/s) or any profile with more than 10 ft (3 m) of soft clay, defined as soil with plasticity index $PI > 20$, water content $w \geq 40$ percent, and undrained shear strength $s_u < 500$ psf (25 kPa)**
F	**Soil requiring site-specific evaluation:** **1. Soils vulnerable to potential failure or collapse under seismic loading; i.e. liquefiable soils, quick and highly sensitive clays, collapsible weakly-cemented soils** **2. Peat and/or highly organic clay layers more than 10 ft (3 m) thick** **3. Very high-plasticity clay ($PI > 75$) layers more than 25 ft (8 m) thick** **4. Soft-to-medium clay layers more than 120 ft (36 m) thick**

Chapter 3. Tables

Table 3-1. Complete schedule of shake table testing (Saiidi et al. 2013)

Test No.	Motion Level	Test Type	Target Motion PGA (g)	
			Trans.	Long.
WN01		White Noise (Transverse)		
WN02		White Noise (Longitudinal)		
1A	1	W/Restrainer1	-	0. 09
1B	1	W/Restrainer2	-	0. 09
1C	1	Longitudinal	-	0. 09
1D	1	Biaxial	0. 075	0. 09
WN11		White Noise (Transverse))		
WN12		White Noise (Longitudinal)		
2	2	Biaxial	0. 15	0. 18
WN21		White Noise (Transverse)		
WN22		White Noise (Longitudinal)		
3	3	Biaxial	0. 25	0. 30
WN31		White Noise (Transverse))		
WN32		White Noise (Longitudinal)		
4A	4	W/Restrainer1	-	0. 60
4B	4	W/Restrainer2	-	0. 60
4C	4	Longitudinal	-	0. 60
4D	4	Biaxial	0. 50	0. 60
WN41		White Noise (Transverse)		
WN42		White Noise (Longitudinal)		
5	5	Biaxial	0. 75	0. 90
WN51		White Noise (Transverse)		
WN52		White Noise (Longitudinal)		
6	6	Biaxial	1. 00	1. 20
WN61		White Noise (Transverse)		
WN62		White Noise (Longitudinal)		
7	7	Biaxial	1. 00	1. 20

Table 3-2. Observed performance of bent 1 east column bottom plastic hinge

Test no.	Observed performance	Damage state
1A	No damage	-
1B	No damage	-
1C	No damage	-
1D	Flexural cracks	DS 1
2	Flexural cracks	-
3	More flexural cracks and spalling begin, few shear cracks	DS 2
4A	More shear cracks, concrete spalling	-
4B	Extensive flexural and shear cracks	-
4C	Extensive flexural and shear cracks	-
4D	Extensive spalling , one visible lateral bar	DS 3
5	Extensive spalling, two visible lateral reinforcement	DS 4
6	Visible five lateral and three longitudinal reinforcement, start of core damage	DS 5
7	Failure of column with fractured longitudinal and lateral reinforcement	DS 6

Table 3-3. Observed performance of bent 1 east column top plastic hinge

Test no.	Observed performance	Damage state
1A	No damage	-
1B	No damage	-
1C	No damage	-
1D	Flexural cracks	DS 1
2	Flexural cracks, crack width is from 0.016 to 0.025 inch	-
3	Flexural cracks	-
4A	Flexural cracks	-
4B	More flexural cracks	-
4C	More flexural cracks, few shear cracks, spalling begin	DS 2
4D	Extensive spalling, one slightly visible lateral bar	DS 3
5	Extensive spalling, one visible lateral bar	-
6	Extensive spalling and two visible lateral bars	DS 4
7	Extensive spalling, visible four lateral and three longitudinal reinforcements.	DS 5

Table 3-4. Observed performance of bent 1 west column bottom plastic hinge

Test no.	Observed Performance	Damage State
1A	No damage	-
1B	No damage	-
1C	No damage	-
1D	No damage	-
2	No damage	-
3	Flexural cracks	DS 1
4A	Spalling of cover concrete begin	DS 2
4B	More flexural cracks	-
4D	Extensive spalling, no visible lateral bar	DS 3
5	Extensive spalling , more shear and flexural cracks, one lateral bar slightly visible	DS 4
6	Extensive spalling and visible lateral reinforcement	-
7	Visible lateral and longitudinal reinforcement, start of core damage, and few longitudinal bars are buckled	DS 5

Table 3-5. Observed performance of bent 1 west column top plastic hinge

Test no.	Observed performance	Damage state
1A	No damage	-
1B	No damage	-
1C	No damage	-
1D	Flexural cracks	DS 1
2	Flexural cracks	-
3	Flexural cracks	-
4A	Flexural cracks	-
4B	Flexural cracks	-
4C	More flexural cracks	-
4D	More flexural cracks and spalling begin	DS 2
5	More spalling and shear cracks	DS 3
6	Extensive spalling , more shear and flexural cracks, one visible lateral bar	-
7	Extensive spalling, 3 visible lateral bars	DS 4

Table 3-6. Observed performance of bent 2 east column bottom plastic hinge

Test no.	Observed performance	Damage state
1A	No damage	-
1B	No damage	-
1C	No damage	-
1D	No damage	-
2	No damage	-
3	Flexural cracks	DS 1
4A	Flexural cracks	-
4B	Flexural cracks	-
4C	Flexural cracks	-
4D	Flexural cracks, crack width 0.007 inch	-
5	Extensive spalling of cover concrete.	DS 3
6	Extensive spalling, two lateral bars are visible.	DS 4
7	Extensive spalling, three lateral bars are visible	-

Table 3-7. Observed performance of bent 2 east column top plastic hinge

Test no.	Observed performance	Damage state
1A	No damage	-
1B	No damage	-
1C	No damage	-
1D	No damage	-
2	No damage	-
3	Flexural cracks	DS 1
4A	Flexural cracks	-
4B	Flexural cracks	-
4C	Flexural cracks	-
4D	Flexural cracks	-
5	shear cracks	DS 2
6	Extensive spalling of cover concrete	DS 3
7	Extensive spalling and shear cracks	-

Table 3-8. Observed performance of bent 2 west column bottom plastic hinge

Test no.	Observed performance	Damage state
1A	No damage	-
1B	No damage	-
1C	No damage	-
1D	No damage	-
2	Flexural cracks	DS 1
3	Flexural cracks	-
4A	Flexural cracks	-
4B	Flexural cracks	-
4C	Flexural cracks	-
4D	Flexural cracks 0.01 inch	-
5	Spalling begin and few shear cracks	DS 2
6	Extensive spalling of cover concrete	DS 3
7	Extensive spalling, two lateral bars are visible	DS 4

Table 3-9. Observed performance of bent 2 west column top plastic hinge

Test no.	Observed performance	Damage state
1A	No damage	-
1B	No damage	-
1C	No damage	-
1D	No damage	-
2	Flexural cracks	DS 1
3	Flexural cracks	-
4A	Flexural cracks	-
4B	Flexural cracks	-
4C	Flexural cracks	-
4D	Flexural cracks	-
5	Flexural cracks 0.01 inch	-
6	shear cracks but no spalling occur	DS 2
7	shear cracks but no spalling occur	-

Table 3-10. Observed performance of bent 3 east column bottom plastic hinge

Test no.	Observed performance	Damage state
1A	No Damage	-
1B	No Damage	-
1C	No Damage	-
1D	No Damage	-
2	No damage	-
3	Flexural cracks	DS 1
4A	Flexural cracks	-
4B	More flexural cracks	-
4C	More flexural cracks	-
4D	Spalling of cover concrete begin	DS 2
5	Extensive spalling, two lateral bars visible	DS 3
6	extensive spalling, two lateral bars visible, core was still intact	-
7	Extensive spalling, four lateral bars visible	DS 4

Table 3-11. Observed performance of bent 3 east column top plastic hinge

Test no.	Observed performance	Damage state
1A	No damage	-
1B	No damage	-
1C	No damage	-
1D	No damage	-
2	No damage	-
3	No damage	-
4A	No damage	-
4B	No damage	-
4C	No damage	-
4D	Spalling of cover concrete begin	DS 2
5	Extensive spalling of cover concrete	DS 3
6	Extensive spalling, one lateral bar is visible	DS 4
7	Extensive spalling , two visible lateral bars	-

Table 3-12. Observed performance of bent 3 west column bottom plastic hinge

Test no.	Observed performance	Damage state
1A	No damage	-
1B	No damage	-
1C	No damage	-
1D	No damage	-
2	No damage	-
3	Flexural cracks	DS 1
4A	More flexural cracks	-
4B	More flexural cracks	-
4C	More flexural cracks	-
4D	Extensive spalling , three visible lateral bars	DS 4
5	Approaching to damage state 5	-
6	Extensive spalling and start of core damage, five lateral and two long bars are visible	DS 5
7	Extensive core damage, four longitudinal and nine lateral bars visible	-

Table 3-13. Observed performance of bent 3 west column top plastic hinge

Test no.	Observed performance	Damage state
1A	No damage	-
1B	No damage	-
1C	No damage	-
1D	No damage	-
2	No damage	-
3	No damage	-
4A	No damage	-
4B	No damage	-
4C	No damage	-
4D	Extensive spalling of cover concrete	DS 3
5	Extensive spalling and shear cracks, two lateral bars are visible	DS 4
6	Extensive spalling, more shear and flexural cracks, four visible lateral bars	-
7	Extensive spalling, more shear and flexural cracks, five visible lateral bars	-

Table 3-14. Maximum drift ratio corresponds to a given damage

Damage State	Maximum Drift Ratios					
	Bent 1		Bent 2		Bent 3	
	East Column	West Column	East Column	West Column	East Column	West Column
DS 1	1.1%	1.1%	2.3%	1.4%	2.9%	2.9%
DS 2	3.4%	-	-	4.4%	4.8%	-
DS 3	5.1%	5.1%	4.4%	5.0%	6.6%	-
DS 4	6.0%	6.0%	5.0%	5.1%	8.8%	4.8%
DS 5	8.0%	9.0%	-	-	-	8.8%
DS 6	9.0%	-	-	-	-	-

Table 3-15. Residual drift ratio corresponds to a given damage state

Damage State	Residual Drift Ratios					
	Bent 1		Bent 2		Bent 3	
	East Column	West Column	East Column	West Column	East Column	West Column
DS 1	0.2%	0.2%	0.1%	0.2%	0.1%	0.1%
DS 2	0.2%	-	-	0.1%	0.4%	-
DS 3	0.3%	0.3%	0.1%	0.2%	0.7%	-
DS 4	0.6%	1.6%	0.5%	0.5%	1.5%	0.4%
DS 5	1.6%	2.7%	-	-	-	1.5%
DS 6	2.7%	-	-	-	-	-

Table 3-16. Frequency ratio corresponds to a given damage state

Damage State	Frequency Ratios					
	Bent 1		Bent 2		Bent 3	
	East Column.	West Column	East Column	West Column	East Column.	West Column
DS 1	52.7%	52.7%	45.6%	58.6%	55.1%	55.2%
DS 2	30.4%	-	-	33.4%	42.8%	-
DS 3	24.7%	24.7%	33.4%	31.1%	36.7%	-
DS 4	22.7%	22.7%	31.1%	30.9%	31.8%	42.8%
DS 5	19.7%	18.6%	-	-	-	31.8%
DS 6	18.6%	-	-	-	-	-

Table 3-17. Damage index of bent 1 East column

Damage State	Maximum Displacement D [in]	Effective Yield Displacement D_Y [in]	Ultimate Displacement D_U [in]	Damage Index DI
DS 1	0.67	0.18	5.38	0.09
DS 2	2.02			0.35
DS 3	3.06			0.55
DS 4	3.62			0.66
DS 5	4.82			0.89
DS 6	5.38			1.00

Table 3-18. Maximum average strain in the column longitudinal bars (microstrain)

Damage State	Bent 1		Bent 2		Bent 3	
	East Column.	West Column	East Column	West Column	East Column.	West Column
DS 1	9298	20729	7859	2708	16540	16465
DS 2	16948	18745	6602	20283	29396	-
DS 3	29558	30248	19117	26610	37380	11275
DS 4	37555	56775	23262	27072	40709	28746
DS 5	39541	-	-	-	-	43574

Table 3-19. Maximum average strain in the column transverse bars (microstrain)

Damage State	Bent 1		Bent 2		Bent 3	
	East Column.	West Column	East Column	West Column	East Column.	West Column
DS 1	432	673	310	178	264	719
DS 2	580	987	355	581	2468	-
DS 3	1520	2112	598	1229	3438	905
DS 4	2861	4466	894	1715	3866	1696
DS 5	6314	4720	-	-		1861

Table 3-20. Median and logarithmic standard deviation of response parameters

		DS-1	DS-2	DS-3	DS-4	DS-5	DS-6
MDR	Median	0.016	0.028	0.043	0.060	0.079	0.089
	Logrithmic Standard Deviation	0.425	0.332	0.264	0.303	0.353	0.284
RDR	Median	0.001	0.002	0.002	0.008	0.014	NA
	Logrithmic Standard Deviation	1.702	0.991	1.843	1.317	1.403	
FR	Median	0.783	0.662	0.526	0.424	0.368	
	Logrithmic Standard Deviation	0.219	0.247	0.295	0.273	0.279	
DI	Median	NA	0.167	0.360	0.589	0.805	
	Logrithmic Standard Deviation	NA	0.418	0.259	0.203	0.147	
MLS	Median	9148	18523	25183	32607	43125	
	Logrithmic Standard Deviation	0.711	0.368	0.303	0.278	0.319	
MTS	Median	329	704	1096	1791	2222	
	Logrithmic Standard Deviation	0.418	0.495	0.530	0.581	0.646	

Note: NA is not applicable.

Chapter 4. Tables

Table 4-1. Ground motions for site class B/C

	NGA No.	Event Name	Magnitude	PGA	$(S_a)_{1sec}$	R_{jb}	V_{S30}	Design Spectrum $(S_a)_{1sec}$=0.4658g Scale Factor
				g	g	km	m/sec	↓
FAR FIELD	164	Imperial Valley	6.53	0.157	0.294	15.2	659.6	1.58
	286	Irpinia, Italy	6.90	0.083	0.255	17.5	1000.0	1.83
	369	Coalinga, US	6.36	0.153	0.269	26.0	684.9	1.73
	755	Loma Prieta	6.93	0.484	0.364	20.0	597.1	1.28
	769	Loma Prieta	6.93	0.170	0.205	17.9	663.3	2.27
	994	Northridge	6.69	0.289	0.361	21.2	1015.9	1.29
	1091	Northridge	6.69	0.139	0.199	23.1	996.4	2.34
	1234	Chi-Chi Taiwan	7.62	0.204	0.298	27.6	680.0	1.56
	1482	Chi-Chi Taiwan	7.62	0.206	0.350	19.9	540.7	1.33
	2626	Chi-Chi Taiwan	6.20	0.224	0.302	18.5	573.0	1.54
NEAR FIELD	126	Gazli, USSR	6.80	0.608	0.797	3.9	659.6	0.58
	143	Tabas, Iran	7.35	0.836	0.713	1.8	766.8	0.65
	265	Victoria, Mexico	6.33	0.621	0.589	13.8	659.6	0.79
	292	Irpinia, Italy	6.9	0.358	0.375	6.8	1000.0	1.24
	495	Nahanni, Canada	6.76	1.096	0.485	2.5	659.6	0.96
	765	Loma Prieta	6.93	0.473	0.310	8.8	1428.0	1.50
	810	Loma Prieta	6.93	0.450	0.298	12.0	714.0	1.56
	828	Cape Mendocino, CA	7.01	0.662	0.985	0.0	712.8	0.47
	879	Landers, CA	7.28	0.727	0.476	2.2	684.9	0.98
	1013	Northridge	6.69	0.511	0.706	0.0	629.0	0.66
	1080	Northridge	6.69	0.877	0.736	0.0	557.4	0.63
	1111	Kobe, Japan	6.9	0.509	0.305	7.1	609.0	1.53
	1197	Chi-Chi, Taiwan	7.62	0.821	1.046	3.1	542.6	0.45
	1517	Chi-Chi, Taiwan	7.62	1.157	2.546	0.0	680.0	0.18
	1787	Hector Mine	7.13	0.337	0.373	10.3	684.9	1.25

Table 4-2. Ground motions for site class D

	NGA No.	Event Name	Magnitude	PGA	$(S_a)_{1sec}$	R_{jb}	V_{S30}	Design Spectrum $(S_a)_{1sec}$=0.845g Scale Factor
				g	g	km	m/sec	↓
FAR FIELD	169	Imperial Valley-06	6.53	0.351	0.481	22.0	274.5	1.76
	338	Coalinga-01	6.36	0.282	1.023	28.1	338.5	0.83
	729	Superstition Hills-02	6.54	0.207	0.440	23.9	207.5	1.92
	778	Loma Prieta	6.93	0.279	0.548	24.5	215.5	1.54
	900	Landers	7.28	0.245	0.499	23.6	353.6	1.69
	978	Northridge-01	6.69	0.246	0.585	17.8	234.9	1.44
	995	Northridge-01	6.69	0.358	0.452	19.7	316.5	1.87
	1003	Northridge-01	6.69	0.439	0.496	21.2	308.7	1.70
	1107	Kobe, Japan	6.90	0.345	0.352	22.5	312.0	2.40
	1203	Chi-Chi, Taiwan	7.62	0.294	0.615	16.1	233.1	1.37
NEAR FIELD	160	Bonds Corner, Imperial Valley-06	6.53	0.775	0.447	0.5	223.0	1.89
	180	El Centro Array#5, Imperial Valley-06	6.53	0.379	0.678	1.8	205.6	1.25
	183	El Centro Array#8, Imperial Valley-06	6.53	0.602	0.365	3.9	206.1	2.31
	368	Pleasant Valley P.P.-Yard, Coalinga-01	6.36	0.592	0.991	7.7	257.4	0.85
	461	Morgan Hill	6.19	0.312	0.423	3.5	281.6	2.00
	529	N. Palm Springs	6.06	0.594	0.859	0.0	345.4	0.98
	723	Parachute Test Site, Superstitons Hills-02	6.54	0.455	0.970	0.9	348.7	0.87
	752	Capitola, Loma Prieta	6.93	0.529	0.456	8.7	288.6	1.85
	821	Erzincan, Turkey	6.69	0.515	0.848	0.0	274.5	1.00
	829	Rio Dell Overpass-FF, Cape Mendocino	7.01	0.385	0.538	7.9	311.8	1.57
	953	Northridge-01	6.69	0.416	1.019	9.4	355.8	0.83
	1063	Northridge-01	6.69	0.825	1.826	0.0	282.2	0.46
	1087	Northridge-01	6.69	1.779	0.787	0.4	257.2	1.07
	1106	Kobe, Japan	6.90	0.821	1.501	0.9	312	0.56
	1503	Chi-Chi Taiwan	7.62	0.814	1.313	0.6	305.9	0.64

Table 4-3. Design spectrum values for site B/C and D

Period	T = 1000 Years		T = 1500 Years		T = 2500 Years	
	Site B/C	Site D	Site B/C	Site D	Site B/C	Site D
	Sa, g		Sa, g		Sa, g	
0	0.636	0.643	0.749	0.729	0.899	0.842
0.1	1.341	1.080	1.583	1.209	1.914	1.399
0.2	1.596	1.361	1.883	1.533	2.306	1.780
0.3	1.328	1.400	1.572	1.594	1.915	1.849
0.5	0.934	1.275	1.103	1.471	1.359	1.745
1	0.466	0.845	0.549	0.982	0.673	1.181
2	0.196	0.420	0.227	0.489	0.273	0.586
3	0.114	0.257	0.131	0.296	0.156	0.353
4	0.078	0.179	0.090	0.206	0.107	0.245
5	0.063	0.145	0.074	0.168	0.088	0.200

Table 4-4. Column diameter and bar size for 1%, 2%, and 3% longitudinal reinforcement

Diameter, D in (mm)	Longitudinal Steel Ratio	Longitudinal Reinforcement
48 (1219)	1%	14 #10
	2%	16 #14
	3%	24 #14
60 (1524)	1%	22 #10
	2%	26 #14
	3%	38 #14
72 (1829)	1%	32 #10
	2%	36 #14
	3%	54 #14

Table 4-5. Single column bent models designed for T = 1000-year

Site Class	Configuration	H/D	Steel Ratio		Period	Δ_Y	Δ_D	Δ_C	DI	V_n / V_s+V_c
			Long.	Trans.	Sec	in	in	in		
B/C	Cantilever	5	1%	0.17%	1.22	3.2	5.3	9.3	0.35	0.82
			2%	*0.23%*	*1.04*	*3.7*	*4.7*	*9.5*	*0.17*	*0.95*
	Fixed-Fixed		*1%*	*0.61%*	*0.64*	*1.8*	*2.9*	*9.9*	*0.13*	*0.98*
D	Cantilever	5	1%	1.05%	1.23	3.5	10.1	22.5	0.346	0.32
			2%	0.84%	1.04	4.0	8.6	17.0	0.353	0.48
			3%	0.66%	0.91	4.0	7.3	13.3	0.351	0.69
	Fixed-Fixed	5	*1%*	*0.53%*	*0.64*	*1.8*	*4.4*	*9.9*	*0.32*	*0.98*
			2%	*0.24%*	*0.55*	*2.3*	*3.6*	*13.1*	*0.12*	*0.87*
			3%	*0.09%*	*0.48*	*2.4*	*2.9*	*13.4*	*0.05*	*0.98*
	Cantilever	10	1%	0.44%	3.39	12.6	24.7	47.2	0.35	0.26
			2%	0.30%	2.84	14.0	21.7	35.8	0.352	0.41
			3%	0.20%	2.49	14.2	19.5	29.5	0.349	0.59
	Fixed-Fixed	10	1%	0.48%	1.73	6.7	14.2	28.2	0.353	0.53
			2%	0.30%	1.47	7.5	12.1	20.7	0.349	0.87
			3%	*0.18%*	*1.29*	*7.8*	*10.6*	*20.6*	*0.22*	*0.97*
	Cantilever	7.5	1%	1.14%	1.91	5.4	15.7	35.0	0.347	0.19
			2%	0.92%	1.65	6.4	13.5	26.6	0.35	0.29
			3%	0.75%	1.46	6.5	12.0	22.0	0.35	0.43
	Fixed-Fixed	7.5	1%	0.84%	1.01	2.9	8.3	18.1	0.35	0.44
			2%	0.50%	0.89	3.6	7.0	13.2	0.35	0.94
			3%	*0.31%*	*0.79*	*3.8*	*5.9*	*14.6*	*0.2*	*0.92*
	Cantilever	15	1%	0.50%	5.23	19.3	38.9	75.2	0.35	0.16
			2%	0.22%	4.44	21.6	31.3	50.3	0.35	0.30
			3%	0.08%	3.92	22.1	27.6	38.2	0.35	0.47
	Fixed-Fixed	15	1%	0.41%	2.70	10.2	20.8	41.3	0.35	0.40
			2%	0.25%	2.32	11.9	18.5	30.4	0.35	0.59
			3%	0.18%	2.05	12.3	16.8	25.6	0.35	0.81

Table 4-6. Single column bent models designed for T = 1500-year

Site Class	Configuration	H/D	Steel Ratio		Period	Δ_Y	Δ_D	Δ_C	DI	V_n / V_s+V_c
			Long.	Trans.	Sec	in	in	in		
D	Cantilever	5	1%	1.32%	1.23	3.6	11.8	26.4	0.35	0.23
			2%	1.19%	1.04	4.1	10.0	20.9	0.35	0.39
			3%	0.97%	0.91	4.1	8.4	16.3	0.35	0.57
	Fixed-Fixed	5	1%	0.74%	0.64	1.9	5.1	11.0	0.35	0.78
			2%	0.41%	0.55	2.1	4.2	8.0	0.35	1.74
			3%	0.26%	0.48	2.2	3.4	6.0	0.35	2.50
	Cantilever	10	1%	0.61%	3.38	12.9	28.5	55.7	0.35	0.21
			2%	0.52%	2.84	14.4	25.0	45.2	0.35	0.31
			3%	0.42%	2.50	14.6	22.7	37.5	0.35	0.42
	Fixed-Fixed	10	1%	0.71%	1.73	6.8	16.6	34.6	0.35	0.42
			2%	0.52%	1.47	7.7	14.1	26.4	0.35	0.66
			3%	0.40%	1.29	7.8	12.4	21.1	0.35	0.92

Table 4-7. Two column bent models designed for T = 1000-year

Site Class	Configuration	H/D	Steel Ratio		Period	Δ_Y	Δ_D	Δ_C	DI	V_n / V_s+V_c
			Long.	Trans.	Sec	in	in	in		
D	Fixed-Pinned	5	1%	1.45%	1.30	4.1	10.7	22.7	0.35	0.22
			2%	0.86%	1.16	5.2	9.5	17.1	0.35	0.51
			3%	0.66%	1.06	5.7	8.7	14.7	0.35	0.73
	Fixed-Fixed	5	1%	0.61%	0.70	2.4	5.0	9.4	0.35	1.05
			2%	*0.79%*	*0.64*	*3.3*	*4.4*	*12.8*	*0.12*	*1.04*
			3%	*1.32%*	*0.58*	*3.7*	*3.8*	*13.5*	*0.01*	*1.05*
	Fixed-Pinned	6	1%	1.06%	1.62	5.2	13.3	28.0	0.35	0.28
			2%	0.83%	1.38	6.2	11.3	20.7	0.35	0.39
			3%	0.63%	1.26	6.6	10.4	17.4	0.35	0.54
	Fixed-Fixed	6	1%	0.75%	0.86	2.8	6.7	13.7	0.35	0.52
			2%	*0.45%*	*0.76*	*3.7*	*5.6*	*10.4*	*0.29*	*1.00*
			3%	*0.97%*	*0.69*	*4.1*	*4.9*	*11.3*	*0.11*	*1.00*
	Fixed-Pinned	10	1%	0.44%	3.62	14.9	25.9	47.3	0.35	0.27
			2%	0.15%	3.13	17.2	23.3	34.4	0.35	0.64
			3%	*0.11%*	*2.81*	*18.4*	*21.5*	*32.0*	*0.22*	*1.01*
	Fixed-Fixed	10	1%	0.56%	1.87	8.2	15.3	29.2	0.35	0.48
			2%	0.30%	1.63	9.7	13.5	21.2	0.35	0.91
			3%	*0.31%*	*1.47*	*10.5*	*12.0*	*21.5*	*0.14*	*1.02*
	Fixed-Pinned	12	1%	0.32%	4.41	18.1	31.0	56.5	0.35	0.31
	Fixed-Fixed	12	1%	0.50%	2.28	9.6	18.1	34.1	0.35	0.44
			2%	0.21%	1.95	11.5	16.0	24.2	0.35	0.98

Table 4-8. Four column bent models designed for T = 1000-year

Site Class	Configuration	H/D	Steel Ratio		Period	Δ_Y	Δ_D	Δ_C	DI	V_n / V_s+V_c
			Long.	Trans.	Sec	in	in	in		
D	Fixed-Pinned	7.5	1%	1.14%	2.06	6.5	16.8	34.4	0.35	0.20
			2%	0.92%	1.85	8.0	15.2	28.6	0.35	0.29
			3%	0.61%	1.67	8.5	13.7	23.3	0.35	0.49
	Fixed-Fixed	7.5	1%	0.49%	1.12	4.0	9.3	20.0	0.35	1.00
			2%	*0.53%*	*1.04*	*5.5*	*8.6*	*17.8*	*0.25*	*0.99*
			3%	*0.71%*	*0.96*	*6.1*	*7.7*	*19.8*	*0.12*	*1.00*

Table 4-9. DI_L for cantilever SCBs with D = 4', H = 30', Site D, and T = 1000

	NGA No.	Long. Steel = 1%		Long. Steel = 2%		Long. Steel = 3%	
		Trans. Steel = 1.14%		Trans. Steel = 0.92%		Trans. Steel = 0.75%	
		Δ_D in	DI_L	Δ_D in	DI_L	Δ_D in	DI_L
Far Field	169	17.44	0.41	7.71	0.07	10.50	0.26
	338	15.16	0.33	10.71	0.22	9.31	0.18
	729	12.37	0.24	14.09	0.38	15.62	0.59
	778	*35.04*	1.00	14.53	0.40	15.48	0.58
	900	12.75	0.25	10.55	0.21	10.96	0.29
	978	16.84	0.39	12.62	0.31	12.00	0.35
	995	11.15	0.19	8.65	0.11	8.58	0.13
	1003	16.16	0.36	10.13	0.19	13.22	0.43
	1107	8.94	0.12	8.98	0.13	12.25	0.37
	1203	10.13	0.16	11.24	0.24	11.42	0.32
Near Field	160	11.36	0.20	9.54	0.16	10.57	0.26
	180	*35.04*	1.00	40.14	1.00	27.17	1.00
	183	16.24	0.37	12.49	0.30	10.38	0.25
	368	15.30	0.33	9.16	0.14	9.12	0.17
	461	12.82	0.25	13.10	0.33	10.56	0.26
	529	15.84	0.35	13.17	0.34	10.64	0.27
	723	14.00	0.29	17.46	0.55	14.47	0.51
	752	10.92	0.19	7.94	0.08	6.21	-0.02
	821	13.34	0.27	13.44	0.35	14.13	0.49
	829	11.40	0.20	12.94	0.33	9.99	0.22
	953	16.62	0.38	7.69	0.07	10.61	0.26
	1063	14.93	0.32	10.37	0.20	11.67	0.33
	1087	16.50	0.37	14.10	0.38	9.61	0.20
	1106	12.66	0.24	10.62	0.21	10.12	0.23
	1503	12.00	0.22	14.39	0.40	13.85	0.47

Table 4-10. DI_L for cantilever SCBs with D = 4', H = 30', Site D, and T = 2500

	NGA No.	Long. Steel = 1% Trans. Steel = 1.14%		Long. Steel = 2% Trans. Steel = 0.92%		Long. Steel = 3% Trans. Steel = 0.75%	
		Δ_D in	DI_L	Δ_D in	DI_L	Δ_D in	DI_L
Far Field	169	*35.04*	1.00	9.42	0.15	13.23	0.43
	338	19.30	0.47	15.41	0.45	12.37	0.38
	729	50.07	1.00	18.66	0.61	18.49	0.77
	778	*35.04*	1.00	27.46	1.00	25.96	1.00
	900	25.43	0.68	13.22	0.34	13.93	0.48
	978	27.88	0.76	17.86	0.57	17.72	0.72
	995	13.77	0.28	9.88	0.17	10.65	0.27
	1003	25.29	0.67	13.14	0.34	17.21	0.69
	1107	9.14	0.13	12.20	0.29	16.60	0.65
	1203	14.99	0.32	12.25	0.29	15.58	0.59
Near Field	160	18.40	0.44	12.21	0.29	14.08	0.49
	180	*35.04*	1.00	26.56	1.00	21.99	1.00
	183	28.00	0.76	16.60	0.51	15.11	0.56
	368	27.22	0.74	13.10	0.33	11.44	0.32
	461	15.71	0.35	17.77	0.57	14.76	0.53
	529	21.82	0.55	18.98	0.62	15.41	0.57
	723	18.38	0.44	21.96	0.77	23.17	1.00
	752	18.80	0.45	10.69	0.21	7.56	0.07
	821	20.69	0.52	18.80	0.62	17.69	0.72
	829	14.71	0.31	15.62	0.46	14.45	0.51
	953	23.63	0.62	10.21	0.19	14.86	0.54
	1063	22.14	0.56	14.13	0.38	13.77	0.47
	1087	18.60	0.45	21.94	0.77	14.43	0.51
	1106	18.50	0.44	13.26	0.34	12.27	0.37
	1503	*35.04*	1.00	27.13	1.00	21.62	0.98

Table 4-11. DI_L for fixed-fixed SCBs with D = 4’, H = 30’, Site D, and T = 1000

	NGA No.	Long. Steel = 1% Trans. Steel = 0.84%		Long. Steel = 2% Trans. Steel = 0.50%		Long. Steel = 3% Trans. Steel = 0.71%	
		Δ_D (in)	DI_L	Δ_D (in)	DI_L	Δ_D (in)	DI_L
Far Field	169	7.77	0.32	6.61	0.32	7.84	0.37
	338	5.40	0.16	7.96	0.46	9.61	0.54
	729	5.80	0.19	7.47	0.41	5.54	0.16
	778	5.18	0.15	5.61	0.21	6.30	0.23
	900	9.60	0.44	7.32	0.39	7.92	0.38
	978	5.53	0.17	5.18	0.17	6.35	0.24
	995	6.30	0.22	5.36	0.19	5.54	0.16
	1003	5.76	0.19	7.88	0.45	7.29	0.32
	1107	7.32	0.29	12.57	0.94	7.77	0.37
	1203	3.86	0.06	6.33	0.29	4.93	0.10
Near Field	160	6.73	0.25	6.83	0.34	4.66	0.08
	180	8.00	0.33	8.55	0.52	11.39	0.70
	183	12.85	0.65	9.28	0.60	6.39	0.24
	368	5.36	0.16	6.93	0.35	6.14	0.22
	461	8.78	0.39	5.61	0.21	5.71	0.18
	529	6.39	0.23	8.55	0.52	9.31	0.51
	723	16.22	0.88	13.62	1.00	6.33	0.23
	752	8.05	0.34	7.54	0.41	4.93	0.11
	821	11.37	0.56	10.11	0.68	9.62	0.54
	829	8.10	0.34	9.02	0.57	7.14	0.31
	953	6.87	0.26	5.83	0.24	6.62	0.26
	1063	9.22	0.41	7.78	0.44	6.96	0.29
	1087	7.60	0.31	5.28	0.18	5.22	0.13
	1106	5.89	0.20	6.59	0.31	7.24	0.32
	1503	6.11	0.21	8.80	0.55	8.63	0.45

Table 4-12. DI_L for fixed-fixed SCBs with D = 4’, H = 30’, Site D, and T = 2500

	NGA No.	Long. Steel = 1% Trans. Steel = 0.84% Δ_D in	DIL	Long. Steel = 2% Trans. Steel = 0.50% Δ_D in	DIL	Long. Steel = 3% Trans. Steel = 0.71% Δ_D in	DIL
Far Field	169	14.45	0.76	9.39	0.61	11.09	0.68
	338	6.58	0.24	10.07	0.68	12.08	0.77
	729	8.44	0.36	11.42	0.82	7.65	0.36
	778	6.15	0.21	6.15	0.27	8.56	0.44
	900	17.25	0.94	12.47	0.93	10.41	0.61
	978	7.54	0.30	6.74	0.33	8.36	0.42
	995	7.21	0.28	7.09	0.37	6.65	0.26
	1003	7.35	0.29	10.39	0.71	10.58	0.63
	1107	12.87	0.65	21.00	1.00	11.99	0.76
	1203	4.64	0.11	7.82	0.44	6.74	0.27
	160	8.53	0.37	9.74	0.64	6.07	0.21
Near Field	180	13.21	0.68	10.65	0.74	14.02	0.95
	183	23.10	1.00	14.66	1.00	10.42	0.61
	368	6.91	0.26	9.51	0.62	6.92	0.29
	461	12.66	0.64	8.18	0.48	7.21	0.32
	529	10.06	0.47	9.51	0.62	11.59	0.72
	723	32.77	1.00	25.91	1.00	12.70	0.82
	752	14.97	0.79	9.75	0.64	7.28	0.32
	821	18.99	1.00	17.41	1.00	16.69	1.00
	829	9.97	0.46	14.56	1.00	10.99	0.67
	953	8.01	0.33	7.72	0.43	8.34	0.42
	1063	12.49	0.63	12.00	0.88	10.80	0.65
	1087	12.83	0.65	6.72	0.33	7.00	0.30
	1106	7.37	0.29	7.08	0.37	9.06	0.49
	1503	8.32	0.36	12.97	0.98	11.18	0.68

Table 4-13. DI_L for cantilever SCBs with D = 4', H = 60', Site D, and T = 1000

	NGA No.	Long. Steel = 1%	Long. Steel = 2%		Long. Steel = 3%	
			Trans. Steel = 0.22%		Trans. Steel = 0.13%	
			Δ_D in	DI_L	Δ_D in	DI_L
Far Field	169	No data for 1% steel	22.44	0.03	31.88	0.52
	338		22.83	0.04	20.57	-0.09
	729		19.20	-0.08	13.31	-0.48
	778		44.82	0.81	25.71	0.19
	900		38.94	0.60	58.43	1.00
	978		30.79	0.32	26.61	0.24
	995		26.27	0.16	15.80	-0.35
	1003		18.72	-0.10	24.41	0.12
	1107		33.64	0.42	28.38	0.33
	1203		19.78	-0.06	12.72	-0.51
Near Field	160		38.72	0.60	41.60	1.00
	180		28.63	0.24	25.55	0.18
	183		31.78	0.35	29.42	0.39
	368		22.17	0.02	27.45	0.28
	461		22.76	0.04	26.97	0.26
	529		27.06	0.19	23.63	0.08
	723		29.81	0.29	28.85	0.36
	752		38.61	0.59	30.58	0.45
	821		26.64	0.17	21.79	-0.02
	829		*50.32*	1.00	43.60	1.00
	953		20.56	-0.04	28.44	0.33
	1063		18.73	-0.10	24.94	0.15
	1087		33.60	0.42	28.09	0.32
	1106		18.35	-0.11	22.25	0.00
	1503		20.70	-0.03	31.34	0.49

Table 4-14. DI_L for cantilever SCBs with D = 4', H = 60', Site D, and T = 2500

	NGA No.	Long. Steel = 1%	Long. Steel = 2%		Long. Steel = 3%	
			Trans. Steel = 0.22%		Trans. Steel = 0.13%	
			Δ_D in	DI_L	Δ_D in	DI_L
Far Field	169	No data for 1% steel	29.92	0.29	40.70	1.00
	338		29.32	0.27	27.59	0.34
	729		27.79	0.21	18.20	-0.24
	778		*50.32*	1.00	30.81	0.54
	900		*50.32*	1.00	53.08	1.00
	978		42.49	0.73	34.87	0.80
	995		39.49	0.62	21.43	-0.04
	1003		23.10	0.05	33.00	0.68
	1107		50.32	1.00	39.53	1.00
	1203		26.49	0.17	16.95	-0.32
	160		38.55	0.59	55.30	1.00
Near Field	180		39.29	0.62	35.23	0.82
	183		64.80	1.00	42.00	1.00
	368		28.71	0.25	35.22	0.82
	461		31.93	0.36	36.18	0.88
	529		36.25	0.51	32.10	0.62
	723		41.87	0.71	38.26	1.00
	752		50.76	1.00	42.08	1.00
	821		36.05	0.50	29.51	0.46
	829		*50.32*	1.00	38.16	1.00
	953		28.18	0.23	38.57	1.00
	1063		25.37	0.13	33.90	0.74
	1087		50.32	1.00	37.70	0.97
	1106		24.93	0.11	30.34	0.51
	1503		28.35	0.23	39.05	1.00

Table 4-15. DI_L for fixed-fixed SCBs with D = 4', H = 60', Site D, and T = 1000

	NGA No.	Long. Steel = 1% Trans. Steel = 0.41%		Long. Steel = 2% Trans. Steel = 0.25%		Long. Steel = 3% Trans. Steel = 0.18%	
		Δ_D in	DI_L	Δ_D in	DI_L	Δ_D in	DI_L
Far Field	169	18.76	0.27	19.87	0.43	16.15	0.29
	338	17.22	0.23	14.80	0.16	16.02	0.28
	729	18.24	0.26	13.61	0.09	12.72	0.03
	778	17.23	0.23	24.44	0.68	19.68	0.56
	900	24.63	0.46	19.64	0.42	16.76	0.34
	978	17.86	0.25	14.94	0.16	17.37	0.38
	995	15.23	0.16	15.61	0.20	16.45	0.31
	1003	17.61	0.24	16.63	0.26	18.47	0.47
	1107	17.55	0.24	12.23	0.02	6.59	-0.43
	1203	*41.33*	1.00	21.01	0.49	10.54	-0.13
Near Field	160	17.57	0.24	12.50	0.03	11.29	-0.07
	180	19.88	0.31	22.90	0.60	25.96	1.00
	183	23.53	0.43	17.99	0.33	14.85	0.19
	368	15.08	0.16	18.51	0.36	16.54	0.32
	461	16.75	0.21	17.51	0.30	15.55	0.25
	529	19.51	0.30	16.50	0.25	15.63	0.25
	723	20.72	0.34	16.73	0.26	16.24	0.30
	752	10.69	0.02	18.19	0.34	17.25	0.37
	821	14.83	0.15	16.53	0.25	16.91	0.35
	829	14.62	0.14	15.43	0.19	15.78	0.26
	953	12.85	0.08	19.59	0.42	21.27	0.68
	1063	16.84	0.21	20.60	0.47	15.85	0.27
	1087	27.69	0.56	13.98	0.11	15.10	0.21
	1106	19.61	0.30	18.87	0.38	13.24	0.07
	1503	14.45	0.14	17.80	0.32	12.90	0.05

Table 4-16. DI_L for fixed-fixed SCBs with D = 4’, H = 60’, Site D, and T = 2500

	NGA No.	Long. Steel = 1% Trans. Steel = 0.41%		Long. Steel = 2% Trans. Steel = 0.25%		Long. Steel = 3% Trans. Steel = 0.18%	
		Δ_D in	DI_L	Δ_D in	DI_L	Δ_D in	DI_L
Far Field	169	18.65	0.27	27.73	0.86	22.63	0.78
	338	21.92	0.38	20.38	0.46	22.48	0.77
	729	19.99	0.31	18.34	0.35	15.96	0.28
	778	26.60	0.53	34.64	1.00	33.96	1.00
	900	30.59	0.65	25.67	0.75	23.09	0.81
	978	21.26	0.35	18.15	0.34	23.59	0.85
	995	19.51	0.30	20.83	0.48	23.28	0.83
	1003	23.92	0.44	22.89	0.59	26.42	1.00
	1107	25.85	0.50	15.67	0.20	8.88	-0.26
	1203	*41.33*	1.00	34.91	1.00	14.15	0.14
Near Field	160	*41.33*	1.00	17.02	0.28	15.25	0.22
	180	34.17	0.77	29.59	0.96	40.33	1.00
	183	35.12	0.80	26.70	0.80	21.35	0.68
	368	21.75	0.37	26.00	0.76	23.27	0.83
	461	21.94	0.38	20.84	0.48	21.85	0.72
	529	25.86	0.50	22.84	0.59	21.87	0.72
	723	26.23	0.51	23.84	0.65	23.67	0.86
	752	18.85	0.28	20.17	0.45	24.20	0.90
	821	20.92	0.34	19.58	0.42	22.15	0.74
	829	21.83	0.37	20.65	0.47	21.98	0.73
	953	19.57	0.30	26.90	0.81	30.91	1.00
	1063	24.67	0.46	29.47	0.95	22.58	0.77
	1087	32.22	0.71	18.84	0.38	20.36	0.61
	1106	28.17	0.58	27.69	0.86	19.10	0.51
	1503	25.09	0.48	32.94	1.00	17.59	0.40

Table 4-17. DI_L for cantilever SCBs with D = 6', H = 30', Site B, and T = 1000

	NGA No.	Long. Steel = 1%		Long. Steel = 2%		Long. Steel = 3%
		Trans. Steel = 0.17%		Trans. Steel = 0.23%		
		Δ_D in	DI_L	Δ_D in	DI_L	
Far Field	164	3.22	0.00	4.55	0.15	No data for 3% steel
	286	5.42	0.36	3.57	-0.02	
	369	3.52	0.05	5.02	0.23	
	755	4.29	0.18	4.74	0.18	
	769	4.84	0.27	4.95	0.21	
	994	4.60	0.23	3.80	0.02	
	1091	4.90	0.28	4.00	0.05	
	1234	4.95	0.28	4.39	0.12	
	1482	5.53	0.38	4.49	0.13	
	2626	5.31	0.34	4.71	0.17	
Near Field	126	6.16	0.48	4.24	0.09	
	143	4.19	0.16	5.96	0.39	
	265	3.96	0.12	4.61	0.16	
	292	6.24	0.50	5.13	0.25	
	495	4.28	0.17	3.34	-0.06	
	765	5.27	0.34	4.01	0.05	
	810	3.71	0.08	4.40	0.12	
	828	5.11	0.31	4.37	0.11	
	879	6.26	0.50	6.54	0.49	
	1013	4.01	0.13	5.00	0.22	
	1080	5.42	0.36	3.71	0.00	
	1111	4.73	0.25	4.80	0.19	
	1197	5.30	0.34	4.77	0.18	
	1517	4.32	0.18	5.47	0.30	
	1787	5.33	0.35	6.64	0.51	

Table 4-18. DI_L for cantilever SCBs with D = 6', H = 30', Site B, and T = 2500

	NGA No.	Long. Steel = 1%		Long. Steel = 2%		Long. Steel = 3%
		Trans. Steel = 0.17%		Trans. Steel = 0.23%		
		Δ_D in	DI_L	Δ_D in	DI_L	
Far Field	164	3.88	0.11	6.13	0.42	No data for 3% steel
	286	7.33	0.68	5.24	0.26	
	369	4.46	0.20	5.85	0.37	
	755	6.27	0.50	6.66	0.51	
	769	6.37	0.52	6.54	0.49	
	994	6.10	0.47	4.93	0.21	
	1091	6.45	0.53	5.13	0.25	
	1234	6.84	0.60	5.32	0.28	
	1482	8.24	0.83	7.93	0.73	
	2626	7.24	0.66	6.90	0.55	
Near Field	126	8.31	0.84	5.76	0.36	
	143	5.92	0.44	9.21	0.95	
	265	4.58	0.22	5.73	0.35	
	292	10.50	1.00	8.44	0.82	
	495	5.40	0.36	4.80	0.19	
	765	8.20	0.82	6.51	0.48	
	810	4.89	0.27	5.44	0.30	
	828	8.08	0.80	5.38	0.29	
	879	11.20	1.00	12.57	1.00	
	1013	5.95	0.45	7.58	0.67	
	1080	5.60	0.39	5.15	0.25	
	1111	7.58	0.72	5.95	0.39	
	1197	6.77	0.58	7.08	0.58	
	1517	5.26	0.34	6.60	0.50	
	1787	6.39	0.52	9.15	0.94	

Table 4-19. DI_L for fixed-fixed SCBs with D = 6’, H = 30’, Site B, and T = 1000

	NGA No.	Long. Steel = 1%		Long. Steel = 2%	Long. Steel = 3%
		Trans. Steel = 0.61%			
		Δ_D in	DI_L		
Far Field	164	1.95	0.01	No data for 2% steel	No data for 3% steel
	286	4.00	0.27		
	369	3.50	0.21		
	755	2.27	0.05		
	769	2.44	0.08		
	994	2.76	0.12		
	1091	2.21	0.05		
	1234	3.59	0.22		
	1482	3.47	0.20		
	2626	3.01	0.15		
Near Field	126	2.60	0.10		
	143	3.48	0.20		
	265	2.37	0.07		
	292	4.44	0.32		
	495	2.60	0.09		
	765	2.70	0.11		
	810	3.00	0.14		
	828	2.46	0.08		
	879	3.58	0.22		
	1013	3.48	0.20		
	1080	2.54	0.09		
	1111	2.60	0.09		
	1197	3.29	0.18		
	1517	3.60	0.22		
	1787	2.95	0.14		

Table 4-20. DI_L for fixed-fixed SCBs with D = 6', H = 30', Site B, and T = 2500

	NGA No.	Long. Steel = 1% Trans. Steel = 0.17% Δ_D (in)	DI_L	Long. Steel = 2%	Long. Steel = 3%
Far Field	164	2.76	0.11	No data for 2% steel	No data for 3% steel
	286	8.32	0.80		
	369	5.68	0.48		
	755	2.76	0.12		
	769	3.85	0.25		
	994	3.42	0.20		
	1091	2.74	0.11		
	1234	5.83	0.49		
	1482	5.23	0.42		
	2626	4.97	0.39		
Near Field	126	3.47	0.20		
	143	5.09	0.40		
	265	2.93	0.14		
	292	10.17	1.00		
	495	4.00	0.27		
	765	3.92	0.26		
	810	5.03	0.40		
	828	2.95	0.14		
	879	7.72	0.73		
	1013	6.47	0.57		
	1080	3.43	0.20		
	1111	3.29	0.18		
	1197	4.49	0.33		
	1517	7.05	0.65		
	1787	4.97	0.39		

Table 4-21. DI_L for cantilever SCBs with D = 6', H = 30', Site D, and T = 1000

	NGA No.	Long. Steel = 1%		Long. Steel = 2%		Long. Steel = 3%	
		Trans. Steel = 1.05%		Trans. Steel = 0.84%		Trans. Steel = 0.66%	
		Δ_D in	DI_L	Δ_D in	DI_L	Δ_D in	DI_L
Far Field	169	12.19	0.46	7.88	0.30	6.58	0.28
	338	6.00	0.13	5.63	0.13	7.85	0.41
	729	9.16	0.30	10.07	0.47	7.79	0.41
	778	9.91	0.34	6.27	0.18	5.71	0.18
	900	10.33	0.36	9.53	0.43	7.42	0.37
	978	6.66	0.17	6.27	0.18	5.82	0.19
	995	5.72	0.12	6.19	0.17	5.79	0.19
	1003	9.79	0.33	6.09	0.16	8.43	0.48
	1107	12.11	0.45	6.55	0.20	10.78	0.73
	1203	9.56	0.32	6.12	0.16	6.56	0.27
Near Field	160	5.12	0.08	7.58	0.28	7.52	0.38
	180	16.32	0.67	6.91	0.23	8.54	0.49
	183	7.83	0.23	11.32	0.56	9.52	0.59
	368	6.39	0.15	5.82	0.14	6.55	0.27
	461	9.72	0.33	7.92	0.30	5.95	0.21
	529	8.20	0.25	7.42	0.26	8.70	0.50
	723	14.65	0.59	16.13	0.93	11.38	0.79
	752	6.11	0.14	7.93	0.30	8.53	0.49
	821	11.15	0.40	9.79	0.45	9.75	0.62
	829	8.38	0.26	9.20	0.40	9.31	0.57
	953	6.78	0.17	7.93	0.30	5.98	0.21
	1063	9.68	0.33	9.04	0.39	7.94	0.42
	1087	8.28	0.25	7.50	0.27	5.47	0.16
	1106	7.76	0.22	6.21	0.17	6.75	0.29
	1503	6.62	0.16	5.96	0.15	8.55	0.49

Table 4-22. DI_L for cantilever SCBs with D = 6', H = 30', Site D, and T = 2500

	NGA No.	Long. Steel = 1%, Trans. Steel = 1.14%		Long. Steel = 2%, Trans. Steel = 0.92%		Long. Steel = 3%, Trans. Steel = 0.75%	
		Δ_D in	DI_L	Δ_D in	DI_L	Δ_D in	DI_L
Far Field	169	14.26	0.57	15.46	0.88	8.26	0.46
	338	6.64	0.16	7.30	0.26	9.20	0.56
	729	12.19	0.46	15.10	0.85	9.95	0.64
	778	16.16	0.67	7.43	0.27	6.41	0.26
	900	13.57	0.53	18.28	1.00	8.82	0.52
	978	9.16	0.30	7.30	0.26	7.20	0.34
	995	7.36	0.20	7.86	0.30	7.00	0.32
	1003	16.44	0.68	7.26	0.25	9.90	0.63
	1107	14.24	0.57	9.39	0.42	16.42	1.00
	1203	12.76	0.49	8.29	0.33	7.77	0.40
Near Field	160	6.57	0.16	8.74	0.37	10.22	0.67
	180	*22.49*	1.00	10.97	0.54	9.83	0.62
	183	10.00	0.34	19.11	1.00	13.27	0.99
	368	9.29	0.30	7.97	0.31	8.72	0.51
	461	13.31	0.52	11.40	0.57	7.86	0.41
	529	12.49	0.47	9.44	0.42	9.70	0.61
	723	18.87	0.81	24.38	1.00	19.77	1.00
	752	10.32	0.36	11.39	0.57	10.29	0.67
	821	18.21	0.77	16.17	0.94	14.45	1.00
	829	10.35	0.36	12.28	0.64	13.29	1.00
	953	8.94	0.29	9.71	0.44	7.72	0.40
	1063	11.77	0.44	12.95	0.69	11.10	0.76
	1087	14.06	0.56	11.42	0.57	6.99	0.32
	1106	10.04	0.34	8.46	0.34	7.34	0.36
	1503	11.36	0.41	7.64	0.28	11.13	0.76

Table 4-23. DI_L for fixed-fixed SCBs with D = 6’, H = 30’, Site D, and T = 1000

	NGA No.	Long. Steel = 1% Trans. Steel = 0.61%		Long. Steel = 2% Trans. Steel = 1.02%		Long. Steel = 3% Trans. Steel = 1.31%	
		Δ_D in	DI_L	Δ_D in	DI_L	Δ_D in	DI_L
Far Field	169	3.14	0.16	4.18	0.18	4.20	0.17
	338	7.72	0.73	2.76	0.05	3.35	0.09
	729	4.08	0.28	4.11	0.17	3.88	0.14
	778	3.92	0.26	3.79	0.14	4.41	0.19
	900	5.77	0.49	5.32	0.28	3.64	0.12
	978	4.87	0.38	4.90	0.24	5.01	0.24
	995	3.32	0.18	3.20	0.09	3.70	0.12
	1003	5.00	0.39	3.04	0.07	3.20	0.08
	1107	4.40	0.32	3.71	0.13	4.63	0.21
	1203	4.47	0.33	3.40	0.10	4.07	0.15
Near Field	160	2.76	0.12	3.57	0.12	4.53	0.20
	180	8.24	0.79	3.63	0.13	2.76	0.04
	183	3.88	0.25	3.69	0.13	3.32	0.09
	368	4.26	0.30	3.05	0.07	3.21	0.08
	461	3.78	0.24	3.89	0.15	4.81	0.22
	529	7.68	0.72	5.31	0.28	3.41	0.10
	723	5.22	0.42	5.26	0.28	3.49	0.10
	752	2.99	0.14	4.53	0.21	4.30	0.18
	821	8.58	0.83	6.66	0.40	4.29	0.18
	829	4.60	0.34	5.57	0.30	3.89	0.14
	953	6.00	0.52	2.55	0.03	4.00	0.15
	1063	6.60	0.59	6.27	0.37	4.07	0.15
	1087	4.78	0.36	3.93	0.15	2.67	0.03
	1106	6.09	0.53	3.58	0.12	2.37	0.00
	1503	7.19	0.66	4.90	0.24	4.55	0.20

Table 4-24. DI_L for fixed-fixed SCBs with D = 6', H = 30', Site D, and T = 2500

	NGA No.	Long. Steel = 1% Trans. Steel = 0.61%		Long. Steel = 2% Trans. Steel = 1.02%		Long. Steel = 3% Trans. Steel = 1.31%	
		Δ_D in	DI_L	Δ_D in	DI_L	Δ_D in	DI_L
Far Field	169	3.98	0.27	5.15	0.27	5.37	0.27
	338	11.36	1.00	4.75	0.23	5.05	0.24
	729	4.84	0.37	5.47	0.30	5.36	0.27
	778	4.73	0.36	4.97	0.25	5.52	0.29
	900	9.14	0.91	8.96	0.62	6.00	0.33
	978	6.82	0.62	6.88	0.43	7.85	0.50
	995	4.77	0.36	4.18	0.18	4.58	0.20
	1003	6.97	0.64	4.15	0.17	3.73	0.12
	1107	7.00	0.64	4.76	0.23	3.13	0.07
	1203	5.73	0.48	4.98	0.25	5.50	0.29
Near Field	160	3.66	0.23	4.28	0.19	6.05	0.34
	180	13.25	1.00	5.65	0.31	3.83	0.13
	183	5.85	0.50	5.53	0.30	4.92	0.23
	368	4.81	0.37	4.21	0.18	4.21	0.17
	461	5.67	0.48	4.50	0.21	6.51	0.38
	529	9.52	0.95	11.80	0.88	6.28	0.36
	723	10.01	1.00	12.79	0.97	5.53	0.29
	752	3.68	0.23	5.18	0.27	5.88	0.32
	821	17.15	1.00	14.18	1.00	8.08	0.52
	829	6.34	0.56	7.79	0.51	5.89	0.32
	953	8.32	0.80	3.51	0.11	5.60	0.29
	1063	10.61	1.00	11.03	0.81	6.99	0.42
	1087	5.97	0.51	5.63	0.31	3.52	0.10
	1106	7.83	0.74	7.39	0.47	3.20	0.08
	1503	12.20	1.00	10.60	0.77	10.01	0.70

Table 4-25. DI_L for cantilever SCBs with D = 6', H = 60', Site D, and T = 1000

	NGA No.	Long. Steel = 1%		Long. Steel = 2%		Long. Steel = 3%	
		Trans. Steel = 0.44%		Trans. Steel = 0.30%		Trans. Steel = 0.20%	
		Δ_D in	DI_L	Δ_D in	DI_L	Δ_D in	DI_L
Far Field	169	23.49	0.31	21.31	0.34	15.74	0.10
	338	17.35	0.14	18.88	0.22	18.18	0.26
	729	14.14	0.04	19.47	0.25	19.44	0.34
	778	16.57	0.11	18.60	0.21	25.25	0.72
	900	42.32	0.86	23.16	0.42	22.07	0.51
	978	19.63	0.20	17.76	0.17	14.33	0.01
	995	16.89	0.12	16.92	0.14	14.39	0.01
	1003	19.83	0.21	18.23	0.20	16.01	0.12
	1107	25.92	0.38	21.43	0.34	13.41	-0.05
	1203	21.33	0.25	41.44	1.00	32.70	1.00
Near Field	160	44.53	0.92	17.76	0.17	14.59	0.03
	180	23.98	0.33	23.82	0.45	24.42	0.67
	183	30.35	0.51	24.61	0.49	21.09	0.45
	368	24.35	0.34	17.48	0.16	16.59	0.16
	461	30.23	0.51	16.99	0.14	14.82	0.04
	529	22.19	0.28	20.00	0.28	18.06	0.25
	723	20.50	0.23	22.42	0.39	16.39	0.14
	752	17.77	0.15	15.75	0.08	15.43	0.08
	821	19.46	0.20	17.29	0.15	16.37	0.14
	829	26.59	0.40	18.44	0.20	15.21	0.07
	953	23.76	0.32	16.91	0.13	18.00	0.25
	1063	25.05	0.36	22.77	0.40	21.30	0.46
	1087	26.20	0.39	24.02	0.46	15.67	0.10
	1106	17.48	0.14	21.27	0.33	22.15	0.52
	1503	31.34	0.54	35.86	1.00	18.89	0.31

Table 4-26. DI_L for cantilever SCBs with D = 6', H = 60', Site D, and T = 2500

	NGA No.	Long. Steel = 1%		Long. Steel = 2%		Long. Steel = 3%	
		Trans. Steel = 0.44%		Trans. Steel = 0.30%		Trans. Steel = 0.20%	
		Δ_D in	DI_L	Δ_D in	DI_L	Δ_D in	DI_L
Far Field	169	25.10	0.36	28.78	0.68	22.65	0.55
	338	20.33	0.22	21.95	0.37	21.61	0.48
	729	18.01	0.16	23.69	0.45	28.68	0.95
	778	21.66	0.26	25.36	0.52	31.37	1.00
	900	38.12	0.74	35.17	0.97	27.83	0.89
	978	20.75	0.23	23.35	0.43	19.93	0.37
	995	23.09	0.30	21.69	0.35	19.20	0.33
	1003	27.86	0.44	24.20	0.47	21.72	0.49
	1107	45.58	0.95	31.42	0.80	18.32	0.27
	1203	24.72	0.35	59.30	1.00	51.32	1.00
Near Field	160	*47.19*	1.00	35.54	0.99	19.60	0.35
	180	*47.19*	1.00	29.26	0.70	28.43	0.93
	183	46.83	0.99	35.89	1.00	30.76	1.00
	368	26.68	0.41	24.91	0.50	22.99	0.57
	461	42.98	0.88	22.98	0.41	20.09	0.38
	529	28.70	0.46	27.40	0.61	24.97	0.70
	723	24.02	0.33	30.46	0.75	23.08	0.58
	752	29.43	0.49	20.45	0.30	19.73	0.36
	821	26.60	0.40	21.35	0.34	21.50	0.48
	829	47.63	1.00	25.67	0.54	20.57	0.42
	953	33.29	0.60	22.77	0.40	24.21	0.65
	1063	34.72	0.64	31.98	0.82	30.10	1.00
	1087	44.11	0.91	34.00	0.92	21.97	0.51
	1106	23.09	0.30	27.88	0.64	31.64	1.00
	1503	*47.19*	1.00	52.57	1.00	37.32	1.00

Table 4-27. DI_L for fixed-fixed SCBs with D = 6’, H = 60’, Site D, and T = 1000

	NGA No.	Long. Steel = 1%		Long. Steel = 2%		Long. Steel = 3%	
		Trans. Steel = 0.48%		Trans. Steel = 0.30%		Trans. Steel = 0.36%	
		Δ_D in	DI_L	Δ_D in	DI_L	Δ_D in	DI_L
Far Field	169	9.14	0.12	11.66	0.32	16.40	0.67
	338	11.96	0.25	10.52	0.23	7.86	0.01
	729	12.80	0.29	15.48	0.60	9.81	0.16
	778	17.34	0.50	12.97	0.41	10.20	0.19
	900	11.50	0.23	11.58	0.31	10.78	0.24
	978	14.00	0.34	10.97	0.26	8.46	0.05
	995	9.12	0.11	8.85	0.10	8.81	0.08
	1003	10.40	0.17	13.21	0.43	12.09	0.34
	1107	8.58	0.09	13.88	0.48	11.16	0.27
	1203	11.18	0.21	10.79	0.25	14.31	0.51
Near Field	160	12.56	0.27	11.58	0.31	7.92	0.01
	180	29.10	1.00	20.10	0.95	14.24	0.51
	183	13.00	0.29	9.84	0.18	9.41	0.13
	368	10.48	0.18	9.61	0.16	9.13	0.11
	461	14.11	0.35	11.00	0.27	11.16	0.27
	529	14.23	0.35	10.57	0.23	9.88	0.16
	723	15.80	0.42	13.09	0.42	15.36	0.59
	752	9.94	0.15	7.22	-0.02	9.69	0.15
	821	14.19	0.35	14.62	0.54	12.90	0.40
	829	11.90	0.24	10.16	0.20	8.07	0.02
	953	20.95	0.66	11.52	0.30	10.46	0.21
	1063	10.93	0.20	11.97	0.34	10.37	0.20
	1087	15.01	0.39	9.13	0.12	10.35	0.20
	1106	11.02	0.20	10.29	0.21	10.43	0.21
	1503	11.01	0.20	12.54	0.38	10.00	0.17

Table 4-28. DI_L for fixed-fixed SCBs with D = 6', H = 60', Site D, and T = 2500

	NGA No.	Long. Steel = 1%		Long. Steel = 2%		Long. Steel = 3%	
		Trans. Steel = 0.48%		Trans. Steel = 0.30%		Trans. Steel = 0.36%	
		Δ_D in	DI_L	Δ_D in	DI_L	Δ_D in	DI_L
Far Field	169	11.77	0.24	13.68	0.47	19.45	0.91
	338	17.00	0.48	12.30	0.36	10.97	0.25
	729	15.13	0.39	20.41	0.97	14.42	0.52
	778	30.86	1.00	21.36	1.00	12.94	0.40
	900	14.38	0.36	15.38	0.60	15.73	0.62
	978	19.64	0.60	16.49	0.68	12.08	0.34
	995	11.74	0.24	11.93	0.34	11.44	0.29
	1003	13.42	0.31	18.43	0.83	18.03	0.80
	1107	11.95	0.25	16.03	0.64	14.84	0.55
	1203	12.81	0.29	14.49	0.53	14.80	0.55
Near Field	160	13.14	0.30	14.01	0.49	11.22	0.27
	180	72.82	1.00	40.48	1.00	25.26	1.00
	183	17.18	0.49	14.74	0.55	11.45	0.29
	368	14.90	0.38	11.53	0.31	12.19	0.35
	461	19.09	0.58	15.33	0.59	15.63	0.61
	529	20.26	0.63	15.18	0.58	12.13	0.34
	723	20.75	0.65	20.58	0.99	23.33	1.00
	752	12.59	0.28	8.93	0.11	12.41	0.36
	821	17.86	0.52	18.83	0.86	17.27	0.74
	829	14.42	0.36	14.37	0.52	11.30	0.28
	953	32.59	1.00	14.85	0.56	15.10	0.57
	1063	14.94	0.39	15.69	0.62	14.89	0.56
	1087	23.53	0.78	13.25	0.43	12.67	0.38
	1106	13.58	0.32	13.42	0.45	13.21	0.43
	1503	21.60	0.69	19.18	0.88	13.04	0.41

Table 4-29. DI_L for cantilever SCBs with D = 6', H = 30', Site D, and T = 1500

	NGA No.	Long. Steel = 1% Trans. Steel = 1.32%		Long. Steel = 2% Trans. Steel = 1.19%		Long. Steel = 3% Trans. Steel = 0.97%	
		Δ_D in	DI_L	Δ_D in	DI_L	Δ_D in	DI_L
Far Field	169	12.90	0.41	10.58	0.39	7.47	0.27
	338	6.27	0.12	6.27	0.13	8.57	0.36
	729	10.79	0.32	12.23	0.48	8.94	0.39
	778	12.41	0.39	6.97	0.17	6.20	0.17
	900	11.84	0.36	13.24	0.54	8.12	0.33
	978	7.62	0.18	6.47	0.14	6.31	0.18
	995	6.35	0.12	7.04	0.17	6.17	0.17
	1003	12.79	0.40	6.18	0.12	9.43	0.43
	1107	13.44	0.43	7.71	0.21	13.31	0.75
	1203	11.87	0.36	7.27	0.19	7.13	0.25
Near Field	160	5.94	0.10	7.87	0.22	9.45	0.44
	180	22.78	0.84	8.06	0.24	9.31	0.42
	183	9.24	0.25	13.71	0.57	11.47	0.60
	368	7.28	0.16	6.84	0.16	7.77	0.30
	461	11.18	0.33	9.30	0.31	6.89	0.23
	529	9.92	0.28	7.59	0.21	9.32	0.43
	723	16.56	0.57	19.69	0.93	15.89	0.96
	752	7.61	0.18	9.08	0.30	10.02	0.48
	821	13.92	0.45	12.18	0.48	12.13	0.66
	829	9.29	0.25	10.64	0.39	11.51	0.61
	953	7.24	0.16	8.76	0.28	6.97	0.23
	1063	10.67	0.31	10.76	0.40	9.60	0.45
	1087	10.44	0.30	9.02	0.29	6.36	0.18
	1106	8.70	0.23	7.26	0.19	7.24	0.25
	1503	7.84	0.19	6.71	0.16	9.99	0.48

Table 4-30. DI_L for fixed-fixed SCBs with D = 6', H = 30', Site D, and T = 1500

	NGA No.	Long. Steel = 1%		Long. Steel = 2%		Long. Steel = 3%	
		Trans. Steel = 0.74%		Trans. Steel = 0.41%		Trans. Steel = 0.26%	
		Δ_D in	DI_L	Δ_D in	DI_L	Δ_D in	DI_L
Far Field	169	3.25	0.15	4.67	0.43	4.89	0.72
	338	9.19	0.80	3.29	0.20	3.99	0.48
	729	4.50	0.29	4.67	0.43	4.30	0.56
	778	4.24	0.26	4.32	0.37	4.94	0.73
	900	7.07	0.57	6.71	0.78	4.27	0.56
	978	5.49	0.40	5.79	0.62	6.13	1.00
	995	4.04	0.24	3.59	0.25	4.15	0.53
	1003	5.97	0.45	3.33	0.20	3.49	0.35
	1107	5.09	0.35	4.13	0.34	5.49	0.88
	1203	4.82	0.32	4.01	0.32	4.68	0.66
Near Field	160	3.06	0.13	3.96	0.31	5.17	0.79
	180	10.49	0.94	4.36	0.38	3.18	0.27
	183	4.68	0.31	4.39	0.38	3.92	0.46
	368	4.52	0.29	3.54	0.24	3.67	0.40
	461	4.52	0.29	4.21	0.35	5.19	0.80
	529	8.96	0.77	7.68	0.95	4.26	0.55
	723	6.80	0.54	7.32	0.88	4.23	0.54
	752	3.35	0.16	4.80	0.45	5.02	0.75
	821	11.35	1.00	9.06	1.00	5.45	0.87
	829	5.33	0.38	6.48	0.74	4.69	0.67
	953	7.24	0.59	2.92	0.13	4.57	0.63
	1063	8.25	0.70	8.01	1.00	5.08	0.77
	1087	5.36	0.38	4.59	0.42	3.06	0.24
	1106	7.02	0.56	4.77	0.45	2.71	0.15
	1503	9.13	0.79	6.77	0.79	5.89	0.98

Table 4-31. DI_L for cantilever SCBs with D = 6', H = 60', Site D, and T = 1500

	NGA No.	Long. Steel = 1% Trans. Steel = 0.61%		Long. Steel = 2% Trans. Steel = 0.52%		Long. Steel = 3% Trans. Steel = 0.42%	
		Δ_D in	DI_L	Δ_D in	DI_L	Δ_D in	DI_L
Far Field	169	24.84	0.28	23.78	0.31	18.38	0.16
	338	17.75	0.11	19.89	0.18	19.97	0.23
	729	16.10	0.08	22.01	0.25	23.27	0.38
	778	18.82	0.14	20.17	0.19	26.63	0.52
	900	53.36	0.94	28.18	0.45	23.58	0.39
	978	21.29	0.20	20.07	0.19	16.54	0.08
	995	19.33	0.15	19.85	0.18	16.30	0.07
	1003	23.80	0.26	20.67	0.20	18.29	0.16
	1107	31.18	0.43	25.20	0.35	15.36	0.03
	1203	23.09	0.24	47.53	1.00	39.42	1.00
Near Field	160	52.33	0.92	23.79	0.31	16.52	0.08
	180	28.96	0.38	24.55	0.33	26.72	0.53
	183	35.67	0.53	29.03	0.48	25.09	0.46
	368	26.00	0.31	20.06	0.18	19.09	0.19
	461	35.48	0.53	19.33	0.16	17.02	0.10
	529	24.84	0.28	22.98	0.28	20.96	0.28
	723	22.22	0.22	26.07	0.38	19.15	0.20
	752	21.89	0.21	17.66	0.11	17.14	0.11
	821	22.12	0.22	18.29	0.13	18.95	0.19
	829	31.55	0.44	21.34	0.23	17.68	0.13
	953	27.25	0.34	19.27	0.16	20.48	0.26
	1063	28.82	0.37	26.46	0.39	24.93	0.45
	1087	31.36	0.43	27.97	0.44	18.42	0.17
	1106	18.95	0.14	24.40	0.33	26.27	0.51
	1503	47.37	0.80	48.79	1.00	23.88	0.40

Table 4-32. DI_L for fixed-fixed SCBs with D = 6’, H = 60’, Site D, and T = 1500

	NGA No.	Long. Steel = 1%		Long. Steel = 2%		Long. Steel = 3%	
		Trans. Steel = 0.71%		Trans. Steel = 0.52%		Trans. Steel = 0.40%	
		Δ_D in	DI_L	Δ_D in	DI_L	Δ_D in	DI_L
Far Field	169	9.73	0.11	12.31	0.25	17.57	0.73
	338	14.05	0.26	11.24	0.19	9.08	0.10
	729	14.94	0.29	18.05	0.55	11.57	0.28
	778	22.81	0.58	16.22	0.46	11.56	0.28
	900	12.70	0.21	13.40	0.31	12.70	0.37
	978	16.38	0.35	13.18	0.29	9.94	0.16
	995	9.73	0.11	10.06	0.13	10.16	0.18
	1003	11.57	0.17	15.40	0.41	14.21	0.48
	1107	9.97	0.11	14.43	0.36	12.07	0.32
	1203	12.85	0.22	12.27	0.25	14.69	0.52
Near Field	160	12.51	0.21	12.53	0.26	9.37	0.12
	180	41.35	1.00	26.84	1.00	18.02	0.77
	183	12.76	0.21	11.72	0.22	10.60	0.21
	368	12.29	0.20	10.72	0.16	10.17	0.18
	461	16.38	0.35	12.76	0.27	12.95	0.39
	529	16.72	0.36	12.43	0.25	10.91	0.23
	723	18.09	0.41	15.89	0.44	18.54	0.81
	752	11.11	0.16	8.01	0.02	10.43	0.20
	821	14.80	0.29	16.35	0.46	14.77	0.52
	829	12.92	0.22	11.83	0.22	9.35	0.12
	953	25.59	0.68	12.43	0.25	12.45	0.35
	1063	12.14	0.19	13.76	0.33	12.11	0.32
	1087	18.64	0.43	10.77	0.17	11.16	0.25
	1106	11.09	0.15	11.79	0.22	11.77	0.30
	1503	15.95	0.33	14.82	0.38	11.31	0.26

Table 4-33. DI_L for fixed-pinned TCBs with D = 5', H = 30', Site D, and T = 1000

	NGA No.	Long. Steel = 1%		Long. Steel = 2%		Long. Steel = 3%	
		Trans. Steel = 1.06%		Trans. Steel = 0.83%		Trans. Steel = 0.68%	
		Δ_D in	DI_L	Δ_D in	DI_L	Δ_D in	DI_L
Far Field	169	6.71	0.06	13.00	0.47	11.34	0.44
	338	10.72	0.24	8.75	0.18	7.15	0.05
	729	13.44	0.36	10.22	0.28	8.53	0.18
	778	11.72	0.29	10.23	0.28	8.06	0.14
	900	9.28	0.18	10.60	0.30	8.76	0.20
	978	11.39	0.27	8.38	0.15	7.51	0.08
	995	7.07	0.08	7.50	0.09	7.68	0.10
	1003	11.32	0.27	9.52	0.23	9.62	0.28
	1107	7.88	0.12	13.44	0.50	11.52	0.46
	1203	8.98	0.16	9.13	0.20	9.89	0.31
Near Field	160	8.33	0.14	8.55	0.16	7.06	0.04
	180	*28.00*	1.00	19.34	0.91	17.95	1.05
	183	10.14	0.22	7.47	0.09	8.67	0.19
	368	9.23	0.18	8.74	0.18	7.98	0.13
	461	11.99	0.30	11.89	0.39	10.50	0.36
	529	13.10	0.35	9.47	0.23	8.55	0.18
	723	15.84	0.47	13.87	0.53	13.45	0.63
	752	7.37	0.09	7.19	0.07	8.00	0.13
	821	12.07	0.30	10.85	0.32	9.31	0.25
	829	12.22	0.31	9.01	0.19	8.23	0.15
	953	9.55	0.19	10.65	0.31	9.64	0.28
	1063	9.12	0.17	11.40	0.36	10.08	0.32
	1087	10.76	0.24	7.98	0.12	8.71	0.20
	1106	8.97	0.16	7.31	0.08	9.00	0.22
	1503	15.91	0.47	8.27	0.14	7.63	0.10

Table 4-34. DI_L for fixed-pinned TCBs with D = 5', H = 30', Site D, and T = 2500

	NGA No.	Long. Steel = 1% Trans. Steel = 1.06%		Long. Steel = 2% Trans. Steel = 0.83%		Long. Steel = 3% Trans. Steel = 0.68%	
		Δ_D in	DI_L	Δ_D in	DI_L	Δ_D in	DI_L
Far Field	169	8.63	0.15	15.71	0.66	19.66	1.00
	338	15.15	0.44	10.40	0.29	9.66	0.28
	729	19.81	0.64	13.99	0.54	12.24	0.52
	778	22.12	0.74	17.67	0.79	12.83	0.58
	900	11.44	0.27	14.02	0.54	13.74	0.66
	978	17.30	0.53	13.22	0.48	9.84	0.30
	995	10.20	0.22	10.36	0.29	9.10	0.23
	1003	13.91	0.38	16.24	0.69	12.94	0.59
	1107	10.30	0.22	14.77	0.59	18.74	1.00
	1203	11.59	0.28	10.95	0.33	12.80	0.57
Near Field	160	10.89	0.25	11.42	0.36	9.03	0.23
	180	*28.00*	1.00	20.70	1.00	17.40	1.00
	183	14.88	0.42	10.90	0.32	12.68	0.56
	368	13.17	0.35	11.33	0.35	9.16	0.24
	461	15.25	0.44	16.85	0.73	14.74	0.75
	529	18.46	0.58	14.14	0.55	11.31	0.44
	723	21.05	0.69	19.30	0.90	20.85	1.00
	752	10.41	0.23	10.36	0.29	9.51	0.27
	821	18.68	0.59	15.80	0.66	14.14	0.70
	829	15.06	0.43	12.51	0.44	11.93	0.49
	953	12.16	0.30	13.15	0.48	11.39	0.44
	1063	12.83	0.33	14.11	0.55	14.38	0.72
	1087	17.98	0.56	12.22	0.42	10.79	0.39
	1106	12.60	0.32	10.00	0.26	11.94	0.49
	1503	12.04	0.30	15.77	0.66	10.46	0.36

Table 4-35. DI_L for fixed-fixed TCBs with D = 5', H = 30', Site D, and T = 1000

	NGA No.	Long. Steel = 1%		Long. Steel = 2%		Long. Steel = 3%	
		Trans. Steel = 0.75%		Trans. Steel = 0.45%		Trans. Steel = 0.97%	
		Δ_D in	DI_L	Δ_D in	DI_L	Δ_D in	DI_L
Far Field	169	6.01	0.29	4.69	0.15	4.19	0.02
	338	6.41	0.33	8.94	0.78	5.99	0.26
	729	5.25	0.22	4.76	0.16	4.80	0.10
	778	4.98	0.20	5.61	0.28	4.98	0.12
	900	7.12	0.39	5.48	0.26	4.57	0.07
	978	4.14	0.12	5.39	0.25	4.52	0.06
	995	3.92	0.10	4.21	0.07	4.19	0.02
	1003	6.65	0.35	6.19	0.37	4.52	0.06
	1107	11.40	0.79	5.58	0.28	4.98	0.12
	1203	5.16	0.21	4.48	0.11	4.16	0.01
Near Field	160	4.85	0.19	4.54	0.12	4.64	0.08
	180	8.61	0.53	7.84	0.61	5.18	0.15
	183	8.54	0.53	5.63	0.29	4.04	-0.01
	368	6.85	0.37	5.37	0.25	4.96	0.12
	461	5.28	0.23	4.84	0.17	4.63	0.08
	529	7.05	0.39	6.53	0.42	4.17	0.01
	723	11.47	0.80	5.23	0.23	4.61	0.07
	752	5.16	0.21	4.39	0.10	4.16	0.01
	821	9.18	0.59	6.73	0.45	5.30	0.17
	829	8.28	0.50	6.19	0.37	5.01	0.13
	953	4.43	0.15	6.64	0.44	4.08	0.00
	1063	6.85	0.37	5.39	0.25	4.80	0.10
	1087	4.89	0.19	5.49	0.26	5.05	0.13
	1106	5.73	0.27	5.54	0.27	3.52	-0.08
	1503	7.77	0.46	4.44	0.11	4.98	0.12

Table 4-36. DI_L for fixed-fixed TCBs with D = 5', H = 30', Site D, and T = 2500

	NGA No.	Long. Steel = 1%		Long. Steel = 2%		Long. Steel = 3%	
		Trans. Steel = 0.75%		Trans. Steel = 0.45%		Trans. Steel = 0.97%	
		Δ_D in	DI_L	Δ_D in	DI_L	Δ_D in	DI_L
Far Field	169	9.69	0.63	5.71	0.30	5.68	0.22
	338	8.51	0.52	11.29	1.00	14.06	1.00
	729	9.55	0.62	5.75	0.30	6.24	0.30
	778	6.08	0.30	7.36	0.54	6.53	0.34
	900	14.75	1.00	8.73	0.75	6.55	0.34
	978	4.91	0.19	6.73	0.45	6.17	0.29
	995	5.65	0.26	5.18	0.22	5.67	0.22
	1003	9.49	0.61	8.86	0.77	6.74	0.37
	1107	16.91	1.00	7.50	0.56	6.91	0.39
	1203	6.31	0.32	5.73	0.30	5.94	0.26
Near Field	160	7.13	0.40	6.21	0.37	6.25	0.30
	180	12.38	0.88	13.33	1.00	8.28	0.58
	183	13.36	0.97	8.86	0.76	5.56	0.20
	368	7.98	0.47	6.38	0.40	6.88	0.39
	461	7.63	0.44	6.14	0.36	5.65	0.22
	529	8.32	0.51	10.52	1.00	7.28	0.44
	723	24.71	1.00	8.12	0.66	7.24	0.44
	752	9.28	0.59	5.21	0.22	4.83	0.10
	821	16.79	1.00	12.50	1.00	9.15	0.70
	829	12.79	0.92	9.12	0.80	7.24	0.44
	953	5.51	0.25	8.93	0.78	8.42	0.60
	1063	10.76	0.73	8.64	0.73	7.52	0.47
	1087	5.55	0.25	7.24	0.52	7.52	0.47
	1106	6.19	0.31	8.26	0.68	5.17	0.15
	1503	12.94	0.93	8.18	0.66	9.49	0.75

Table 4-37. DI_L for fixed-pinned TCBs with D = 5', H = 60', Site D, and T = 1000

	NGA No.	Long. Steel = 1%		Long. Steel = 2%	Long. Steel = 3%
		Trans. Steel = 0.32%			
		Δ_D in	DI_L		
Far Field	169	20.74	0.07	No data for 2% steel	No data for 3% steel
	338	21.17	0.08		
	729	18.44	0.01		
	778	47.20	0.76		
	900	32.17	0.37		
	978	29.18	0.29		
	995	32.08	0.36		
	1003	20.60	0.07		
	1107	42.22	0.63		
	1203	15.47	-0.07		
Near Field	160	28.46	0.27		
	180	30.48	0.32		
	183	56.55	1.00		
	368	20.96	0.07		
	461	26.59	0.22		
	529	26.90	0.23		
	723	33.52	0.40		
	752	36.70	0.48		
	821	28.45	0.27		
	829	56.55	1.00		
	953	30.36	0.32		
	1063	29.66	0.30		
	1087	34.09	0.42		
	1106	22.21	0.11		
	1503	23.89	0.15		

Table 4-38. DI_L for fixed-fixed TCBs with D = 5', H = 60', Site D, and T = 1000

	NGA No.	Long. Steel = 1%		Long. Steel = 2%		Long. Steel = 3%
		Trans. Steel = 0.50%		Trans. Steel = 0.21%		
		Δ_D in	DI_L	Δ_D in	DI_L	
Far Field	169	18.79	0.38	13.71	0.17	No data for 3% steel
	338	16.08	0.26	15.79	0.33	
	729	10.37	0.03	15.92	0.34	
	778	20.72	0.45	17.76	0.49	
	900	17.15	0.31	15.58	0.32	
	978	17.79	0.33	16.57	0.40	
	995	13.94	0.18	12.16	0.05	
	1003	16.83	0.30	14.45	0.23	
	1107	12.79	0.13	11.05	-0.04	
	1203	17.84	0.34	12.01	0.04	
Near Field	160	10.37	0.03	15.56	0.32	
	180	17.65	0.33	20.28	0.69	
	183	16.34	0.28	15.77	0.33	
	368	18.58	0.37	14.77	0.25	
	461	17.45	0.32	15.71	0.33	
	529	17.31	0.31	15.77	0.33	
	723	16.93	0.30	13.97	0.19	
	752	16.15	0.27	13.42	0.15	
	821	14.39	0.20	16.15	0.36	
	829	14.80	0.21	15.70	0.33	
	953	17.47	0.32	14.65	0.24	
	1063	18.67	0.37	13.53	0.16	
	1087	17.32	0.32	17.17	0.44	
	1106	17.72	0.33	14.14	0.20	
	1503	15.40	0.24	13.50	0.15	

Table 4-39. DI_L for fixed-pinned TCBs with D = 6', H = 30', Site D, and T = 1000

	NGA No.	Long. Steel = 1%		Long. Steel = 2%		Long. Steel = 3%	
		Trans. Steel = 1.45%		Trans. Steel = 0.84%		Trans. Steel = 0.66%	
		Δ_D in	DI_L	Δ_D in	DI_L	Δ_D in	DI_L
Far Field	169	12.00	0.42	15.87	0.90	7.58	0.21
	338	6.32	0.12	5.57	0.03	6.48	0.09
	729	9.06	0.27	8.80	0.30	8.70	0.34
	778	11.06	0.37	7.37	0.18	6.35	0.08
	900	9.51	0.29	8.82	0.31	7.81	0.24
	978	7.81	0.20	6.29	0.09	6.53	0.10
	995	6.29	0.12	7.02	0.16	6.14	0.05
	1003	11.17	0.38	7.22	0.17	8.02	0.26
	1107	12.61	0.46	7.38	0.19	7.04	0.15
	1203	8.89	0.26	9.78	0.39	6.51	0.09
Near Field	160	5.85	0.09	6.74	0.13	10.10	0.49
	180	25.39	1.00	8.13	0.25	8.11	0.27
	183	6.97	0.15	8.32	0.26	10.15	0.50
	368	6.75	0.14	7.96	0.23	5.87	0.02
	461	11.08	0.37	9.28	0.35	7.26	0.18
	529	8.95	0.26	7.44	0.19	8.55	0.32
	723	14.65	0.57	11.51	0.53	11.51	0.65
	752	6.47	0.13	7.55	0.20	8.44	0.31
	821	4.81	0.04	9.17	0.34	8.34	0.30
	829	8.21	0.22	9.25	0.34	8.41	0.30
	953	7.37	0.18	8.22	0.26	7.67	0.22
	1063	9.86	0.31	9.24	0.34	8.31	0.29
	1087	8.83	0.25	7.73	0.21	8.23	0.28
	1106	7.27	0.17	7.62	0.21	7.13	0.16
	1503	7.55	0.19	6.24	0.09	6.65	0.11

Table 4-40. DI_L for fixed-fixed TCBs with D = 6', H = 30', Site D, and T = 1000

	NGA No.	Long. Steel = 1%		Long. Steel = 2%		Long. Steel = 3%	
		Trans. Steel = 0.61%		Trans. Steel =0.79%		Trans. Steel = 1.32%	
		Δ_D in	DI_L	Δ_D in	DI_L	Δ_D in	DI_L
Far Field	169	3.39	0.15	3.46	0.02	3.52	-0.02
	338	9.21	0.98	3.70	0.04	3.09	-0.06
	729	4.12	0.25	3.98	0.07	3.56	-0.01
	778	4.44	0.30	4.21	0.09	3.77	0.01
	900	5.00	0.38	4.55	0.13	3.68	0.00
	978	4.13	0.25	4.81	0.16	3.62	-0.01
	995	3.43	0.15	3.62	0.03	3.27	-0.04
	1003	5.22	0.41	3.52	0.02	3.60	-0.01
	1107	4.99	0.37	4.09	0.08	3.38	-0.03
	1203	3.98	0.23	4.08	0.08	3.93	0.03
Near Field	160	4.05	0.24	3.41	0.01	3.37	-0.03
	180	8.84	0.93	4.93	0.17	3.93	0.03
	183	4.33	0.28	3.49	0.02	3.14	-0.05
	368	4.61	0.32	4.38	0.11	3.78	0.01
	461	3.88	0.22	4.08	0.08	3.57	-0.01
	529	6.86	0.64	3.73	0.04	3.29	-0.04
	723	6.35	0.57	3.51	0.02	3.72	0.00
	752	3.18	0.12	3.89	0.06	3.48	-0.02
	821	7.94	0.80	4.99	0.18	3.87	0.02
	829	5.40	0.43	4.47	0.12	3.72	0.00
	953	6.53	0.59	3.74	0.05	3.32	-0.04
	1063	5.87	0.50	4.77	0.15	3.79	0.01
	1087	5.25	0.41	4.28	0.10	3.13	-0.06
	1106	4.83	0.35	3.51	0.02	3.60	-0.01
	1503	6.43	0.58	4.65	0.14	3.26	-0.04

Table 4-41. DI_L for fixed-pinned TCBs with D = 6', H = 60', Site D, and T = 1000

	NGA No.	Long. Steel = 1% Trans. Steel = 0.44%		Long. Steel = 2% Trans. Steel = 0.15%		Long. Steel = 3% Trans. Steel = 0.11%	
		Δ_D in	DI_L	Δ_D in	DI_L	Δ_D in	DI_L
Far Field	169	23.01	0.25	22.90	0.33	21.93	0.26
	338	16.78	0.06	18.87	0.10	19.90	0.11
	729	15.08	0.01	19.04	0.11	18.66	0.02
	778	17.11	0.07	17.58	0.02	20.70	0.17
	900	41.99	0.84	25.67	0.49	20.01	0.12
	978	19.69	0.15	19.28	0.12	19.14	0.05
	995	16.69	0.05	20.71	0.20	18.14	-0.02
	1003	23.92	0.28	20.10	0.17	19.57	0.08
	1107	26.99	0.37	26.98	0.57	18.98	0.04
	1203	20.52	0.17	26.85	0.56	36.71	1.35
Near Field	160	43.64	0.89	40.36	1.00	16.66	-0.13
	180	24.36	0.29	23.44	0.36	22.94	0.33
	183	30.48	0.48	26.35	0.53	22.28	0.28
	368	24.71	0.30	22.08	0.28	17.81	-0.05
	461	31.80	0.52	22.47	0.31	19.31	0.06
	529	23.25	0.26	22.02	0.28	20.65	0.16
	723	21.03	0.19	23.17	0.35	21.64	0.24
	752	23.92	0.28	18.92	0.10	15.75	-0.20
	821	5.33	-0.30	18.20	0.06	18.67	0.02
	829	30.97	0.50	22.04	0.28	19.03	0.04
	953	26.70	0.36	20.19	0.17	18.64	0.01
	1063	26.39	0.35	24.09	0.40	22.31	0.29
	1087	26.37	0.35	25.64	0.49	22.31	0.29
	1106	18.47	0.11	21.62	0.26	21.94	0.26
	1503	30.00	0.47	43.96	1.00	21.28	0.21

Table 4-42. DI_L for fixed-fixed TCBs with D = 6’, H = 60’, Site D, and T = 1000

	NGA No.	Long. Steel = 1%		Long. Steel = 2%		Long. Steel = 3%	
		Trans. Steel = 0.56%		Trans. Steel = 0.30%		Trans. Steel = 0.31%	
		Δ_D in	DI_L	Δ_D in	DI_L	Δ_D in	DI_L
Far Field	169	11.07	0.14	9.16	-0.05	14.64	0.38
	338	14.49	0.30	11.04	0.12	11.67	0.11
	729	13.26	0.24	16.03	0.55	12.54	0.19
	778	18.59	0.49	9.77	0.01	11.82	0.12
	900	13.41	0.25	12.75	0.26	12.00	0.14
	978	16.27	0.38	10.80	0.10	12.04	0.14
	995	10.53	0.11	10.52	0.07	9.84	-0.06
	1003	12.63	0.21	12.96	0.28	11.45	0.09
	1107	9.45	0.06	11.19	0.13	13.48	0.27
	1203	10.81	0.12	10.18	0.04	12.94	0.22
Near Field	160	12.65	0.21	10.72	0.09	11.74	0.11
	180	22.63	0.69	17.76	0.70	14.30	0.35
	183	13.12	0.23	12.13	0.21	10.21	-0.03
	368	13.85	0.27	10.37	0.06	10.06	-0.04
	461	15.19	0.33	13.27	0.31	12.09	0.15
	529	15.42	0.34	12.35	0.23	10.99	0.04
	723	14.08	0.28	13.54	0.33	12.87	0.22
	752	12.74	0.21	8.65	-0.09	9.17	-0.12
	821	14.13	0.28	14.24	0.39	12.71	0.20
	829	14.53	0.30	13.00	0.29	10.00	-0.05
	953	12.87	0.22	10.77	0.09	12.67	0.20
	1063	11.42	0.15	12.97	0.28	12.10	0.15
	1087	15.84	0.36	9.69	0.00	10.34	-0.01
	1106	11.19	0.14	12.31	0.23	10.09	-0.04
	1503	12.51	0.20	13.36	0.32	10.47	0.00

Table 4-43. DI_L for fixed-pinned FCBs with D = 4', H = 30', Site D, and T = 1000

	NGA No.	Long. Steel = 1%		Long. Steel = 2%		Long. Steel = 3%	
		Trans. Steel =1.14%		Trans. Steel = 0.92%		Trans. Steel = 0.61%	
		Δ_D in	DI_L	Δ_D in	DI_L	Δ_D in	DI_L
Far Field	169	17.53	0.39	10.84	0.14	8.58	0.01
	338	16.83	0.37	14.11	0.30	10.78	0.15
	729	8.77	0.08	13.34	0.26	14.98	0.44
	778	*34.42*	1.00	21.09	0.64	11.62	0.21
	900	16.38	0.35	13.14	0.25	12.68	0.28
	978	18.59	0.43	15.94	0.39	11.77	0.22
	995	11.04	0.16	10.50	0.12	10.32	0.12
	1003	23.29	0.60	12.22	0.20	12.93	0.30
	1107	9.00	0.09	9.26	0.06	10.51	0.14
	1203	12.21	0.20	11.09	0.15	10.41	0.13
Near Field	160	8.29	0.06	12.42	0.21	10.37	0.13
	180	*34.42*	1.00	26.30	0.89	20.90	0.84
	183	16.55	0.36	12.04	0.20	13.17	0.32
	368	20.21	0.49	13.63	0.27	9.57	0.07
	461	13.36	0.24	15.21	0.35	13.69	0.35
	529	16.71	0.37	15.27	0.35	13.11	0.31
	723	15.62	0.33	14.32	0.31	14.19	0.38
	752	12.41	0.21	12.74	0.23	8.65	0.01
	821	13.14	0.24	12.64	0.23	12.88	0.30
	829	11.59	0.18	14.11	0.30	13.73	0.35
	953	17.18	0.38	11.95	0.19	10.13	0.11
	1063	15.51	0.32	11.34	0.16	12.77	0.29
	1087	15.34	0.32	16.29	0.40	10.64	0.14
	1106	15.03	0.30	10.51	0.12	12.13	0.25
	1503	12.59	0.22	12.69	0.23	13.60	0.34

Table 4-44. DI_L for fixed-pinned FCBs with D = 4’, H = 30’, Site D, and T = 2500

	NGA No.	Long. Steel = 1%		Long. Steel = 2%		Long. Steel = 3%	
		Trans. Steel =1.14%		Trans. Steel = 0.92%		Trans. Steel = 0.61%	
		Δ_D in	DI_L	Δ_D in	DI_L	Δ_D in	DI_L
Far Field	169	*34.42*	1.00	17.79	0.48	10.50	0.14
	338	20.80	0.51	20.21	0.59	15.74	0.49
	729	15.36	0.32	16.20	0.40	16.63	0.55
	778	*34.42*	1.00	*28.58*	1.00	19.01	0.71
	900	*34.42*	1.00	15.99	0.39	14.78	0.42
	978	29.12	0.81	22.75	0.72	17.35	0.60
	995	17.89	0.41	14.30	0.31	11.27	0.19
	1003	*34.42*	1.00	17.55	0.46	16.77	0.56
	1107	11.23	0.17	12.23	0.21	11.57	0.21
	1203	17.52	0.39	11.33	0.16	13.98	0.37
Near Field	160	14.54	0.29	18.44	0.51	13.71	0.35
	180	*34.42*	1.00	*28.58*	1.00	*23.33*	1.00
	183	29.85	0.84	19.89	0.58	16.68	0.55
	368	*34.42*	1.00	19.04	0.54	13.37	0.33
	461	16.45	0.36	19.90	0.58	18.39	0.67
	529	23.22	0.60	21.94	0.68	19.24	0.72
	723	19.99	0.48	19.00	0.53	22.99	0.98
	752	21.96	0.55	15.64	0.37	12.38	0.26
	821	19.41	0.46	16.85	0.43	16.46	0.54
	829	16.67	0.36	16.43	0.41	18.53	0.68
	953	*34.42*	1.00	17.53	0.46	14.10	0.38
	1063	23.02	0.59	16.72	0.42	14.18	0.38
	1087	17.43	0.39	24.10	0.78	16.16	0.52
	1106	19.03	0.45	15.53	0.37	13.43	0.33
	1503	*34.42*	1.00	19.87	0.58	20.86	0.83

Table 4-45. DI_L for fixed-fixed FCBs with D = 4’, H = 30’, Site D, and T = 1000

	NGA No.	Long. Steel = 1%		Long. Steel = 2%		Long. Steel = 3%	
		Trans. Steel = 0.49%		Trans. Steel =0.53%		Trans. Steel = 0.71%	
		Δ_D in	DI_L	Δ_D in	DI_L	Δ_D in	DI_L
Far Field	169	13.58	0.60	7.16	0.14	5.84	-0.02
	338	4.59	0.03	6.02	0.04	6.27	0.01
	729	9.95	0.37	7.77	0.18	6.17	0.01
	778	5.99	0.12	6.08	0.05	6.09	0.00
	900	9.87	0.37	7.00	0.12	6.29	0.01
	978	5.88	0.12	5.91	0.03	6.33	0.02
	995	6.58	0.16	5.74	0.02	6.04	0.00
	1003	6.32	0.14	7.83	0.19	7.49	0.10
	1107	6.32	0.14	6.55	0.09	7.26	0.08
	1203	7.25	0.20	6.23	0.06	5.43	-0.05
Near Field	160	6.58	0.16	10.32	0.39	6.08	0.00
	180	7.77	0.23	8.04	0.21	7.47	0.10
	183	10.05	0.38	9.90	0.36	8.01	0.14
	368	6.33	0.14	6.45	0.08	6.43	0.02
	461	8.42	0.27	6.48	0.08	6.57	0.03
	529	6.53	0.16	8.34	0.23	7.68	0.12
	723	12.69	0.54	9.49	0.33	5.95	-0.01
	752	7.19	0.20	7.50	0.16	8.67	0.19
	821	11.34	0.46	8.60	0.25	7.30	0.09
	829	9.63	0.35	7.33	0.15	6.74	0.05
	953	7.14	0.19	7.18	0.14	6.23	0.01
	1063	8.97	0.31	7.94	0.20	6.93	0.06
	1087	6.45	0.15	7.59	0.17	7.64	0.11
	1106	6.73	0.17	7.13	0.13	7.59	0.11
	1503	5.27	0.08	6.49	0.08	6.82	0.05

Table 4-46. DI_L for fixed-fixed FCBs with D = 4', H = 30', Site D, and T = 2500

	NGA No.	Long. Steel = 1%		Long. Steel = 2%		Long. Steel = 3%	
		Trans. Steel = 0.49%		Trans. Steel =0.53%		Trans. Steel = 0.71%	
		Δ_D in	DI_L	Δ_D in	DI_L	Δ_D in	DI_L
Far Field	169	18.45	0.90	10.35	0.39	8.73	0.19
	338	6.31	0.14	7.16	0.14	8.95	0.21
	729	14.15	0.63	11.77	0.51	8.69	0.19
	778	9.97	0.37	7.49	0.16	8.38	0.17
	900	18.45	0.90	8.77	0.27	8.60	0.18
	978	7.26	0.20	8.07	0.21	7.94	0.13
	995	7.65	0.23	8.14	0.22	7.53	0.10
	1003	8.96	0.31	10.44	0.40	10.91	0.35
	1107	10.39	0.40	8.63	0.26	10.54	0.32
	1203	9.22	0.32	7.89	0.20	7.76	0.12
Near Field	160	6.83	0.17	10.67	0.42	9.22	0.23
	180	15.22	0.70	10.04	0.37	10.98	0.36
	183	19.89	0.99	15.74	0.83	13.05	0.51
	368	7.73	0.23	7.23	0.14	7.66	0.11
	461	12.40	0.52	9.69	0.34	9.48	0.25
	529	9.91	0.37	9.80	0.35	10.99	0.36
	723	20.12	1.00	20.51	1.00	7.98	0.14
	752	12.15	0.51	9.83	0.35	12.56	0.47
	821	18.18	0.89	14.14	0.70	11.95	0.43
	829	12.60	0.54	11.77	0.51	10.26	0.30
	953	8.42	0.27	9.32	0.31	7.93	0.13
	1063	12.59	0.54	12.26	0.55	10.70	0.34
	1087	10.93	0.43	9.60	0.33	8.26	0.16
	1106	8.09	0.25	8.33	0.23	9.44	0.24
	1503	7.28	0.20	7.97	0.20	9.52	0.25

Table 4-47. Reliability index and probability of failure

β	Probability of exceedance	Rounded reciprocal
		approx. 1-in-N
0	0.5	2
0.5	0.308537539	3
1	0.158655254	6
1.5	0.066807201	15
2	0.022750132	50
2.5	0.006209665	200
3	0.001349898	1000
3.5	0.000232629	5000
4	3.16712E-05	30000
4.5	3.3977E-06	300000
5	2.867E-07	3500000

Chapter 5. Tables

Table 5-1. Mean and standard deviation of DI_R

	DS3	DS4	DS5	DS6
μ_R	0.375	0.600	0.822	1.000
σ_R	0.100	0.119	0.114	0.000

Table 5-2. Mean and standard deviation of DI_L

	SCBs	TCBs	FCBs
μ_L	0.325	0.239	0.279
σ_L	0.204	0.195	0.185

Table 5-3. The β_6'' to be used to obtain desired β_6'

Desired β_6'	$P_{EQ} \cap P_{CF}$	P_{EQ}	$P_{CF} \vert P_{EQ}$	β_6''
2	0.022750	0.072257	0.314852	0.48
2.5	0.006210	0.072257	0.085939	1.37
3	0.001350	0.072257	0.018682	2.08
3.5	0.000233	0.072257	0.003219	2.72
4	0.000032	0.072257	0.000438	3.33

Table 5-4. The DI's for various β_6's for SCBs

Target β'_6	Design DI'	Probability of exceedance of other damage states					
		DS1	DS2	DS3	DS4	DS5	DS6
2.5	0.58	7%	7%	5%	2%	1%	0.6%
3.0	0.38	7%	6%	3%	1%	0%	0%
3.5	0.26	7%	5%	1%	0%	0%	0%
4.0	0.19	7%	3%	1%	0%	0%	0%

Table 5-5. Probability of exceedance of DSs for SCBs excluding P_{EQ}

Target β'_6	Probability of exceedance of other damage states					
	DS1	DS2	DS3	DS4	DS5	DS6
2.5	100%	93%	64%	34%	16%	9%
3.0	99%	81%	38%	14%	5%	2%
3.5	99%	63%	19%	4%	1%	0%
4.0	98%	43%	8%	1%	0%	0%

Table 5-6. The DI's for various β_6's for TCBs

Target β'_6	Design DI'	Probability of exceedance of other damage states					
		DS1	DS2	DS3	DS4	DS5	DS6
2.5	0.63	7%	7%	4%	2%	1%	0.6%
3.0	0.41	7%	6%	3%	1%	0%	0%
3.5	0.28	7%	4%	1%	0%	0%	0%
4.0	0.19	7%	3%	0%	0%	0%	0%

Table 5-7. The DI's for various β_6's for FCBs

Target β'_6	Design DI'	Probability of exceedance of other damage states					
		DS1	DS2	DS3	DS4	DS5	DS6
2.5	0.66	7%	7%	4%	2%	1%	0.6%
3.0	0.43	7%	6%	3%	1%	0%	0%
3.5	0.29	7%	4%	1%	0%	0%	0%
4.0	0.20	7%	3%	0%	0%	0%	0%

Chapter 6. Tables

Table 6-1. Damage index for repaired columns NHS1-R and NHS2-R

Name	Damage State	Repaired Column			
		Δ_Y	Δ_C	Δ_D	DI
		in	in	in	
NHS1-R	DS3	3.33	10.48	4.04	0.10
NHS2-R	DS3	2.05	10.65	3.99	0.23

Table 6-2. Damage index for original columns NHS1 and NHS2

Name	Damage State	Original Column			
		Δ_Y	Δ_C	Δ_D	DI_R
		in	in	in	
NHS1	DS3	1.40	7.54	2.53	0.18
NHS2	DS3	1.00	6.41	2.82	0.34

Table 6-3. Original cantilever column design properties

Original Column						
Column Configuration	Diameter	Height	Steel Ratio		Δ_Y	Δ_C
			Longitudinal	Transverse		
	in [mm]	in [mm]	%	%	in [mm]	in [mm]
Cantilever	72 [1829]	360 [9144]	2	0.84	4.0 [102]	16.5 [419]

Table 6-4. Modified steel properties for repaired columns

Damage State	α	Point A			Point B			Point C		
		Stress		Strain	Stress		Strain	Stress		Strain
		[ksi]	[MPa]		[ksi]	[MPa]		[ksi]	[MPa]	
DS-5	0.2	68	469	0.012	95	655	0.046	95	655	0.060

Table 6-5. CFRP material properties (Tyfo® SCH-41 composite using Tyfo® S epoxy)

Property	Composite Gross Laminate Properties
Ultimate tensile strength in primary fiber direction, psi	121000 psi [834 Mpa]
Elongation at break	0.85%
Tensile modulus, psi	11.9 x 10^6 [82 Gpa]
Nominal laminate thickness	0.04 in. [1 mm]

Table 6-6. CFRP confined concrete properties for repaired columns

Repaired Column	f'_{co}		f'_{cu}		ε_{cu}
	[ksi]	[Mpa]	[ksi]	[Mpa]	
Cover	4.56	31.4	6.96	50.0	0.01512
Core	5.56	38.3	7.96	54.9	0.01678

Table 6-7. Repair design for the cantilever column for DI = 0.15

Repaired Column					
Target DI	CFRP Layers	Δ_Y	Δ_C	Δ_D	DI, Calculated
		in [mm]	in [mm]	in [mm]	
0.15	7	11.1[282]	23.0 [584]	12.8 [325]	0.15

Table 6-8. DI_L for repaired cantilever column for T = 1000

	NGA No.	Δ_D	DI_L
FAR FIELD	169	9.92	-0.10
	338	11.72	0.05
	729	16.15	0.42
	778	17.26	0.52
	900	10.96	-0.01
	978	14.01	0.24
	995	9.06	-0.17
	1003	9.63	-0.13
	1107	8.16	-0.25
	1203	10.86	-0.02
NEAR FIELD	160	14.39	0.28
	180	23.66	1.00
	183	13.69	0.22
	368	10.66	-0.04
	461	13.89	0.23
	529	10.18	-0.08
	723	13.42	0.19
	752	9.00	-0.18
	821	15.52	0.37
	829	12.45	0.11
	953	8.35	-0.23
	1063	11.20	0.01
	1087	16.09	0.42
	1106	11.65	0.04
	1503	15.74	0.39

Figures

Chapter 2. Figures

Damage State 1 Damage State 2 Damage State 3

Damage State 4 Damage State 5 Damage State 6

Figure 2-1. Possible apparent damage states of bridge columns

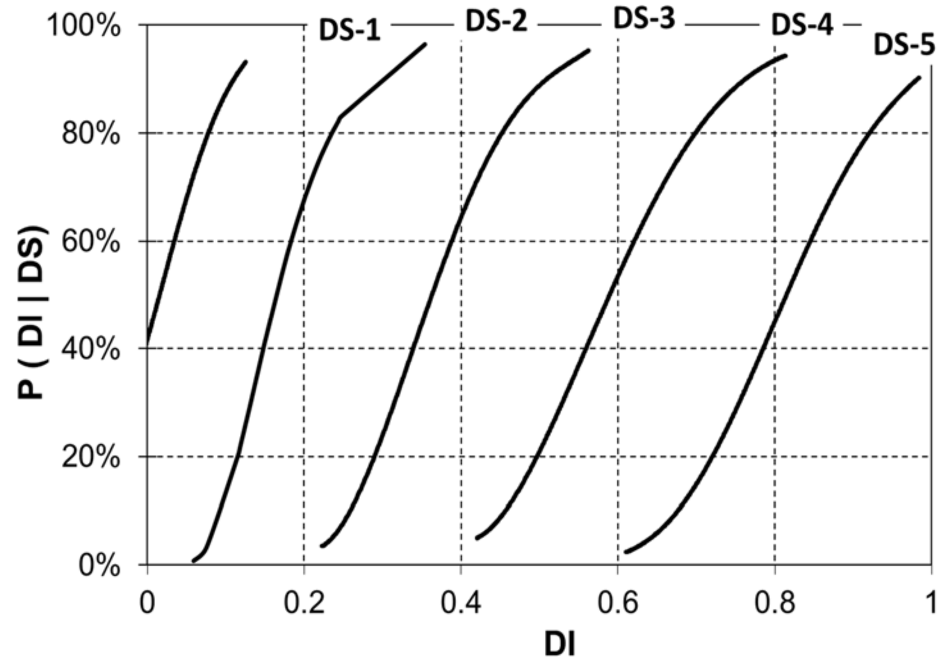

Figure 2-2. Correlation between damage states and damage indices

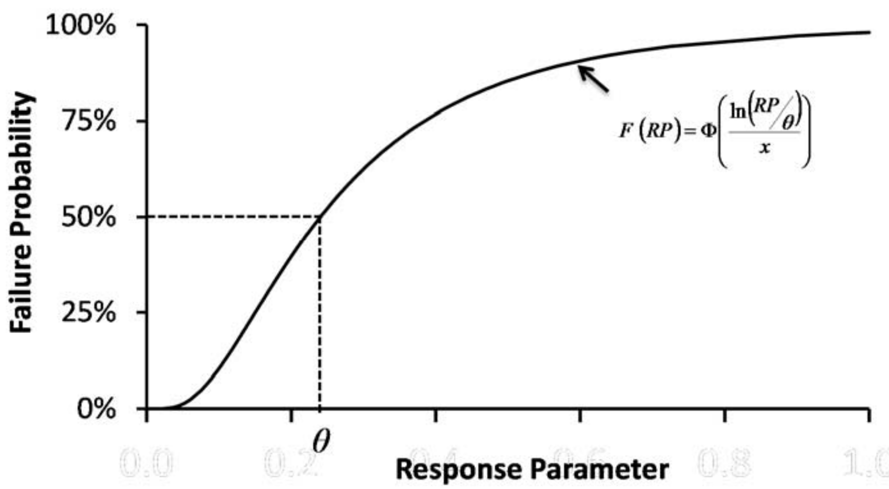

Figure 2-3. Fragility curve using lognormal distribution

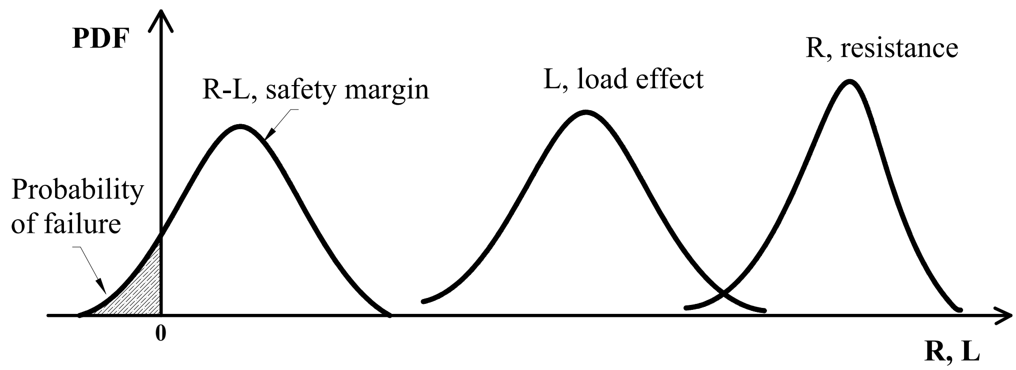

Figure 2-4. Probability distribution functions of load, resistance, and safety margin (Nowak & Collins 2000).

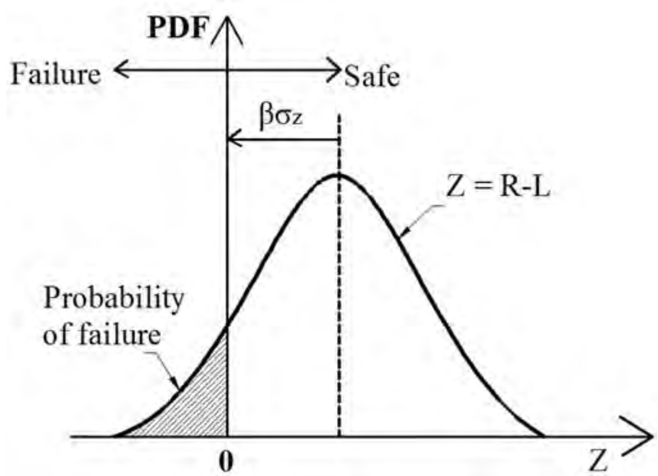

Figure 2-5. Graphical representation of reliability index and probability of failure (Cornell 1969)

Chapter 3. Figures

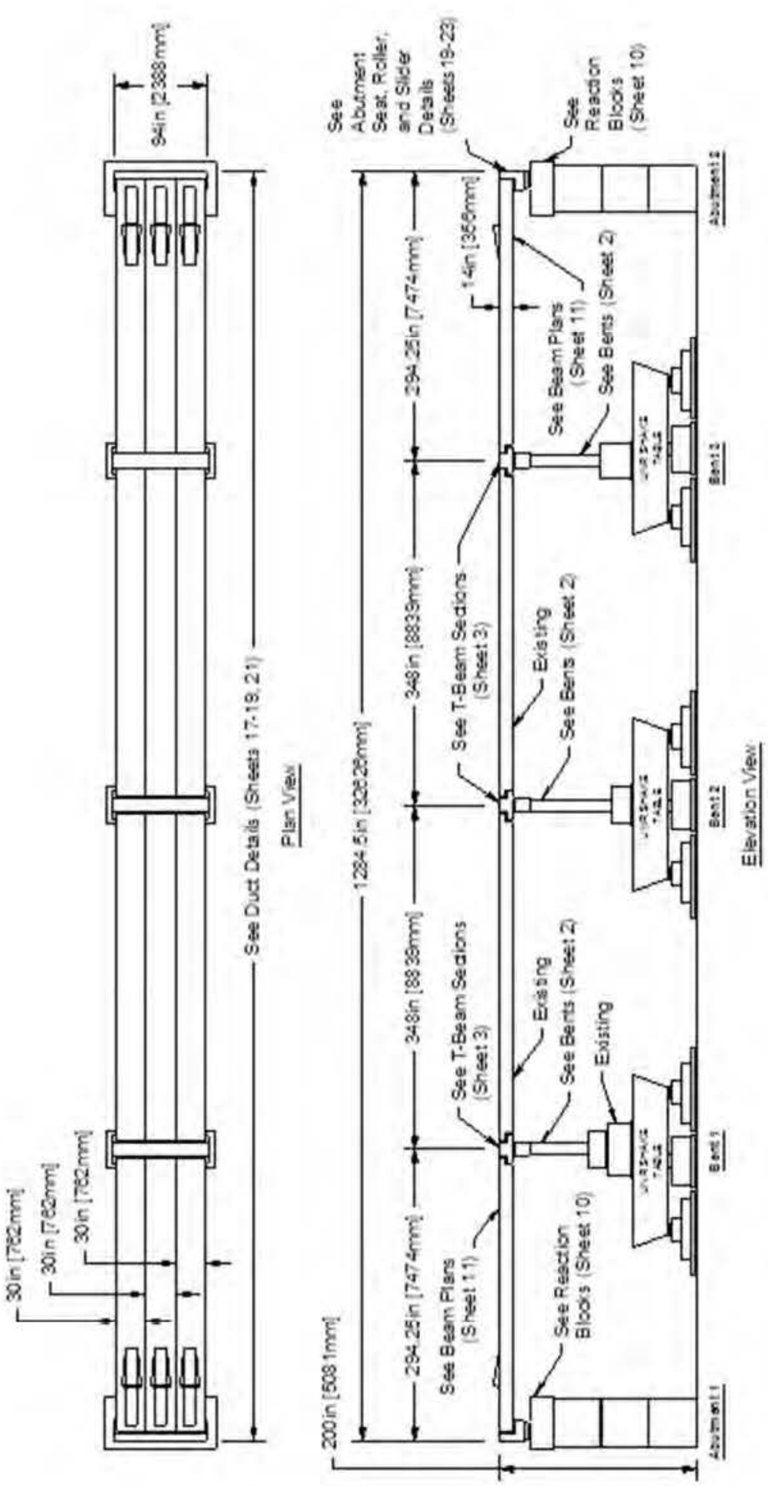

Figure 3-1. Plan and elevation of four span bridge (Saiidi et al. 2013)

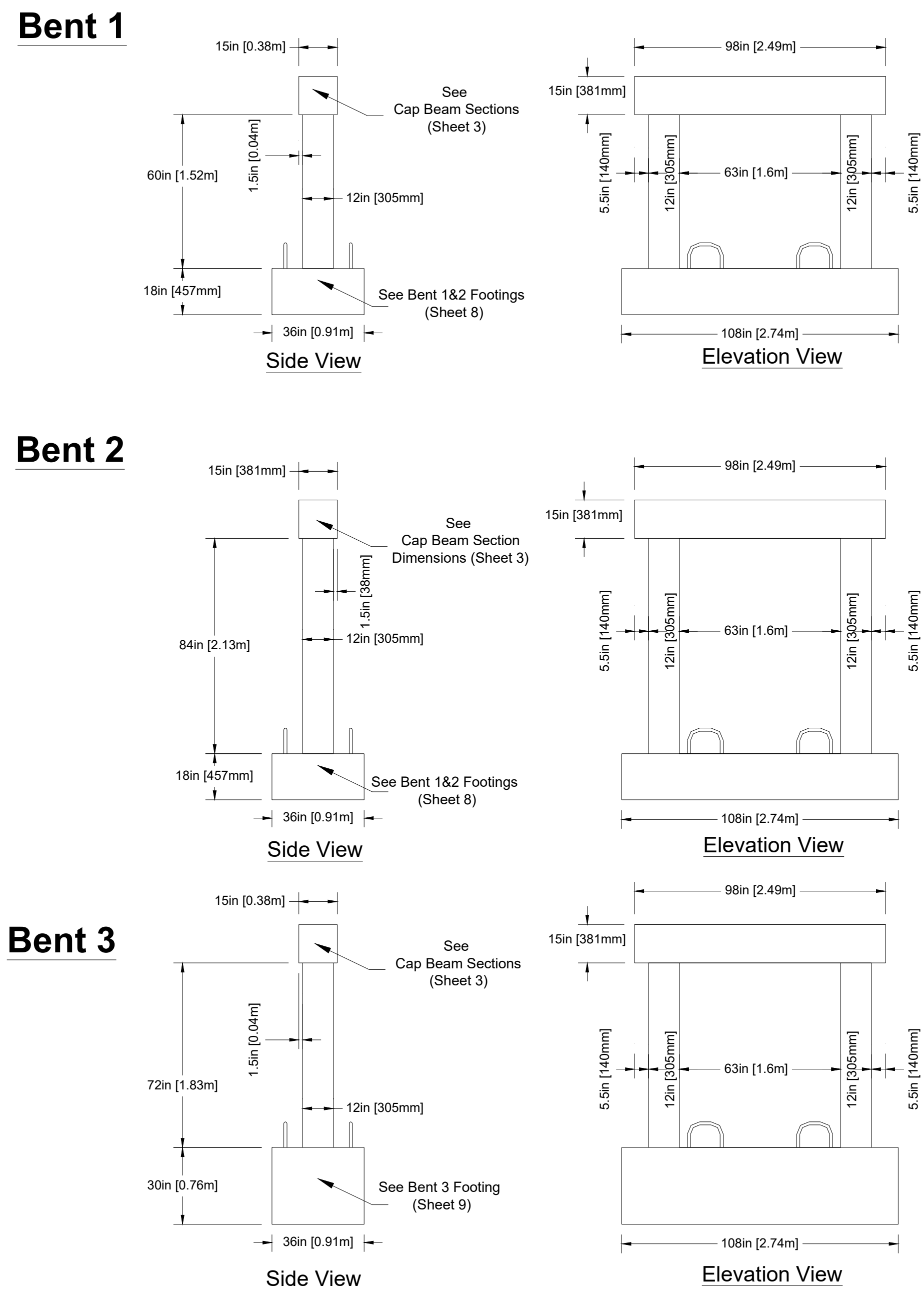

Figure 3-2. Bents configuration (Saiidi et al. 2013)

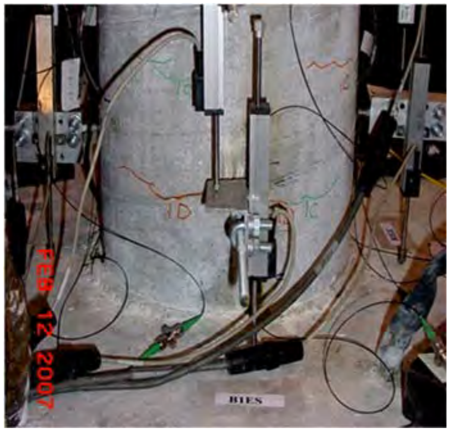

Damage State 1 (after test 1D)

Damage State 2 (after test 3)

Damage State 3 (after test 4D)

Damage State 4 (after test 5)

Damage State 5 (after test 6)

Damage State 6 (after test 7)

Figure 3-3. Apparent damage states for bent 1 East column bottom plastic hinge

Damage State 1 (after test 1D)

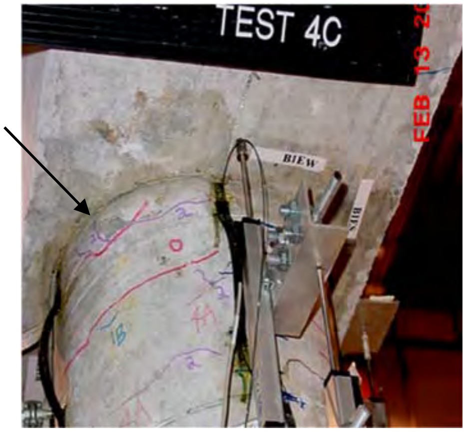

Damage State 2 (after test 4C)

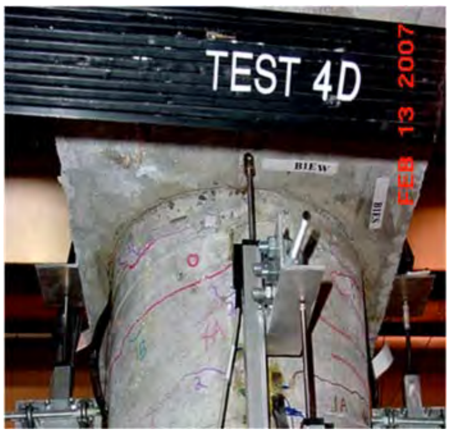

Damage State 3 (after test 4D)

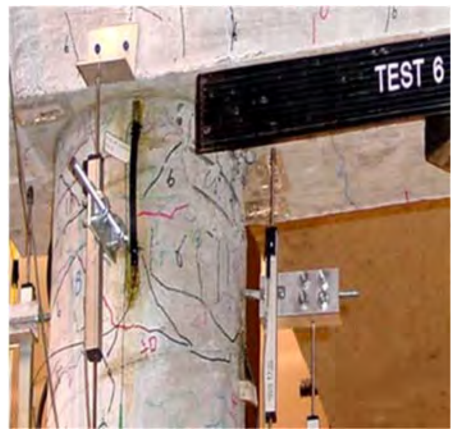

Damage State 4 (after test 6)

Damage State 5 (after test 7)

Figure 3-4. Apparent damage states for bent 1 East column top plastic hinge

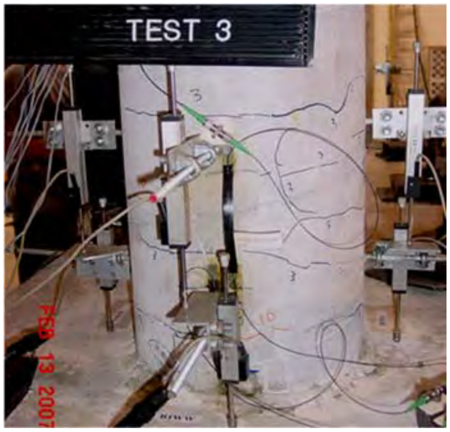

Damage State 1 (after test 3)

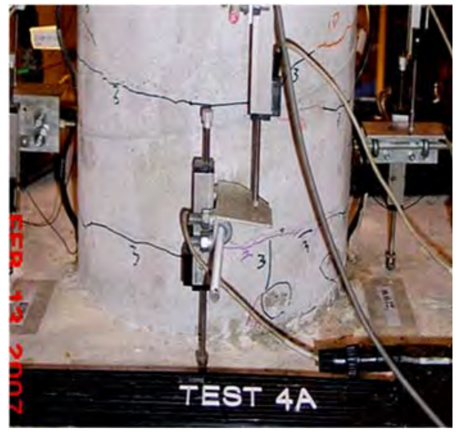

Damage State 2 (after test 4A)

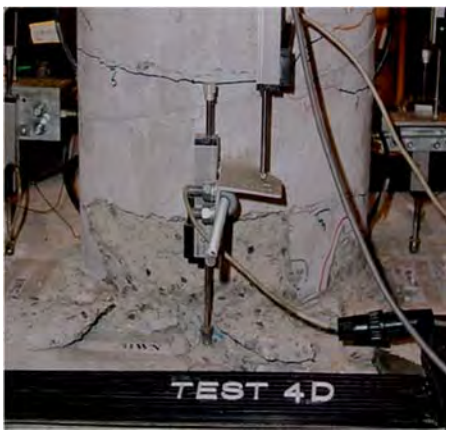

Damage State 3 (after test 4D)

Damage State 4 (after test 5)

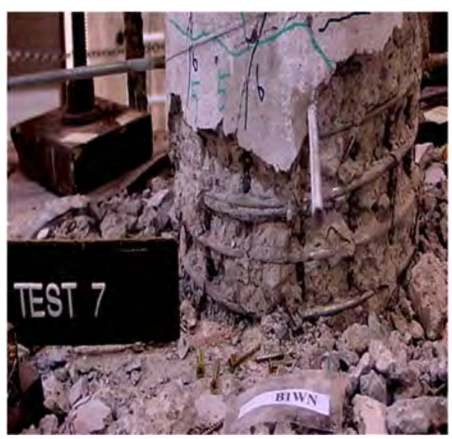

Damage State 5 (after test 7)

Figure 3-5. Apparent damage states for bent 1 West column bottom plastic hinge

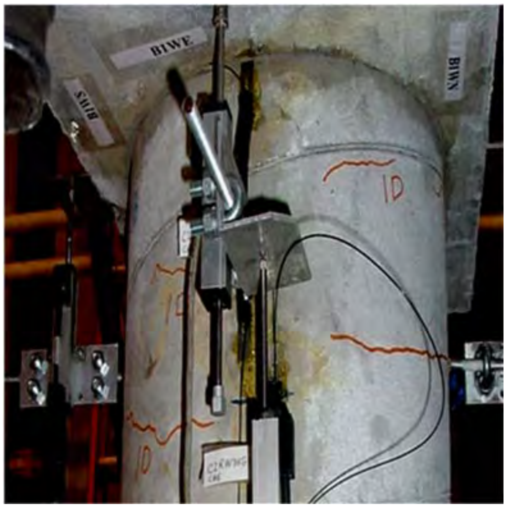

Damage State 1 (after test 1D)

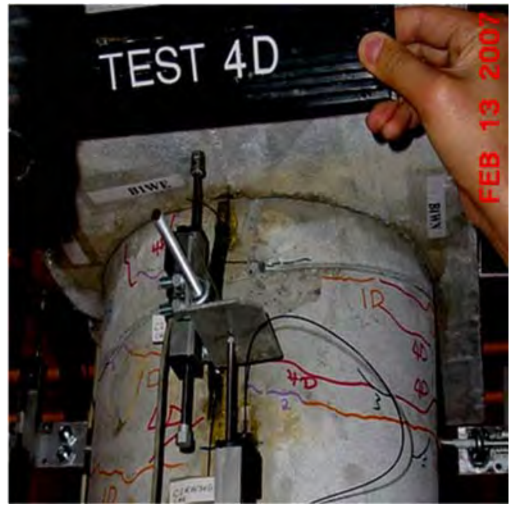

Damage State 2 (after test 4D)

Damage State 3 (after test 5)

Damage State 3 (after test 7)

Figure 3-6. Apparent damage states for bent 1 West column top plastic hinge

Damage State 1 (after test 3)

Damage State 3 (after test 5)

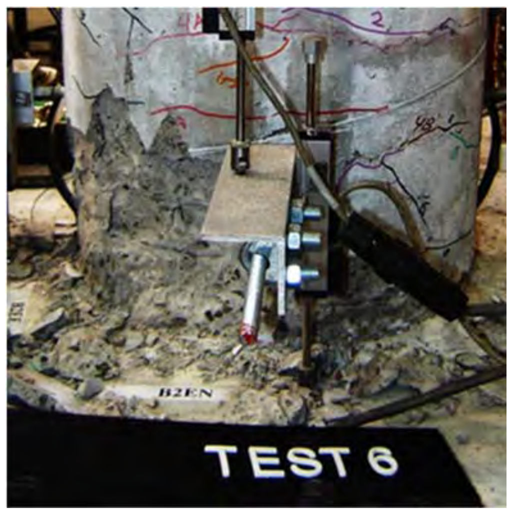

Damage State 4 (after test 6)

Figure 3-7. Apparent damage states for bent 2 East column bottom plastic hinge

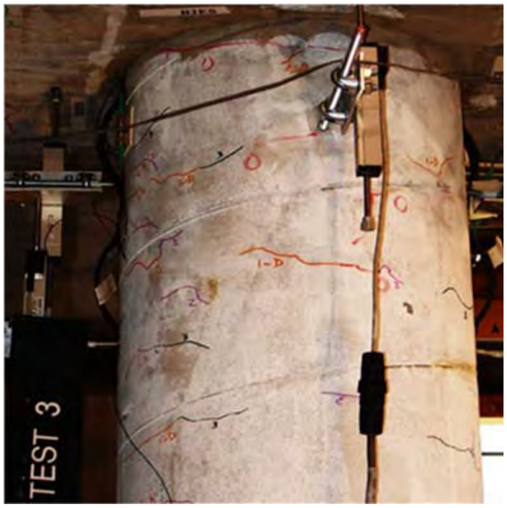

Damage State 1 (after test 3)

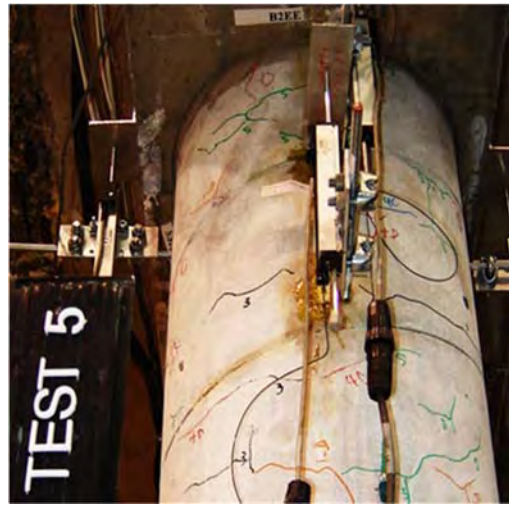

Damage State 2 (after test 5)

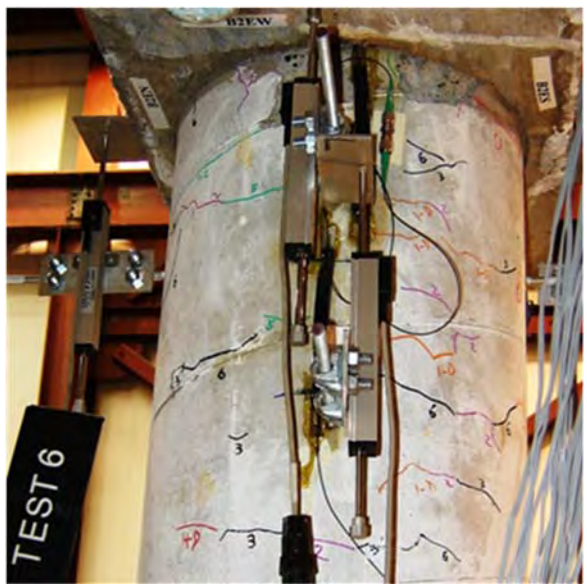

Damage State 3 (after test 6)

Figure 3-8. Apparent damage states for bent 2 East column top plastic hinge

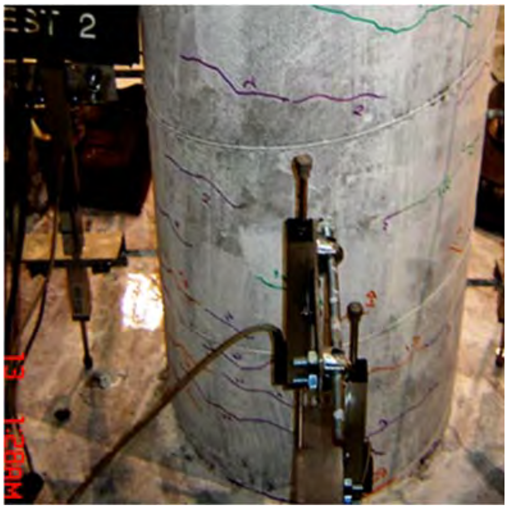

Damage State 1 (after test 2)

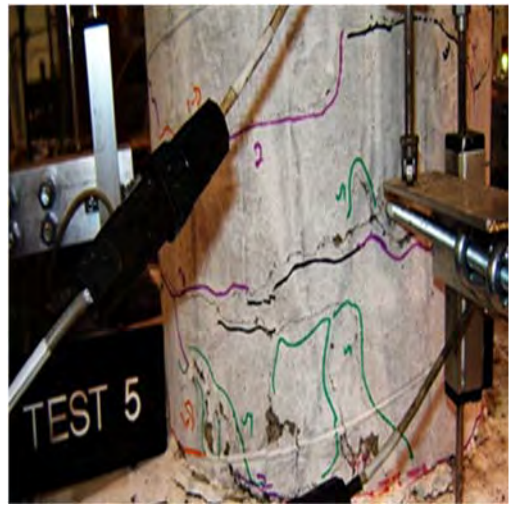

Damage State 2 (after test 5)

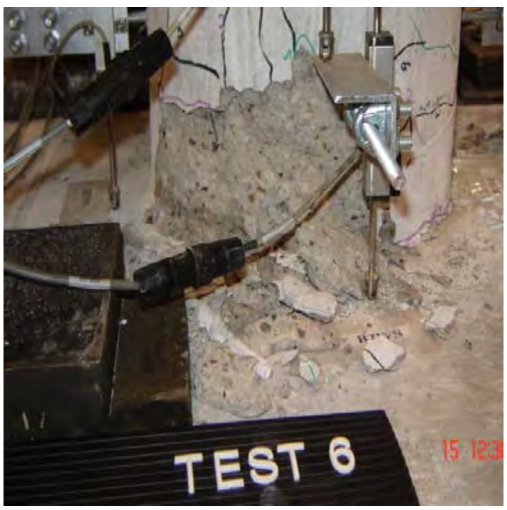

Damage State 3 (after test 6)

Damage State 4 (after test 7)

Figure 3-9. Apparent damage states for bent 2 West column bottom plastic hinge

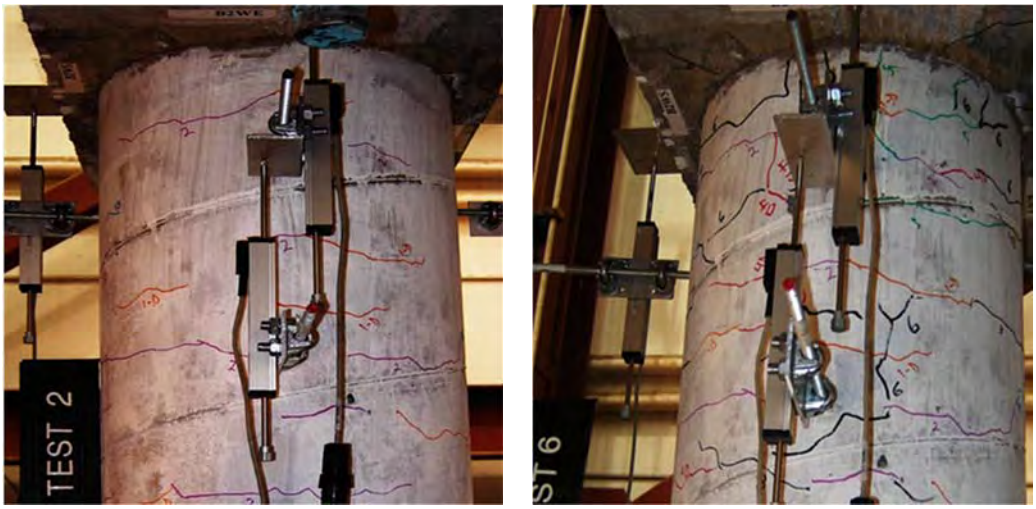

Damage State 1 (after test 2) Damage State 2 (after test 6)

Figure 3-10. Apparent damage states for bent 2 West column top plastic hinge

Damage State 1 (after test 3)

Damage State 2 (after test 4D)

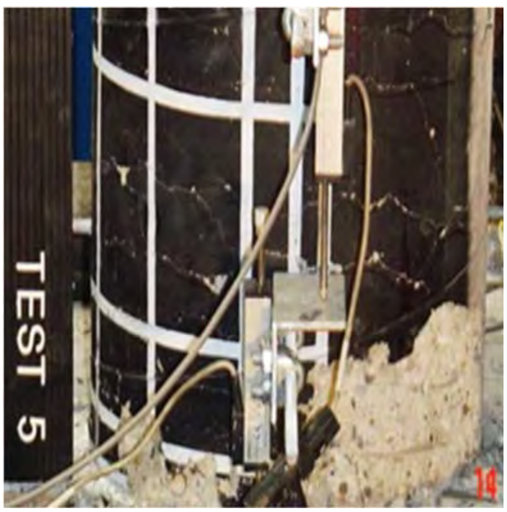

Damage State 3 (after test 5)

Damage State 4 (after test 7)

Figure 3-11. Apparent damage states for bent 3 East column bottom plastic hinge

Damage State 2 (after test 4D)

Damage State 3 (after test 5)

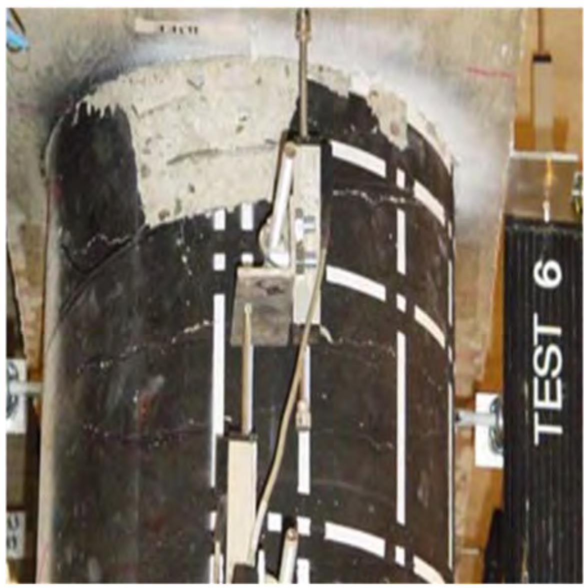

Damage State 4 (after test 6)

Figure 3-12. Apparent damage states for bent 3 East column top plastic hinge

Damage State 1 (after test 3)

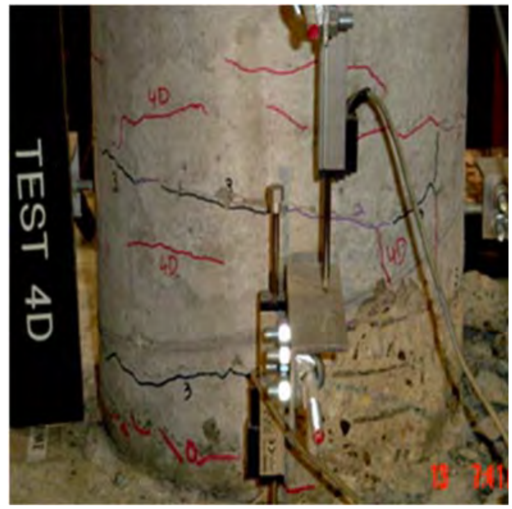

Damage State 4 (after test 4D)

Damage State 5 (after test 6)

Figure 3-13. Apparent damage states for bent 3 West column bottom plastic hinge

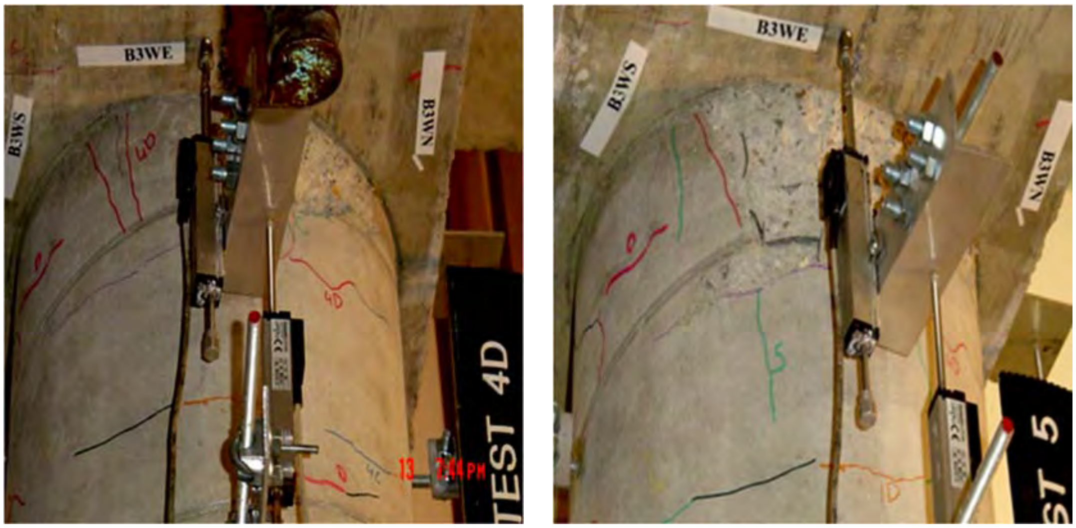

Damage State 3 (after test 4D) Damage State 4 (after test 5)

Figure 3-14. Apparent damage states for bent 3 West column top plastic hinge

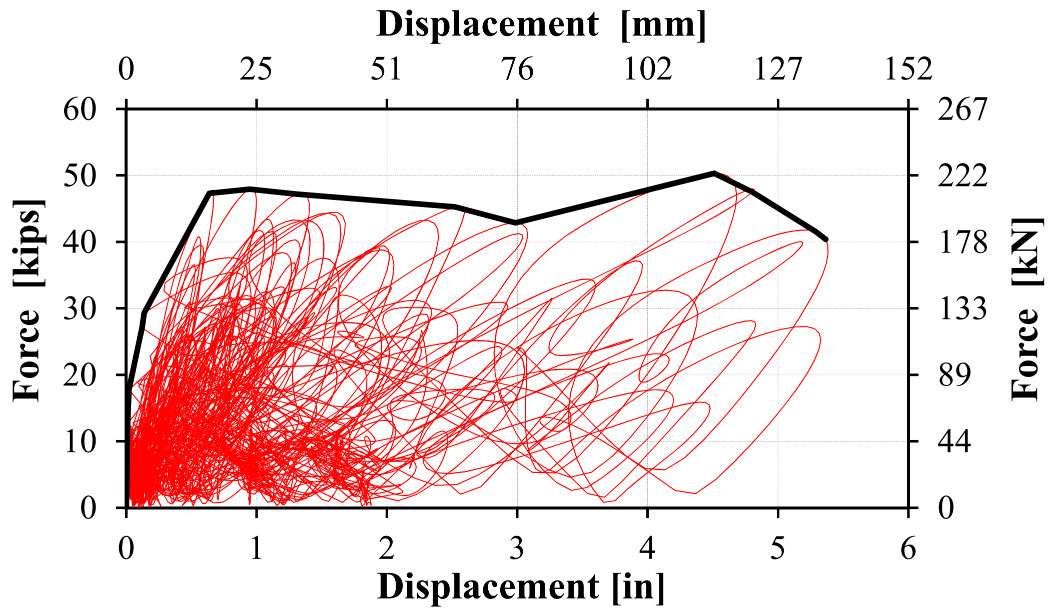

Figure 3-15. Bent 1 measured force-displacement hysteresis curves and envelope

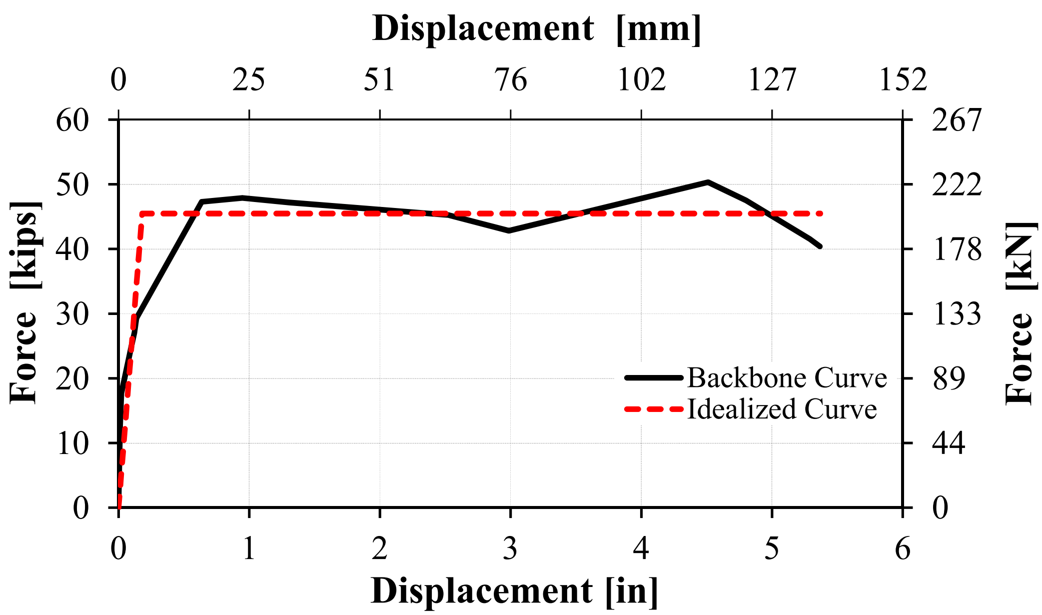

Figure 3-16. Bent 1 measured envelope and idealized force-displacement curve

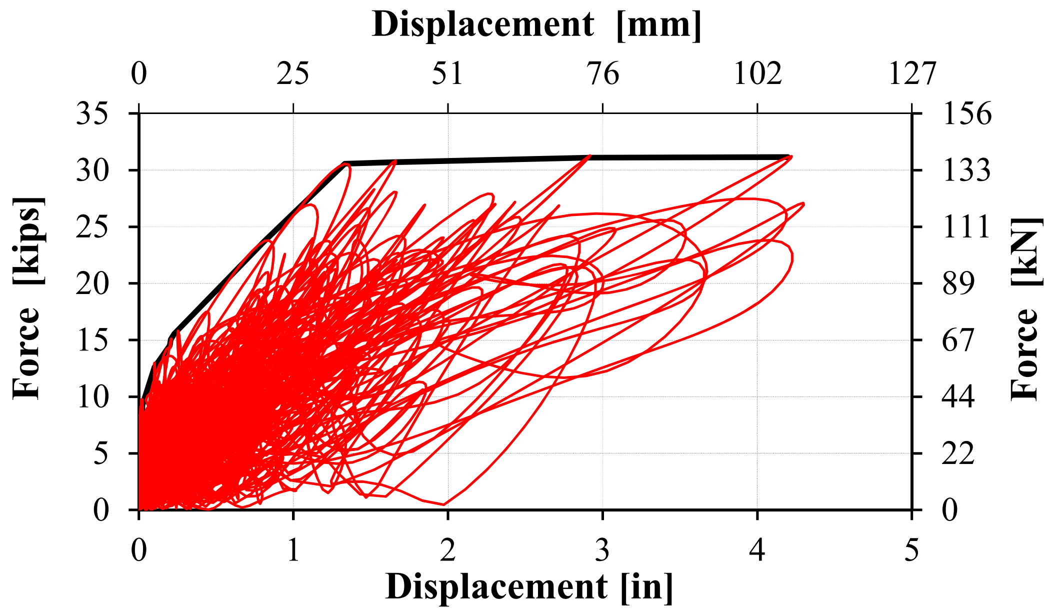

Figure 3-17. Bent 2 measured force-displacement hysteresis curves and envelope

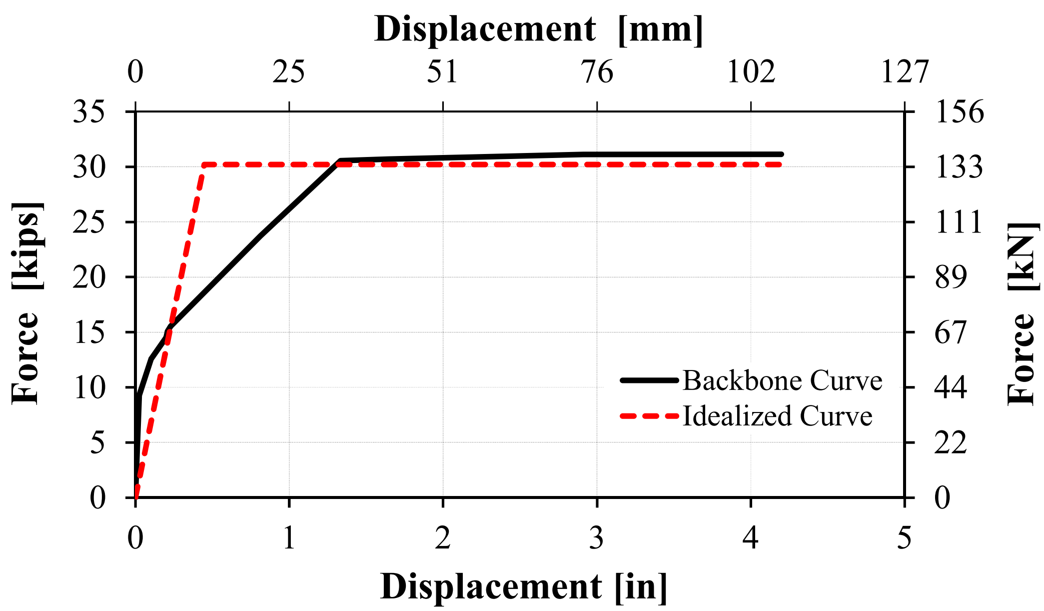

Figure 3-18. Bent 2 measured envelope and idealized force-displacement curve

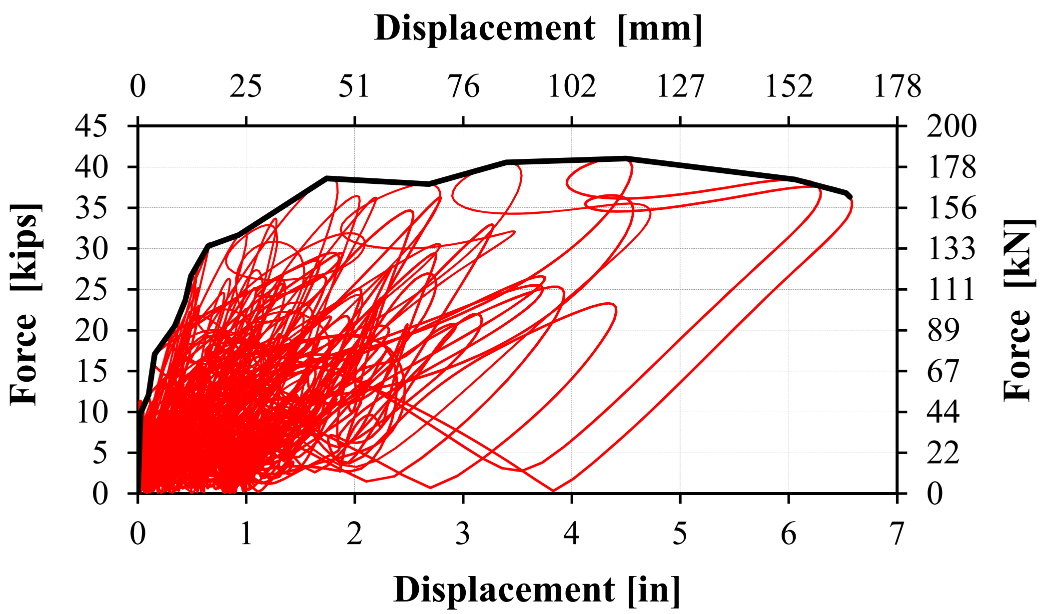

Figure 3-19. Bent 3 measured force-displacement hysteresis curves and envelope

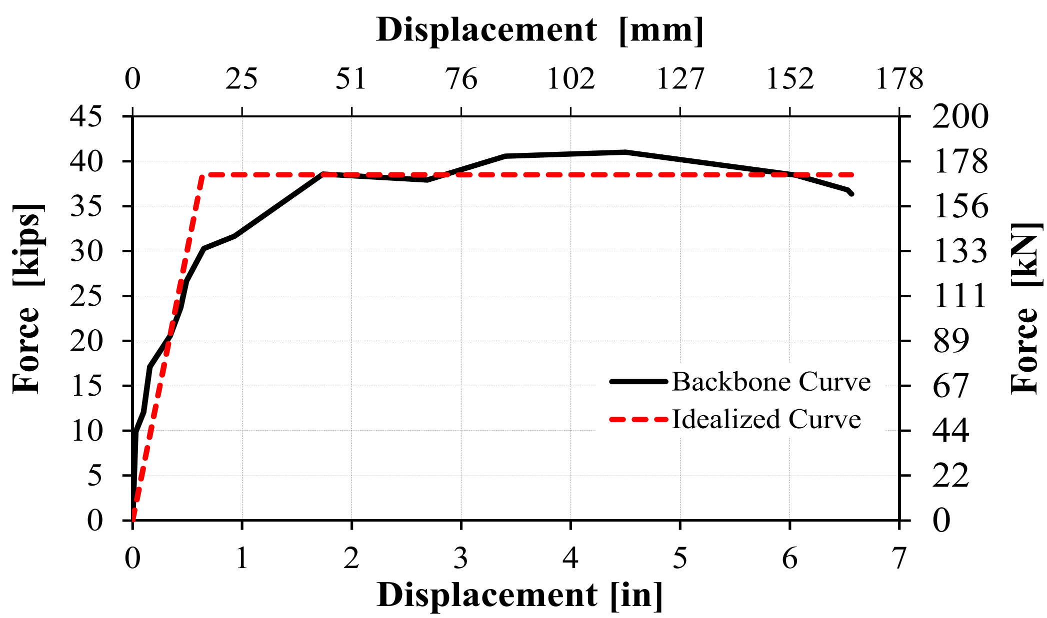

Figure 3-20. Bent 3 measured envelope and idealized force-displacement curve

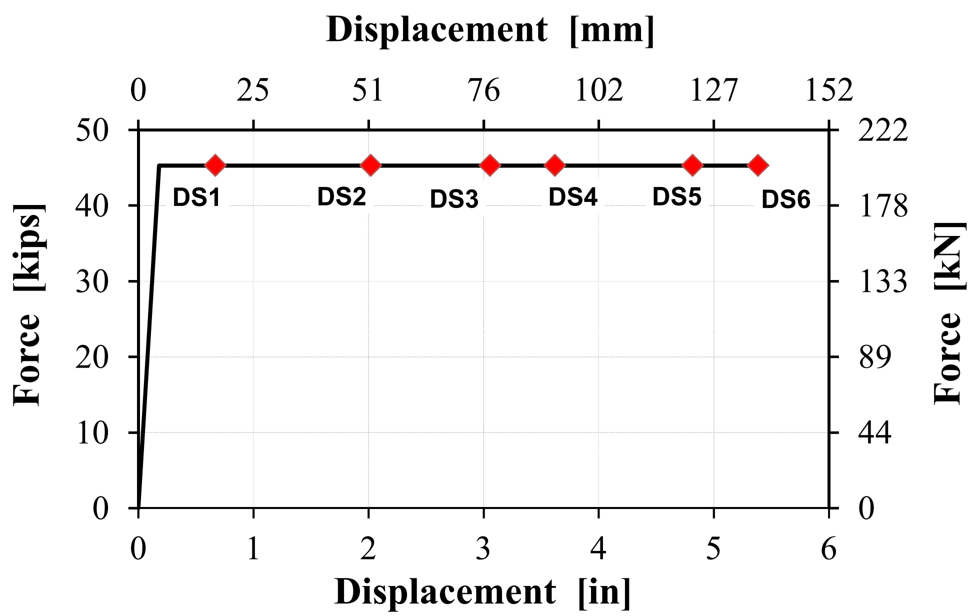

Figure 3-21. Idealized pushover curve and damage states for bent 1 East column

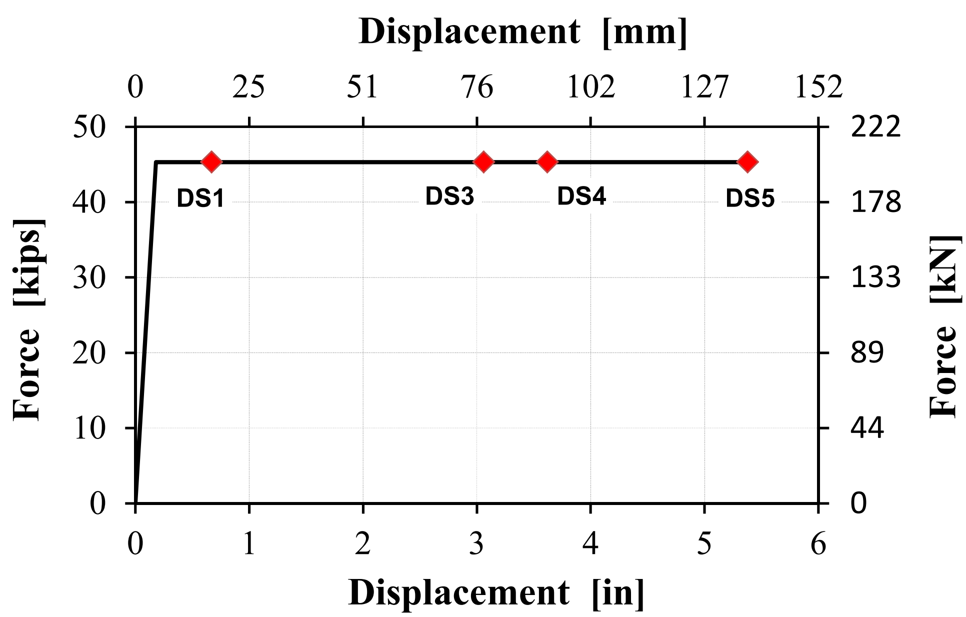

Figure 3-22. Idealized pushover curve and damage states for bent 1 West column

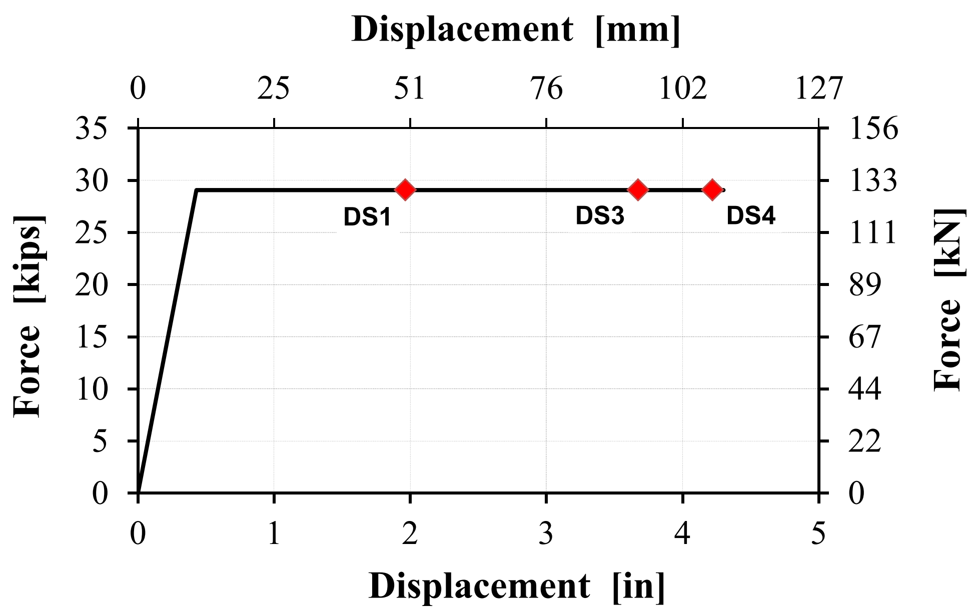

Figure 3-23. Idealized pushover curve and damage states for bent 2 East column

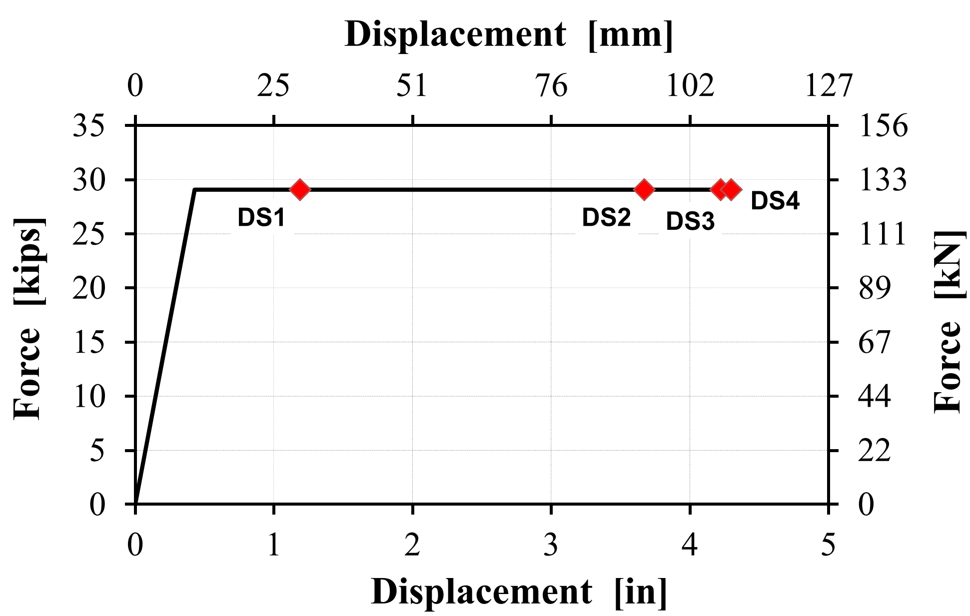

Figure 3-24. Idealized pushover curve and damage states for bent 2 West column

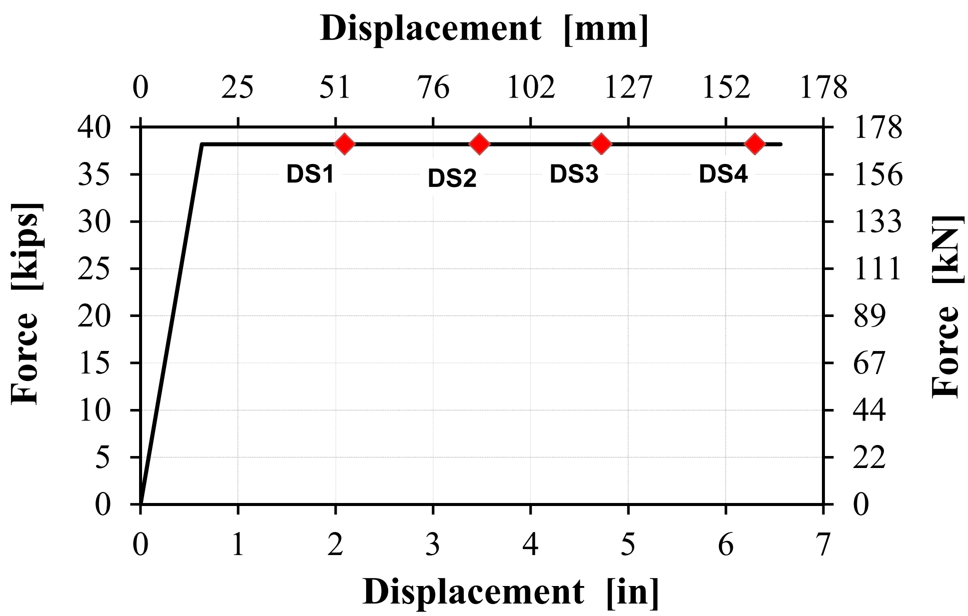

Figure 3-25. Idealized pushover curve and damage states for bent 3 East column

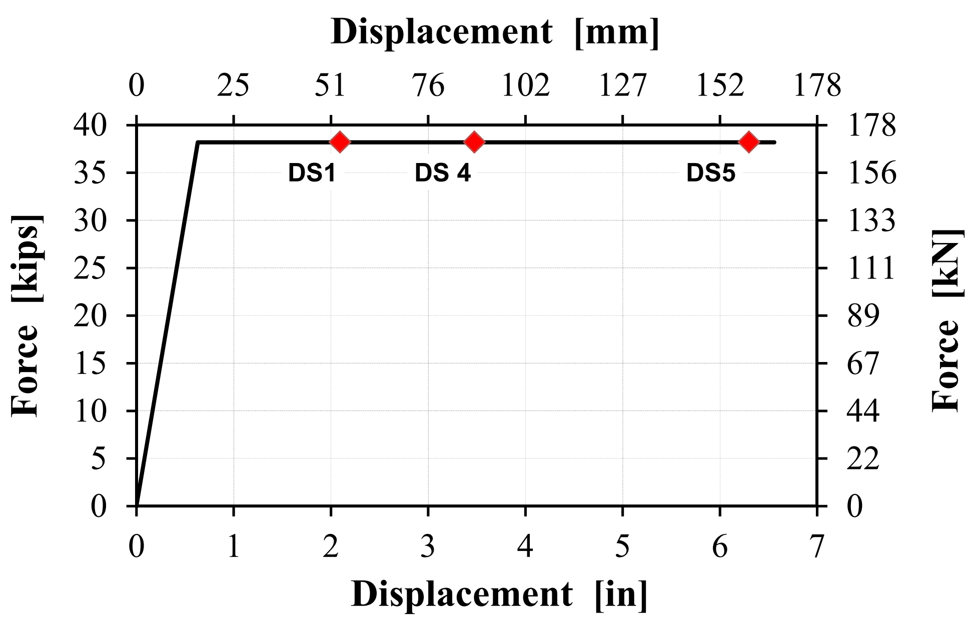

Figure 3-26. Idealized pushover curve and damage states for bent 3 West column

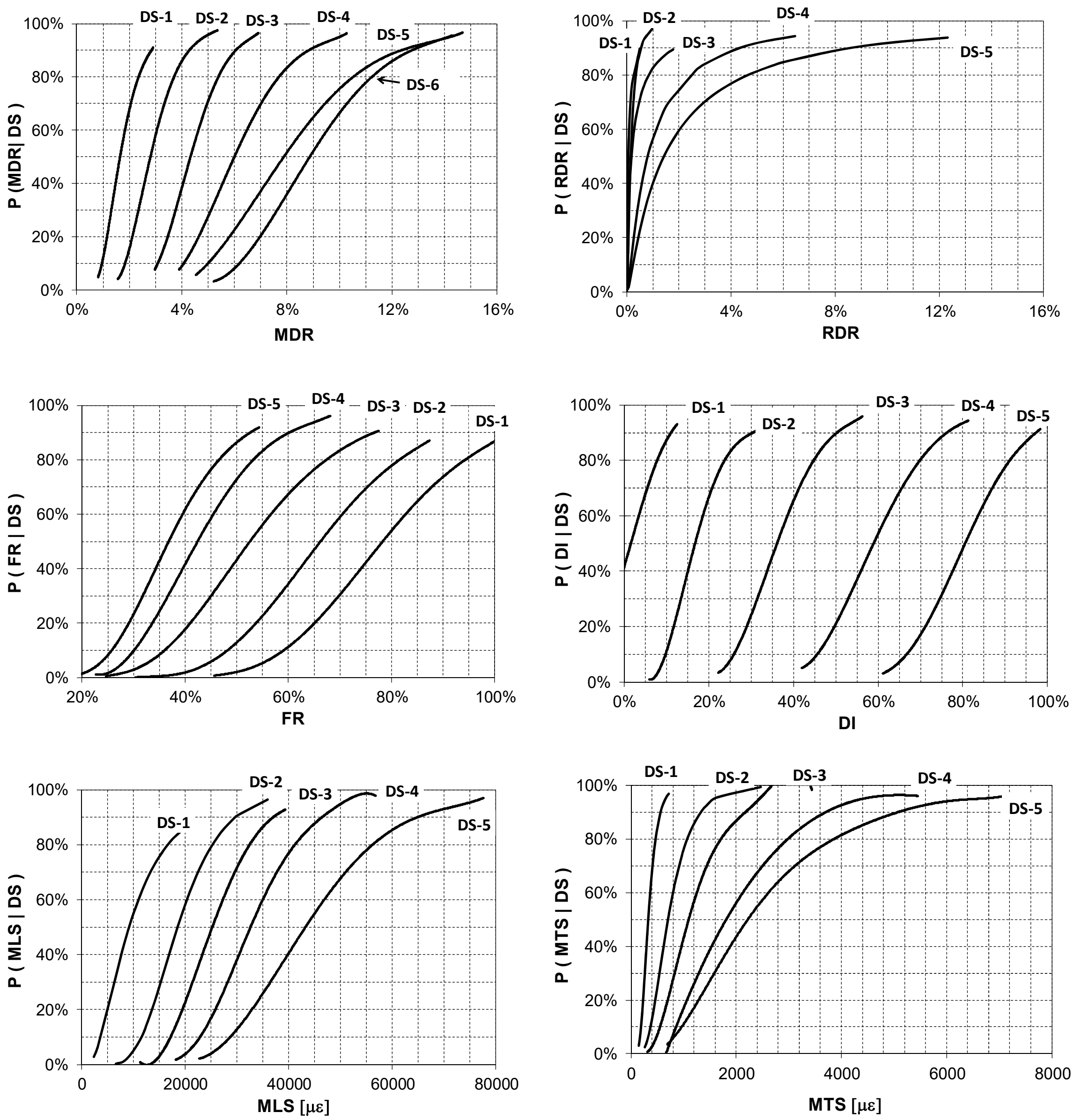

Figure 3-27. Combined fragility curves of response parameters

Chapter 4. Figures

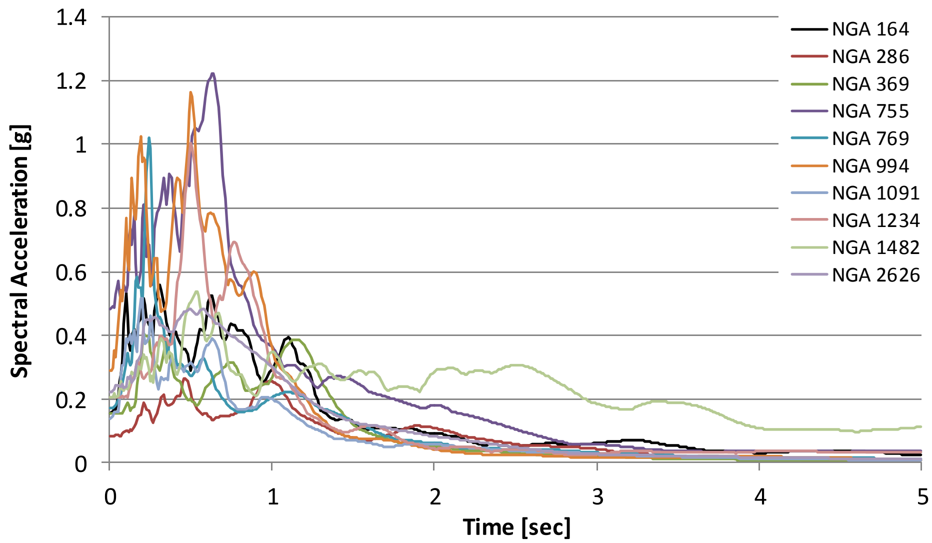

Figure 4-1. Far-field ground motions response spectrum of site class B/C

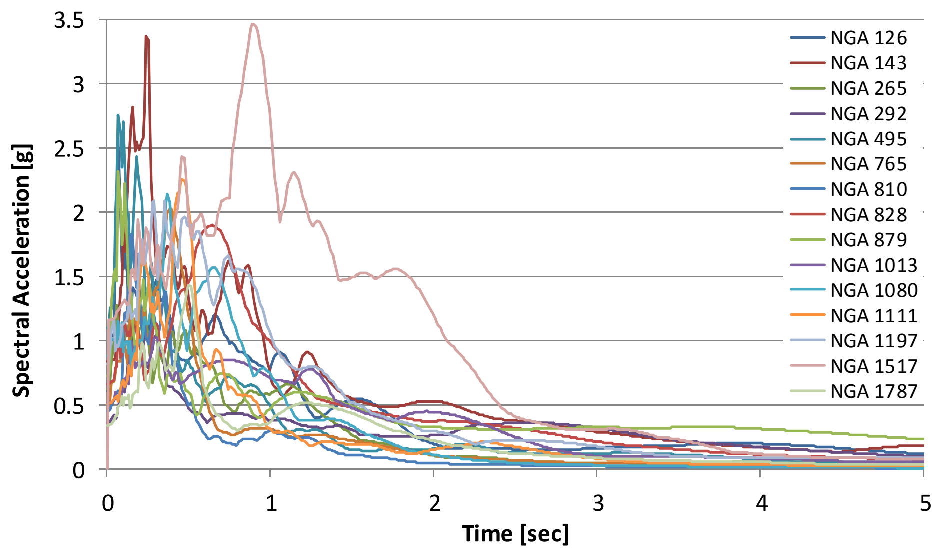

Figure 4-2. Near-field ground motions response spectrum of site class B/C

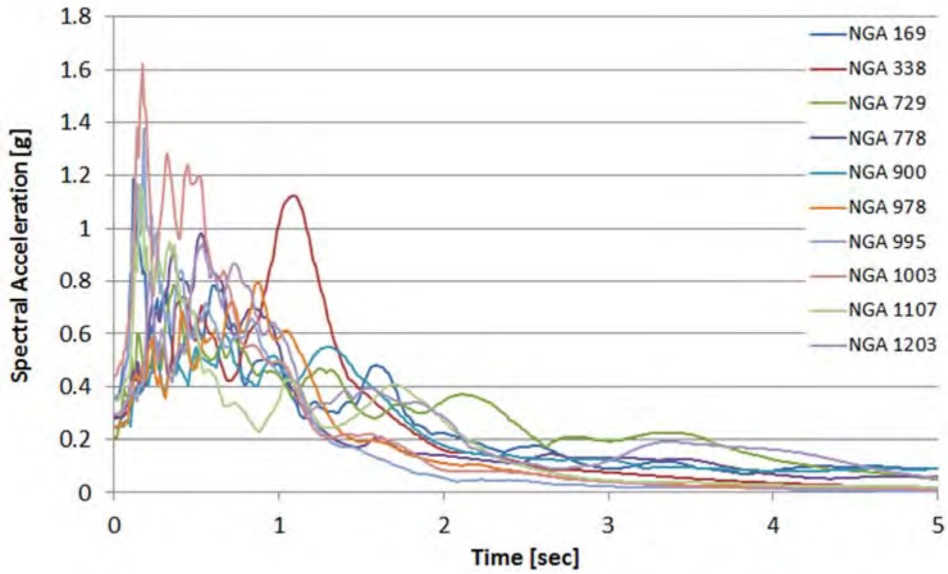

Figure 4-3. Far-field ground motions response spectrum of site class D

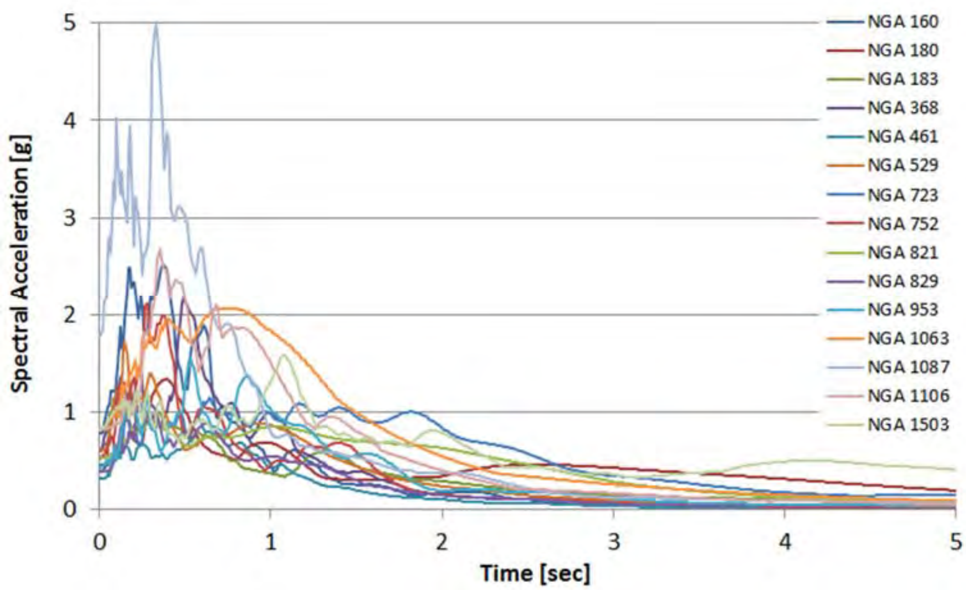

Figure 4-4. Near-field ground motions response spectrum of site class D

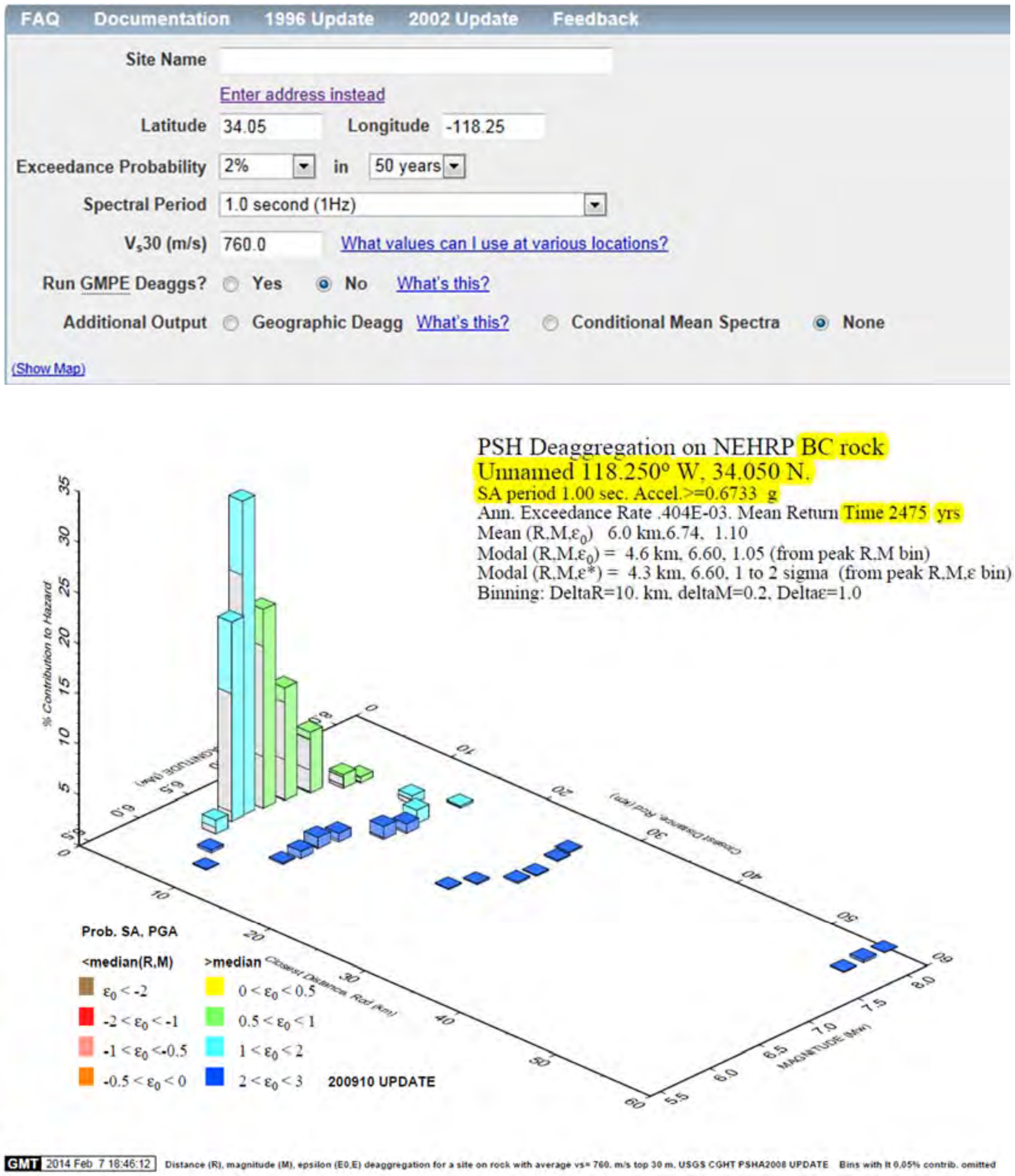

Figure 4-5. USGS Interactive Deaggregation Tool (Beta)

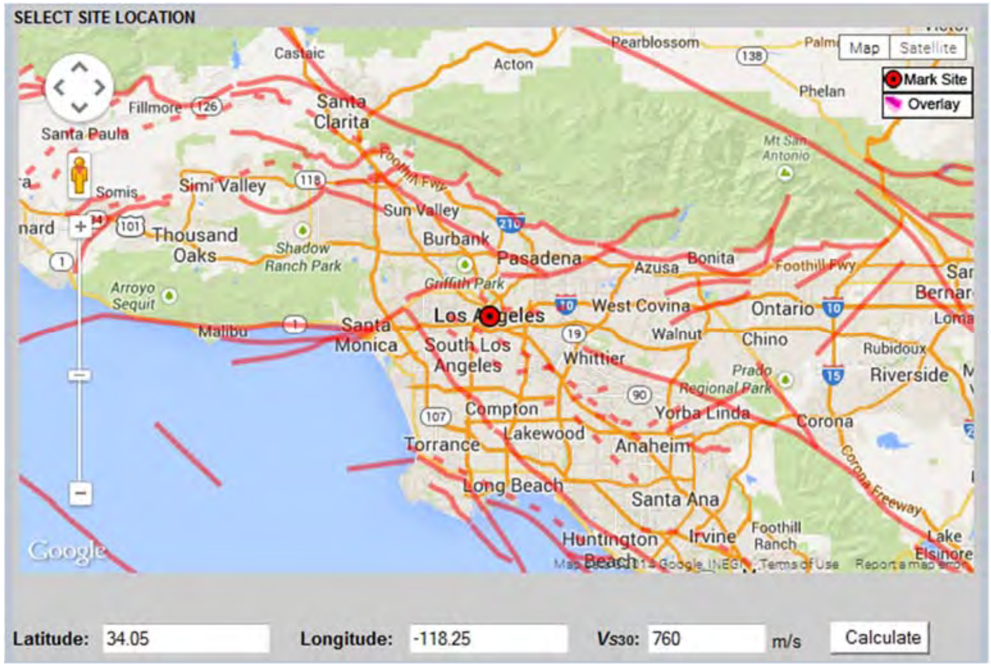

Figure 4-6. Site location (latitude = 34.05, longitude = -118.25)

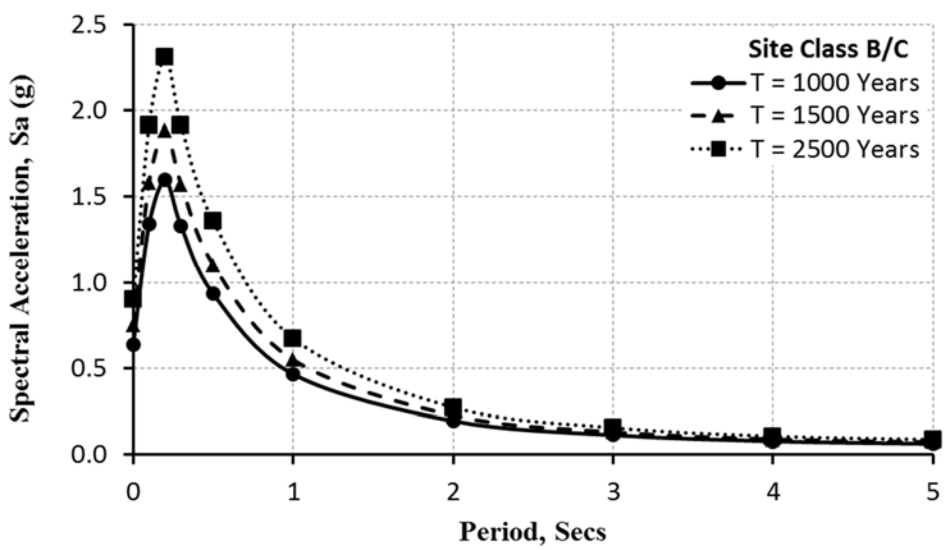

Figure 4-7. Design spectrum for site class B/C

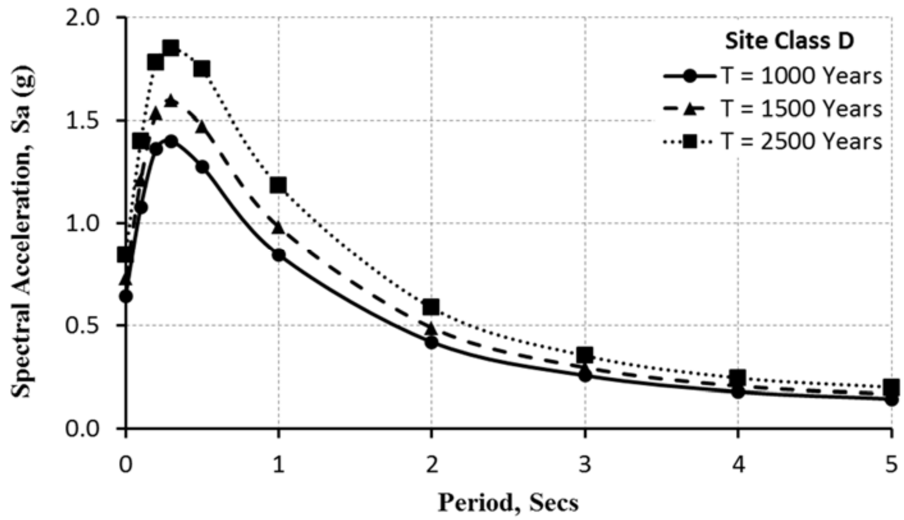

Figure 4-8. Design spectrum for site class D

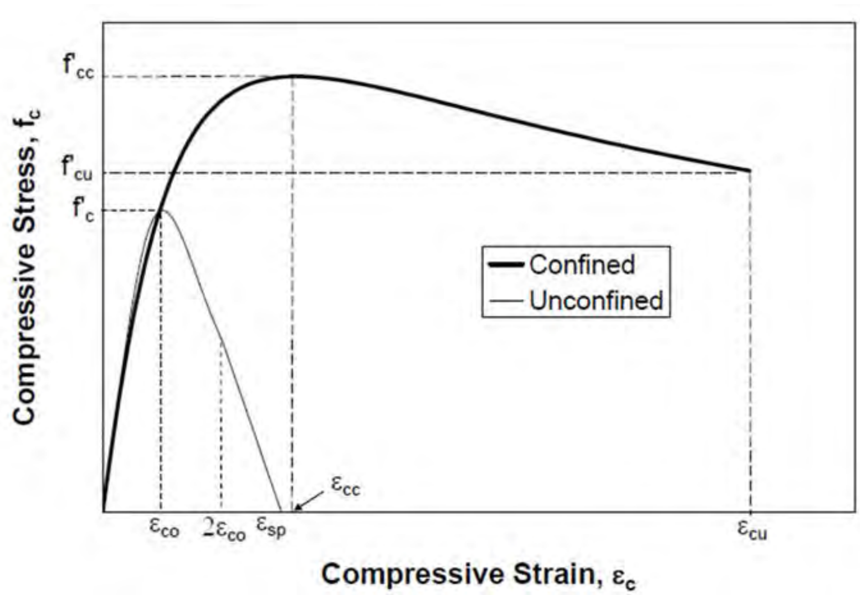

Figure 4-9. Mander's confined and unconfined concrete model

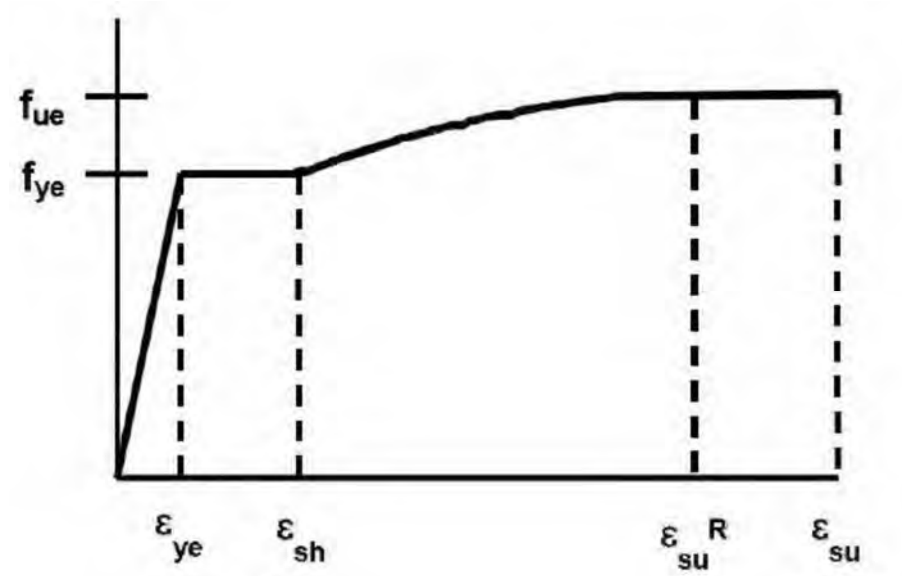

Figure 4-10. Steel stress strain model

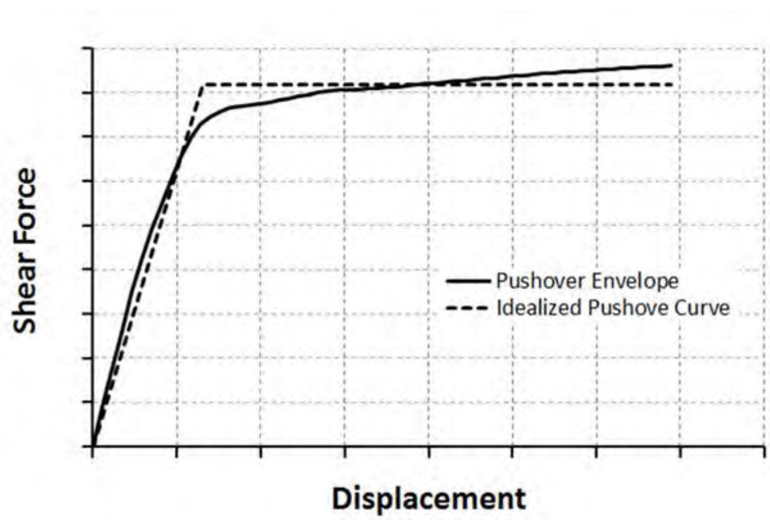

Figure 4-11. Typical idealized pushover curve

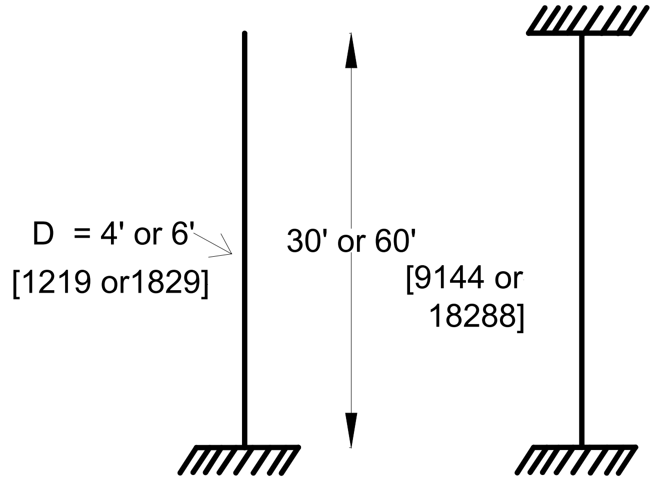

Figure 4-12. Typical single column bents configuration

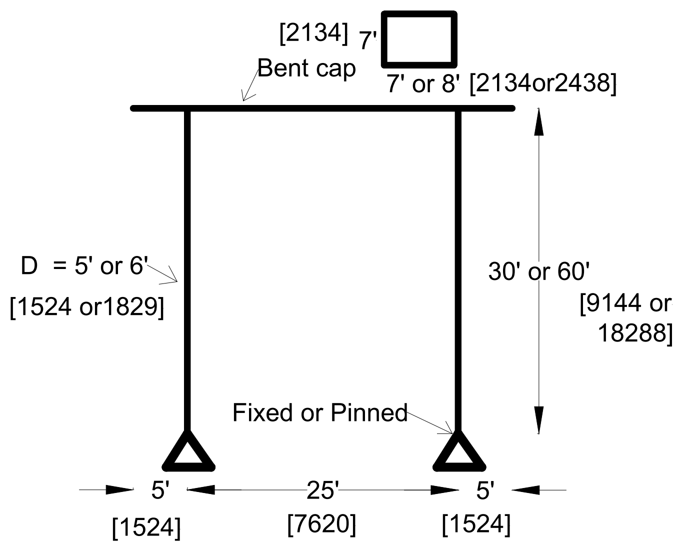

Figure 4-13. Typical two column bents configuration

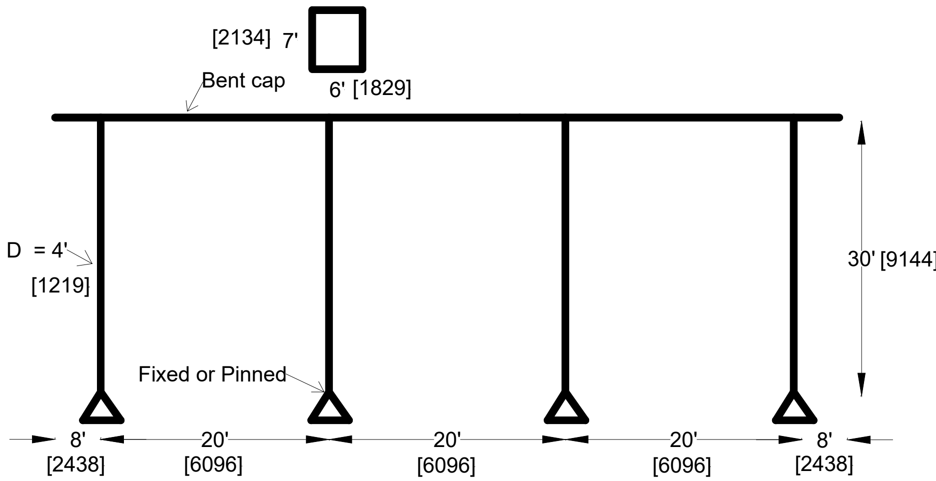

Figure 4-14. Typical four Column Bents configuration

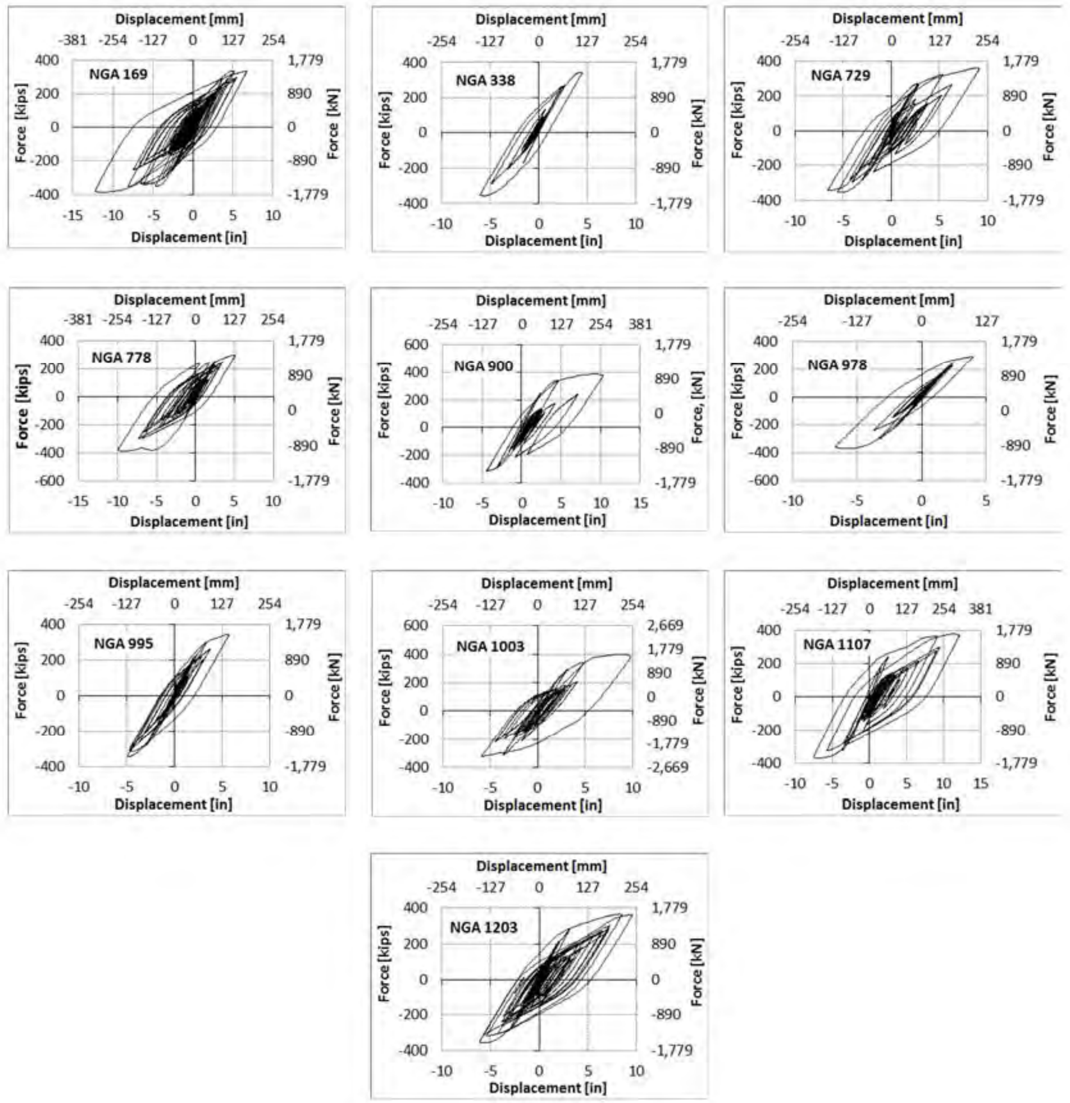

Figure 4-15. Force-displacement hysteresis curves for far-field GMs

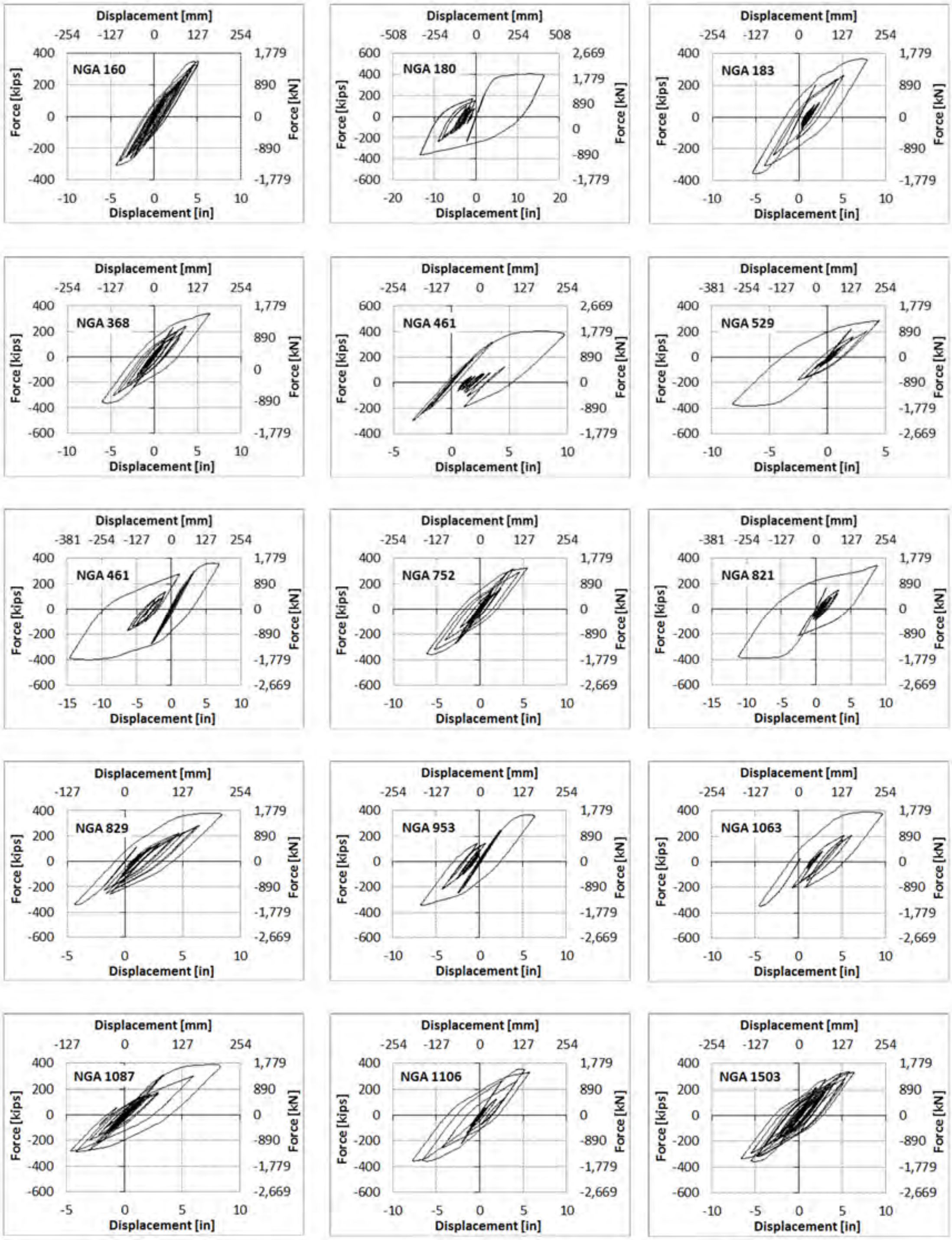

Figure 4-16. Force-displacement hysteresis curves for near-field GMs

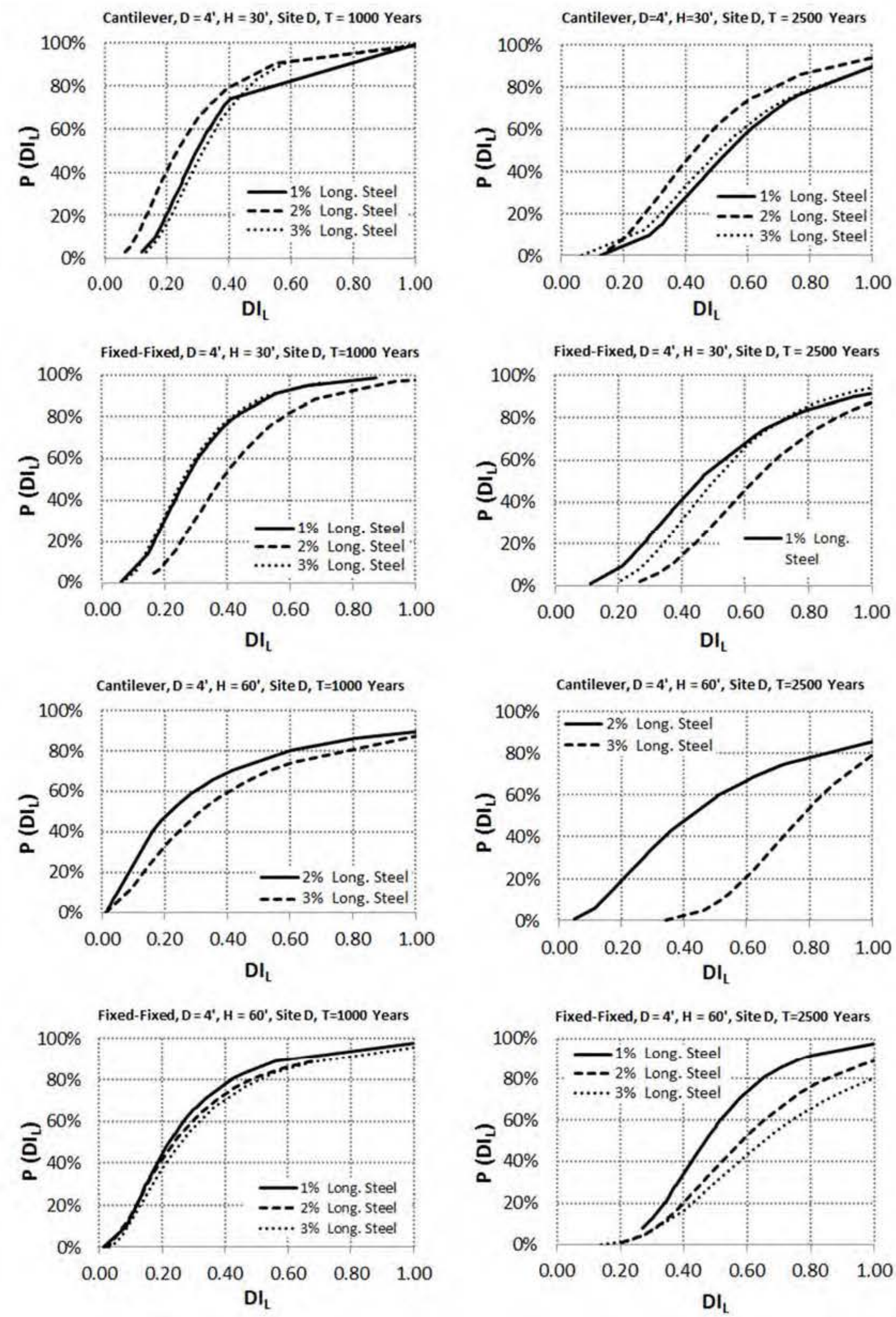

Figure 4-17. Fragility curves for SCBs with four foot diameter columns for Site D

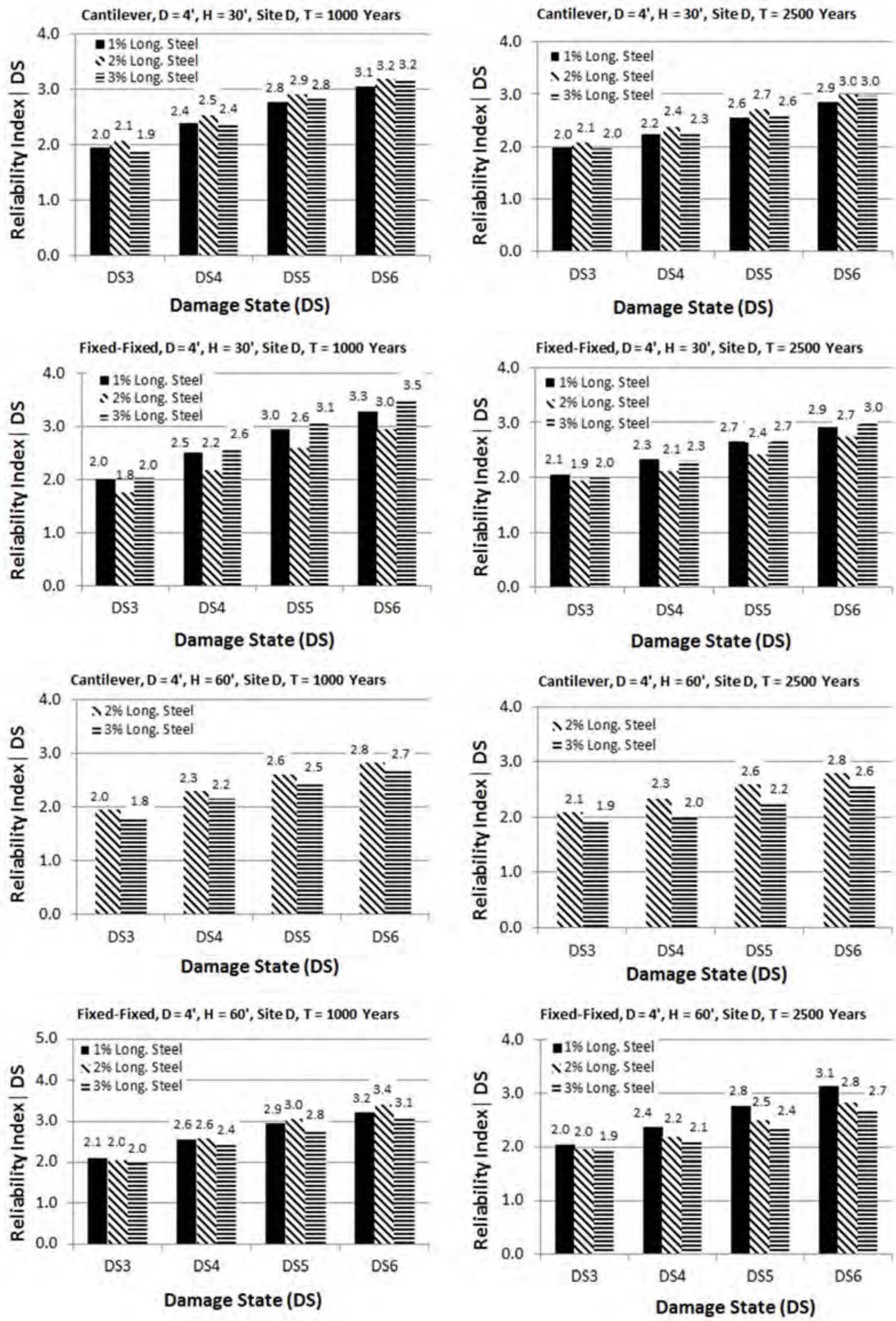

Figure 4-18. Reliability indices for SCBs with four foot diameter columns for Site D

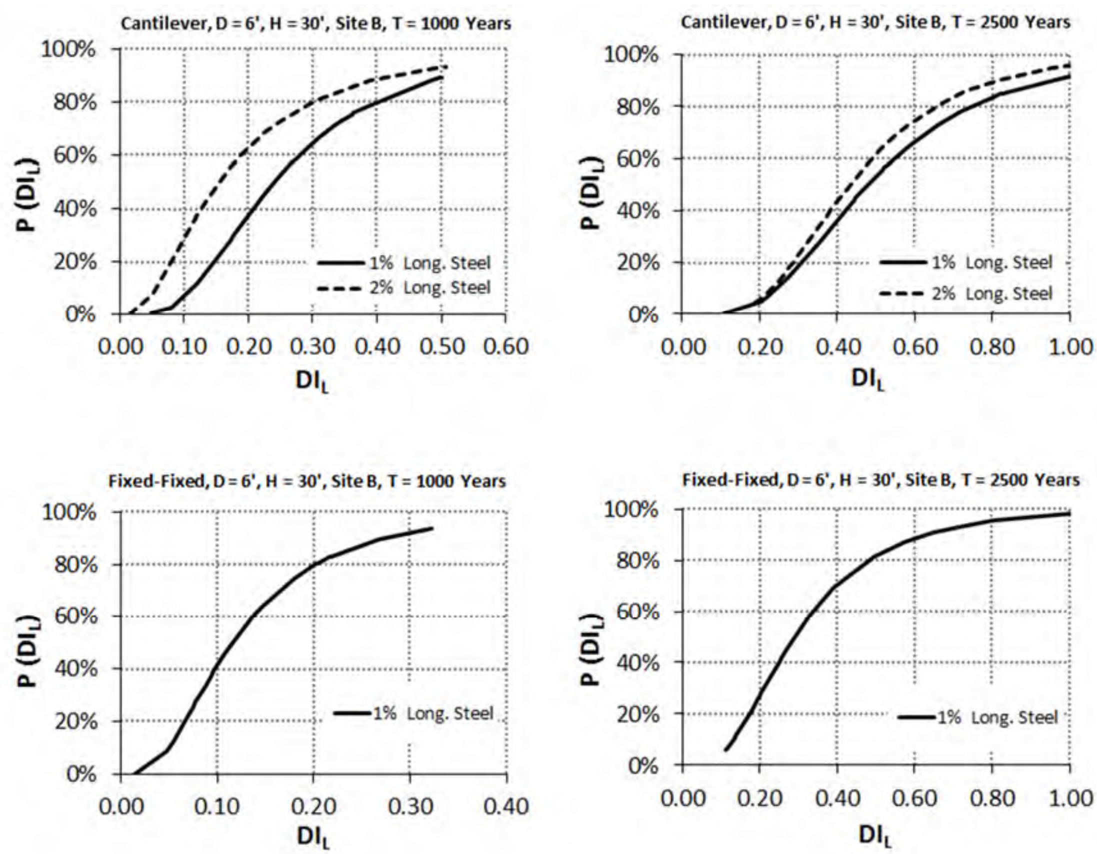

Figure 4-19. Fragility curves for SCBs with six foot diameter columns for Site B/C

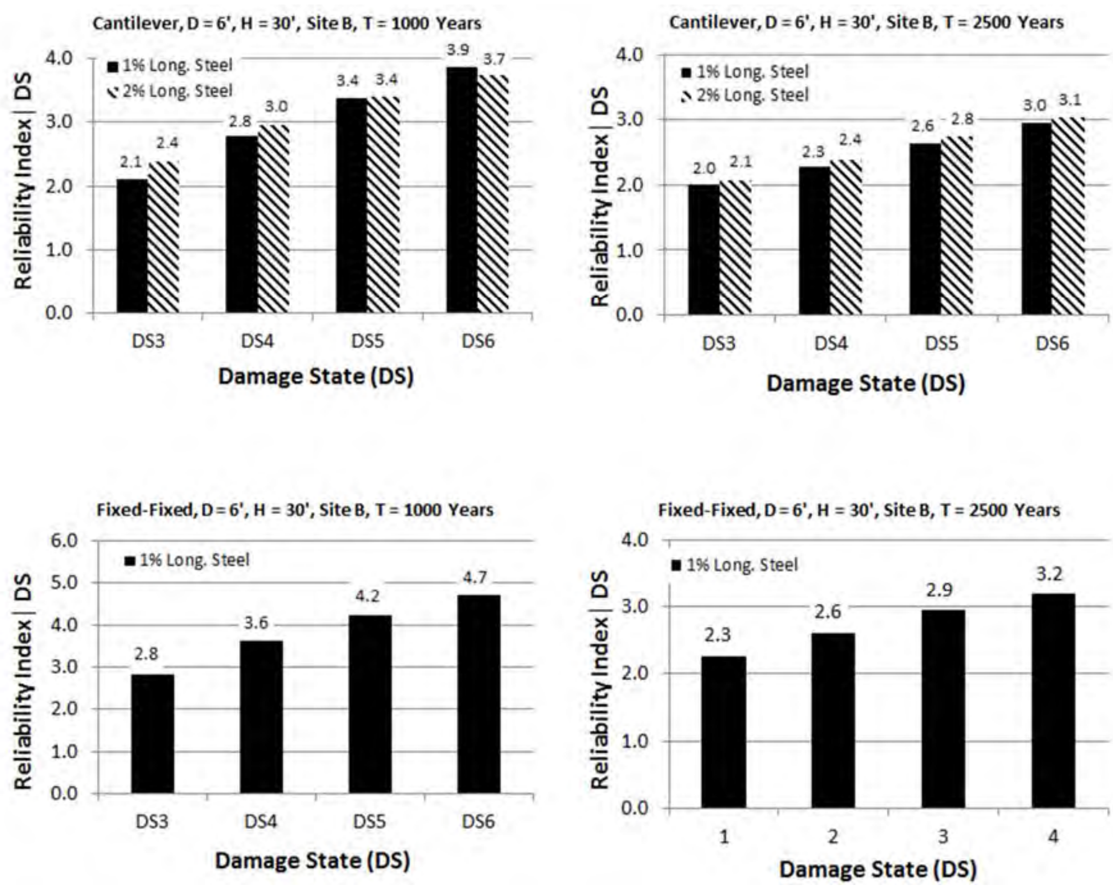

Figure 4-20. Reliability indices for SCBs with six foot diameter columns for Site B/C

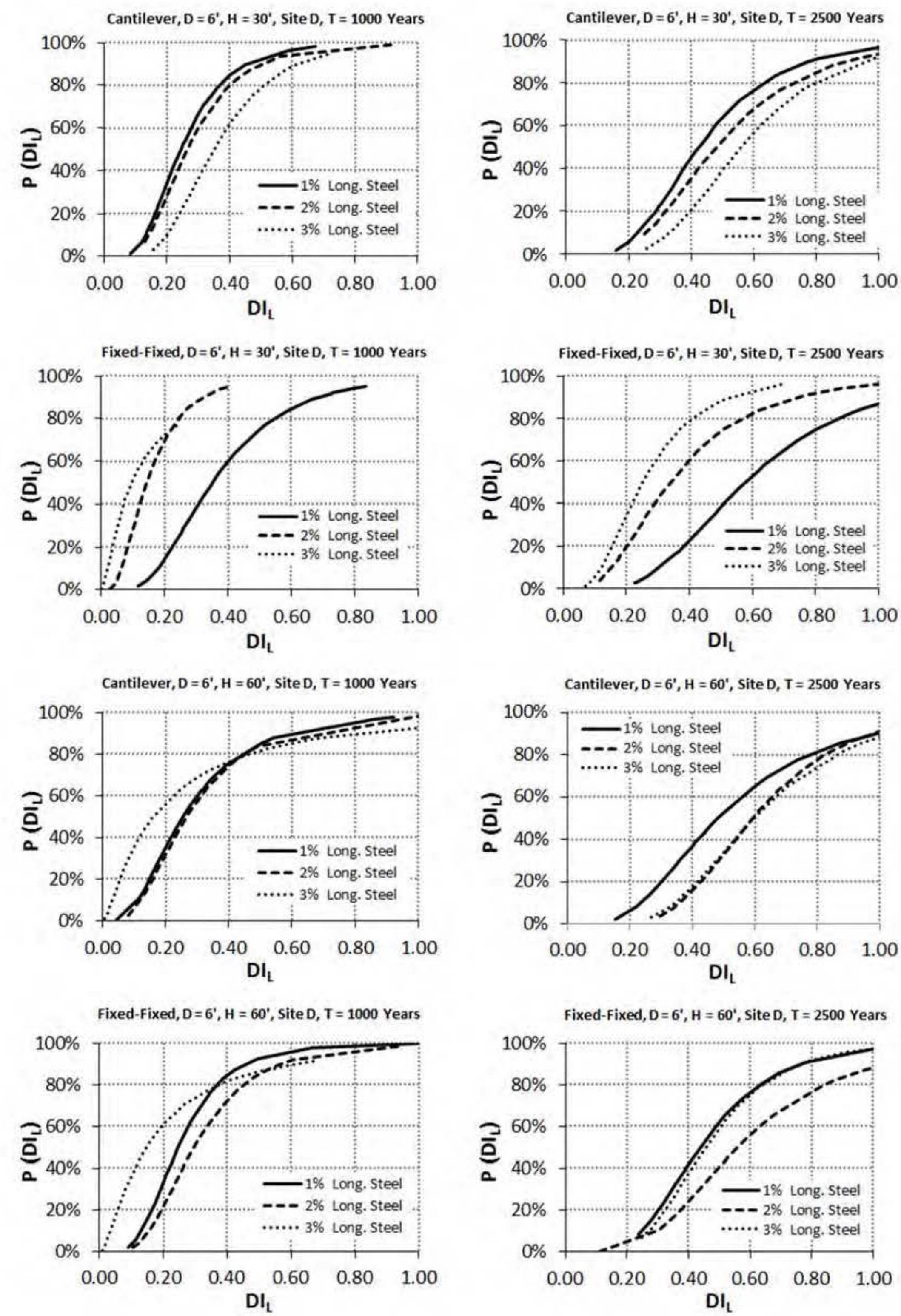

Figure 4-21. Fragility curves for SCBs with six foot diameter columns for Site D

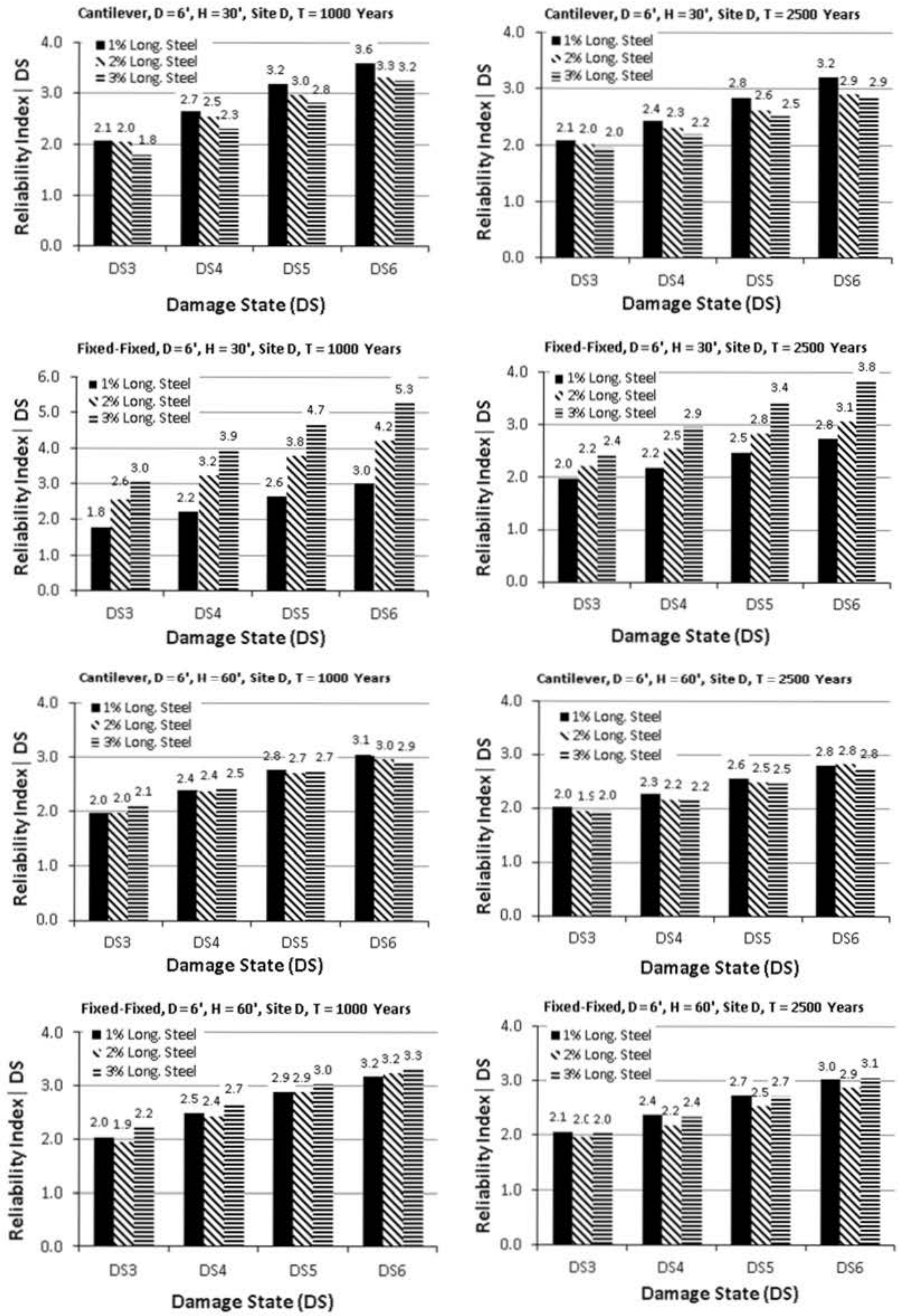

Figure 4-22. Reliability indices for SCBs with six foot diameter columns for Site D

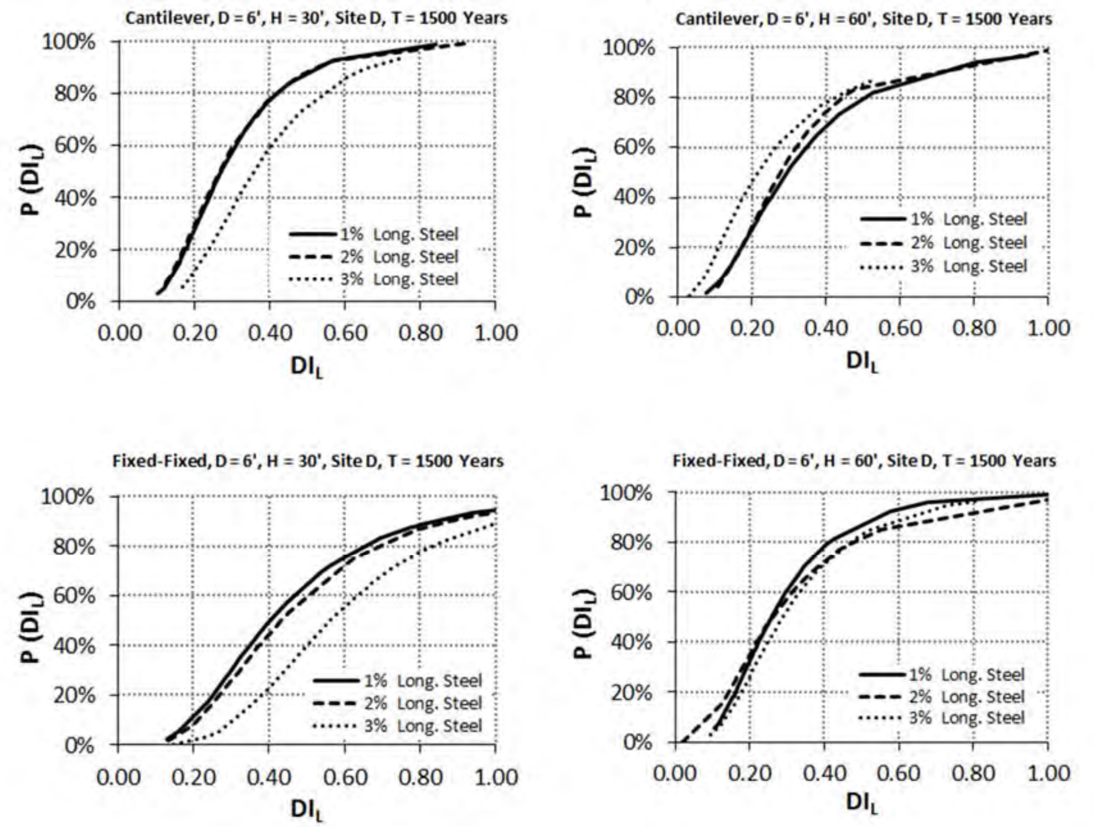

Figure 4-23. Fragility curves for SCBs with six foot diameter columns for Site D analyzed under 1500-year earthquake

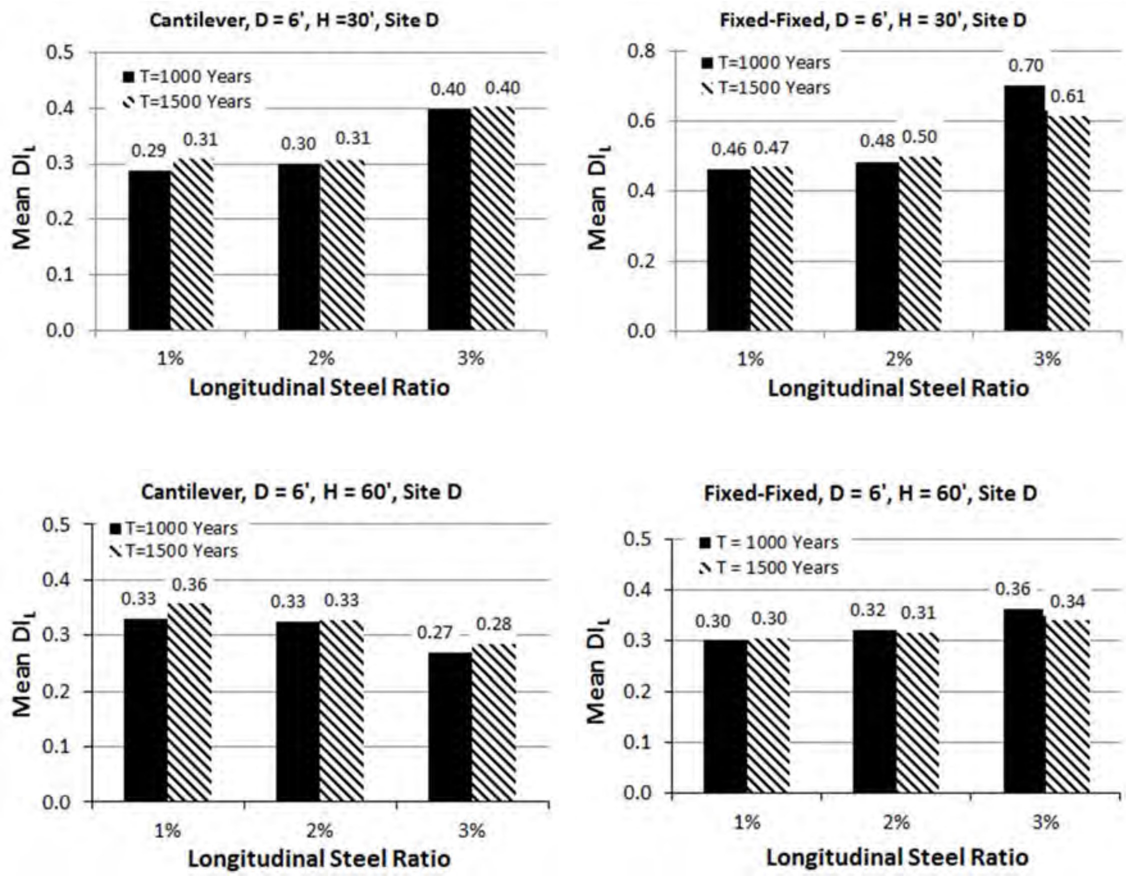

Figure 4-24. Mean DI_L for T=1000 and 1500-year earthquake

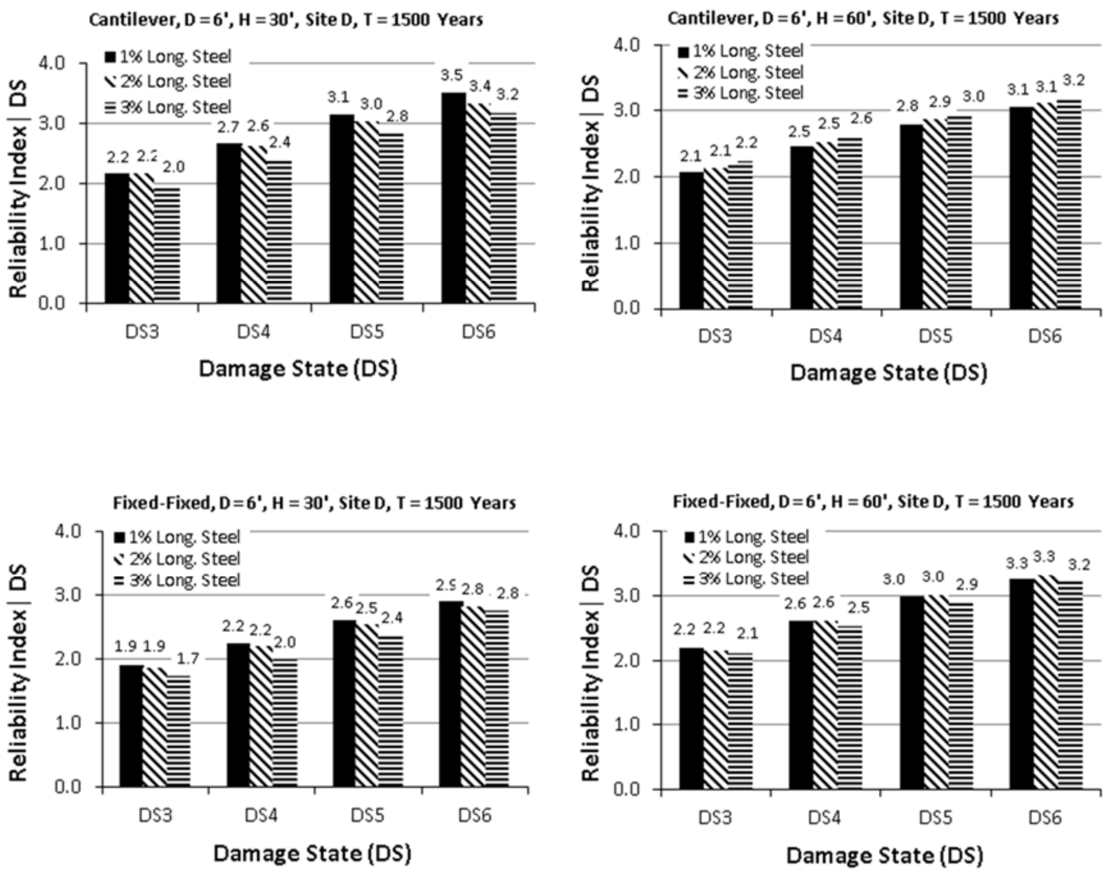

Figure 4-25. Reliability indices for SCBs with six foot diameter columns for Site D

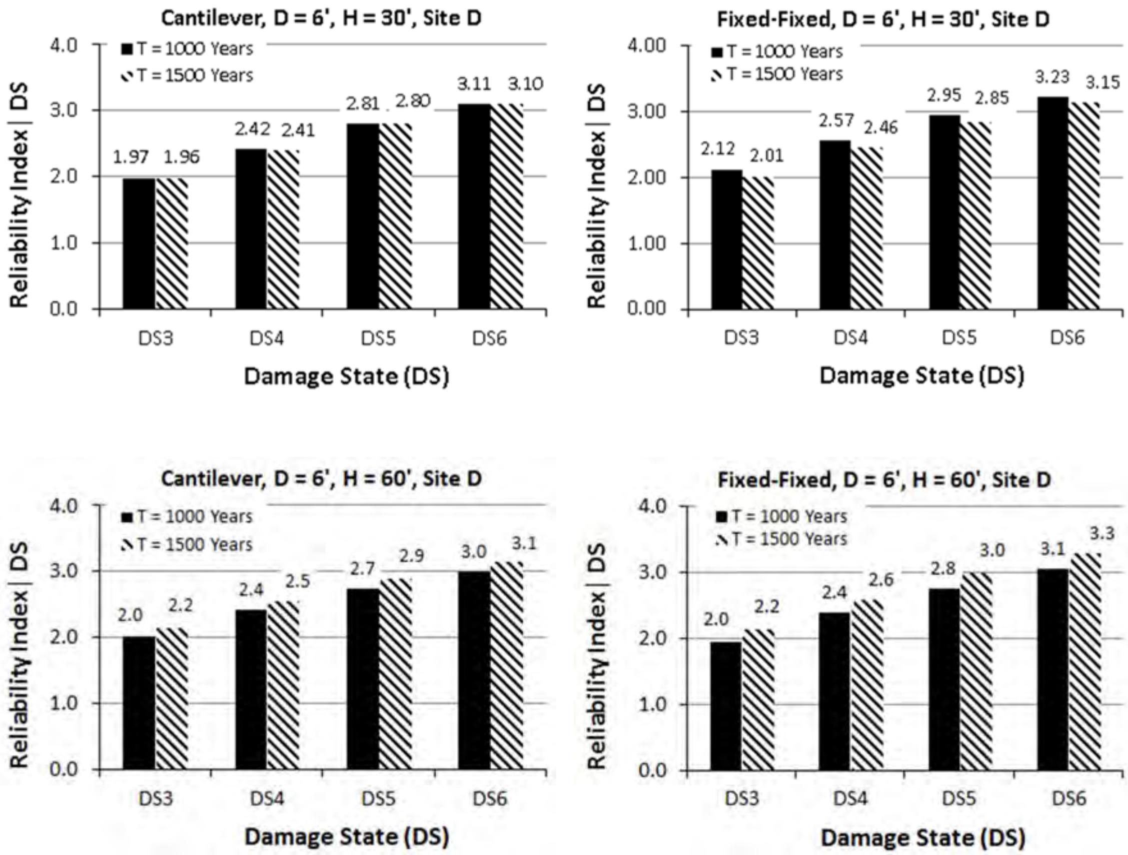

Figure 4-26. Reliability indices for T=1000 and 1500-year earthquake

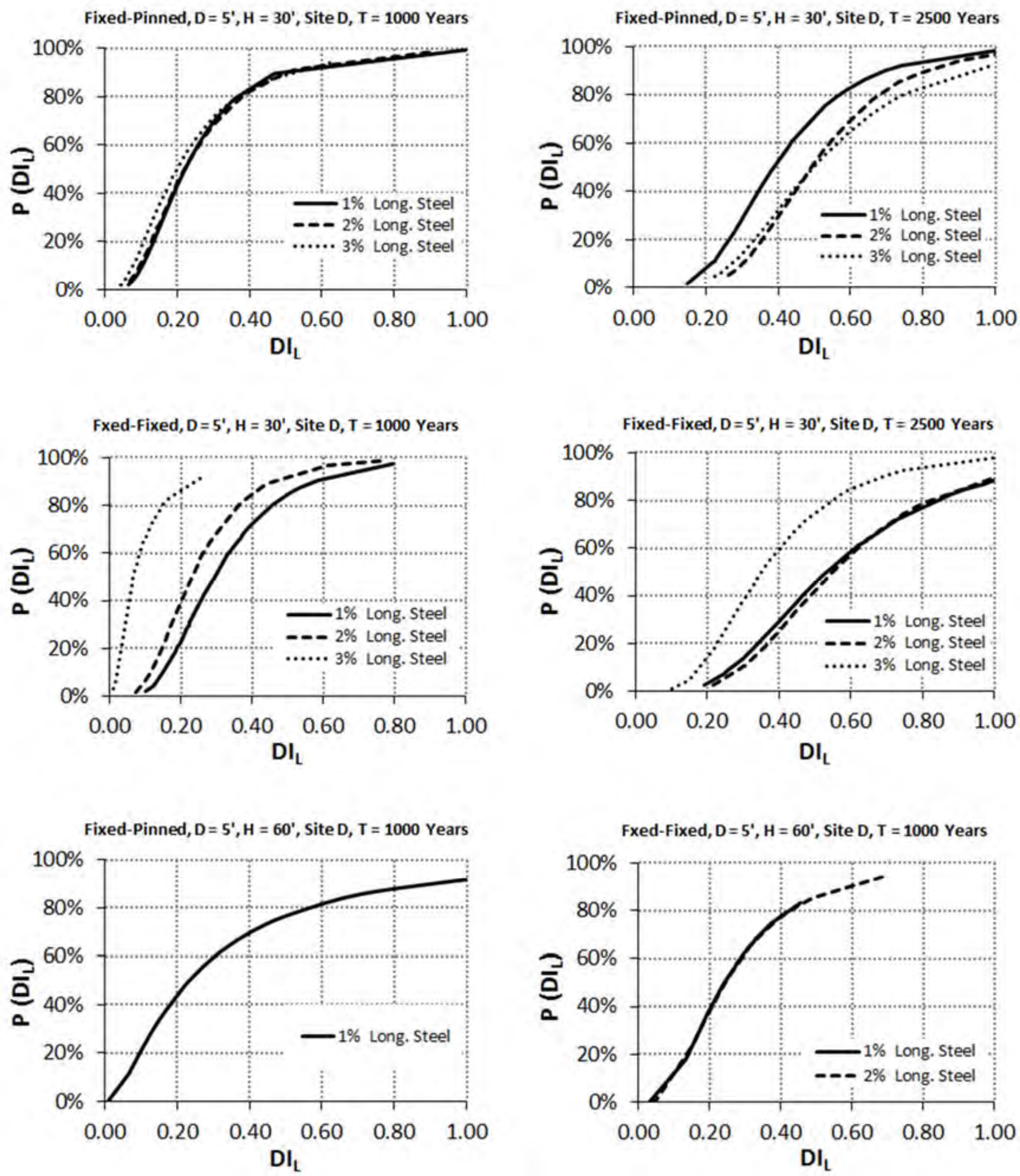

Figure 4-27. Fragility curves for TCBs with five foot diameter columns for Site D

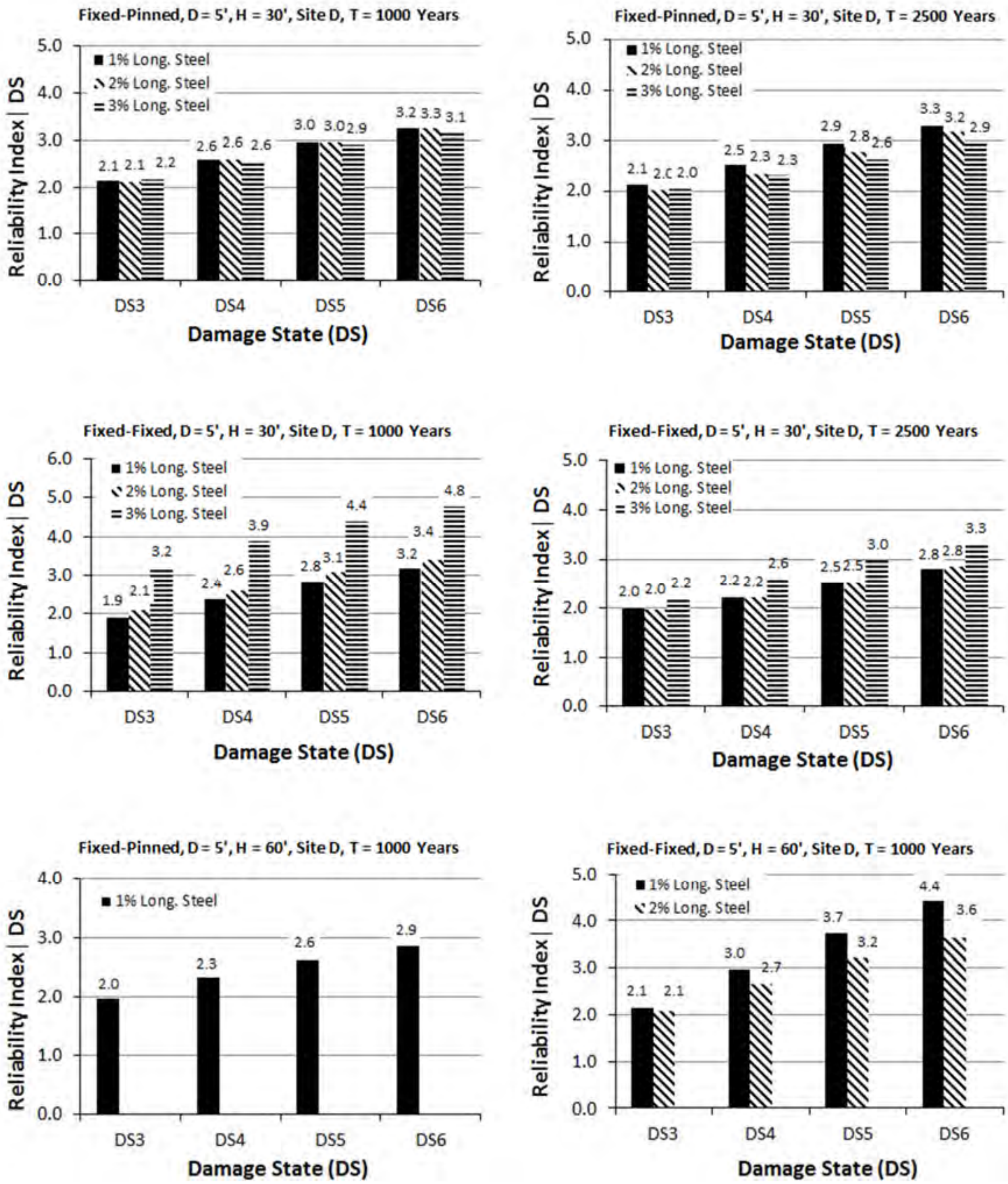

Figure 4-28. Reliability indices for TCBs with five foot diameter columns for Site D

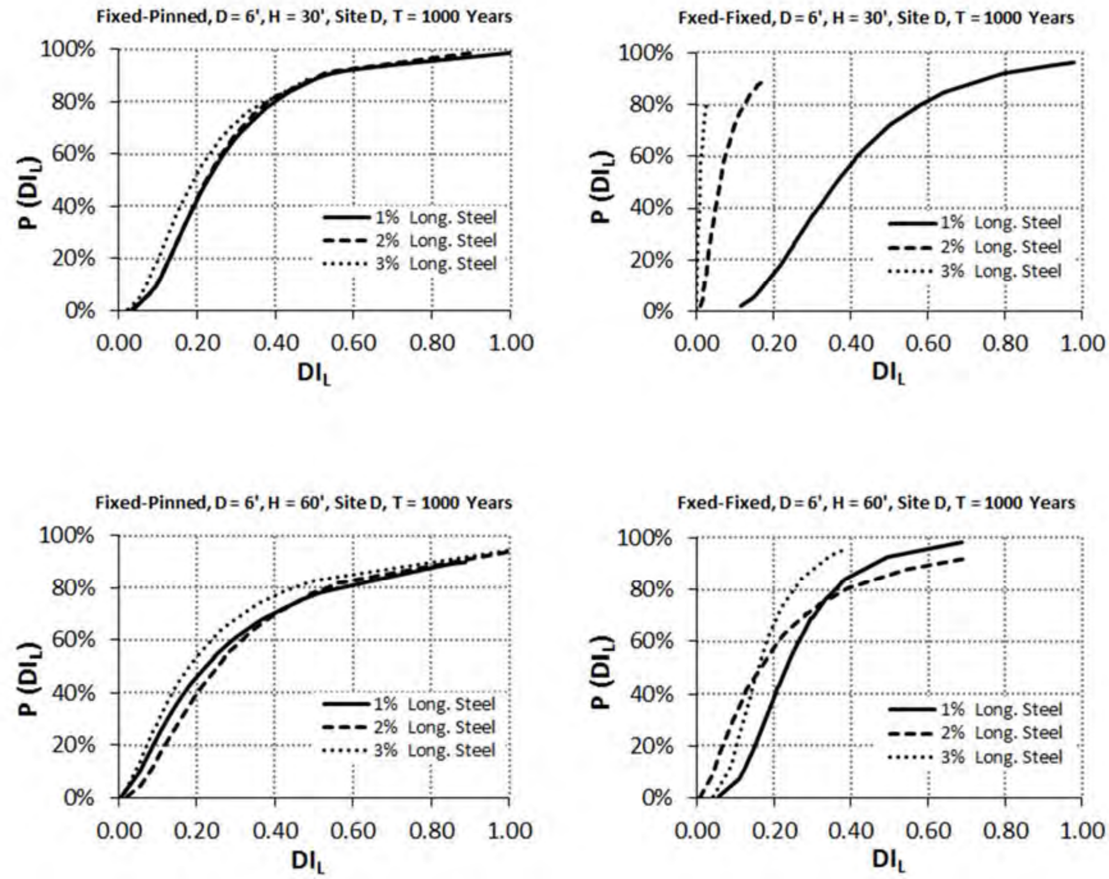

Figure 4-29. Fragility curves for TCBs with six foot diameter columns for Site D

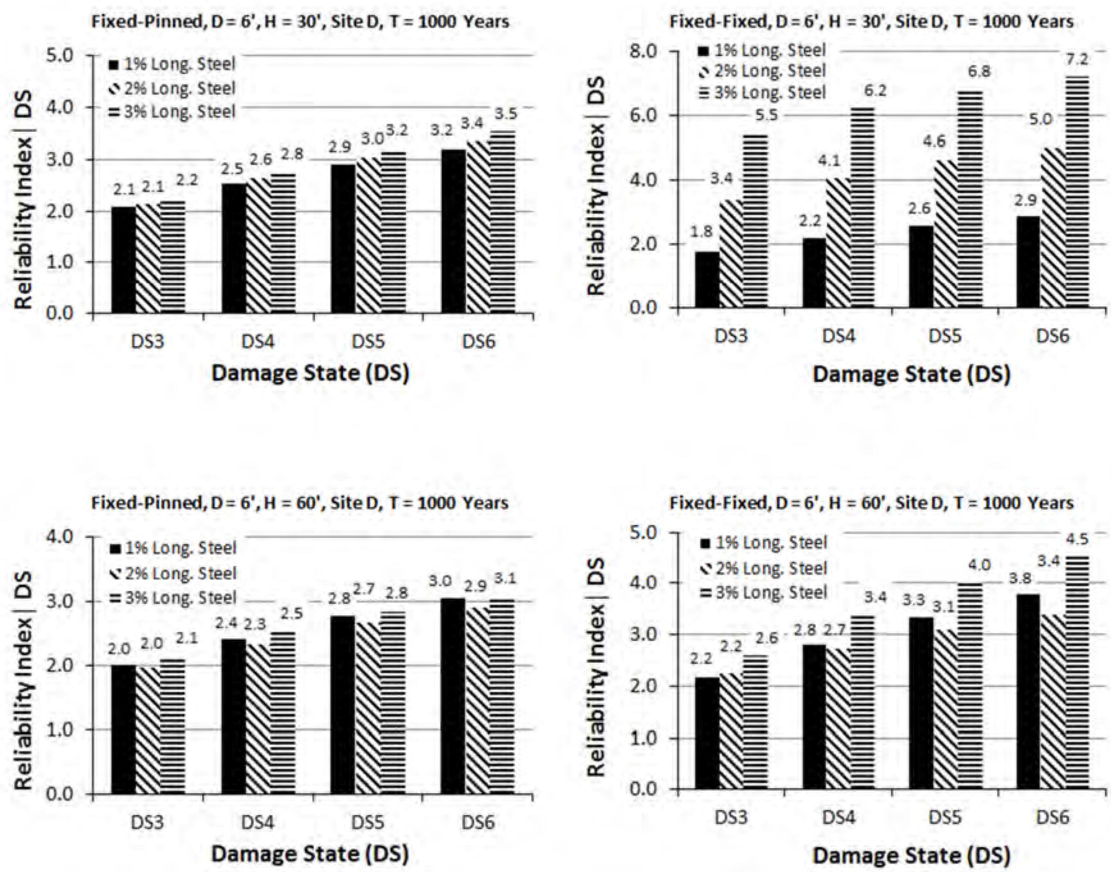

Figure 4-30. Reliability indices for TCBs with six foot diameter columns for Site D

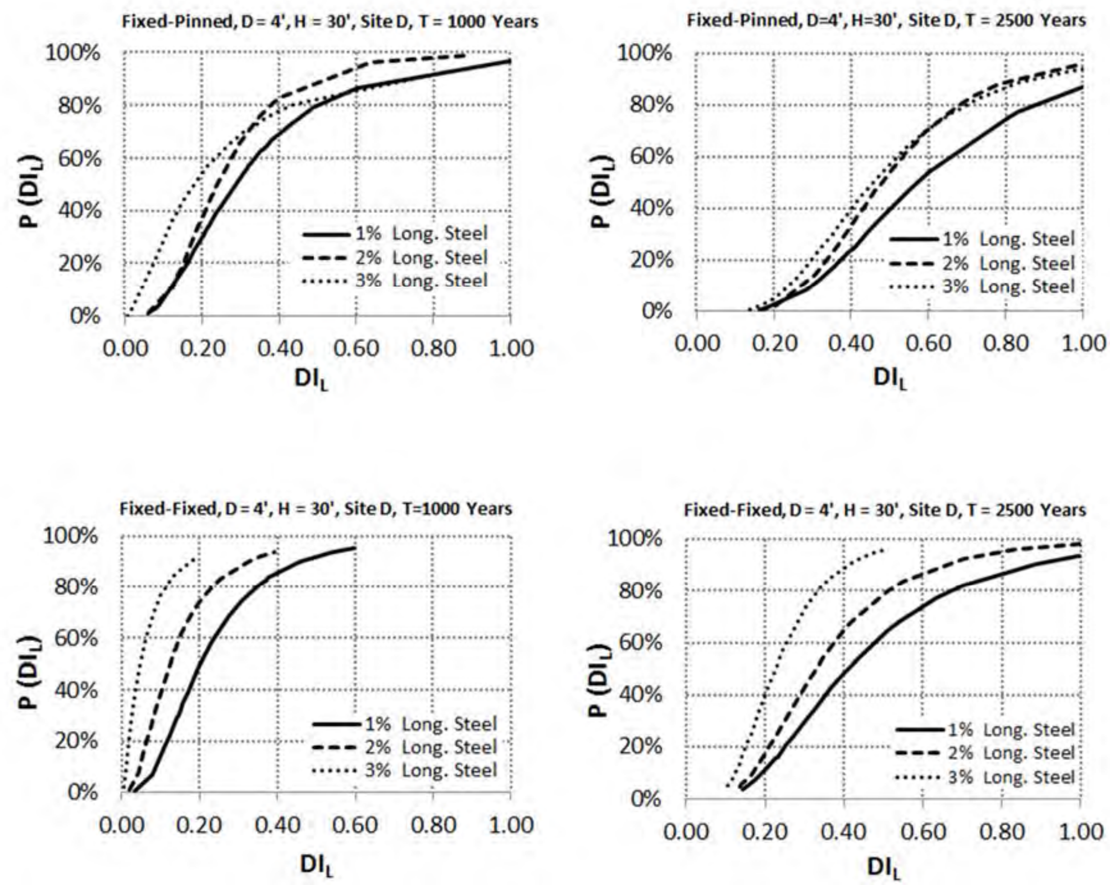

Figure 4-31. Fragility curves for FCBs with four foot diameter columns for Site D

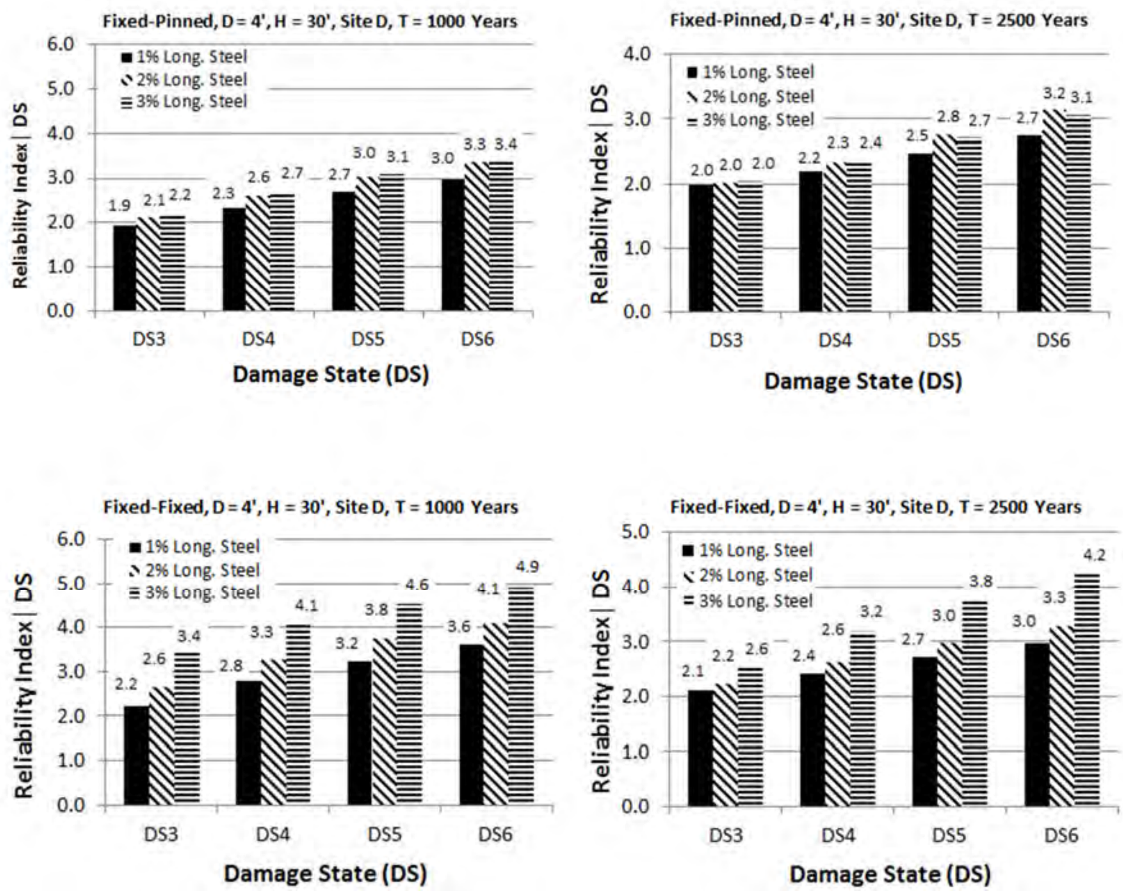

Figure 4-32. Reliability indices for FCBs with four foot diameter columns for Site D

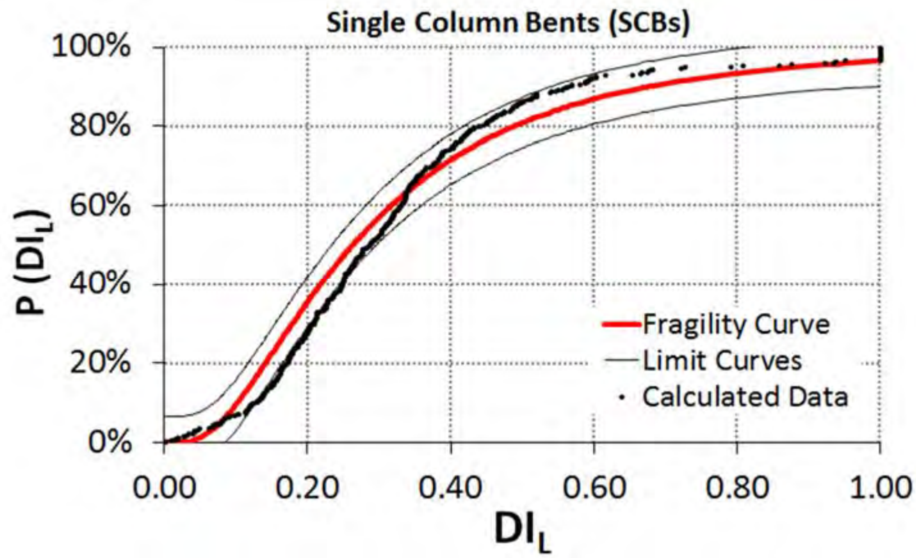

Figure 4-33. Combined fragility curve for SCBs

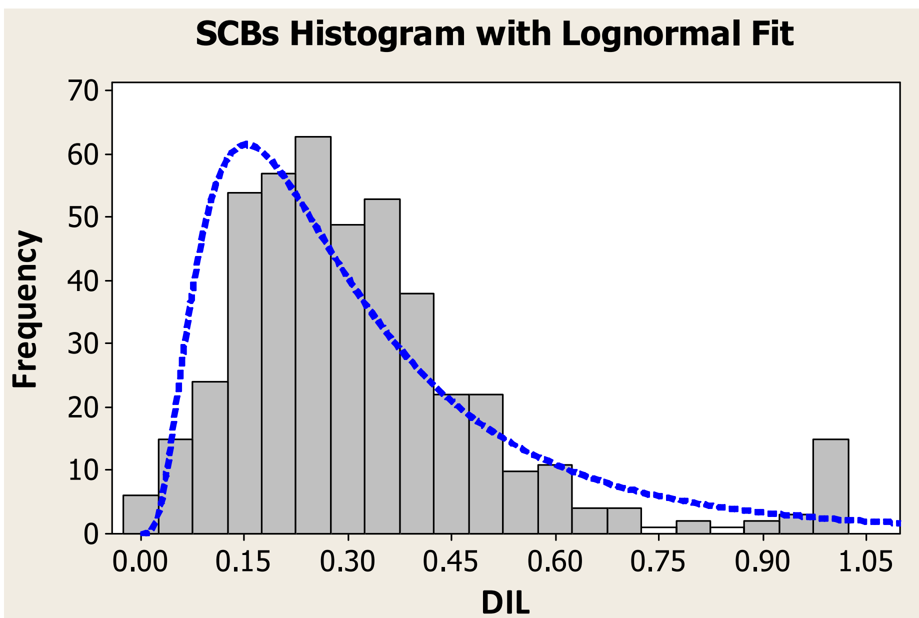

Figure 4-34. Histogram for SCBs with lognormal fit

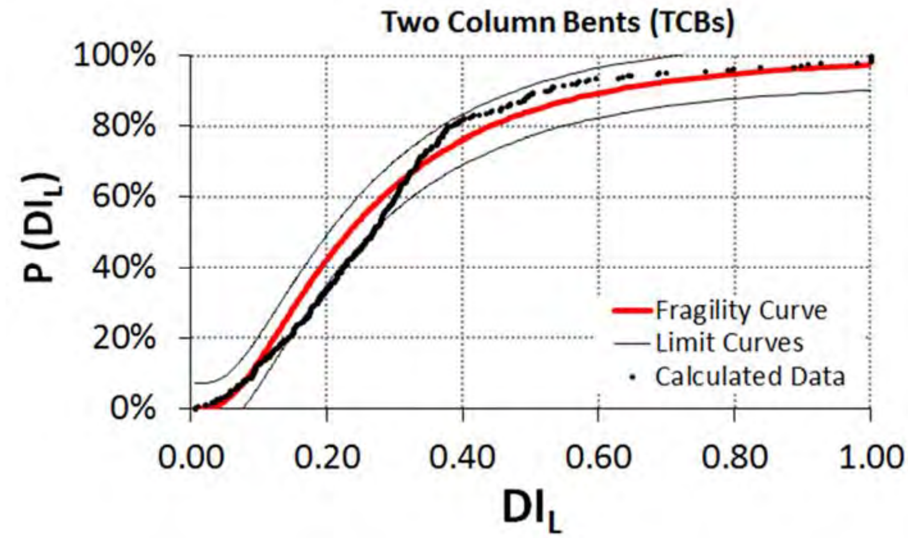

Figure 4-35. Combined fragility curve for TCBs

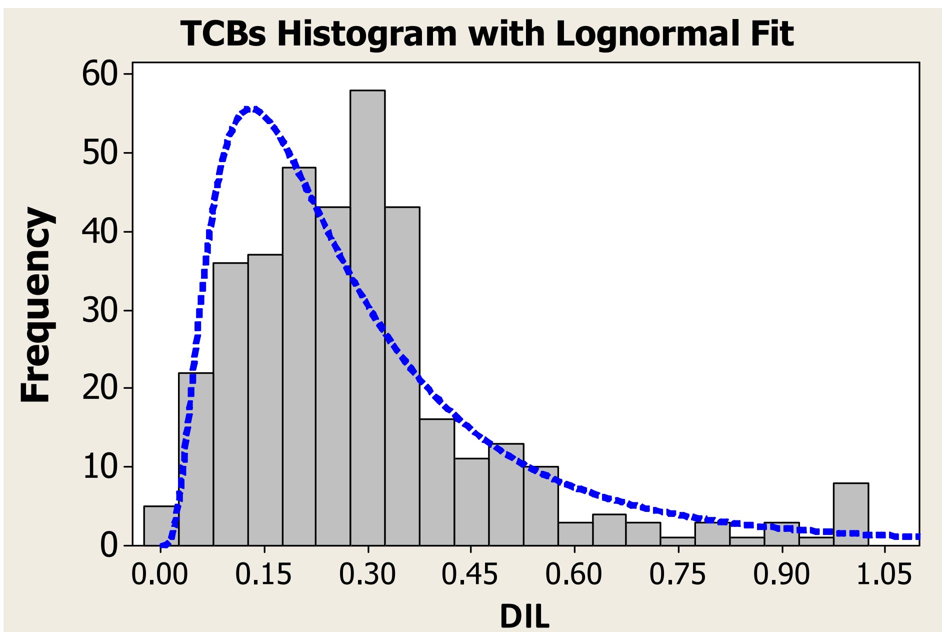

Figure 4-36. Histogram for TCBs with lognormal fit

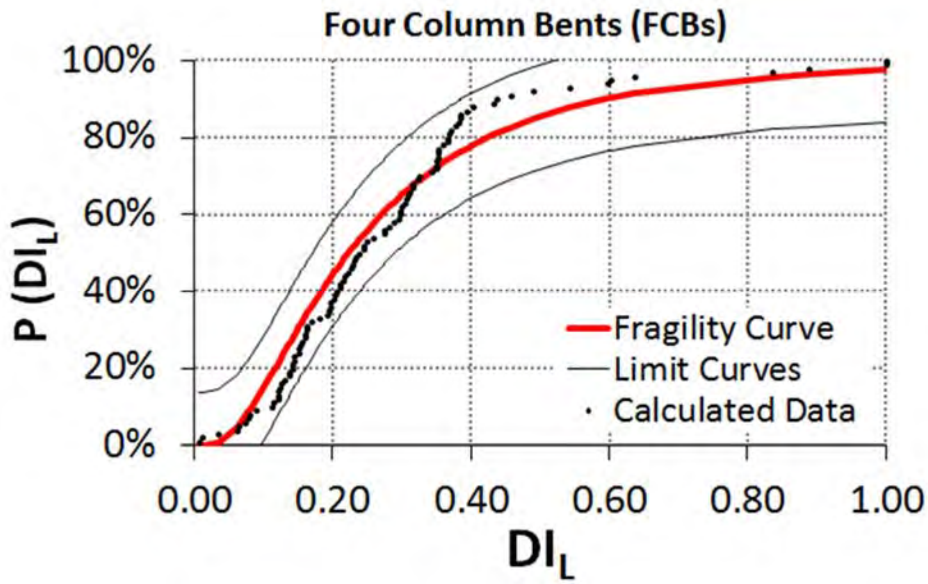

Figure 4-37. Combined fragility curve for FCBs

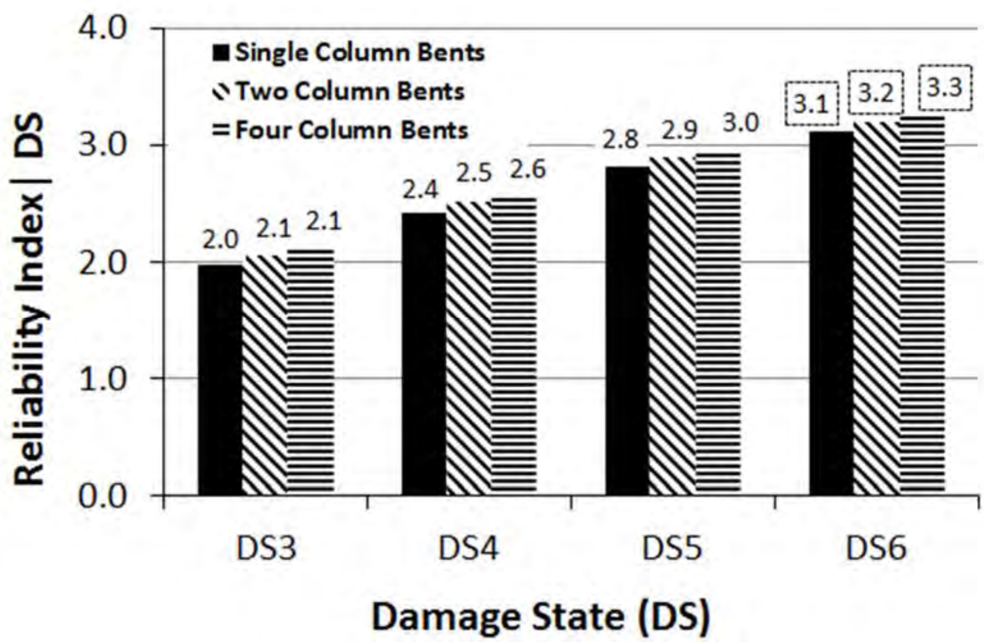

Figure 4-38. Reliability indices comparison

Chapter 5. Figures

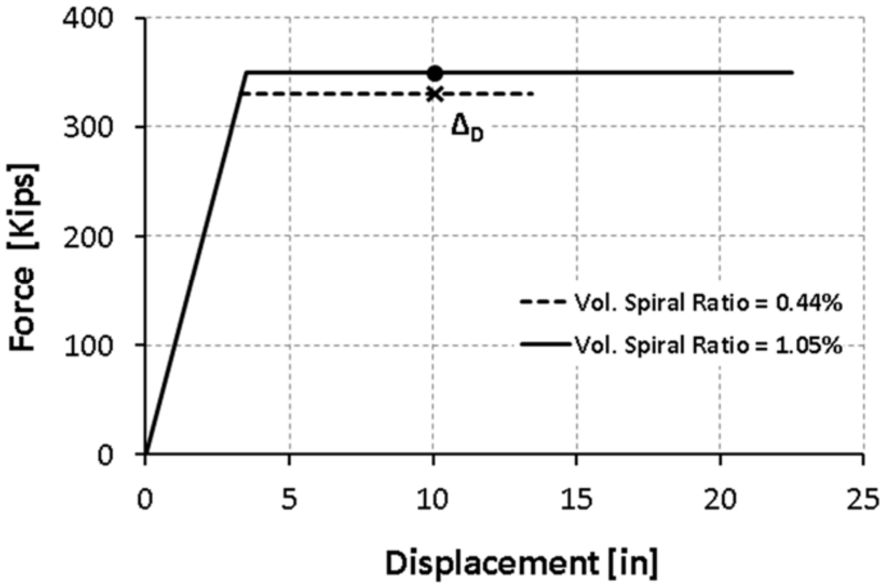

Figure 5-1. Displacement demand for different spiral ratios

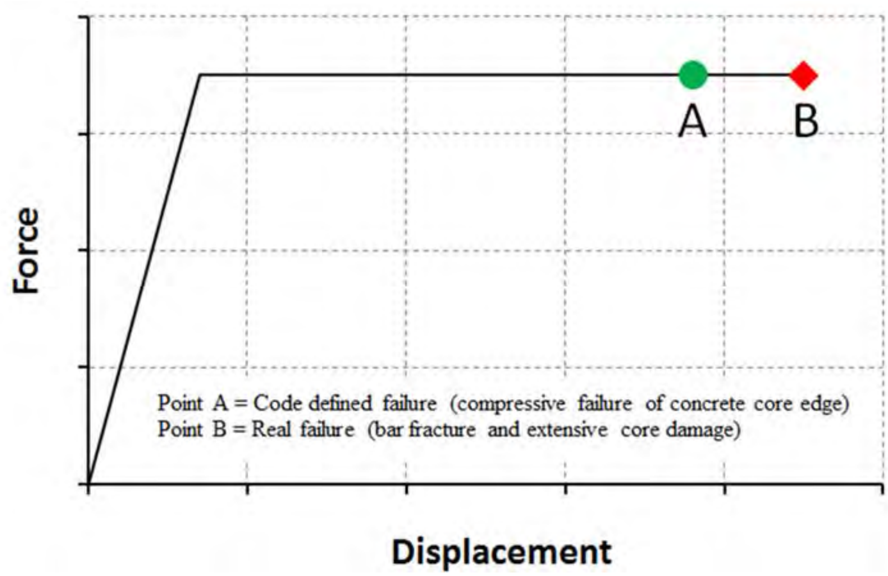

Figure 5-2. Definition of column failure

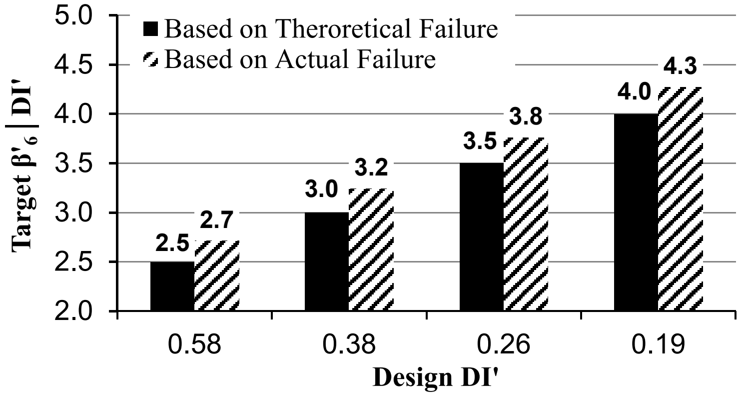

Figure 5-3. The target β_6' for a given design DI' for SCBs

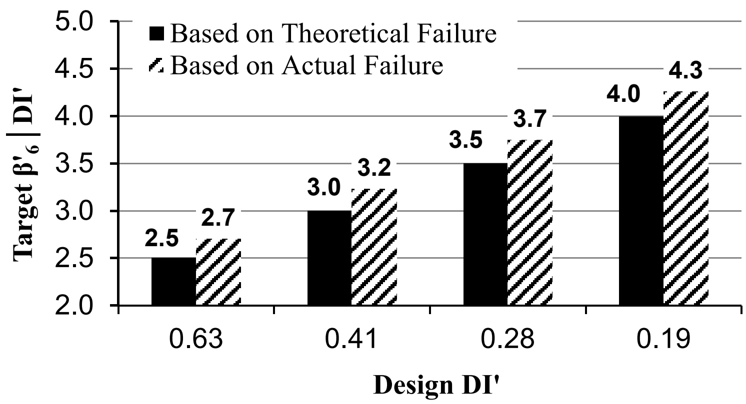

Figure 5-4. The target β_6' for a given design DI' for TCBs

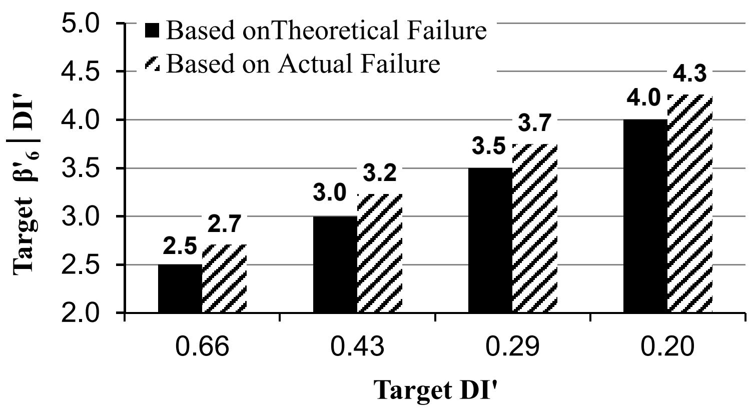

Figure 5-5. The target β_6' for a given design DI' for FCBs

Chapter 6. Figures

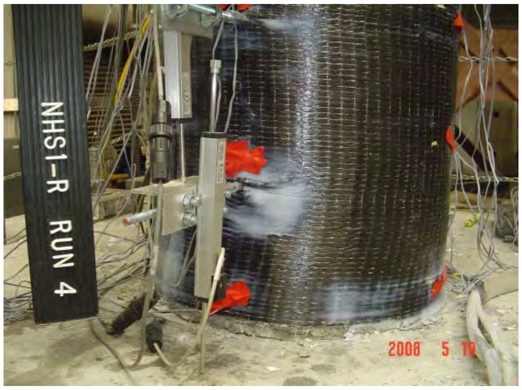

NHS1-R (DS3)

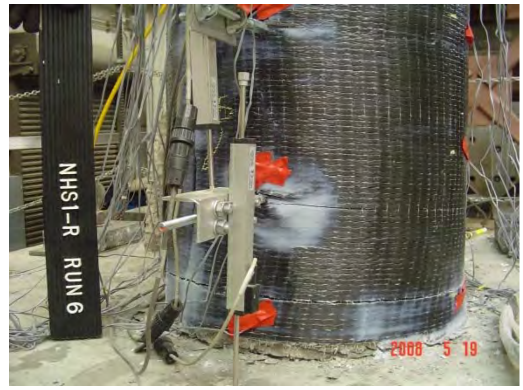

NHS1-R (DS6)

NHS2-R (DS3)

NHS2-R (DS6)

Figure 6-1. Damage states for repaired columns

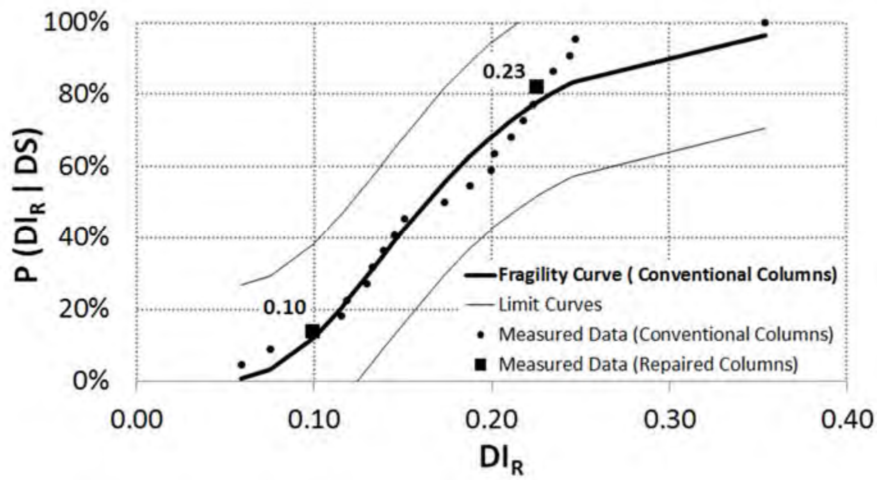

Figure 6-2. Resistance fragility curve for DS2 in conventional columns

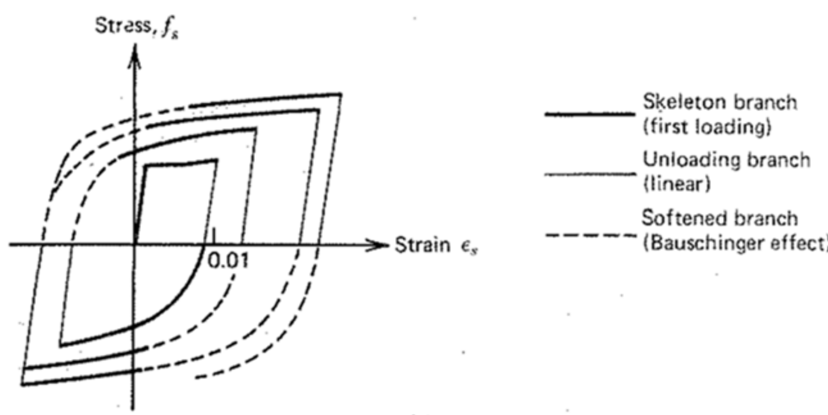

Figure 6-3. Stress-strain curves for steel with reversed loading (Park and Paulay 1975)

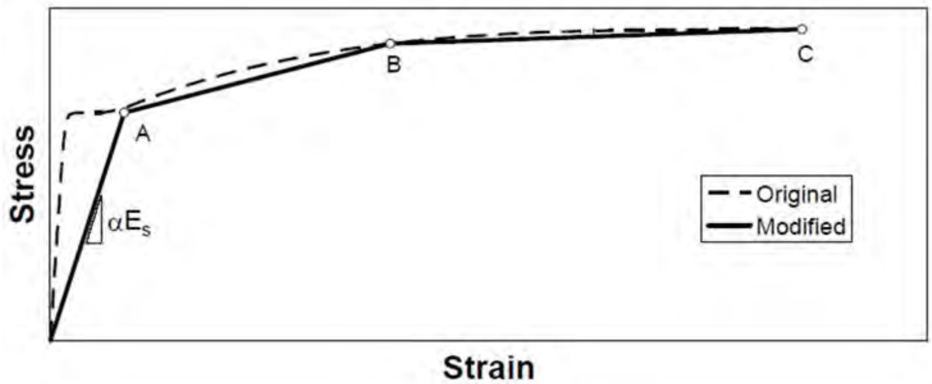

Figure 6-4. Original and modified stress-strain relationship for steel (Vosooghi and Saiidi 2010)

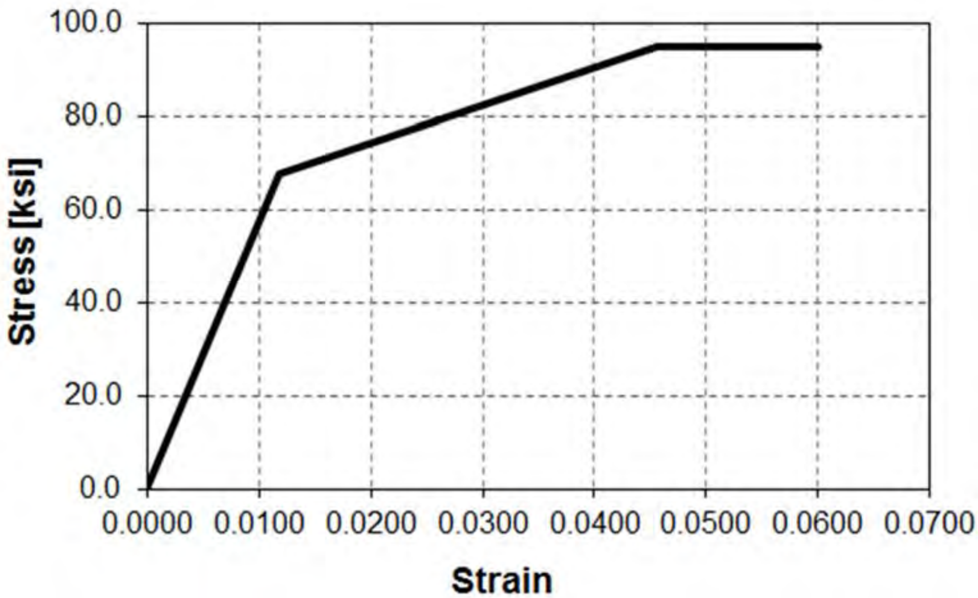

Figure 6-5. Modified stress-strain relationship for steel used for cantilever SCB

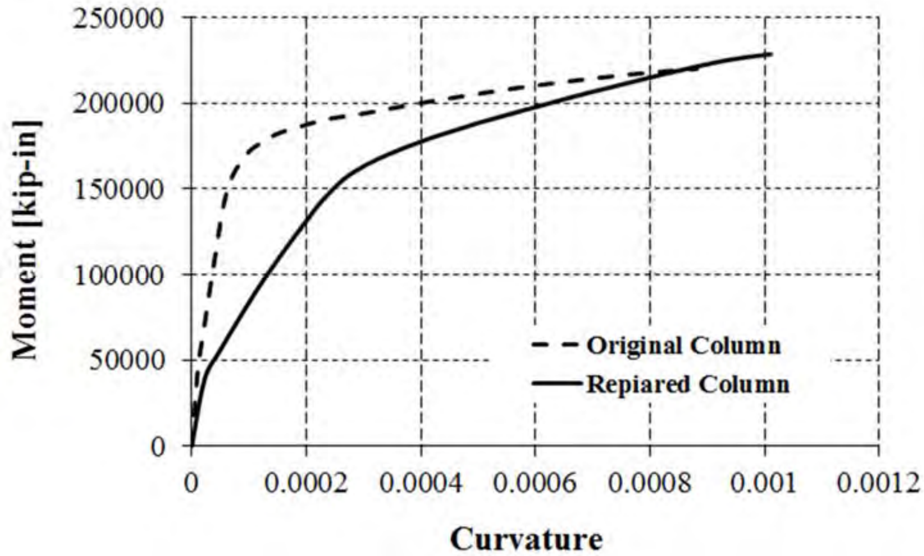

Figure 6-6. Moment curvature curves for the original and repaired columns

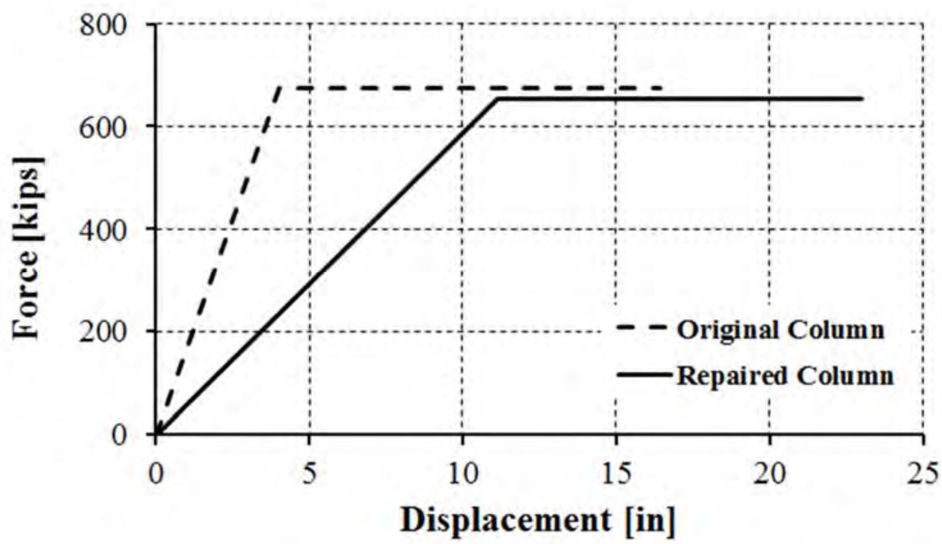

Figure 6-7. Idealized force-Displacement curves for the original and repaired columns

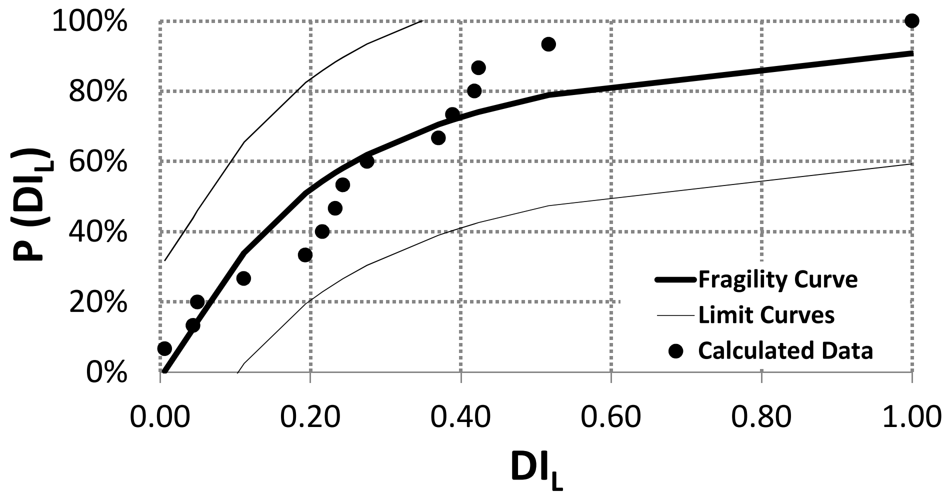

Figure 6-8. Fragility curve for DI_L for the repaired column

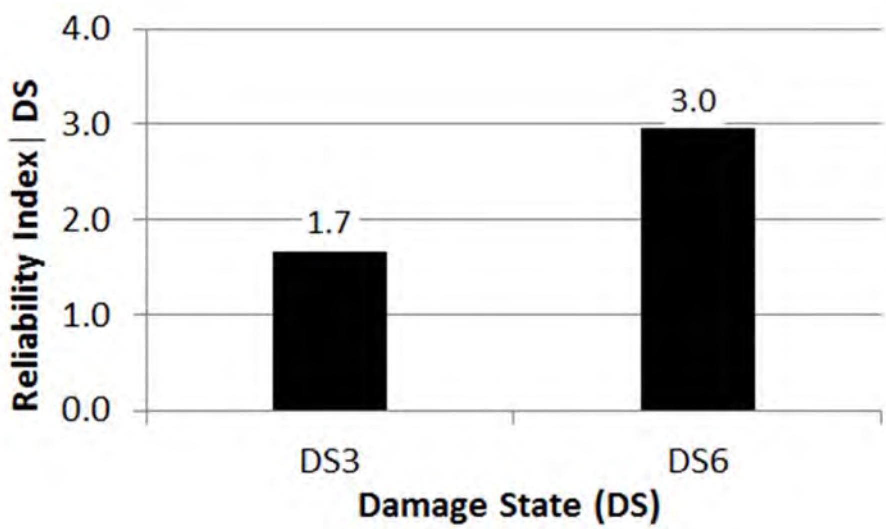

Figure 6-9. Reliability indices for the repaired column

Appendix A- Column Design Using Direct Formulation of PDCA

Four design examples for a single column bent (SCB) are presented in this appendix. These examples are associated with the two design scenarios discussed in Chapter 5.

Example A-1: Determine reliability index against failure (β_6') for a circular bridge column deigned to be at 50% probability of exceedance of DS3 (or *DI*=0.35) under 1000-year earthquake for site class D. Also, determine the reliability index against other damage states (DS3, DS4, and DS5). The properties of the column to be designed are listed in Table A-1.

Table A- 1. Column properties

Site Class	Configuration	Diameter	Height	Steel Ratio
		in	ft	Longitudinal
D	Cantilever	72	30	2%

Solution: The procedure to design a column for given *DI*, and reliability indices charts described in Sections 4.5.1 and 4.7.1.3, respectively are used to solve this example using the following steps:

Step 1. Design the column for *DI* of 0.35 (or 50% probability of exceeding DS3) using the procedure described in Section 4.5.1.

Table A- 2. The properties of the column designed for *DI* of 0.35

Site Class	Configuration	Diameter	Height	Steel Ratio		Period	Δ_Y	Δ_D	Δ_C	*DI*
		in	ft	Long.	Trans.	Sec	in	in	in	
D	Cantilever	72	30	2%	0.84%	1.04	3.97	8.58	17.00	0.35

Step 2. Determine the reliability index against failure and other damage states using charts in Figure 4-22. Figure A-1 shows the reliability indices for DS3 and higher for SCB designed for *DI* of 0.35.

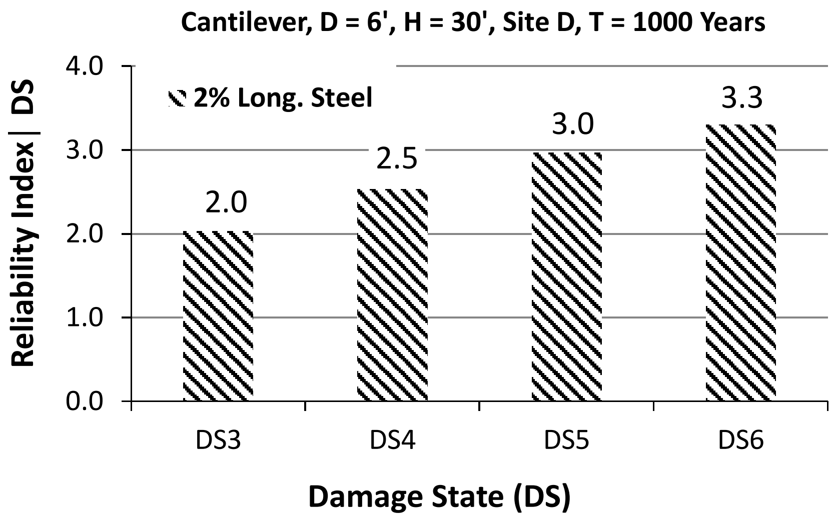

Figure A- 1. Reliability indices for SCB designed for DI = 0.35

Note: The reliability indices charts described in Chapter 4 are only applicable when the column is to be designed for a *DI* of 0.35.

Example A-2: Determine β_6' for a single-column bent designed for *DI* of 0.40 (or 65% probability of exceeding DS3). The properties of the column designed for 1000-year earthquake and site class D are listed in Table A-1. Assume a bridge design life of t = 75 years (AASHTO 2010).

Solution: The direct PDCA method described in Chapter 5 is used to solve this example using the following steps:

Step 1. Design the column for *DI* of 0.40 using Section 4.5.1. Table A-3 lists the properties of SCB designed for DI of 0.40.

Table A- 3. The properties of the column designed for *DI* of 0.40

Site Class	Configuration	Diameter	Height	Steel Ratio		Period	Δ_Y	Δ_D	Δ_C	*DI*
		in	ft	Long.	Trans.	Sec	in	in	in	
D	Cantilever	72	30	2%	0.74%	1.04	3.93	8.56	15.86	0.40

Step 2. Determine α, μ_L', and σ_L' corresponding to *DI* of 0.40. For single column bents, μ_L and σ_L are equal to 0.325 and 0.204, respectively (Table 5-2). Because Tables 5-4, 5-6, and 5-7 are based on the cumulative data for bents designed for tentative *DI* of 0.35, the factor of 0.35 is to be used to calculate α (Section 5.4).

$\alpha = 0.40/0.35 = 1.14$ (Eq. 5-6)

$\mu_L' = \alpha\mu_L = 1.14 \times 0.325 = 0.371$ (Eq. 5-4)

$\sigma'_L = \alpha\sigma_L = 1.14 \times 0.204 = 0.233$ (Eq. 5-4)

Where μ_L and σ_L are the mean and standard deviation of the combined DI_L data for SCBs (Section 5.5).

Step 3. Use Eqs. 2-8 to 2-12 to determine β'_6. Note that μ_R and σ_R for DS6 are one and zero, respectively (Table 5-1).

$$\beta_6 = \frac{\ln\left(\frac{\mu_R}{\mu'_L}\sqrt{\frac{\delta'^2_L + 1}{\delta^2_R + 1}}\right)}{\sqrt{\ln\left[\left(\delta^2_R + 1\right)\left(\delta'^2_L + 1\right)\right]}} = 2.0 \text{ (Eq. 2-8) (This value does not include } P_{EQ}.)$$

Where $\delta'_L = \sigma'_L / \mu'_L = 0.628$ and $\delta_R = \sigma_R / \mu_R = 0$

$$P_{EQ} = 1 - \left(1 - \frac{1}{T}\right)^t = 0.072256 \text{ (Eq. 2-9)}$$

$P_{CF}|P_{EQ} = 1 - \Phi(\beta_6) = 0.0227501$ (Eq. 2-11), [use Table A-4 to determine $\Phi(\beta_6)$]

$P_{CF} \cap P_{EQ} = (P_{CF}|P_{EQ}) \times (P_{EQ}) = 0.0016438$ (Eq. 2-10)

$\beta'_6 = \Phi^{-1}(1 - P_{CF} \cap P_{EQ}) = 2.94$ (Eq . 2-12) (included P_{EQ}) [use Table A-4 to back calculate β'_6]

Where Φ is defined as normal standard distribution function. β'_6 is 2.94 for column designed for DI of 0.40. Similarly, Eqs. 2-8 to 2-12 can be used to calculate reliability indices for other damage states by selecting the corresponding μ_R and σ_R from Table 5-1.

Table A- 4. Cumulative Distribution Function of Standard Normal (Φ (β))

β	Φ(β)	β	Φ(β)	β	Φ(β)	β	Φ(β)	β	Φ(β)
0.00	0.50000	0.90	0.81594	1.70	0.95543	2.50	0.99379	3.30	0.99952
0.02	0.50798	0.92	0.82121	1.72	0.95728	2.52	0.99413	3.32	0.99955
0.04	0.51595	0.94	0.82639	1.74	0.95907	2.54	0.99446	3.34	0.99958
0.06	0.52392	0.96	0.83147	1.76	0.96080	2.56	0.99477	3.36	0.99961
0.08	0.53188	0.98	0.83646	1.78	0.96246	2.58	0.99506	3.38	0.99964
0.10	0.53983	1.00	0.84134	1.80	0.96407	2.60	0.99534	3.40	0.99966
0.12	0.54776	1.02	0.84614	1.82	0.96562	2.62	0.99560	3.42	0.99969
0.14	0.55567	1.04	0.85083	1.84	0.96712	2.64	0.99585	3.44	0.99971
0.16	0.56356	1.06	0.85543	1.86	0.96856	2.66	0.99609	3.46	0.99973
0.18	0.57142	1.08	0.85993	1.88	0.96995	2.68	0.99632	3.48	0.99975
0.20	0.57926	1.10	0.86433	1.90	0.97128	2.70	0.99653	3.50	0.99977
0.22	0.58706	1.12	0.86864	1.92	0.97257	2.72	0.99674	3.52	0.99978
0.24	0.59483	1.14	0.87286	1.94	0.97381	2.74	0.99693	3.54	0.99980
0.26	0.60257	1.16	0.87698	1.96	0.97500	2.76	0.99711	3.56	0.99981
0.28	0.61026	1.18	0.88100	1.98	0.97615	2.78	0.99728	3.58	0.99983
0.30	0.61791	1.20	0.88493	2.00	0.97725	2.80	0.99744	3.60	0.99984
0.32	0.62552	1.22	0.88877	2.02	0.97831	2.82	0.99760	3.62	0.99985
0.34	0.63307	1.24	0.89251	2.04	0.97932	2.84	0.99774	3.64	0.99986
0.36	0.64058	1.26	0.89617	2.06	0.98030	2.86	0.99788	3.66	0.99987
0.38	0.64803	1.28	0.89973	2.08	0.98124	2.88	0.99801	3.68	0.99988
0.40	0.65542	1.30	0.90320	2.10	0.98214	2.90	0.99813	3.70	0.99989
0.42	0.66276	1.32	0.90658	2.12	0.98300	2.92	0.99825	3.72	0.99990
0.44	0.67003	1.34	0.90988	2.14	0.98382	2.94	0.99836	3.74	0.99991
0.46	0.67724	1.36	0.91309	2.16	0.98461	2.96	0.99846	3.76	0.99992
0.48	0.68439	1.38	0.91621	2.18	0.98537	2.98	0.99856	3.78	0.99992
0.50	0.69146	1.40	0.91924	2.20	0.98610	3.00	0.99865	3.80	0.99993
0.52	0.69847	1.42	0.92220	2.22	0.98679	3.02	0.99874	3.82	0.99993
0.54	0.70540	1.44	0.92507	2.24	0.98745	3.04	0.99882	3.84	0.99994
0.56	0.71226	1.46	0.92785	2.26	0.98809	3.06	0.99889	3.86	0.99994
0.58	0.71904	1.48	0.93056	2.28	0.98870	3.08	0.99896	3.88	0.99995
0.60	0.72575	1.50	0.93319	2.30	0.98928	3.10	0.99903	3.90	0.99995
0.62	0.73237	1.52	0.93574	2.32	0.98983	3.12	0.99910	3.92	0.99996
0.64	0.73891	1.54	0.93822	2.34	0.99036	3.14	0.99916	3.94	0.99996
0.66	0.74537	1.56	0.94062	2.36	0.99086	3.16	0.99921	3.96	0.99996
0.68	0.75175	1.58	0.94295	2.38	0.99134	3.18	0.99926	3.98	0.99997
0.70	0.75804	1.60	0.94520	2.40	0.99180	3.20	0.99931	4.00	0.99997
0.72	0.76424	1.62	0.94738	2.42	0.99224	3.22	0.99936		
0.74	0.77035	1.64	0.94950	2.44	0.99266	3.24	0.99940		
0.76	0.77637	1.66	0.95154	2.46	0.99305	3.26	0.99944		
0.78	0.78230	1.68	0.95352	2.48	0.99343	3.28	0.99948		

Example A-3: Determine design damage index (DI') for a bridge column for a target β_6' of 3.5 under 1000-year earthquake for site class D and design the transverse reinforcement for this DI. The properties of the column are listed in Table A-1.

Solution: The direct PDCA method described in Chapter 5 is used to solve this example using the following steps:

Step 1. Determine DI' for a given β_6' of 3.5 from Table 5-4.

$$DI' = 0.26$$

Step 2. Design column for a target DI' of 0.26 using Section 4.5.1. Table A-5 lists the transverse steel ratio and the properties of the column designed for DI' of 0.26.

Table A- 5. The properties of the column designed for DI' of 0.26

Site Class	Configuration	Diameter	H/D	Steel Ratio		Period	Δ_Y	Δ_D	Δ_C	DI'
		in		Longitudinal	Transverse	Sec	in	in	in	
D	Cantilever	72	5	2%	1.23%	1.04	4.12	8.60	21.30	0.26

Example A-4: Determine the reliability index for DS3, DS4, and DS5 for SCB designed for DI' of 0.26 in Example A-3 (associated with β_6' of 3.5). Assume a bridge design life of t=75 years.

Solution: The direct PDCA method described in Chapter 5 is used to solve this example using the following steps:

Step 3. Using the same procedure as used in step 3 of Example A-2 the new μ_L' and σ_L', can be calculated as:

$\alpha = 0.26/0.35 = 0.743$ (Eq. 5-6)

$\mu_L' = \alpha\mu_L = 0.743 \times 0.325 = 0.241$ (Eq. 5-4)

$\sigma_L' = \alpha\sigma_L = 0.743 \times 0.204 = 0.152$ (Eq. 5-4)

Step 4. Having μ_L' and σ_L', the reliability indices against DS3 and higher can be calculated using Eqs. 2-8 to 2-12. For example reliability index against DS3 (μ_R = 0.375 and σ_R = 0.100 (Table 5-1)) can be calculated as:

$$\beta_3 = \frac{\ln\left(\frac{\mu_R}{\mu_L'}\sqrt{\frac{\delta_L'^2+1}{\delta_R^2+1}}\right)}{\sqrt{\ln\left[\left(\delta_R^2+1\right)\left(\delta_L'^2+1\right)\right]}} = 0.90 \quad \text{(Eq. 2-8)} \quad \text{(This value does not include } P_{EQ}\text{)}$$

Where $\delta_L^{'} = \sigma_L^{'} / \mu_L^{'} = 0.63$ and $\delta_R = \sigma_R / \mu_R = 0.27$

$$P_{EQ} = 1 - \left(1 - \frac{1}{T}\right)^t = 0.07225 \quad \text{(Eq. 2-9)}$$

$(P_{CF}|P_{EQ}) = 1 - \Phi(\beta_3) = 0.18406$ (Eq. 2-11), [use Table A-4 to determine $\Phi(\beta_3)$]

$P_{CF} \cap P_{EQ} = (P_{CF}|P_{EQ}) \times (P_{EQ}) = 0.013298$ (Eq. 2-10)

$\beta_3' = \Phi^{-1}(1 - P_{CF} \cap P_{EQ}) = 2.22$ (Eq . 2-12) (included P_{EQ}), [use Table A-4 to back calculate β_3']

Where, subscript 3 represents the reliability index for DS3. The same procedure can be followed to determine reliability index against DS4 and DS5 by selecting the corresponding μ_R and σ_R from Table 5-1. The reliability indices for different damage states when the column was designed for DI' of 0.26 are listed in Table A-6.

Table A- 6. Reliability indices for the column designed for DI' of 0.26

Direct Method	
Damage State	Reliability Index
DS3	2.2
DS4	2.7
DS5	3.2
DS6	3.5

LIST OF CCEER PUBLICATIONS

Report No.	Publication
CCEER-84-1	Saiidi, M., and R. Lawver, “User's Manual for LZAK-C64, A Computer Program to Implement the Q-Model on Commodore 64,” Civil Engineering Department, Report No. CCEER-84-1, University of Nevada, Reno, January 1984.
CCEER-84-1	Douglas, B., Norris, G., Saiidi, M., Dodd, L., Richardson, J. and Reid, W., “Simple Bridge Models for Earthquakes and Test Data,” Civil Engineering Department, Report No. CCEER-84-1 Reprint, University of Nevada, Reno, January 1984.
CCEER-84-2	Douglas, B. and T. Iwasaki, “Proceedings of the First USA-Japan Bridge Engineering Workshop,” held at the Public Works Research Institute, Tsukuba, Japan, Civil Engineering Department, Report No. CCEER-84-2, University of Nevada, Reno, April 1984.
CCEER-84-3	Saiidi, M., J. Hart, and B. Douglas, “Inelastic Static and Dynamic Analysis of Short R/C Bridges Subjected to Lateral Loads,” Civil Engineering Department, Report No. CCEER-84-3, University of Nevada, Reno, July 1984.
CCEER-84-4	Douglas, B., “A Proposed Plan for a National Bridge Engineering Laboratory,” Civil Engineering Department, Report No. CCEER-84-4, University of Nevada, Reno, December 1984.
CCEER-85-1	Norris, G. and P. Abdollaholiaee, “Laterally Loaded Pile Response: Studies with the Strain Wedge Model,” Civil Engineering Department, Report No. CCEER-85-1, University of Nevada, Reno, April 1985.
CCEER-86-1	Ghusn, G. and M. Saiidi, “A Simple Hysteretic Element for Biaxial Bending of R/C in NEABS-86,” Civil Engineering Department, Report No. CCEER-86-1, University of Nevada, Reno, July 1986.
CCEER-86-2	Saiidi, M., R. Lawver, and J. Hart, “User's Manual of ISADAB and SIBA, Computer Programs for Nonlinear Transverse Analysis of Highway Bridges Subjected to Static and Dynamic Lateral Loads,” Civil Engineering Department, Report No. CCEER-86-2, University of Nevada, Reno, September 1986.
CCEER-87-1	Siddharthan, R., “Dynamic Effective Stress Response of Surface and Embedded Footings in Sand,” Civil Engineering Department, Report No. CCEER-86-2, University of Nevada, Reno, June 1987.
CCEER-87-2	Norris, G. and R. Sack, “Lateral and Rotational Stiffness of Pile Groups for Seismic Analysis of Highway Bridges,” Civil Engineering Department, Report No. CCEER-87-2, University of Nevada, Reno, June 1987.
CCEER-88-1	Orie, J. and M. Saiidi, “A Preliminary Study of One-Way Reinforced Concrete Pier Hinges Subjected to Shear and Flexure,” Civil Engineering Department, Report No. CCEER-88-1, University of Nevada, Reno, January 1988.
CCEER-88-2	Orie, D., M. Saiidi, and B. Douglas, “A Micro-CAD System for Seismic Design of Regular Highway Bridges,” Civil Engineering Department, Report No. CCEER-88-2, University of Nevada, Reno, June 1988.
CCEER-88-3	Orie, D. and M. Saiidi, “User's Manual for Micro-SARB, a Microcomputer Program for Seismic Analysis of Regular Highway Bridges,” Civil Engineering Department, Report No. CCEER-88-3, University of Nevada, Reno, October 1988.

CCEER-89-1 Douglas, B., M. Saiidi, R. Hayes, and G. Holcomb, “A Comprehensive Study of the Loads and Pressures Exerted on Wall Forms by the Placement of Concrete,” Civil Engineering Department, Report No. CCEER-89-1, University of Nevada, Reno, February 1989.

CCEER-89-2 Richardson, J. and B. Douglas, “Dynamic Response Analysis of the Dominion Road Bridge Test Data,” Civil Engineering Department, Report No. CCEER-89-2, University of Nevada, Reno, March 1989.

CCEER-89-2 Vrontinos, S., M. Saiidi, and B. Douglas, “A Simple Model to Predict the Ultimate Response of R/C Beams with Concrete Overlays,” Civil Engineering Department, Report NO. CCEER-89-2, University of Nevada, Reno, June 1989.

CCEER-89-3 Ebrahimpour, A. and P. Jagadish, “Statistical Modeling of Bridge Traffic Loads - A Case Study,” Civil Engineering Department, Report No. CCEER-89-3, University of Nevada, Reno, December 1989.

CCEER-89-4 Shields, J. and M. Saiidi, “Direct Field Measurement of Prestress Losses in Box Girder Bridges,” Civil Engineering Department, Report No. CCEER-89-4, University of Nevada, Reno, December 1989.

CCEER-90-1 Saiidi, M., E. Maragakis, G. Ghusn, Y. Jiang, and D. Schwartz, “Survey and Evaluation of Nevada's Transportation Infrastructure, Task 7.2 - Highway Bridges, Final Report,” Civil Engineering Department, Report No. CCEER 90-1, University of Nevada, Reno, October 1990.

CCEER-90-2 Abdel-Ghaffar, S., E. Maragakis, and M. Saiidi, “Analysis of the Response of Reinforced Concrete Structures During the Whittier Earthquake 1987,” Civil Engineering Department, Report No. CCEER 90-2, University of Nevada, Reno, October 1990.

CCEER-91-1 Saiidi, M., E. Hwang, E. Maragakis, and B. Douglas, “Dynamic Testing and the Analysis of the Flamingo Road Interchange,” Civil Engineering Department, Report No. CCEER-91-1, University of Nevada, Reno, February 1991.

CCEER-91-2 Norris, G., R. Siddharthan, Z. Zafir, S. Abdel-Ghaffar, and P. Gowda, “Soil-Foundation-Structure Behavior at the Oakland Outer Harbor Wharf,” Civil Engineering Department, Report No. CCEER-91-2, University of Nevada, Reno, July 1991.

CCEER-91-3 Norris, G., “Seismic Lateral and Rotational Pile Foundation Stiffnesses at Cypress,” Civil Engineering Department, Report No. CCEER-91-3, University of Nevada, Reno, August 1991.

CCEER-91-4 O'Connor, D. and M. Saiidi, “A Study of Protective Overlays for Highway Bridge Decks in Nevada, with Emphasis on Polyester-Styrene Polymer Concrete,” Civil Engineering Department, Report No. CCEER-91-4, University of Nevada, Reno, October 1991.

CCEER-91-5 O'Connor, D.N. and M. Saiidi, “Laboratory Studies of Polyester-Styrene Polymer Concrete Engineering Properties,” Civil Engineering Department, Report No. CCEER-91-5, University of Nevada, Reno, November 1991.

CCEER-92-1 Straw, D.L. and M. Saiidi, “Scale Model Testing of One-Way Reinforced Concrete Pier Hinges Subject to Combined Axial Force, Shear and Flexure,” edited by D.N. O'Connor, Civil Engineering Department, Report No. CCEER-92-1, University of Nevada, Reno, March 1992.

CCEER-92-2 Wehbe, N., M. Saiidi, and F. Gordaninejad, “Basic Behavior of Composite Sections Made of Concrete Slabs and Graphite Epoxy Beams,” Civil Engineering Department, Report No. CCEER-92-2, University of Nevada, Reno, August 1992.

CCEER-92-3 Saiidi, M. and E. Hutchens, “A Study of Prestress Changes in A Post-Tensioned Bridge

During the First 30 Months," Civil Engineering Department, Report No. CCEER-92-3, University of Nevada, Reno, April 1992.

CCEER-92-4 Saiidi, M., B. Douglas, S. Feng, E. Hwang, and E. Maragakis, "Effects of Axial Force on Frequency of Prestressed Concrete Bridges," Civil Engineering Department, Report No. CCEER-92-4, University of Nevada, Reno, August 1992.

CCEER-92-5 Siddharthan, R., and Z. Zafir, "Response of Layered Deposits to Traveling Surface Pressure Waves," Civil Engineering Department, Report No. CCEER-92-5, University of Nevada, Reno, September 1992.

CCEER-92-6 Norris, G., and Z. Zafir, "Liquefaction and Residual Strength of Loose Sands from Drained Triaxial Tests," Civil Engineering Department, Report No. CCEER-92-6, University of Nevada, Reno, September 1992.

CCEER-92-6-A Norris, G., Siddharthan, R., Zafir, Z. and Madhu, R. "Liquefaction and Residual Strength of Sands from Drained Triaxial Tests," Civil Engineering Department, Report No. CCEER-92-6-A, University of Nevada, Reno, September 1992.

CCEER-92-7 Douglas, B., "Some Thoughts Regarding the Improvement of the University of Nevada, Reno's National Academic Standing," Civil Engineering Department, Report No. CCEER-92-7, University of Nevada, Reno, September 1992.

CCEER-92-8 Saiidi, M., E. Maragakis, and S. Feng, "An Evaluation of the Current Caltrans Seismic Restrainer Design Method," Civil Engineering Department, Report No. CCEER-92-8, University of Nevada, Reno, October 1992.

CCEER-92-9 O'Connor, D., M. Saiidi, and E. Maragakis, "Effect of Hinge Restrainers on the Response of the Madrone Drive Undercrossing During the Loma Prieta Earthquake," Civil Engineering Department, Report No. CCEER-92-9, University of Nevada, Reno, February 1993.

CCEER-92-10 O'Connor, D., and M. Saiidi, "Laboratory Studies of Polyester Concrete: Compressive Strength at Elevated Temperatures and Following Temperature Cycling, Bond Strength to Portland Cement Concrete, and Modulus of Elasticity," Civil Engineering Department, Report No. CCEER-92-10, University of Nevada, Reno, February 1993.

CCEER-92-11 Wehbe, N., M. Saiidi, and D. O'Connor, "Economic Impact of Passage of Spent Fuel Traffic on Two Bridges in Northeast Nevada," Civil Engineering Department, Report No. CCEER-92-11, University of Nevada, Reno, December 1992.

CCEER-93-1 Jiang, Y., and M. Saiidi, "Behavior, Design, and Retrofit of Reinforced Concrete One-way Bridge Column Hinges," edited by D. O'Connor, Civil Engineering Department, Report No. CCEER-93-1, University of Nevada, Reno, March 1993.

CCEER-93-2 Abdel-Ghaffar, S., E. Maragakis, and M. Saiidi, "Evaluation of the Response of the Aptos Creek Bridge During the 1989 Loma Prieta Earthquake," Civil Engineering Department, Report No. CCEER-93-2, University of Nevada, Reno, June 1993.

CCEER-93-3 Sanders, D.H., B.M. Douglas, and T.L. Martin, "Seismic Retrofit Prioritization of Nevada Bridges," Civil Engineering Department, Report No. CCEER-93-3, University of Nevada, Reno, July 1993.

CCEER-93-4 Abdel-Ghaffar, S., E. Maragakis, and M. Saiidi, "Performance of Hinge Restrainers in the Huntington Avenue Overhead During the 1989 Loma Prieta Earthquake," Civil Engineering Department, Report No. CCEER-93-4, University of Nevada, Reno, June 1993 (in final preparation).

CCEER-93-5 Maragakis, E., M. Saiidi, S. Feng, and L. Flournoy, "Effects of Hinge Restrainers on the Response of the San Gregorio Bridge during the Loma Prieta Earthquake," (in final preparation) Civil Engineering Department, Report No. CCEER-93-5, University of

Nevada, Reno.

CCEER-93-6 Saiidi, M., E. Maragakis, S. Abdel-Ghaffar, S. Feng, and D. O'Connor, "Response of Bridge Hinge Restrainers during Earthquakes -Field Performance, Analysis, and Design," Civil Engineering Department, Report No. CCEER-93-6, University of Nevada, Reno, May 1993.

CCEER-93-7 Wehbe, N., Saiidi, M., Maragakis, E., and Sanders, D., "Adequacy of Three Highway Structures in Southern Nevada for Spent Fuel Transportation," Civil Engineering Department, Report No. CCEER-93-7, University of Nevada, Reno, August 1993.

CCEER-93-8 Roybal, J., Sanders, D.H., and Maragakis, E., "Vulnerability Assessment of Masonry in the Reno-Carson City Urban Corridor," Civil Engineering Department, Report No. CCEER-93-8, University of Nevada, Reno, May 1993.

CCEER-93-9 Zafir, Z. and Siddharthan, R., "MOVLOAD: A Program to Determine the Behavior of Nonlinear Horizontally Layered Medium Under Moving Load," Civil Engineering Department, Report No. CCEER-93-9, University of Nevada, Reno, August 1993.

CCEER-93-10 O'Connor, D.N., Saiidi, M., and Maragakis, E.A., "A Study of Bridge Column Seismic Damage Susceptibility at the Interstate 80/U.S. 395 Interchange in Reno, Nevada," Civil Engineering Department, Report No. CCEER-93-10, University of Nevada, Reno, October 1993.

CCEER-94-1 Maragakis, E., B. Douglas, and E. Abdelwahed, "Preliminary Dynamic Analysis of a Railroad Bridge," Report CCEER-94-1, January 1994.

CCEER-94-2 Douglas, B.M., Maragakis, E.A., and Feng, S., "Stiffness Evaluation of Pile Foundation of Cazenovia Creek Overpass," Civil Engineering Department, Report No. CCEER-94-2, University of Nevada, Reno, March 1994.

CCEER-94-3 Douglas, B.M., Maragakis, E.A., and Feng, S., "Summary of Pretest Analysis of Cazenovia Creek Bridge," Civil Engineering Department, Report No. CCEER-94-3, University of Nevada, Reno, April 1994.

CCEER-94-4 Norris, G.M., Madhu, R., Valceschini, R., and Ashour, M., "Liquefaction and Residual Strength of Loose Sands from Drained Triaxial Tests," Report 2, Vol. 1&2, Civil Engineering Department, Report No. CCEER-94-4, University of Nevada, Reno, August 1994.

CCEER-94-5 Saiidi, M., Hutchens, E., and Gardella, D., "Prestress Losses in a Post-Tensioned R/C Box Girder Bridge in Southern Nevada," Civil Engineering Department, CCEER-94-5, University of Nevada, Reno, August 1994.

CCEER-95-1 Siddharthan, R., El-Gamal, M., and Maragakis, E.A., "Nonlinear Bridge Abutment , Verification, and Design Curves," Civil Engineering Department, CCEER-95-1, University of Nevada, Reno, January 1995.

CCEER-95-2 Ashour, M. and Norris, G., "Liquefaction and Undrained Response Evaluation of Sands from Drained Formulation," Civil Engineering Department, Report No. CCEER-95-2, University of Nevada, Reno, February 1995.

CCEER-95-3 Wehbe, N., Saiidi, M., Sanders, D. and Douglas, B., "Ductility of Rectangular Reinforced Concrete Bridge Columns with Moderate Confinement," Civil Engineering Department, Report No. CCEER-95-3, University of Nevada, Reno, July 1995.

CCEER-95-4 Martin, T.., Saiidi, M. and Sanders, D., "Seismic Retrofit of Column-Pier Cap Connections in Bridges in Northern Nevada," Civil Engineering Department, Report No. CCEER-95-4, University of Nevada, Reno, August 1995.

CCEER-95-5 Darwish, I., Saiidi, M. and Sanders, D., "Experimental Study of Seismic Susceptibility Column-Footing Connections in Bridges in Northern Nevada," Civil Engineering Department, Report No. CCEER-95-5, University of Nevada, Reno, September 1995.

CCEER-95-6 Griffin, G., Saiidi, M. and Maragakis, E., "Nonlinear Seismic Response of Isolated Bridges and Effects of Pier Ductility Demand," Civil Engineering Department, Report No. CCEER-95-6, University of Nevada, Reno, November 1995.

CCEER-95-7 Acharya, S.., Saiidi, M. and Sanders, D., "Seismic Retrofit of Bridge Footings and Column-Footing Connections," Civil Engineering Department, Report No. CCEER-95-7, University of Nevada, Reno, November 1995.

CCEER-95-8 Maragakis, E., Douglas, B., and Sandirasegaram, U., "Full-Scale Field Resonance Tests of a Railway Bridge," A Report to the Association of American Railroads, Civil Engineering Department, Report No. CCEER-95-8, University of Nevada, Reno, December 1995.

CCEER-95-9 Douglas, B., Maragakis, E. and Feng, S., "System Identification Studies on Cazenovia Creek Overpass," Report for the National Center for Earthquake Engineering Research, Civil Engineering Department, Report No. CCEER-95-9, University of Nevada, Reno, October 1995.

CCEER-96-1 El-Gamal, M.E. and Siddharthan, R.V., "Programs to Computer Translational Stiffness of Seat-Type Bridge Abutment," Civil Engineering Department, Report No. CCEER-96-1, University of Nevada, Reno, March 1996.

CCEER-96-2 Labia, Y., Saiidi, M. and Douglas, B., "Evaluation and Repair of Full-Scale Prestressed Concrete Box Girders," A Report to the National Science Foundation, Research Grant CMS-9201908, Civil Engineering Department, Report No. CCEER-96-2, University of Nevada, Reno, May 1996.

CCEER-96-3 Darwish, I., Saiidi, M. and Sanders, D., "Seismic Retrofit of R/C Oblong Tapered Bridge Columns with Inadequate Bar Anchorage in Columns and Footings," A Report to the Nevada Department of Transportation, Civil Engineering Department, Report No. CCEER-96-3, University of Nevada, Reno, May 1996.

CCEER-96-4 Ashour, M., Pilling, R., Norris, G. and Perez, H., "The Prediction of Lateral Load Behavior of Single Piles and Pile Groups Using the Strain Wedge Model," A Report to the California Department of Transportation, Civil Engineering Department, Report No. CCEER-96-4, University of Nevada, Reno, June 1996.

CCEER-97-1-A Rimal, P. and Itani, A. "Sensitivity Analysis of Fatigue Evaluations of Steel Bridges," Center for Earthquake Research, Department of Civil Engineering, University of Nevada, Reno, Nevada Report No. CCEER-97-1-A, September, 1997.

CCEER-97-1-B Maragakis, E., Douglas, B., and Sandirasegaram, U. "Full-Scale Field Resonance Tests of a Railway Bridge," A Report to the Association of American Railroads, Civil Engineering Department, University of Nevada, Reno, May, 1996.

CCEER-97-2 Wehbe, N., Saiidi, M., and D. Sanders, "Effect of Confinement and Flares on the Seismic Performance of Reinforced Concrete Bridge Columns," Civil Engineering Department, Report No. CCEER-97-2, University of Nevada, Reno, September 1997.

CCEER-97-3 Darwish, I., M. Saiidi, G. Norris, and E. Maragakis, "Determination of In-Situ Footing Stiffness Using Full-Scale Dynamic Field Testing," A Report to the Nevada Department of Transportation, Structural Design Division, Carson City, Nevada, Report No. CCEER-97-3, University of Nevada, Reno, October 1997.

CCEER-97-4-A Itani, A. "Cyclic Behavior of Richmond-San Rafael Tower Links," Center for Civil Engineering Earthquake Research, Department of Civil Engineering, University of Nevada, Reno, Nevada, Report No. CCEER-97-4, August 1997.

CCEER-97-4-B Wehbe, N., and M. Saiidi, "User's Manual for RCMC v. 1.2 : A Computer Program for Moment-Curvature Analysis of Confined and Unconfined Reinforced Concrete Sections," Center for Civil Engineering Earthquake Research, Department of Civil Engineering, University of Nevada, Reno, Nevada, Report No. CCEER-97-4, November, 1997.

CCEER-97-5 Isakovic, T., M. Saiidi, and A. Itani, "Influence of new Bridge Configurations on Seismic Performance," Department of Civil Engineering, University of Nevada, Reno, Report No. CCEER-97-5, September, 1997.

CCEER-98-1 Itani, A., Vesco, T. and Dietrich, A., "Cyclic Behavior of "as Built" Laced Members With End Gusset Plates on the San Francisco Bay Bridge," Center for Civil Engineering Earthquake Research, Department of Civil Engineering, University of Nevada, Reno, Nevada Report No. CCEER-98-1, March, 1998.

CCEER-98-2 G. Norris and M. Ashour, "Liquefaction and Undrained Response Evaluation of Sands from Drained Formulation," Center for Civil Engineering Earthquake Research, Department of Civil Engineering, University of Nevada, Reno, Nevada, Report No. CCEER-98-2, May, 1998.

CCEER-98-3 Qingbin, Chen, B. M. Douglas, E. Maragakis, and I. G. Buckle, "Extraction of Nonlinear Hysteretic Properties of Seismically Isolated Bridges from Quick-Release Field Tests," Center for Civil Engineering Earthquake Research, Department of Civil Engineering, University of Nevada, Reno, Nevada, Report No. CCEER-98-3, June, 1998.

CCEER-98-4 Maragakis, E., B. M. Douglas, and C. Qingbin, "Full-Scale Field Capacity Tests of a Railway Bridge," Center for Civil Engineering Earthquake Research, Department of Civil Engineering, University of Nevada, Reno, Nevada, Report No. CCEER-98-4, June, 1998.

CCEER-98-5 Itani, A., Douglas, B., and Woodgate, J., "Cyclic Behavior of Richmond-San Rafael Retrofitted Tower Leg," Center for Civil Engineering Earthquake Research, Department of Civil Engineering, University of Nevada, Reno. Report No. CCEER-98-5, June 1998

CCEER-98-6 Moore, R., Saiidi, M., and Itani, A., "Seismic Behavior of New Bridges with Skew and Curvature," Center for Civil Engineering Earthquake Research, Department of Civil Engineering, University of Nevada, Reno. Report No. CCEER-98-6, October, 1998.

CCEER-98-7 Itani, A and Dietrich, A, "Cyclic Behavior of Double Gusset Plate Connections," Center for Civil Engineering Earthquake Research, Department of Civil Engineering, University of Nevada, Reno, Nevada, Report No. CCEER-98-5, December, 1998.

CCEER-99-1 Caywood, C., M. Saiidi, and D. Sanders, "Seismic Retrofit of Flared Bridge Columns with Steel Jackets," Civil Engineering Department, University of Nevada, Reno, Report No. CCEER-99-1, February 1999.

CCEER-99-2 Mangoba, N., M. Mayberry, and M. Saiidi, "Prestress Loss in Four Box Girder Bridges in Northern Nevada," Civil Engineering Department, University of Nevada, Reno, Report No. CCEER-99-2, March 1999.

CCEER-99-3 Abo-Shadi, N., M. Saiidi, and D. Sanders, "Seismic Response of Bridge Pier Walls in the Weak Direction," Civil Engineering Department, University of Nevada, Reno, Report No. CCEER-99-3, April 1999.

CCEER-99-4 Buzick, A., and M. Saiidi, "Shear Strength and Shear Fatigue Behavior of Full-Scale Prestressed Concrete Box Girders," Civil Engineering Department, University of Nevada, Reno, Report No. CCEER-99-4, April 1999.

CCEER-99-5 Randall, M., M. Saiidi, E. Maragakis and T. Isakovic, "Restrainer Design Procedures For Multi-Span Simply-Supported Bridges," Civil Engineering Department, University of Nevada, Reno, Report No. CCEER-99-5, April 1999.

CCEER-99-6 Wehbe, N. and M. Saiidi, "User's Manual for RCMC v. 1.2, A Computer Program for

Moment-Curvature Analysis of Confined and Unconfined Reinforced Concrete Sections," Civil Engineering Department, University of Nevada, Reno, Report No. CCEER-99-6, May 1999.

CCEER-99-7 Burda, J. and A. Itani, "Studies of Seismic Behavior of Steel Base Plates," Civil Engineering Department, University of Nevada, Reno, Report No. CCEER-99-7, May 1999.

CCEER-99-8 Ashour, M. and G. Norris, "Refinement of the Strain Wedge Model Program," Civil Engineering Department, University of Nevada, Reno, Report No. CCEER-99-8, March 1999.

CCEER-99-9 Dietrich, A., and A. Itani, "Cyclic Behavior of Laced and Perforated Steel Members on the San Francisco-Oakland Bay Bridge," Civil Engineering Department, University, Reno, Report No. CCEER-99-9, December 1999.

CCEER 99-10 Itani, A., A. Dietrich, "Cyclic Behavior of Built Up Steel Members and their Connections," Civil Engineering Department, University of Nevada, Reno, Report No. CCEER-99-10, December 1999.

CCEER 99-10-A Itani, A., E. Maragakis and P. He, "Fatigue Behavior of Riveted Open Deck Railroad Bridge Girders," Civil Engineering Department, University of Nevada, Reno, Report No. CCEER-99-10-A, August 1999.

CCEER 99-11 Itani, A., J. Woodgate, "Axial and Rotational Ductility of Built Up Structural Steel Members," Civil Engineering Department, University of Nevada, Reno, Report No. CCEER-99-11, December 1999.

CCEER-99-12 Sgambelluri, M., Sanders, D.H., and Saiidi, M.S., "Behavior of One-Way Reinforced Concrete Bridge Column Hinges in the Weak Direction," Department of Civil Engineering, University of Nevada, Reno, Report No. CCEER-99-12, December 1999.

CCEER-99-13 Laplace, P., Sanders, D.H., Douglas, B, and Saiidi, M, "Shake Table Testing of Flexure Dominated Reinforced Concrete Bridge Columns", Department of Civil Engineering, University of Nevada, Reno, Report No. CCEER-99-13, December 1999.

CCEER-99-14 Ahmad M. Itani, Jose A. Zepeda, and Elizabeth A. Ware "Cyclic Behavior of Steel Moment Frame Connections for the Moscone Center Expansion," Department of Civil Engineering, University of Nevada, Reno, Report No. CCEER-99-14, December 1999.

CCEER 00-1 Ashour, M., and Norris, G. "Undrained Lateral Pile and Pile Group Response in Saturated Sand," Civil Engineering Department, University of Nevada, Reno, Report No. CCEER-00-1, May 1999. January 2000.

CCEER 00-2 Saiidi, M. and Wehbe, N., "A Comparison of Confinement Requirements in Different Codes for Rectangular, Circular, and Double-Spiral RC Bridge Columns," Civil Engineering Department, University of Nevada, Reno, Report No. CCEER-00-2, January 2000.

CCEER 00-3 McElhaney, B., M. Saiidi, and D. Sanders, "Shake Table Testing of Flared Bridge Columns With Steel Jacket Retrofit," Civil Engineering Department, University of Nevada, Reno, Report No. CCEER-00-3, January 2000.

CCEER 00-4 Martinovic, F., M. Saiidi, D. Sanders, and F. Gordaninejad, "Dynamic Testing of Non-Prismatic Reinforced Concrete Bridge Columns Retrofitted with FRP Jackets," Civil Engineering Department, University of Nevada, Reno, Report No. CCEER-00-4, January 2000.

CCEER 00-5 Itani, A., and M. Saiidi, "Seismic Evaluation of Steel Joints for UCLA Center for Health Science Westwood Replacement Hospital," Civil Engineering Department, University of Nevada, Reno, Report No. CCEER-00-5, February 2000.

CCEER 00-6 Will, J. and D. Sanders, "High Performance Concrete Using Nevada Aggregates," Civil Engineering Department, University of Nevada, Reno, Report No. CCEER-00-6, May 2000.

CCEER 00-7 French, C., and M. Saiidi, "A Comparison of Static and Dynamic Performance of Models of Flared Bridge Columns," Civil Engineering Department, University of Nevada, Reno, Report No. CCEER-00-7, October 2000.

CCEER 00-8 Itani, A., H. Sedarat, "Seismic Analysis of the AISI LRFD Design Example of Steel Highway Bridges," Civil Engineering Department, University of Nevada, Reno, Report No. CCEER 00-08, November 2000.

CCEER 00-9 Moore, J., D. Sanders, and M. Saiidi, "Shake Table Testing of 1960's Two Column Bent with Hinges Bases," Civil Engineering Department, University of Nevada, Reno, Report No. CCEER 00-09, December 2000.

CCEER 00-10 Asthana, M., D. Sanders, and M. Saiidi, "One-Way Reinforced Concrete Bridge Column Hinges in the Weak Direction," Civil Engineering Department, University of Nevada, Reno, Report No. CCEER 00-10, April 2001.

CCEER 01-1 Ah Sha, H., D. Sanders, M. Saiidi, "Early Age Shrinkage and Cracking of Nevada Concrete Bridge Decks," Civil Engineering Department, University of Nevada, Reno, Report No. CCEER 01-01, May 2001.

CCEER 01-2 Ashour, M. and G. Norris, "Pile Group program for Full Material Modeling a Progressive Failure," Civil Engineering Department, University of Nevada, Reno, Report No. CCEER 01-02, July 2001.

CCEER 01-3 Itani, A., C. Lanaud, and P. Dusicka, "Non-Linear Finite Element Analysis of Built-Up Shear Links," Civil Engineering Department, University of Nevada, Reno, Report No. CCEER 01-03, July 2001.

CCEER 01-4 Saiidi, M., J. Mortensen, and F. Martinovic, "Analysis and Retrofit of Fixed Flared Columns with Glass Fiber-Reinforced Plastic Jacketing," Civil Engineering Department, University of Nevada, Reno, Report No. CCEER 01-4, August 2001

CCEER 01-5 Not Published

CCEER 01-6 Laplace, P., D. Sanders, and M. Saiidi, "Experimental Study and Analysis of Retrofitted Flexure and Shear Dominated Circular Reinforced Concrete Bridge Columns Subjected to Shake Table Excitation," Civil Engineering Department, University of Nevada, Reno, Report No. CCEER 01-6, June 2001.

CCEER 01-7 Reppi, F., and D. Sanders, "Removal and Replacement of Cast-in-Place, Post-tensioned, Box Girder Bridge," Civil Engineering Department, University of Nevada, Reno, Report No. CCEER 01-7, December 2001.

CCEER 02-1 Pulido, C., M. Saiidi, D. Sanders, and A. Itani, "Seismic Performance and Retrofitting of Reinforced Concrete Bridge Bents," Civil Engineering Department, University of Nevada, Reno, Report No. CCEER 02-1, January 2002.

CCEER 02-2 Yang, Q., M. Saiidi, H. Wang, and A. Itani, "Influence of Ground Motion Incoherency on Earthquake Response of Multi-Support Structures," Civil Engineering Department, University of Nevada, Reno, Report No. CCEER 02-2, May 2002.

CCEER 02-3 M. Saiidi, B. Gopalakrishnan, E. Reinhardt, and R. Siddharthan, "A Preliminary Study of Shake Table Response of A Two-Column Bridge Bent on Flexible Footings," Civil Engineering Department, University of Nevada, Reno, Report No. CCEER 02-03, June 2002.

CCEER 02-4 Not Published

CCEER 02-5 Banghart, A., Sanders, D., Saiidi, M., "Evaluation of Concrete Mixes for Filling the Steel Arches in the Galena Creek Bridge," Civil Engineering Department, University of Nevada, Reno, Report No. CCEER 02-05, June 2002.

CCEER 02-6 Dusicka, P., Itani, A., Buckle, I. G., "Cyclic Behavior of Shear Links and Tower Shaft Assembly of San Francisco – Oakland Bay Bridge Tower," Civil Engineering Department, University of Nevada, Reno, Report No. CCEER 02-06, July 2002.

CCEER 02-7 Mortensen, J., and M. Saiidi, "A Performance-Based Design Method for Confinement in Circular Columns," Civil Engineering Department, University of Nevada, Reno, Report No. CCEER 02-07, November 2002.

CCEER 03-1 Wehbe, N., and M. Saiidi, "User's manual for SPMC v. 1.0 : A Computer Program for Moment-Curvature Analysis of Reinforced Concrete Sections with Interlocking Spirals," Center for Civil Engineering Earthquake Research, Department of Civil Engineering, University of Nevada, Reno, Nevada, Report No. CCEER-03-1, May, 2003.

CCEER 03-2 Wehbe, N., and M. Saiidi, "User's manual for RCMC v. 2.0 : A Computer Program for Moment-Curvature Analysis of Confined and Unconfined Reinforced Concrete Sections," Center for Civil Engineering Earthquake Research, Department of Civil Engineering, University of Nevada, Reno, Nevada, Report No. CCEER-03-2, June, 2003.

CCEER 03-3 Nada, H., D. Sanders, and M. Saiidi, "Seismic Performance of RC Bridge Frames with Architectural-Flared Columns," Civil Engineering Department, University of Nevada, Reno, Report No. CCEER 03-3, January 2003.

CCEER 03-4 Reinhardt, E., M. Saiidi, and R. Siddharthan, "Seismic Performance of a CFRP/ Concrete Bridge Bent on Flexible Footings," Civil Engineering Department, University of Nevada, Reno, Report No. CCEER 03-4, August 2003.

CCEER 03-5 Johnson, N., M. Saiidi, A. Itani, and S. Ladkany, "Seismic Retrofit of Octagonal Columns with Pedestal and One-Way Hinge at the Base," Center for Civil Engineering Earthquake Research, Department of Civil Engineering, University of Nevada, Reno, Nevada, and Report No. CCEER-03-5, August 2003.

CCEER 03-6 Mortensen, C., M. Saiidi, and S. Ladkany, "Creep and Shrinkage Losses in Highly Variable Climates," Center for Civil Engineering Earthquake Research, Department of Civil Engineering, University of Nevada, Reno, Report No. CCEER-03-6, September 2003.

CCEER 03- 7 Ayoub, C., M. Saiidi, and A. Itani, "A Study of Shape-Memory-Alloy-Reinforced Beams and Cubes," Center for Civil Engineering Earthquake Research, Department of Civil Engineering, University of Nevada, Reno, Nevada, Report No. CCEER-03-7, October 2003.

CCEER 03-8 Chandane, S., D. Sanders, and M. Saiidi, "Static and Dynamic Performance of RC Bridge Bents with Architectural-Flared Columns," Center for Civil Engineering Earthquake Research, Department of Civil Engineering, University of Nevada, Reno, Nevada, Report No. CCEER-03-8, November 2003.

CCEER 04-1 Olaegbe, C., and Saiidi, M., "Effect of Loading History on Shake Table Performance of A Two-Column Bent with Infill Wall," Center for Civil Engineering Earthquake Research, Department of Civil Engineering, University of Nevada, Reno, Nevada, Report No. CCEER-04-1, January 2004.

CCEER 04-2 Johnson, R., Maragakis, E., Saiidi, M., and DesRoches, R., "Experimental Evaluation of Seismic Performance of SMA Bridge Restrainers," Center for Civil Engineering Earthquake Research, Department of Civil Engineering, University of Nevada, Reno, Nevada, Report No. CCEER-04-2, February 2004.

CCEER 04-3 Moustafa, K., Sanders, D., and Saiidi, M., "Impact of Aspect Ratio on Two-Column Bent Seismic Performance," Center for Civil Engineering Earthquake Research, Department of

Civil Engineering, University of Nevada, Reno, Nevada, Report No. CCEER-04-3, February 2004.

CCEER 04-4 Maragakis, E., Saiidi, M., Sanchez-Camargo, F., and Elfass, S., “Seismic Performance of Bridge Restrainers At In-Span Hinges,” Center for Civil Engineering Earthquake Research, Department of Civil Engineering, University of Nevada, Reno, Nevada, Report No. CCEER-04-4, March 2004.

CCEER 04-5 Ashour, M., Norris, G. and Elfass, S., “Analysis of Laterally Loaded Long or Intermediate Drilled Shafts of Small or Large Diameter in Layered Soil,” Center for Civil Engineering Earthquake Research, Department of Civil Engineering, University of Nevada, Reno, Nevada, Report No. CCEER-04-5, June 2004.

CCEER 04-6 Correal, J., Saiidi, M. and Sanders, D., “Seismic Performance of RC Bridge Columns Reinforced with Two Interlocking Spirals,” Center for Civil Engineering Earthquake Research, Department of Civil Engineering, University of Nevada, Reno, Nevada, Report No. CCEER-04-6, August 2004.

CCEER 04-7 Dusicka, P., Itani, A. and Buckle, I., “Cyclic Response and Low Cycle Fatigue Characteristics of Plate Steels,” Center for Civil Engineering Earthquake Research, Department of Civil Engineering, University of Nevada, Reno, Nevada, Report No. CCEER-04-7, November 2004.

CCEER 04-8 Dusicka, P., Itani, A. and Buckle, I., “Built-up Shear Links as Energy Dissipaters for Seismic Protection of Bridges,” Center for Civil Engineering Earthquake Research, Department of Civil Engineering, University of Nevada, Reno, Nevada, Report No. CCEER-04-8, November 2004.

CCEER 04-9 Sureshkumar, K., Saiidi, S., Itani, A. and Ladkany, S., “Seismic Retrofit of Two-Column Bents with Diamond Shape Columns,” Center for Civil Engineering Earthquake Research, Department of Civil Engineering, University of Nevada, Reno, Nevada, Report No. CCEER-04-9, November 2004.

CCEER 05-1 Wang, H. and Saiidi, S., “A Study of RC Columns with Shape Memory Alloy and Engineered Cementitious Composites,” Center for Civil Engineering Earthquake Research, Department of Civil Engineering, University of Nevada, Reno, Nevada, Report No. CCEER-05-1, January 2005.

CCEER 05-2 Johnson, R., Saiidi, S. and Maragakis, E., “A Study of Fiber Reinforced Plastics for Seismic Bridge Restrainers,” Center for Civil Engineering Earthquake Research, Department of Civil Engineering, University of Nevada, Reno, Nevada, Report No. CCEER-05-2, January 2005.

CCEER 05-3 Carden, L.P., Itani, A.M., Buckle, I.G, “Seismic Load Path in Steel Girder Bridge Superstructures,” Center for Civil Engineering Earthquake Research, Department of Civil Engineering, University of Nevada, Reno, Nevada, Report No. CCEER-05-3, January 2005.

CCEER 05-4 Carden, L.P., Itani, A.M., Buckle, I.G, “Seismic Performance of Steel Girder Bridge Superstructures with Ductile End Cross Frames and Seismic Isolation,” Center for Civil Engineering Earthquake Research, Department of Civil Engineering, University of Nevada, Reno, Nevada, Report No. CCEER-05-4, January 2005.

CCEER 05-5 Goodwin, E., Maragakis, M., Itani, A. and Luo, S., “Experimental Evaluation of the Seismic Performance of Hospital Piping Subassemblies,” Center for Civil Engineering Earthquake Research, Department of Civil Engineering, University of Nevada, Reno, Nevada, Report No. CCEER-05-5, February 2005.

CCEER 05-6 Zadeh M. S., Saiidi, S, Itani, A. and Ladkany, S., “Seismic Vulnerability Evaluation and Retrofit Design of Las Vegas Downtown Viaduct,” Center for Civil Engineering

Earthquake Research, Department of Civil Engineering, University of Nevada, Reno, Nevada, Report No. CCEER-05-6, February 2005.

CCEER 05-7 Phan, V., Saiidi, S. and Anderson, J., "Near Fault (Near Field) Ground Motion Effects on Reinforced Concrete Bridge Columns," Center for Civil Engineering Earthquake Research, Department of Civil Engineering, University of Nevada, Reno, Nevada, Report No. CCEER-05-7, August 2005.

CCEER 05-8 Carden, L., Itani, A. and Laplace, P., "Performance of Steel Props at the UNR Fire Science Academy subjected to Repeated Fire," Center for Civil Engineering Earthquake Research, Department of Civil Engineering, University of Nevada, Reno, Nevada, Report No. CCEER-05-8, August 2005.

CCEER 05-9 Yamashita, R. and Sanders, D., "Shake Table Testing and an Analytical Study of Unbonded Prestressed Hollow Concrete Column Constructed with Precast Segments," Center for Civil Engineering Earthquake Research, Department of Civil Engineering, University of Nevada, Reno, Nevada, Report No. CCEER-05-9, August 2005.

CCEER 05-10 Not Published

CCEER 05-11 Carden, L., Itani., A., and Peckan, G., "Recommendations for the Design of Beams and Posts in Bridge Falsework," Center for Civil Engineering Earthquake Research, Department of Civil Engineering, University of Nevada, Reno, Nevada, Report No. CCEER-05-11, October 2005.

CCEER 06-01 Cheng, Z., Saiidi, M., and Sanders, D., "Development of a Seismic Design Method for Reinforced Concrete Two-Way Bridge Column Hinges," Center for Civil Engineering Earthquake Research, Department of Civil Engineering, University of Nevada, Reno, Nevada, Report No. CCEER-06-01, February 2006.

CCEER 06-02 Johnson, N., Saiidi, M., and Sanders, D., "Large-Scale Experimental and Analytical Studies of a Two-Span Reinforced Concrete Bridge System," Center for Civil Engineering Earthquake Research, Department of Civil Engineering, University of Nevada, Reno, Nevada, Report No. CCEER-06-02, March 2006.

CCEER 06-03 Saiidi, M., Ghasemi, H. and Tiras, A., "Seismic Design and Retrofit of Highway Bridges," Proceedings, Second US-Turkey Workshop, Center for Civil Engineering Earthquake Research, Department of Civil Engineering, University of Nevada, Reno, Nevada, Report No. CCEER-06-03, May 2006.

CCEER 07-01 O'Brien, M., Saiidi, M. and Sadrossadat-Zadeh, M., "A Study of Concrete Bridge Columns Using Innovative Materials Subjected to Cyclic Loading," Center for Civil Engineering Earthquake Research, Department of Civil Engineering, University of Nevada, Reno, Nevada, Report No. CCEER-07-01, January 2007.

CCEER 07-02 Sadrossadat-Zadeh, M. and Saiidi, M., "Effect of Strain rate on Stress-Strain Properties and Yield Propagation in Steel Reinforcing Bars," Center for Civil Engineering Earthquake Research, Department of Civil Engineering, University of Nevada, Reno, Nevada, Report No. CCEER-07-02, January 2007.

CCEER 07-03 Sadrossadat-Zadeh, M. and Saiidi, M., "Analytical Study of NEESR-SG 4-Span Bridge Model Using OpenSees," Center for Civil Engineering Earthquake Research, Department of Civil Engineering, University of Nevada, Reno, Nevada, Report No. CCEER-07-03, January 2007.

CCEER 07-04 Nelson, R., Saiidi, M. and Zadeh, S., "Experimental Evaluation of Performance of Conventional Bridge Systems," Center for Civil Engineering Earthquake Research, Department of Civil Engineering, University of Nevada, Reno, Nevada, Report No. CCEER-07-04, October 2007.

CCEER 07-05 Bahen, N. and Sanders, D., "Strut-and-Tie Modeling for Disturbed Regions in Structural Concrete Members with Emphasis on Deep Beams," Center for Civil Engineering Earthquake Research, Department of Civil Engineering, University of Nevada, Reno, Nevada, Report No. CCEER-07-05, December 2007.

CCEER 07-06 Choi, H., Saiidi, M. and Somerville, P., "Effects of Near-Fault Ground Motion and Fault-Rupture on the Seismic Response of Reinforced Concrete Bridges," Center for Civil Engineering Earthquake Research, Department of Civil Engineering, University of Nevada, Reno, Nevada, Report No. CCEER-07-06, December 2007.

CCEER 07-07 Ashour M. and Norris, G., "Report and User Manual on Strain Wedge Model Computer Program for Files and Large Diameter Shafts with LRFD Procedure," Center for Civil Engineering Earthquake Research, Department of Civil Engineering, University of Nevada, Reno, Nevada, Report No. CCEER-07-07, October 2007.

CCEER 08-01 Doyle, K. and Saiidi, M., "Seismic Response of Telescopic Pipe Pin Connections," Center for Civil Engineering Earthquake Research, Department of Civil Engineering, University of Nevada, Reno, Nevada, Report No. CCEER-08-01, February 2008.

CCEER 08-02 Taylor, M. and Sanders, D., "Seismic Time History Analysis and Instrumentation of the Galena Creek Bridge," Center for Civil Engineering Earthquake Research, Department of Civil Engineering, University of Nevada, Reno, Nevada, Report No. CCEER-08-02, April 2008.

CCEER 08-03 Abdel-Mohti, A. and Pekcan, G., "Seismic Response Assessment and Recommendations for the Design of Skewed Post-Tensioned Concrete Box-Girder Highway Bridges," Center for Civil Engineering Earthquake Research, Department of Civil and Environmental Engineering, University of Nevada, Reno, Nevada, Report No. CCEER-08-03, September 2008.

CCEER 08-04 Saiidi, M., Ghasemi, H. and Hook, J., "Long Term Bridge Performance Monitoring, Assessment & Management," Proceedings, FHWA/NSF Workshop on Future Directions," Center for Civil Engineering Earthquake Research, Department of Civil and Environmental Engineering, University of Nevada, Reno, Nevada, Report No. CCEER 08-04, September 2008.

CCEER 09-01 Brown, A., and Saiidi, M., "Investigation of Near-Fault Ground Motion Effects on Substandard Bridge Columns and Bents," Center for Civil Engineering Earthquake Research, Department of Civil and Environmental Engineering, University of Nevada, Reno, Nevada, Report No. CCEER-09-01, July 2009.

CCEER 09-02 Linke, C., Pekcan, G., and Itani, A., "Detailing of Seismically Resilient Special Truss Moment Frames," Center for Civil Engineering Earthquake Research, Department of Civil and Environmental Engineering, University of Nevada, Reno, Nevada, Report No. CCEER-09-02, August 2009.

CCEER 09-03 Hillis, D., and Saiidi, M., "Design, Construction, and Nonlinear Dynamic Analysis of Three Bridge Bents Used in a Bridge System Test," Center for Civil Engineering Earthquake Research, Department of Civil and Environmental Engineering, University of Nevada, Reno, Nevada, Report No. CCEER-09-03, August 2009.

CCEER 09-04 Bahrami, H., Itani, A., and Buckle, I., "Guidelines for the Seismic Design of Ductile End Cross Frames in Steel Girder Bridge Superstructures," Center for Civil Engineering Earthquake Research, Department of Civil and Environmental Engineering, University of Nevada, Reno, Nevada, Report No. CCEER-09-04, September 2009.

CCEER 10-01 Zaghi, A. E., and Saiidi, M., "Seismic Design of Pipe-Pin Connections in Concrete Bridges," Center for Civil Engineering Earthquake Research, Department of Civil and Environmental Engineering, University of Nevada, Reno, Nevada, Report No. CCEER-10-01, January 2010.

CCEER 10-02 Pooranampillai, S., Elfass, S., and Norris, G., "Laboratory Study to Assess Load Capacity Increase of Drilled Shafts through Post Grouting," Center for Civil Engineering Earthquake Research, Department of Civil and Environmental Engineering, University of Nevada, Reno, Nevada, Report No. CCEER-10-02, January 2010.

CCEER 10-03 Itani, A., Grubb, M., and Monzon, E, "Proposed Seismic Provisions and Commentary for Steel Plate Girder Superstructures," Center for Civil Engineering Earthquake Research, Department of Civil and Environmental Engineering, University of Nevada, Reno, Nevada, Report No. CCEER-10-03, June 2010.

CCEER 10-04 Cruz-Noguez, C., Saiidi, M., "Experimental and Analytical Seismic Studies of a Four-Span Bridge System with Innovative Materials," Center for Civil Engineering Earthquake Research, Department of Civil and Environmental Engineering, University of Nevada, Reno, Nevada, Report No. CCEER-10-04, September 2010.

CCEER 10-05 Vosooghi, A., Saiidi, M., "Post-Earthquake Evaluation and Emergency Repair of Damaged RC Bridge Columns Using CFRP Materials," Center for Civil Engineering Earthquake Research, Department of Civil and Environmental Engineering, University of Nevada, Reno, Nevada, Report No. CCEER-10-05, September 2010.

CCEER 10-06 Ayoub, M., Sanders, D., "Testing of Pile Extension Connections to Slab Bridges," Center for Civil Engineering Earthquake Research, Department of Civil and Environmental Engineering, University of Nevada, Reno, Nevada, Report No. CCEER-10-06, October 2010.

CCEER 10-07 Builes-Mejia, J. C. and Itani, A., "Stability of Bridge Column Rebar Cages during Construction," Center for Civil Engineering Earthquake Research, Department of Civil and Environmental Engineering, University of Nevada, Reno, Nevada, Report No. CCEER-10-07, November 2010.

CCEER 10-08 Monzon, E.V., "Seismic Performance of Steel Plate Girder Bridges with Integral Abutments," Center for Civil Engineering Earthquake Research, Department of Civil and Environmental Engineering, University of Nevada, Reno, Nevada, Report No. CCEER-10-08, November 2010.

CCEER 11-01 Motaref, S., Saiidi, M., and Sanders, D., "Seismic Response of Precast Bridge Columns with Energy Dissipating Joints," Center for Civil Engineering Earthquake Research, Department of Civil and Environmental Engineering, University of Nevada, Reno, Nevada, Report No. CCEER-11-01, May 2011.

CCEER 11-02 Harrison, N. and Sanders, D., "Preliminary Seismic Analysis and Design of Reinforced Concrete Bridge Columns for Curved Bridge Experiments," Center for Civil Engineering Earthquake Research, Department of Civil and Environmental Engineering, University of Nevada, Reno, Nevada, Report No. CCEER-11-02, May 2011.

CCEER 11-03 Vallejera, J. and Sanders, D., "Instrumentation and Monitoring the Galena Creek Bridge," Center for Civil Engineering Earthquake Research, Department of Civil and Environmental Engineering, University of Nevada, Reno, Nevada, Report No. CCEER-11-03, September 2011.

CCEER 11-04 Levi, M., Sanders, D., and Buckle, I., "Seismic Response of Columns in Horizontally Curved Bridges," Center for Civil Engineering Earthquake Research, Department of Civil and Environmental Engineering, University of Nevada, Reno, Nevada, Report No. CCEER-11-04, December 2011.

CCEER 12-01 Saiidi, M., "NSF International Workshop on Bridges of the Future – Wide Spread Implementation of Innovation," Center for Civil Engineering Earthquake Research, Department of Civil and Environmental Engineering, University of Nevada, Reno, Nevada, Report No. CCEER-12-01, January 2012.

CCEER 12-02 Larkin, A.S., Sanders, D., and Saiidi, M., "Unbonded Prestressed Columns for Earthquake Resistance," Center for Civil Engineering Earthquake Research, Department of Civil and Environmental Engineering, University of Nevada, Reno, Nevada, Report No. CCEER-12-02, January 2012.

CCEER 12-03 Arias-Acosta, J. G., Sanders, D., "Seismic Performance of Circular and Interlocking Spirals RC Bridge Columns under Bidirectional Shake Table Loading Part 1," Center for Civil Engineering Earthquake Research, Department of Civil and Environmental Engineering, University of Nevada, Reno, Nevada, Report No. CCEER-12-03, September 2012.

CCEER 12-04 Cukrov, M.E., Sanders, D., "Seismic Performance of Prestressed Pile-To-Bent Cap Connections," Center for Civil Engineering Earthquake Research, Department of Civil and Environmental Engineering, University of Nevada, Reno, Nevada, Report No. CCEER-12-04, September 2012.

CCEER 13-01 Carr, T. and Sanders, D., "Instrumentation and Dynamic Characterization of the Galena Creek Bridge," Center for Civil Engineering Earthquake Research, Department of Civil and Environmental Engineering, University of Nevada, Reno, Nevada, Report No. CCEER-13-01, January 2013.

CCEER 13-02 Vosooghi, A. and Buckle, I., "Evaluation of the Performance of a Conventional Four-Span Bridge During Shake Table Tests," Center for Civil Engineering Earthquake Research, Department of Civil and Environmental Engineering, University of Nevada, Reno, Nevada, Report No. CCEER-13-02, January 2013.

CCEER 13-03 Amirihormozaki, E. and Pekcan, G., "Analytical Fragility Curves for Horizontally Curved Steel Girder Highway Bridges," Center for Civil Engineering Earthquake Research, Department of Civil and Environmental Engineering, University of Nevada, Reno, Nevada, Report No. CCEER-13-03, February 2013.

CCEER 13-04 Almer, K. and Sanders, D., "Longitudinal Seismic Performance of Precast Bridge Girders Integrally Connected to a Cast-in-Place Bentcap," Center for Civil Engineering Earthquake Research, Department of Civil and Environmental Engineering, University of Nevada, Reno, Nevada, Report No. CCEER-13-04, April 2013.

CCEER 13-05 Monzon, E.V., Itani, A.I., and Buckle, I.G., "Seismic Modeling and Analysis of Curved Steel Plate Girder Bridges," Center for Civil Engineering Earthquake Research, Department of Civil and Environmental Engineering, University of Nevada, Reno, Nevada, Report No. CCEER-13-05, April 2013.

CCEER 13-06 Monzon, E.V., Buckle, I.G., and Itani, A.I., "Seismic Performance of Curved Steel Plate Girder Bridges with Seismic Isolation," Center for Civil Engineering Earthquake Research, Department of Civil and Environmental Engineering, University of Nevada, Reno, Nevada, Report No. CCEER-13-06, April 2013.

CCEER 13-07 Monzon, E.V., Buckle, I.G., and Itani, A.I., "Seismic Response of Isolated Bridge Superstructure to Incoherent Ground Motions," Center for Civil Engineering Earthquake Research, Department of Civil and Environmental Engineering, University of Nevada, Reno, Nevada, Report No. CCEER-13-07, April 2013.

CCEER 13-08 Haber, Z.B., Saiidi, M.S., and Sanders, D.H., "Precast Column-Footing Connections for Accelerated Bridge Construction in Seismic Zones," Center for Civil Engineering Earthquake Research, Department of Civil and Environmental Engineering, University of Nevada, Reno, Nevada, Report No. CCEER-13-08, April 2013.

CCEER 13-09 Ryan, K.L., Coria, C.B., and Dao, N.D., "Large Scale Earthquake Simulation of a Hybrid Lead Rubber Isolation System Designed under Nuclear Seismicity Considerations," Center for Civil Engineering Earthquake Research, Department of Civil and Environmental Engineering, University of Nevada, Reno, Nevada, Report No. CCEER-13-09, April 2013.

CCEER 13-10 Wibowo, H., Sanford, D.M., Buckle, I.G., and Sanders, D.H., "The Effect of Live Load on the Seismic Response of Bridges," Center for Civil Engineering Earthquake Research, Department of Civil and Environmental Engineering, University of Nevada, Reno, Nevada, Report No. CCEER-13-10, May 2013.

CCEER 13-11 Sanford, D.M., Wibowo, H., Buckle, I.G., and Sanders, D.H., "Preliminary Experimental Study on the Effect of Live Load on the Seismic Response of Highway Bridges," Center for Civil Engineering Earthquake Research, Department of Civil and Environmental Engineering, University of Nevada, Reno, Nevada, Report No. CCEER-13-11, May 2013.

CCEER 13-12 Saad, A.S., Sanders, D.H., and Buckle, I.G., "Assessment of Foundation Rocking Behavior in Reducing the Seismic Demand on Horizontally Curved Bridges," Center for Civil Engineering Earthquake Research, Department of Civil and Environmental Engineering, University of Nevada, Reno, Nevada, Report No. CCEER-13-12, June 2013.

CCEER 13-13 Ardakani, S.M.S. and Saiidi, M.S., "Design of Reinforced Concrete Bridge Columns for Near-Fault Earthquakes," Center for Civil Engineering Earthquake Research, Department of Civil and Environmental Engineering, University of Nevada, Reno, Nevada, Report No. CCEER-13-13, July 2013.

CCEER 13-14 Wei, C. and Buckle, I., "Seismic Analysis and Response of Highway Bridges with Hybrid Isolation," Center for Civil Engineering Earthquake Research, Department of Civil and Environmental Engineering, University of Nevada, Reno, Nevada, Report No. CCEER-13-14, August 2013.

CCEER 13-15 Wibowo, H., Buckle, I.G., and Sanders, D.H., "Experimental and Analytical Investigations on the Effects of Live Load on the Seismic Performance of a Highway Bridge," Center for Civil Engineering Earthquake Research, Department of Civil and Environmental Engineering, University of Nevada, Reno, Nevada, Report No. CCEER-13-15, August 2013.

CCEER 13-16 Itani, A.M., Monzon, E.V., Grubb, M., and Amirihormozaki, E. "Seismic Design and Nonlinear Evaluation of Steel I-Girder Bridges with Ductile End Cross-Frames," Center for Civil Engineering Earthquake Research, Department of Civil and Environmental Engineering, University of Nevada, Reno, Nevada, Report No. CCEER-13-16, September 2013.

CCEER 13-17 Kavianipour, F. and Saiidi, M.S., "Experimental and Analytical Seismic Studies of a Four-span Bridge System with Composite Piers," Center for Civil Engineering Earthquake Research, Department of Civil and Environmental Engineering, University of Nevada, Reno, Nevada, Report No. CCEER-13-17, September 2013.

CCEER 13-18 Mohebbi, A., Ryan, K., and Sanders, D., "Seismic Response of a Highway Bridge with Structural Fuses for Seismic Protection of Piers," Center for Civil Engineering Earthquake Research, Department of Civil and Environmental Engineering, University of Nevada, Reno, Nevada, Report No. CCEER-13-18, December 2013.

CCEER 13-19 Guzman Pujols, Jean C., Ryan, K.L., "Development of Generalized Fragility Functions for Seismic Induced Content Disruption," Center for Civil Engineering Earthquake Research, Department of Civil and Environmental Engineering, University of Nevada, Reno, Nevada, Report No. CCEER-13-19, December 2013.

CCEER 14-01 Salem, M. M. A., Pekcan, G., and Itani, A., "Seismic Response Control Of Structures Using Semi-Active and Passive Variable Stiffness Devices," Center for Civil Engineering Earthquake Research, Department of Civil and Environmental Engineering, University of Nevada, Reno, Nevada, Report No. CCEER-14-01, May 2014.

CCEER 14-02 Saini, A. and Saiidi, M., "Probabilistic Damage Control Approach for Seismic Design of Bridge Columns," Center For Civil Engineering Earthquake Research, Department Of

Civil and Environmental Engineering, University of Nevada, Reno, Nevada, Report No. CCEER-14-02, June 2014.

CCEER 14-03 Saini, A. and Saiidi, M., "Post Earthquake Damage Repair of Various Reinforced Concrete Bridge Components," Center For Civil Engineering Earthquake Research, Department Of Civil and Environmental Engineering, University of Nevada, Reno, Nevada, Report No. CCEER-14-03, May 2014.